

**TRANSFORMATION OF VETERINARY IONOPHORE ANTIBIOTICS  
UNDER CONDITIONS RELATED TO WATER-SOIL-LITTER SYSTEMS**

A Dissertation  
Presented to  
The Academic Faculty

by

Peizhe Sun

In Partial Fulfillment  
of the Requirements for the Degree  
Doctor of Philosophy in the  
School of Civil and Environmental Engineering

Georgia Institute of Technology  
May, 2014

**COPYRIGHT 2014 BY PEIZHE SUN**

**TRANSFORMATION OF VETERINARY IONOPHORE  
ANTIBIOTICS UNDER CONDITIONS RELATED TO WATER-  
SOIL-LITTER SYSTEMS**

Approved by:

Dr. Ching-Hua Huang, Advisor  
School of Civil and Environmental  
Engineering  
*Georgia Institute of Technology*

Dr. Yuanzhi Tang  
School of Earth and Atmospheric  
Science  
*Georgia Institute of Technology*

Dr. Spyros G. Pavlostathis, Advisor  
School of Civil and Environmental  
Engineering  
*Georgia Institute of Technology*

Dr. Miguel Cabrera  
College of Agricultural and  
Environmental Science  
*The University of Georgia*

Dr. Jim Spain  
School of Civil and Environmental  
Engineering  
*Georgia Institute of Technology*

Dr. Aaron Thompson  
College of Agricultural and  
Environmental Science  
*The University of Georgia*

Dr. John Crittenden  
School of Civil and Environmental  
Engineering  
*Georgia Institute of Technology*

Date Approved: March 28, 2014

*To my family*

## ACKNOWLEDGEMENTS

First of all, I would like to express my deepest gratitude to Dr. Ching-Hua Huang, who guided me through my graduate studies, provided me with patient assistance, and encouraged me when I had difficulties. My sincere thanks also go to Dr. Spyros Pavlostathis, who invested countless hours on my research. I feel extremely lucky to have two such wonderful mentors in my PhD study.

I would also like to thank my committee members Dr. Jim Spain, Dr. John Crittenden, Dr. Yuanzhi Tang, Dr. Miguel Cabrera and Dr. Aaron Thompson for their time and constructive advice on my research. Especially, I would like to thank Dr. Spain for his interesting and inspirational biotransformation course, Dr. Crittenden for his help on multiple research areas, and Dr. Cabrera for his assistant in field studies.

My thanks also go to Dr. Guangxuan Zhu who maintains and fixes every instrument in our department. I cannot imagine a well-working environmental lab without Dr. Zhu's help. I also wish to thank Jenny Eaton and other staff in CEE department for their consistent support and service for me and other graduate students.

I would like to express my special thanks to them who I worked with, including Dr. Lokesh Padhye, Dr. Daisuke Minakata, Delphine Barmaz, Dr. Yao Hong, Yung-Li Wang and Zhanguang Liu. I also appreciate the support from my current lab-mates, Wenlong Zhang, Xiaofei Zeng, Jiabin Chen, Christina Dykstra, Jon Callura, Jay Renew, Ruochun Zhang and Wan-Ning Lee. Also, many thanks go to my friends, Biao Chang, Kungang Li, Chen Chen, Ran Yin and Jia Yang.

Last but foremost, I would like to thank my family. My mother, Suting Wu, and my father, Yunzhu Sun, supported me with persistent understanding, love and encouragement.

# TABLE OF CONTENTS

	Page
ACKNOWLEDGEMENTS	iii
LIST OF TABLES	ix
LIST OF FIGURES	xi
LIST OF SYMBOLS AND ABBREVIATIONS	xvi
SUMMARY	xix
<u>CHAPTER</u>	
1 Introduction	1
1.1 Background	1
1.1.1 Veterinary pharmaceuticals and poultry industry	1
1.1.2 Ionophore antibiotics (IPAs)	3
1.1.3 Eco-toxicity and antimicrobial mechanisms of IPAs	6
1.1.4 Physicochemical properties of IPAs	8
1.1.5 Quantification and occurrence of IPAs in environmental samples	10
1.1.6 Abiotic transformation of IPAs	13
1.1.7 Biotic transformation/degradation of IPAs	18
1.2 Research Objectives	22
2 Detection and Quantification of Ionophore Antibiotics in Standard Matrix, Runoff, Soil and Poultry Litter	26
2.1 Introduction	26
2.2 Materials and Methods	28
2.2.1 Chemicals and reagents	28
2.2.2 Sample collection and pre-treatment	28

2.2.3	Water sample analysis - solid phase extraction (SPE)	29
2.2.4	Solid sample analysis - solvent extraction	30
2.2.5	LC-MS analysis	30
2.2.6	Calibration and method validation	32
2.3	Results and Discussion	34
2.3.1	Optimization of standard matrix and LC conditions	34
2.3.2	Water sample extraction and clean-up	38
2.3.3	Soil/litter sample extraction and clean-up	42
2.3.4	Method validation	45
2.3.5	Occurrence of IPAs in the environment	49
2.4	Conclusions	51
3	Estimation of Acidity Constants, Metal Complexation Constants and Aqueous Solubility of IPAs	52
3.1	Introduction	52
3.2	Materials and Methods	53
3.2.1	General Methodology	53
3.2.2	Chemicals	54
3.2.3	Experimental set-up	54
3.2.4	IPA analysis	55
3.3	Experimental Results	56
3.3.1	pKa determination	56
3.3.2	$K_{\text{diss}}$ determination	56
3.4	Discussion	60
3.4.1	Justifications of assumptions	60
3.4.2	pKa of IPAs	61
3.4.3	$K_{\text{diss}}$ of IPAs	62

3.4.4	Intrinsic water solubility of IPA species	63
3.5	Conclusions	64
4	Acid-catalyzed Transformation of Ionophore Veterinary Antibiotics: Reaction Mechanism and Product Implications	65
4.1	Introduction	65
4.2	Materials and Methods	66
4.2.1	Chemicals	66
4.2.2	Hydrolysis experiment	66
4.2.3	Analytical methods	67
4.2.4	Toxicity tests for transformation products	69
4.3	Results and Discussion	69
4.3.1	Hydrolysis of IPAs under acidic conditions	69
4.3.2	Kinetic modeling of IPA transformation	75
4.3.3	Transformation products and pathways	77
4.3.4	Toxicity of transformation products	94
4.3.5	Preliminary study of environmental occurrence of IPAs and transformation products	97
4.4	Environmental Implications	99
5	Photodegradation of Veterinary Ionophore Antibiotics under UV and Solar Irradiation	100
5.1	Introduction	100
5.2	Materials and Methods	102
5.2.1	Chemicals, reagents and water samples	102
5.2.2	Photolysis experimental set-up	104
5.2.3	Chemical and instrumental analysis	106
5.3	Results and Discussion	107

5.3.1	Direct photolysis of IPAs with LP UV, simulated sunlight and natural sunlight	107
5.3.2	Indirect photolysis of IPAs	113
5.3.3	Product identification and photolytic transformation mechanism	122
5.3.4	Toxicity tests	132
5.4	Environmental Implications	134
6	Biodegradation of Veterinary Ionophore Antibiotics in Poultry Litter and Soil Microcosms	136
6.1	Introduction	136
6.2	Materials and Methods	138
6.2.1	Chemicals	138
6.2.2	Poultry litter microcosms	138
6.2.3	Soil microcosms	140
6.2.4	Field study	140
6.2.5	Analytical methods	141
6.3	Results and Discussion	144
6.3.1	Poultry litter and soil characteristics	144
6.3.2	IPA degradation in poultry litter microcosms	144
6.3.3	IPA degradation in soil microcosms	163
6.3.4	Field study	175
6.4	Environmental Implications	177
7	Inhibition and Biotransformation Potential of Veterinary Ionophore Antibiotics under Different Redox Conditions	178
7.1	Introduction	178
7.2	Materials and Methods	181
7.2.1	Chemicals	181

7.2.2 Culture development and maintenance	181
7.2.3 Inhibition and biotransformation assays	185
7.2.4 Analytical methods	189
7.3 Results and Discussion	190
7.3.1 Energetics of IPA biodegradation	190
7.3.2 Characterization of PL-enriched aerobic/anoxic culture	190
7.3.3 Biodegradation of IPAs under aerobic conditions	193
7.3.4 Inhibition and biodegradation of IPAs under nitrate-reducing conditions	197
7.3.5 Inhibition and biodegradation of IPAs under fermentative/sulfate-reducing conditions	198
7.3.6 Inhibition and biodegradation of IPAs under fermentative/methanogenic conditions	202
7.3.7 Biotransformation products of IPAs	206
7.4 Environmental Implications	217
8 Conclusions and Recommendations	219
8.1 Quantification of IPAs in the Environment Matrices	219
8.2 Abiotic Transformation of IPAs	220
8.3 Biotransformation of IPAs	221
8.4 Implications of IPA Transformation Reactions in the Environment	223
8.5 Recommendations	224
8.6 Future Work	225
APPENDIX A: Gibbs Free Energy Estimations of IPAs	226
REFERENCES	228

## LIST OF TABLES

	Page
<b>Table 1.1</b> Properties of IPAs	9
<b>Table 1.2</b> Environmental occurrence of IPAs	11
<b>Table 2.1</b> LC/MS parameters of IPAs	31
<b>Table 2.2</b> Recovery of IPAs	46
<b>Table 2.3</b> Calibration linearity, instrument detection limit (IDL), and method detection limit (MDL) in runoff samples from unfertilized field, poultry litter fertilized field soil and poultry litter.	46
<b>Table 2.4</b> Signal suppression (%) of IPAs in the final extracts.	46
<b>Table 2.5</b> The environmental occurrence of IPAs.	50
<b>Table 3.1</b> Acidity constant ( $pK_a$ ), dissociation constant ( $K_{diss}$ ), and intrinsic solubility of different forms of IPAs in water (at 22°C).	57
<b>Table 3.2</b> Dissociation constant ( $\text{Log}(K_{diss})$ (M)) of IPAs in different solvents.	57
<b>Table 4.1</b> Hydrolysis rate constants and half-lives of IPAs at pH 3-5.	76
<b>Table 5.1</b> Characteristics of real water samples	103
<b>Table 5.2</b> Rate constants of MON and SAL ( $\text{hour}^{-1}$ ) ( $R^2 > 0.98$ )	110
<b>Table 5.3</b> Direct photolysis of SAL under simulated sunlight: effects of the presence of <i>t</i> -butanol or MON	129
<b>Table 6.1</b> Characteristics of Poultry Litter (PL), Non-fertilized Soil, and PL-fertilized Soil	143
<b>Table 6.2</b> Datasets for factor analysis	159
<b>Table 6.3</b> ANOVA of SAL Data	159
<b>Table 6.4</b> ANOVA of NAR Data	159
<b>Table 6.5</b> Proposed fragment structures of MON and its biotransformation product (TP-MON).	173
<b>Table 7.1</b> Characteristics of water extract from poultry litter (PL).	180

<b>Table 7.2</b> Stock cultures used to test inhibition and biotransformation assays.	184
<b>Table 7.3</b> Experimental set-up and conditions for the inhibition and biotransformation assays.	188
<b>Table 7.4</b> Proposed structures of primary biotransformation products of MON.	216
<b>Table 7.5</b> Proposed structures of primary biotransformation products of SAL.	217

## LIST OF FIGURES

	Page
<b>Figure 1.1</b> Structures of ionophore antibiotics (IPAs)	5
<b>Figure 1.2</b> Illustration of pseudo-cyclic conformation of MON-sodium complex	5
<b>Figure 1.3</b> Mechanism of IPA as antiporter between proton and metal ions	7
<b>Figure 1.4</b> MON transformation in acidic condition proposed by Agtarap <i>et al.</i> , 1967	15
<b>Figure 1.5</b> Acid-catalytic transformation of spiro-ketal moiety	16
<b>Figure 1.6</b> SAL and NAR transformation in the presence of formic acid	17
<b>Figure 1.7</b> Decomposition of SAL by enzymatic retroaldol cleavage	20
<b>Figure 1.8</b> Bioconversion of MON by the soil bacterium <i>Sebekia benihana</i>	21
<b>Figure 2.1</b> MON signal intensity in different standard sample matrices buffered with phosphate	35
<b>Figure 2.2</b> Example of total ion chromatograms of IPA in a standard mixture, an extract of runoff from PL-fertilized plots, or an extract of PL.	37
<b>Figure 2.3</b> Recovery, signal suppression and extraction efficiency of MON with different clean-up methods after HLB SPE.	40
<b>Figure 2.4</b> Recovery, signal suppression and extraction efficiency of MON in poultry litter extract by different extraction solvents.	44
<b>Figure 2.5</b> Peak areas of MON (A) and SAL (C) obtained in standard matrix (STD), rainfall runoff (RF) and poultry litter (PL). Peak areas of MON (B) and SAL (D) normalized by the NIG peak area in each sample matrix.	48
<b>Figure 3.1</b> Total dissolved MON in water at pH 3.55 – 4.94.	58
<b>Figure 3.2</b> Total dissolved MON in water at pH 8.5 with sodium concentration 0.01 – 1.0 M.	58
<b>Figure 3.3</b> Total dissolved MON in water at pH 8.5 with potassium concentration 0.15 – 0.4 M.	59
<b>Figure 3.4</b> Total dissolved SAL in water at pH 8.5 with sodium concentration 0.3 – 1.0 M.	59

<b>Figure 4.1</b> The ratio of IPA concentration after 7 days of reaction to the initial IPA concentration at different pH values.	71
<b>Figure 4.2</b> Hydrolysis of (A) MON, (B) SAL and (C) NAR at acidic conditions. Initial concentration of IPA was 1 $\mu$ M.	73
<b>Figure 4.3</b> Regression of the log of first-order rate constant $k_{obs}$ versus pH plot for SAL and NAR.	76
<b>Figure 4.4</b> MON hydrolysis products at pH 3 (A) and pH 5 (B) buffered by acetic acid and HCl.	81
<b>Figure 4.5</b> LC/MS/MS spectra of (A) MON, (B) MP1 and (C) MP2.	83
<b>Figure 4.6</b> Proposed acid-catalyzed transformation pathways of MON with mechanism of reactions from parent MON to MP1 and MP2.	84
<b>Figure 4.7</b> MON hydrolyzed at pH 2.0, yielding two new transformation products (MP4 and MP5) with strong UV absorption at 235 nm and 290 nm, respectively.	85
<b>Figure 4.8</b> Structure of MP5.	85
<b>Figure 4.9</b> SAL hydrolysis products at pH 3 (A) and pH 5 (B) buffered by acetic acid and HCl.	89
<b>Figure 4.10</b> SAL hydrolyzed at pH 3.0, yielding SP1 with UV absorption peaked at 285 nm.	90
<b>Figure 4.11</b> LC/MS/MS spectra of (a) SAL and (b) SP1.	91
<b>Figure 4.12</b> Proposed acid-catalyzed transformation pathways and mechanism of SAL.	92
<b>Figure 4.13</b> Aqueous phase optimized structure of SP1 sodium form.	92
<b>Figure 4.14</b> Aqueous phase UV-VIS spectrum of SP1.	93
<b>Figure 4.15</b> Molecular orbital of 199alpha.	93
<b>Figure 4.16</b> [C(71)=O(73)] moiety of SP1 structure.	93
<b>Figure 4.17</b> Growth inhibition (represented by bars) by MON hydrolysis samples (obtained after different hydrolysis time) and by reference samples containing the same MON concentration as that remained in the hydrolysis samples at each time point.	96
<b>Figure 4.18</b> Detection of (a) m/z 693 and (b) m/z 773 ions in samples of (i) hydrolysis experiments (DI water pH 3), (ii) poultry litter extract (PL) and (iii) extract of runoff from PL-fertilized grass plots.	98

<b>Figure 5.1</b> Illustrations of photolysis experimental set-up.	105
<b>Figure 5.2</b> Direct photolysis of IPAs under (A) LP UV, (B) simulated sunlight, and (C) natural sunlight.	111
<b>Figure 5.3</b> Light emission spectra and UV absorbance of IPAs.	111
<b>Figure 5.4</b> Overlapping of SAL absorbance with light source spectra ( $\epsilon_{\lambda} \cdot I_{\lambda}$ ).	112
<b>Figure 5.5</b> MON and SAL degradation rates under simulated sunlight irradiation with $\text{NaNO}_3$ .	116
<b>Figure 5.6</b> Reactive species generation by the photolysis of nitrate.	116
<b>Figure 5.7</b> UV-Vis absorbance of DOM working solutions.	119
<b>Figure 5.8</b> Ion chromatograms of TP-SALs on LC/MS.	125
<b>Figure 5.9</b> SAL photolytic transformation products under LP UV (A), simulated sunlight (B), and natural sunlight (C) irradiation in DI water matrix.	125
<b>Figure 5.10</b> MS/MS fragmentation patterns of selected TP-SALs.	128
<b>Figure 5.11</b> SAL photolytic transformation pathways.	128
<b>Figure 5.12</b> MON (A) and SAL (B) photolytic transformation products under simulated sunlight irradiation with 5 mg/L $\text{NaNO}_3$ .	131
<b>Figure 5.13</b> Toxicity test of SAL photolytic transformation products. Dashed lines represent 95% confidence level.	133
<b>Figure 6.1</b> Headspace gas composition of PL microcosms set-up with 24, 40, 57, and 72% water content and incubated at 35°C.	146
<b>Figure 6.2</b> Moisture release curve for poultry litter.	147
<b>Figure 6.3</b> Normalized IPA content in PL microcosms after 14-day incubation at 35°C and a range of PL water content.	148
<b>Figure 6.4</b> Headspace gas composition of PL microcosms set-up with 24% and 72% water content and incubated at (A) 35°C, (B) 45°C and (C) 60°C.	151
<b>Figure 6.5</b> Normalized IPA concentration in PL microcosms after 14-day incubation at 35, 45, and 60°C with 24% (A) and 72% (B) water content.	152
<b>Figure 6.6</b> Correlation of observed IPA removal with $\text{CO}_2$ production in PL microcosms set-up with water content from 24 to 72% and incubated at a temperature range from 35 to 60°C.	156

<b>Figure 6.7</b> Simulation of SAL and NAR degradation rates in PL microcosms using MatLab curve fitting toolbox.	156
<b>Figure 6.8</b> Estimated values of IPA degradation rates versus experimentally measured values.	157
<b>Figure 6.9</b> Water content-temperature domain (shaded areas) where degradation of SAL (A) and NAR (B) in PL is not expected (i.e., $k = 0$ ).	158
<b>Figure 6.10</b> Transformation product of SAL (TP-SAL) in the PL microcosms with 72% water content incubated at 35°C. At day 14, replicate microcosms were amended with non-fertilized soil (1/1, w/w) or 50 mg/kg SAL..	161
<b>Figure 6.11</b> Transformation of SAL yielding two products which have the same m/z of 531 $[M+Na]^+$	161
<b>Figure 6.12.</b> MS/MS spectrum of SAL.	162
<b>Figure 6.13</b> MS/MS spectrum of TP-SAL.	162
<b>Figure 6.14</b> MON (A) and SAL (B) normalized to initial IPA concentration (1 mg IPA/kg soil) in microcosms set up with non-fertilized (1) and PL-fertilized soil (2) after 7-day incubation. Abiotic controls were prepared with autoclaved soil.	165
<b>Figure 6.15</b> Normalized MON (A) and MON product (TP-MON) (B) in PL-fertilized soil microcosms set up at a range of initial MON concentration (0.2 – 10 mg MON/kg soil).	168
<b>Figure 6.16</b> Sum of peak areas of parent MON and TP-MON normalized to the initial MON peak area, over a 10-day incubation of soil microcosms amended with different initial MON.	169
<b>Figure 6.17</b> (A) Initial steps of MON biotransformation predicted by UM-BBD. (B) Proposed molecular structure of MON product (TP-MON).	171
<b>Figure 6.18</b> MS/MS spectrum of MON. The arrows represent elimination of a water molecule.	172
<b>Figure 6.19</b> MS/MS spectrum of TP-MON. The arrows represent elimination of a water molecule.	173
<b>Figure 6.20</b> IPA concentration during the PL stacking process. IPAs were spiked into PL at 1500 – 2000 mg/kg.	176
<b>Figure 6.21</b> IPA concentration in upper layer soil fertilized with PL containing MON and SAL, subjected to simulated rainfall right after PL application. Samples were collected at 0, 7, 14, and 21 days after rainfall.	176

<b>Figure 7.1</b> Performance of the PL-enriched aerobic/anoxic culture during a typical feeding cycle. (A) soluble COD (sCOD) and total COD (tCOD); (B) nitrogen species; (C) dissolved oxygen (DO); (D) IPA concentration.	192
<b>Figure 7.2</b> MON (A) and SAL (B) degradation under aerobic conditions at a low medium buffer capacity.	195
<b>Figure 7.3</b> MON (A) and SAL (B) degradation under aerobic conditions at a high medium buffer capacity.	196
<b>Figure 7.4</b> Cumulative nitrogen gas production in culture series under anoxic conditions with or without IPAs, dextrin, or PL-extract. (1 atm and 25°C).	197
<b>Figure 7.5</b> Cumulative total gas production in culture series under fermentative/sulfate reducing conditions with or without IPAs. (1 atm and 25°C).	200
<b>Figure 7.6</b> Cumulative CO <sub>2</sub> and H <sub>2</sub> S production in culture series under fermentative/sulfate reducing conditions with or without IPAs. (1 atm and 25°C).	200
<b>Figure 7.7</b> Degradation of IPAs under fermentative/sulfate-reducing conditions. Initial concentrations of IPAs were 1 mg/L; an additional 0.5 mg/L SAL was added on day 7.5.	201
<b>Figure 7.8</b> Sulfate concentration in culture series under fermentative/sulfate-reducing conditions, without or with molybdate added on day 7.5.	201
<b>Figure 7.9</b> Inhibitory effect of MON under fermentative/methanogenic conditions, based on total gas production (A), and cumulative methane production (B).	204
<b>Figure 7.10</b> Performance of the cultures with and without MON -amendment. (A) Cumulative gas production; (B) Cumulative CH <sub>4</sub> production; (C) Cumulative CO <sub>2</sub> production; (D) Acetate concentration; (E) Propionate concentration (All gas data are at 1 atm and 25°C).	205
<b>Figure 7.11</b> Primary biotransformation products of MON (A) and SAL (B) in dextrin-amended culture series incubated under aerobic conditions.	209
<b>Figure 7.12</b> MSMS fragments of the biotransformation products of IPAs.	213
<b>Figure 7.13</b> CAD fragmentation sites of the parent IPAs. Arrows represent elimination of water.	214

## LIST OF SYMBOLS AND ABBREVIATIONS

ACN	Acetonitrile
CAD	Collision activated dissociation
COD	Chemical oxygen demand
DI water	Deionized water
DO	Dissolved oxygen
DOC	Dissolved organic carbon
DOM	Dissolved organic matter
ESI+	Positive electrospray ionization mode
FDA	Food and drug administration
GC	Gas chromatography
HLB	Hydrophilic–lipophilic balance
HPLC	High performance liquid chromatography
IPA	Ionophore antibiotics
$K_a$	Acidity constant
$K_{diss}$	Dissociation constant
LC/MS	Liquid chromatography / mass spectrometry
LC/MS/MS	Liquid chromatography/tandem mass spectrometry
LLE	Liquid-liquid extraction
LP	Low pressure
MDL	Method detection limit
MeOH	Methanol

MON	Monensin
MPHA	Humic acid purchased from MP biomedical
MW	Molecular weight
NAR	Narasin
NIG	Nigericin
NOM	Natural organic matter
OC	Organic carbon
OD600	Optical density at 600 nm
PL	Poultry litter
PL-ext	Water extracts from poultry litter
RNS	Reactive nitrogen species
ROS	Reactive oxygen species
SAL	Salinomycin
SIM	Selected ion monitoring
SPE	Solid-phase extraction
SRHA	Suwannee river humic acid
$t_{1/2}$	Half-life
TOC	Total organic carbon
TP	Transformation product
UV	Ultraviolet
VFA	Volatile fatty acid
WWTP	Wastewater treatment plant
$\epsilon$	Molar absorption coefficient

$\Phi$

Quantum yield

## SUMMARY

Veterinary pharmaceuticals are routinely used in livestock production to treat diseases, prevent infections, and promote growth. However, the potential release of pharmaceuticals from agricultural activities has raised concerns because they may pose detrimental effects to the ecosystems and human health, for example fostering the evolution of antibiotic-resistant bacteria in the natural environment. A better understanding of the environmental fate of veterinary pharmaceuticals is critical to properly assess and mitigate their risks. This dissertation focuses on a major group of veterinary pharmaceuticals, ionophore antibiotics (IPAs), which is sold at over 4 million kilograms per year and constitutes more than one third of the total antibiotic consumption by the livestock industry in the U.S. Despite the extensive usage of IPAs, their environmental fate was not well-understood. Therefore, this study aimed at achieving a comprehensive understanding of the occurrence, persistence, and transformation of IPAs from poultry litter before and after applications to the agricultural lands. Three of the most commonly used members of IPAs were investigated in this study: monensin (MON), salinomycin (SAL), and narasin (NAR). Based on the common management practices of poultry litter, the potential abiotic and biotic transformation reactions of IPAs were examined under varying conditions relevant to the water-soil-litter systems.

This dissertation consists of three sections. First, a robust analytical method was developed to quantify IPAs in various environmental compartments, especially in high organic-containing matrices such as poultry litter, and soil and runoff from litter-fertilized lands. Efforts were made to optimize the analytical method with respect to improving extraction recovery, reducing matrix effects, and validating a surrogate standard. Second, lab-scale experiments were

set up to determine the chemical properties of IPAs in aqueous environments and to study the abiotic transformation of IPAs, including hydrolysis and photolysis. The results showed that IPAs are prone to hydrolytic transformation in acidic environments, which are likely to be encountered in acidic soils, alum-amended litter (alum:  $\text{Al}_2(\text{SO}_4)_3 \cdot 12\text{H}_2\text{O}$ ), and acidic runoff. Multiple transformation pathways were proposed based on the identified hydrolysis products. It is also noteworthy that the hydrolysis products of MON still exhibited a toxic effect on the selected microorganism (*Bacillus subtilis*). SAL and NAR were found to undergo direct photolysis under both UV light and sunlight irradiation. In natural water matrix, IPAs were also degraded by indirect photolysis with hydroxyl radicals generated by light-excited nitrate. Dissolved organic matter can shield IPAs from light and slow down their photolysis. Third, the biodegradation potential of IPAs was first tested in litter and soil microcosms. Factor analysis was conducted to delineate the interaction of water and temperature on IPA degradation in the litter. Litter-fertilized and non-fertilized soil microcosms were compared on the degradation of MON and SAL. Furthermore, the inhibition and biotransformation potential of IPAs were assessed under different redox conditions with litter-enriched cultures. Inhibition tests focused on examining IPAs' impact on microbial community functions, including denitrification, sulfate-reduction, and methane production. Biodegradation tests were conducted with different electron acceptors, including oxygen, nitrate, sulfate, and organic carbons, with efforts to elucidate primary biotransformation products.

On the basis of the results obtained in this study, several recommendations on litter management and IPA selection were made to help mitigate the release and transport of IPAs, as well as enhance their degradation. Overall, this study significantly improved the understanding of the environmental fate of IPAs and the obtained knowledge can aid proper selection of IPAs

and management strategies in future applications to minimize the risks of antibiotic micropollutants in the environment.

# CHAPTER 1

## INTRODUCTION

### 1.1 Background

#### *1.1.1 Veterinary pharmaceuticals and poultry industry*

Veterinary pharmaceuticals are routinely used in livestock production (i.e., poultry, cattle, swine, etc.) as antibiotics, coccidiostats, and prophylactics to treat diseases, prevent infections and promote growth. In the U.S., it was estimated that around 4.7 million kg per year of antimicrobials were consumed in poultry industry, compared to 4.7, 1.7 and 1.4 million kg used in swine industry, cattle industry, and human medicine, respectively (Mellon, 2001). The total domestic consumption of veterinary antimicrobials has been increasing over the recent years, increasing from 12,570,257 kg in 2009, 12,861,103 kg in 2010, to 13,110,423 kg in 2011 (FDA, 2009; 2010; 2011). Production of veterinary pharmaceuticals has also increased worldwide, especially in developing countries, since they are playing major roles in modern agriculture and livestock industries (Sarmah *et al.*, 2006). In addition, the application of antibiotics as growth-promoters is evaluated as a cost-effective way to mitigate green-house gases and ammonia emissions based on a partial life cycle analysis (Stackhouse *et al.*, 2012).

In 2012, the U.S. poultry industry produced 8.4 billion broilers (<http://usda01.library.cornell.edu/usda/current/PoulProdVa/PoulProdVa-04-29-2013.pdf>).

Broilers are raised on bedding materials such as wood shavings or peanut shells, which become poultry litter (PL) when mixed with broiler excreta, wasted feed, and feathers during the growth of one or more flocks. In 2012, the U.S. broiler production was estimated to generate about 13 billion kilograms of litter. Most of this litter was used to fertilize grasslands because it is rich in

nitrogen, phosphorus, and potassium (Moore *et al.*, 1995). It was estimated that the PL is used to fertilize agricultural fields at a rate of at least 5 metric tons/hectare/application (Kuykendall *et al.*, 1999).

However, a considerable portion of veterinary pharmaceuticals also stay with the PL, due to the poor absorption and metabolism in the gut of broilers. The introduction of veterinary pharmaceuticals to the environment has brought a lot of concerns. A major impact is that the antibiotics will foster evolution of antibiotic-resistant bacteria in soil and aquatic systems. In addition, the effects of chronic low-level exposure to antibiotics remain unclear. Although much research has been devoted to the issue of pharmaceutical contaminants in recent decades, significant knowledge gaps still exist in the understanding of the transformation and transport of antibiotics, especially veterinary antibiotics, in natural systems.

### ***1.1.2 Ionophore antibiotics (IPAs)***

IPAs are polyether organic compounds used in livestock production to promote animal growth and prevent infections. Most of the commonly used IPAs are produced by microbial fermentation (e.g., from *Streptomyces*). IPAs were initially designed to control coccidiosis for chickens (Russell and Strobel, 1989). Later, the usage of IPAs was expanded to food additives for cattle and sheep, after showing growth promoting effect on ruminal animals (Russell and Houlihan, 2003). In addition, IPAs can control swine dysentery caused by *Brachyspira hyodysenteriae* (Kyriakis, 1989) and *Clostridium perfringens* type A infections (Kyriakis *et al.*, 1995). IPAs are also active against an *Enterococcus*-like pathogen in rainbow trout (Carson and Statham, 1993).

The U.S. was among the first regions to introduce IPAs to livestock industry, when U.S. Food and Drug Administration (FDA) approved the use of IPAs in 1970. Commonly, IPAs are given as veterinary feed additives. For example, in broiler production, it is estimated that one kilogram of feed consists of over 300 milligrams of IPAs ([http://www.ucsusa.org/assets/documents/food\\_and\\_agriculture/hog\\_apps.pdf](http://www.ucsusa.org/assets/documents/food_and_agriculture/hog_apps.pdf)). IPAs (including arsenicals) accounted for about 47.5% (by weight) of the total usage of antibiotics in the U.S. (Sarmah *et al.*, 2006). The U.S. FDA reported the annual sales of 3,821,138 kg of IPAs domestically in the year of 2010 and 3,740,627 kg in 2009, which was the second top-selling pharmaceutical group next to tetracyclines (FDA, 2009; 2010). Since the sale of arsenicals, another type of growth promoter, was suspended in 2011 due to its high environmental risks, the consumption of IPAs is expected to significantly increase in the future (<http://www.fda.gov/NewsEvents/Newsroom/PressAnnouncements/ucm258342.htm>). The most commonly used IPAs (Figure 1.1) are monensin (MON), salinomycin (SAL), and narasin (NAR).

Nigericin (NIG) is not commercially applied in livestock industry; it is used as an analytical surrogate for the other IPAs.

MON, SAL, and NAR belong to carboxylic ionophores. From a structural perspective, they are aliphatic chains which bear five cyclic ether rings, with a carboxylic group on one end, and one or more hydroxyl groups on the other end. Because of their unique structure, IPAs are able to form pseudo-cyclic neutral complexes with alkali metal ions at  $\text{pH} > \text{pK}_a$ , by head-to-tail hydrogen bonding (e.g., MON-sodium complex shown in Figure 1.2). This conformation makes them extremely hydrophobic, enabling low energy barrier to pass through cytoplasmic membranes.

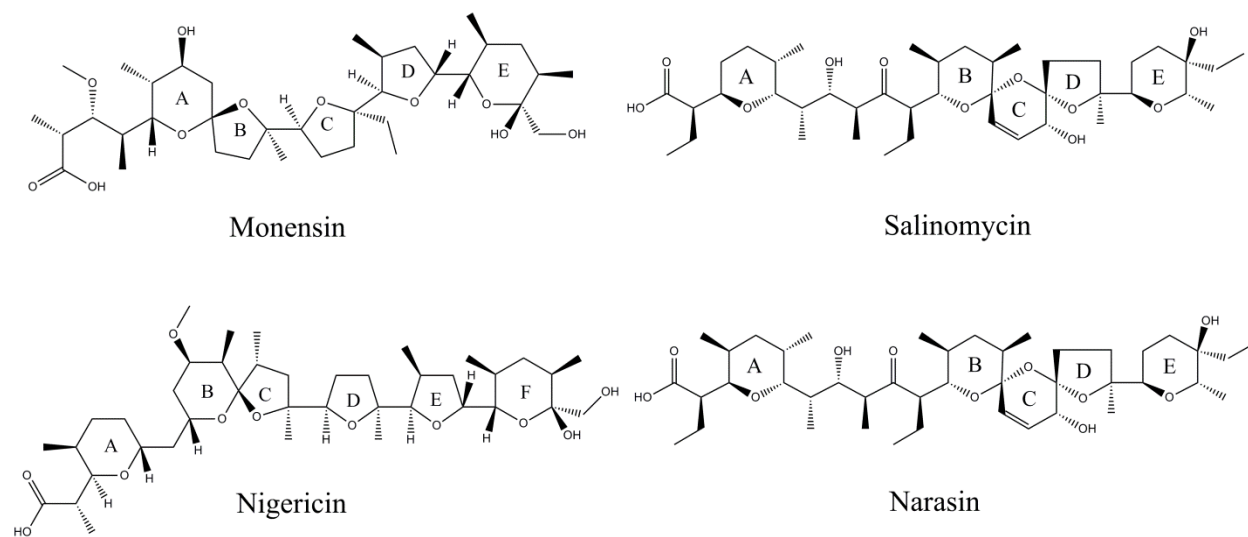


**Figure 1.1** Structures of ionophore antibiotics (IPAs).

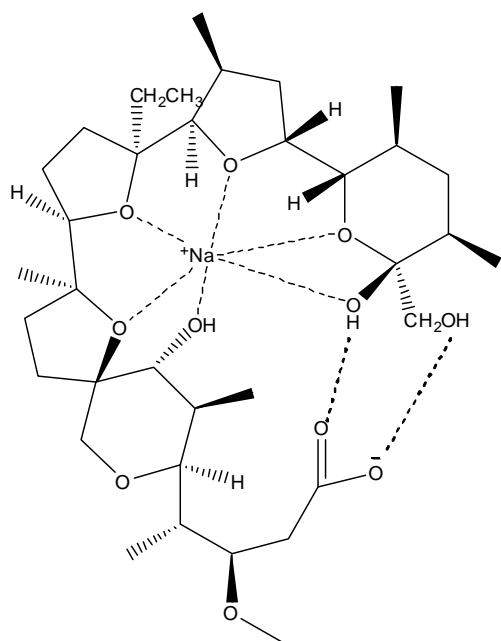


**Figure 1.2** Illustration of pseudo-cyclic conformation of MON-sodium complex. (adapted from Lopes *et al.*, 2002)

### ***1.1.3 Eco-toxicity and antimicrobial mechanisms of IPAs***

Although the detailed mechanisms of IPA's inhibitory effects on microorganisms are controversial, the general belief is that they disrupt trans-membrane cation concentration gradients, required for the proper functioning and survival of microorganisms (Westley, 1983). Specifically, IPAs lower the energy barrier of ion-transport through lipid bilayer membranes by acting as antiporters of metal ions and protons (Figure 1.3). Consequently, the normal gradients of  $\text{Ca}^{2+}$ ,  $\text{Mg}^{2+}$ ,  $\text{K}^{+}$ , and  $\text{Na}^{+}$  are disrupted, causing cell death usually by cell-lysis (Westley, 1983). However, most gram-negative bacteria are not affected by IPAs, because the cell walls have a 600 Dalton molecular weight cut-off, which is smaller than the molecular weight of most IPAs.

The residual IPAs in the environment may be a risk to living organisms in soils, waters, and sediments, and may have eco-toxicological effects (Brain *et al.*, 2004; Dorkov *et al.*, 2008; Hansen *et al.*, 2009b; Hanson *et al.*, 2007; Hillis *et al.*, 2007; Jensen *et al.*, 2009; Kart and Bilgili, 2008). Hillis *et al.* found that, although MON did not significantly affect zooplankton community structure, significant changes were observed within specific taxonomic groups such as Rotifers (Hillis *et al.*, 2007). To quantitatively express the inhibitory effects of IPAs, researchers have measured the  $\text{EC}_{50}$  values of IPAs toward various aquatic species (Brain *et al.*, 2004; Jensen *et al.*, 2009; McGregor *et al.*, 2007). Hansen *et al.* (2009b) reviewed the toxic effects from IPAs on various species in soil and water environments and the presence of IPAs in the environment, and stated that the reported concentrations of IPAs in sediments and predicted concentrations of IPAs in environmental compartments were higher than the no-effect concentrations. Applying a methodology based on three criteria (usage, the potential to reach the environment, and toxicity profile), Capleton *et al.* (2006) assessed a total of 83 veterinary medicines and ranked IPAs as one of the high priority veterinary pharmaceutical groups that

merit further detailed risk assessment.

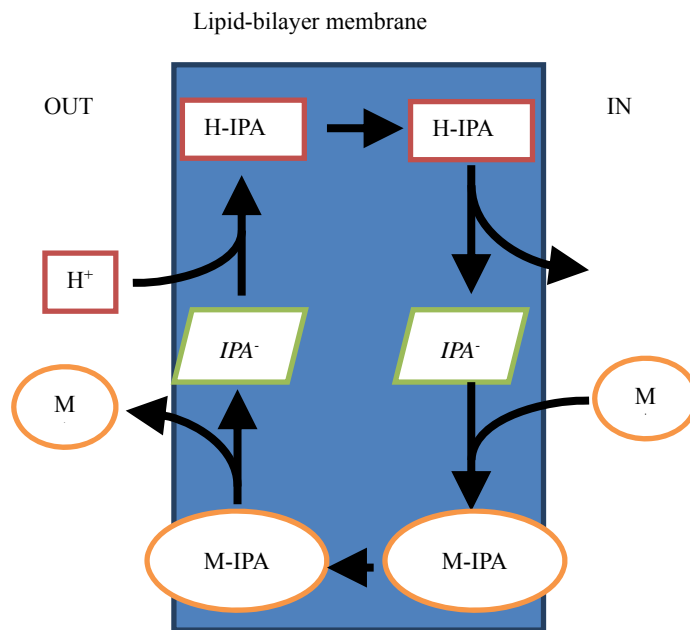


**Figure 1.3** Mechanism of IPA as antiporter between proton and metal ions.

#### ***1.1.4 Physicochemical properties of IPAs***

Due to IPA's low solubility in water, environmentally relevant properties, such as water solubility,  $pK_a$ , and  $K_{ow}$ , were not easily measured in aqueous phase. Instead, they were usually determined in organic solvent or water/solvent mixture. Table 1.1 summarizes the physicochemical properties of IPAs from previous studies as well as predicted values by SPARC (<https://archemcalc.com/sparc/test/login.cfm>). It is noteworthy that the reported water solubility values covered a wide range, which may be due to different experimental conditions, such as pH and counter ion concentrations. Overall, IPAs are highly-hydrophobic, protonated at acidic pH values.

Adsorption of IPAs on soil particles are described by  $K_{oc}$  and  $K_d$  values, which were mainly tested by Sassman and Lee (2007), who measured the sorption of MON in eight different soils of varying physicochemical properties. Other reported values are also shown in Table 1.1; however, the related experimental details were not stated in the original documents. Additionally, some field studies indicated that, compared to other commonly used antibiotics, MON had the highest potential to be transported with runoff, although less than 10% of MON was transported with sediments (Davis *et al.*, 2006; Kim *et al.*, 2010).

One of the major properties of IPAs is their affinity to complex with alkali metal ions. Different IPAs have different tendency to complex with alkali metal ions. For examples, MON is more favorable to complex with  $Na^+$  than with  $K^+$ , whereas SAL favors the opposite. However, it should be noted that, while many studies have reported the relative tendency of certain IPAs to complex with cations such as  $H^+$ ,  $Na^+$ ,  $K^+$ , and  $NH_4^+$  (Cox *et al.*, 1984a; b; Degani, 1977; Duax *et al.*, 1980; Lutz *et al.*, 1970; Morf and Simon, 1971; Steinrau.Lk *et al.*, 1971), all of these experiments were conducted in organic solvents and thus the associated results may not be

directly applicable to aqueous environmental systems.

**Table 1.1** Properties of IPAs

Name	pK <sub>a</sub>	Log K <sub>ow</sub>	Water		EC <sub>50</sub> for soil bacteria (µM)
			solubility (mg/L)	K <sub>oc</sub> (L/kg)	
Monensin (MON)	6.65 <sup>a</sup> 4.26 <sup>b</sup>	5.4 – 8.5 <sup>d</sup> 2.75 – 4.24 <sup>c</sup>	0.85 - 63 <sup>c</sup> 5 – 63 <sup>e</sup>	125 – 5700 <sup>f</sup>	0.915 – 78.6 <sup>f,c</sup> 10 (4.6 – 22) <sup>e</sup>
C36H62O11 M.W. = 670.9	6.7 <sup>c</sup> 4.25 <sup>g</sup>				
Salinomycin (SAL)	4.5, 6.4 <sup>a</sup> 4.37 <sup>g</sup>	5.15 <sup>a</sup>	17 – 905 <sup>e</sup>	N.A.	N.A. 5.7 (3.2 – 10) <sup>e</sup>
C42H70O11 M.W. = 751.0					
Narasin (NAR)	7.9 <sup>a</sup> 4.37 <sup>g</sup>	4.9 – 6.2 <sup>a</sup>	102 at pH 7 681 at pH 9 <sup>e</sup>	Log K <sub>oc</sub> = 6.06 – 6.88 <sup>a</sup>	N.A. 19.6 (6.5 – 56.2) <sup>e</sup>
C43H72O11 M.W. = 765.0					

<sup>a</sup> ESFA, 2005

<sup>b</sup> (Franco *et al.*, 2009)

<sup>c</sup> (Dolliver *et al.*, 2008a)

<sup>d</sup> (Thiele-Bruhn, 2003)

<sup>e</sup> (Hansen *et al.*, 2009c)

<sup>f</sup> (Sassman and Lee, 2007)

<sup>g</sup> predicted by Sparc®

### ***1.1.5 Quantification and occurrence of IPAs in environmental samples***

A number of analytical methods have been developed to detect IPAs in animal tissues (e.g. (Blanchflower and Kennedy, 1996; Matabudul *et al.*, 2001; Mortier *et al.*, 2005)), manure (e.g. (Blackwell *et al.*, 2004; Schlusener *et al.*, 2003a)), soil (e.g. (Furtula *et al.*, 2009; Schlusener *et al.*, 2003b; Watanabe *et al.*, 2008)), surface water (e.g. (Cha *et al.*, 2005; Dolliver *et al.*, 2008b; Hao *et al.*, 2006; Kim and Carlson, 2007a)) and wastewater (e.g. (Herrero *et al.*, 2013; Herrero *et al.*, 2012)). Commonly, IPAs in water were extracted using Oasis HLB cartridges followed by methanol as elution solvent (Hansen *et al.*, 2009a; Hao *et al.*, 2006; Kim and Carlson, 2007a). IPAs in solid samples were extracted by organic solvents (Carlson and Kim, 2006; Schlusener *et al.*, 2003a; Schlusener *et al.*, 2003b). Quantification of IPAs typically requires LC/MS with electrospray ionization at positive mode (ESI(+)). In some studies, LC/MS/MS was applied for confirmatory purposes (Cha *et al.*, 2005; Kim and Carlson, 2007a).

With the reported analytical methods, the presence of IPAs in sediments, sewage, surface water, and groundwater has been reported by several studies, shown in Table 1.2. For example, IPAs were found from 0.001 to 0.22 µg/L in surface water near agricultural lands (Carlson and Mabury, 2006; Carlson and Kim, 2006; Cha *et al.*, 2005), 1.89 to 16.24 µg/L in lagoons near dairy farms (Watanabe *et al.*, 2008), 0.002 to 0.022 µg/L in wastewater treatment plant (WWTP) effluent (Hao *et al.*, 2008), and 0.9 to 31.5 µg/kg in river sediments in agriculture-influenced areas (Kim and Carlson, 2006; 2007a).

**Table 1.2** Environmental occurrence of IPAs.

Matrix	Sample sites	IPAs	Concentration ( $\mu\text{g/L}$ or $\mu\text{g/kg}$ )	$n_q/n_a$	References
Water	River, five sampling sites	Monensin	0.001–0.036	10/16	(Carlson and Kim, 2006)
	downstream agricultural land	Salinomycin	0.002–0.007	5/16	
	use and animal-feeding operations with seasonal variation	Narasin	0.007–0.038	7/16	
	Watershed, five sampling sites, including pristine area; entrance of urban area; urban area; agriculture influenced area; and urban and agriculture-influenced area.	Monensin	0.009-0.011	2/5	(Kim and Carlson, 2007a)
		Salinomycin	0.006-0.007	2/5	
		Narasin	0.025-0.038	4/5	
	River, five sampling sites	Monensin	0.03–0.05	3/45	(Cha <i>et al.</i> , 2005)
	downstream agricultural land	Salinomycin	0.04	1/45	
	use and animal-feeding operations	Narasin	0.04–0.06	3/45	
	Surface run-off from livestock farm, drainage and stagnant water	Monensin	0.002–0.037	6/11	(Song <i>et al.</i> , 2007)
	Surface waters from agricultural run-off	Monensin	0.020–0.220	7/8	(Hao <i>et al.</i> , 2006)
	Surface waters and wastewater treatment plant (WWTP) effluent	Monensin	0.002–0.022	5/16	(Hao <i>et al.</i> , 2008)
Lagoon, flush water from two dairy farms with seasonal	Monensin	1.89-16.24	8/8	(Watanabe <i>et al.</i> , 2008)	

	variation				
	WWTP influent and effluent,	Monensin	N.D.-0.15	98/140	(Watkinson <i>et al.</i> , 2009)
	environmental water	Salinomycin	N.D.-0.30	19/127	
Sediment	River, five sampling sites	Monensin	1.5–31.5	8/16	(Carlson and Kim, 2006)
	downstream agricultural land	Salinomycin	0.9–30.1	7/16	
	use and animal-feeding operations with seasonal variation	Narasin	2.0–16.3	8/16	
	Watershed, five sampling sites, including pristine area; entrance of urban area; urban area; agriculture influenced area; and urban and agriculture- influenced area.	Monensin	2.9-14.6	2/5	(Kim and Carlson, 2007a)
		Salinomycin	2.3-3.7	2/5	
		Narasin	2.5-5.3	4/5	

---

n<sub>a</sub> Total number of samples analyzed

n<sub>q</sub> Number of samples quantified

### ***1.1.6 Abiotic transformation of IPAs***

Abiotic transformation of antibiotics may occur via hydrolysis, photolysis, and redox reaction with metal oxides. However, very limited research has been conducted to investigate any such types of degradation for IPAs. Sassman and Lee indicated that abiotic degradation of MON may be important in soil after observing 40% loss of parent MON in  $^{60}\text{Co}$ -irradiated soils after 30 d of incubation in the dark (Sassman and Lee, 2007). Agtarap et al. studied MON transformation at acidic conditions and showed occurrence of transformation on the spiroketal region of MON (Figure 1.4) (Agtarap *et al.*, 1967). The ring (ring A and ring B) opening reaction by acid catalysis was also presented in other studies focusing solely on spiroketal chemistry (Figure 1.5) (Woodward *et al.*, 1959). Wells et al. detected degradation products of SAL and NAR after treating them with high concentrations of formic acid in tetrahydrofuran solvent (Figure 1.6) (Wells *et al.*, 1988). While these findings are valuable, both studies were conducted in organic solvent due to the low solubility of IPAs and thus the results are difficult to be applied to water.

The tendency of various IPAs to complex with different metal ions is well documented (Westley, 1983). Additionally, Pangborn et al. stated that coordination of MON to  $\text{K}^+$  ion may involve a distortion of the spiro-fused ring and lead to a higher-energy conformation compared to complexation with  $\text{Na}^+$  ion (Pangborn *et al.*, 1987). The above findings suggest that different metal ion complexation may result in different reactivity of IPAs for transformation.

Information related to photolysis of IPAs is scarce. Hansen et al. reported no observable additional loss of SAL when the samples were exposed to light compared to being in the dark (Hansen *et al.*, 2009c). However, this study was conducted in glass bottles which blocked the UV range of the light source. Considering the occurrence and the ability of IPAs to be

transported with water, photolysis may contribute to the abiotic degradation of IPAs. The structures of IPAs such as SAL (Figure 1.1) suggest potential direct photolysis due to its ketone moiety. Additionally, indirect photolysis involving natural photosensitizers such as nitrate and humic acids may also play a role in runoff and surface waters. Andreozzi *et al.* and Jiao *et al.* showed that the presence of nitrate or humic acids may enhance or slow down the photolysis of antibiotics in water depending on the structures of the antibiotics and the concentration of nitrate and humic acids (Andreozzi *et al.*, 2003; Jiao *et al.*, 2008).

A number of studies have shown that mineral surfaces may facilitate the abiotic transformation of various antibiotics via hydrolysis, substitution, redox, and polymerization. For example, the tetracycline antibiotics can undergo oxidative transformation in the presence of manganese oxides (Chen *et al.*, 2010). Aluminum oxides can also catalyze the isomerization and dehydration transformation of tetracyclines (Chen and Huang, 2010). In poultry industry, amending litter with aluminum sulfate is a common practice in order to control gaseous ammonia release and pathogens. Such a chemical amendment will likely affect the abiotic transformation of IPAs because of the resulted lower pH and the presence of aluminum species. The dissolved or precipitated aluminum species will likely affect the dynamics of metal complexation of IPAs, thereby affecting their abiotic reactivity.

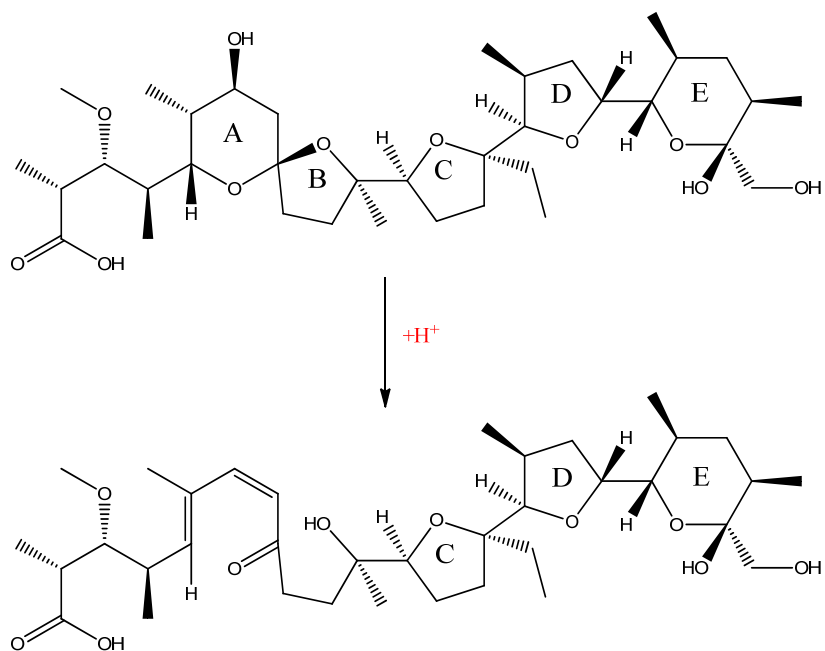


**Figure 1.4** MON transformation in acidic condition proposed by Agtarap *et al.*, 1967.

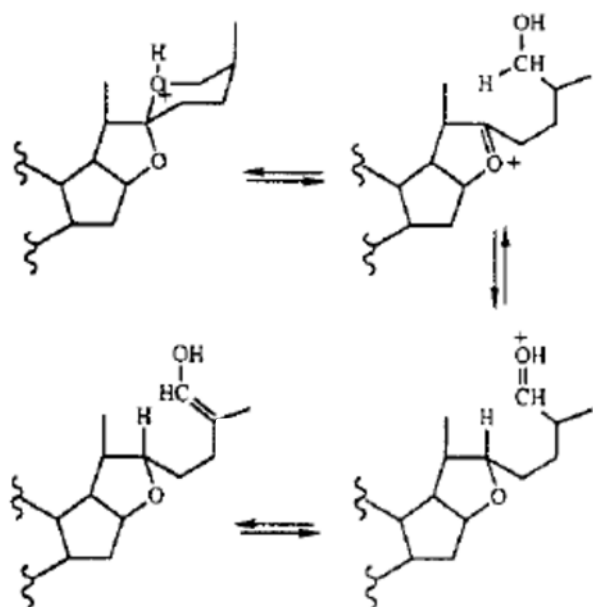


**Figure 1.5** Acid-catalytic transformation of spiro-ketal moiety (Perron and Albizati, 1989).

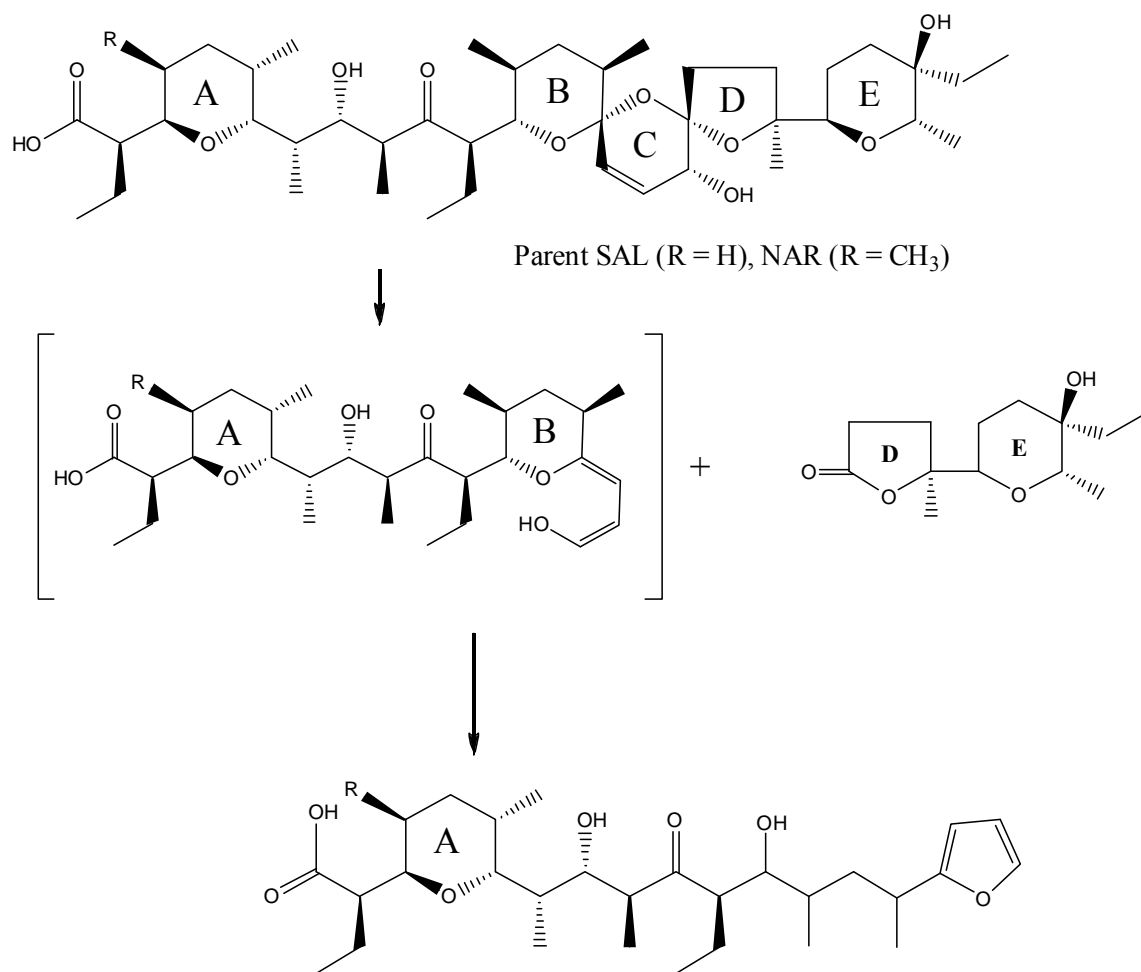


**Figure 1.6** SAL and NAR transformation in the presence of formic acid (Wells *et al.*, 1988).

### ***1.1.7 Biotic transformation/degradation of IPAs***

Although detailed biotransformation studies on IPAs with specific information relative to the transformation pathways, products, and microorganisms responsible for the degradation do not exist, a number of studies have attributed the disappearance of the parent IPAs to biodegradation. Disappearance of MON from MON-fed cow fresh feces (from 4.5 to 2.6 mg/kg in 10 weeks) and a cattle manure pile (from 4.7 to 0.7 mg/kg in 11 weeks) was attributed to biodegradation (Donoho, 1984). The relatively lower rate of MON disappearance in the feces was attributed to anaerobic conditions in the first test. This result agrees with the general belief that IPAs persist in anaerobic environments, and that they are degraded only under aerobic conditions (Russell and Houlihan, 2003). However, a recent study on the fate of SAL in stored pig manure under anaerobic conditions at 20°C reported degradation of SAL with a half-life of 5 days and two SAL cleavage metabolites were identified (Schlusener *et al.*, 2006). Results of this study agree with previous observations by Vértesy *et al.* who reported microbial cleavage of SAL (Vertesy *et al.*, 1987). The half-life of MON applied to an agricultural soil at an initial concentration of 300 µg/kg was 3.8 and 3.3 days without and with manure amendment, respectively; its disappearance was attributed to degradation in the upper soil layer, but direct evidence for microbial degradation was not reported (Carlson and Mabury, 2006). SAL-amended soil (2 mg/kg) incubated under aerobic conditions resulted in its disappearance with a 5-day half-life (Schlusener and Bester, 2006). It is noteworthy that, with the exception of a single study, IPA biotransformation products and/or any evidence for complete mineralization of the parent compounds was not provided in the above-mentioned studies.

As mentioned above, detailed information on the degradation pathways of IPAs is very limited. Decomposition of SAL, shown in Figure 1.7, by enzymes extracted from a

*Pseudomonas stutzeri* FH 1796 isolate was characterized as a retroaldol cleavage of the  $\beta$ -hydroxyl-ketone group; the SAL metabolite had no antibiotic activity and could not complex sodium or potassium (Vertesy *et al.*, 1987). In 2012, Hansen *et al.* investigated the biodegradation of SAL using bacteria extracted from agricultural soil, showing that SAL was readily biodegraded under aerobic conditions yielding a metabolite at  $m/z$  531.3 on mass spectrometry, which, the author claimed, was the same product as the one via the retroaldol cleavage reaction (Hansen *et al.*, 2012) (Note: *Pseudomonas stutzeri* is a Gram-negative, rod-shaped, motile, single, polar-flagellated, soil bacterium, first isolated from human spinal fluid. It is a denitrifying bacterium.).

MON was converted by the soil bacterium *Sebekia benihana* to three major compounds as follows (Vaufrey *et al.*, 1990): a) reduction of the  $\delta$ -hydroxyl-ketone leading to the opening of the terminal ring; b) oxidation of the  $\text{CH}_3$  to  $\text{CH}_2\text{OH}$  in the sub-terminal ring; and c) oxidation of an ethyl group to  $-\text{CHOH}-\text{CH}_3$  (Figure 1.8). Note that the two oxidations (b and c) proceed in parallel. An indirect assessment of the biodegradability of MON under aerobic conditions based on oxygen consumption reported 26.9% degradation at an initial MON concentration of 2.35 mg/L after 28 days of incubation (Alexy *et al.*, 2004). The same study also concluded that the biodegradability of the antibiotics tested, including MON, improved when a readily biodegradable carbon source was available, indicating possible cometabolism. (Note: *Sebekia benihana* is a Gram-positive, aerobic, thermophilic actinomycete isolated from soil.)

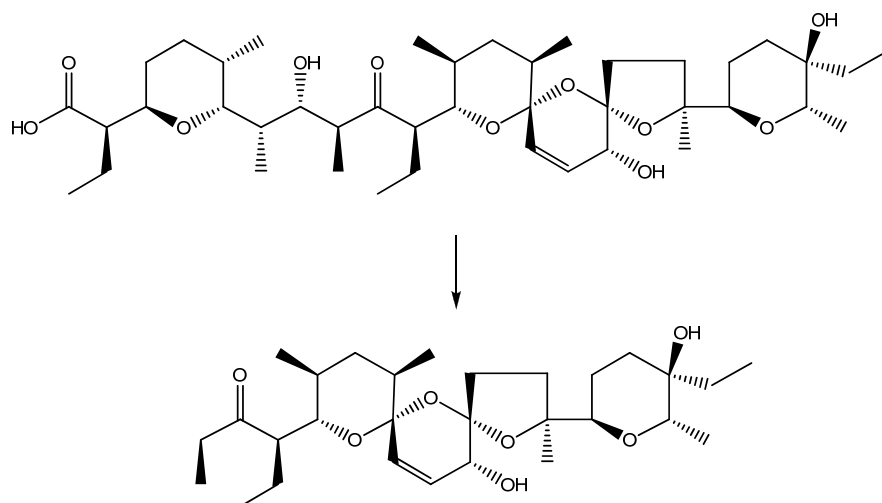


**Figure 1.7** Decomposition of SAL by enzymatic retroaldol cleavage (Vertesy *et al.*, 1987).

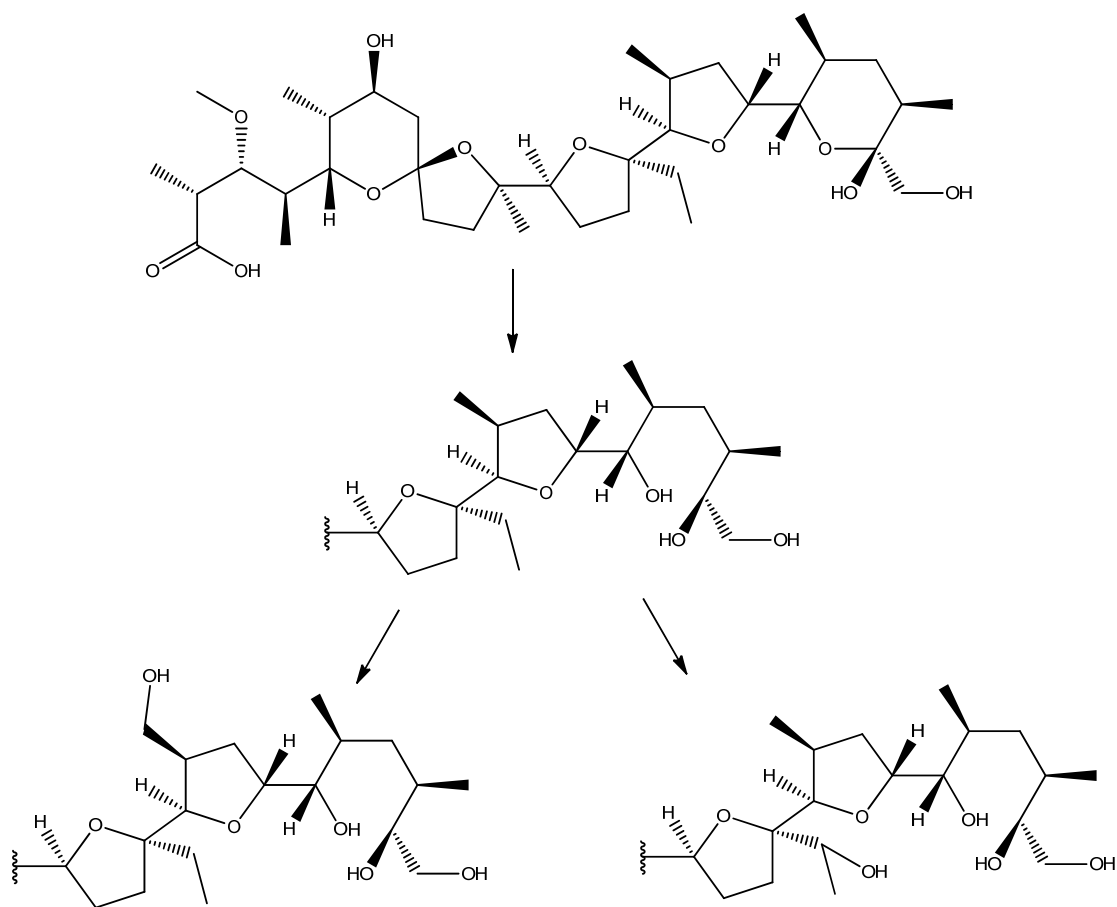


**Figure 1.8** Bioconversion of MON by the soil bacterium *Sebekia benihana* (Vaufery *et al.*, 1990).

## 1.2 Research Objectives

The overall goal of this research was to obtain a better understanding of the abiotic and biotic transformation of IPAs under conditions relevant in water-litter-soil systems.

The specific objectives of this research were:

- 1) To develop analytical methods for quantification of IPAs in various environmental matrices;
- 2) To estimate chemical properties (acidity, solubility, and metal ion complexation) of IPAs in aqueous phase;
- 3) To investigate the abiotic (i.e., hydrolysis and photolysis) and biotic transformation potential of IPAs under conditions relevant in the water-litter-soil environment;
- 4) To systematically evaluate the impact of environmental, chemical and biological conditions on the abiotic and biotic biotransformation of IPAs;
- 5) To determine the reaction kinetics, pathways and mechanisms of the abiotic and biotic transformation of IPAs;
- 6) To use laboratory-scale study to interpret the results from field study.

Chapter 2 describes the development of a robust analytical method that can quantify IPAs in various environmental compartments, especially in high-organic matrices such as poultry litter, and soil and runoff from litter-applied lands. The method for water samples involves solid-phase extraction (SPE) followed by liquid-liquid extraction (LLE) post-clean up steps. The method for detecting IPAs in solid samples includes bi-solvent LLE. IPAs were detected by HPLC-MS, with optimized parameters to achieve the highest sensitivity. Nigericin (NIG), an IPA not used in livestock industry, was successfully applied and validated as a surrogate standard. The method recoveries were at 92-95% and 81-85% in runoff samples from unfertilized and

litter-fertilized fields, respectively. For solids, the method recoveries were at 93-99% in soils, and 79-83% in poultry litter samples. SAL was detected at up to 22 mg/kg and MON and NAR at up to 4 mg/kg in broiler litter from different farms. Up to 183  $\mu\text{g}/\text{kg}$  of MON was detected in litter-fertilized soils. All three IPAs were detected in the rainfall runoff from litter-fertilized lands at concentrations up to 9  $\mu\text{g}/\text{L}$ .

Chapter 3 describes the research efforts to estimate the physicochemical properties of IPAs in aqueous phase, including acidity constant ( $K_a$ ), metal-complex dissociation constant ( $K_{\text{diss}}$ ), and the intrinsic solubility of protonated IPAs and metal-IPA complexes. The general methodology to estimate  $K_a$ ,  $K_{\text{diss}}$ , and the solubility of each species was by measuring the total dissolved IPAs at saturation level under different pH and metal ion concentration conditions with the assumption that the solubility of protonated IPAs or metal-IPA complexes controlled the concentration of total dissolved IPAs. Results showed that the  $pK_a$  of MON was  $4.50 \pm 0.05$ ,  $K_{\text{diss}}$  of MON with sodium ion was  $0.058 \pm 0.008$  (M), and  $K_{\text{diss}}$  of MON with potassium ion was  $0.573 \pm 0.072$  (M). The intrinsic water solubility of protonated MON, sodium-MON, and potassium-MON were  $76.6 \pm 7.5$ ,  $2.67 \pm 0.35$ ,  $199.6 \pm 24.3$   $\mu\text{M}$ , respectively.  $K_{\text{diss}}$  of SAL with sodium ion was estimated to be  $1.31 \pm 0.25$  (M).

Chapters 4 and 5 summarize the investigation of abiotic transformation of IPAs under environmentally relevant conditions. Specifically, chapter 4 assessed different IPAs' hydrolytic transformation potential under different pH conditions. Efforts were also made to characterize the reaction kinetics, elucidate transformation products and mechanisms, and evaluate toxicity of the transformation products. Results showed that IPAs are susceptible to acid-catalyzed transformation. MON reacted much more slowly than SAL and NAR and exhibited a different kinetic behavior that was further evaluated by a reversible reaction kinetic model. Extensive

product characterization identified that the spiro-ketal group of IPAs was the reactive site for the acid-catalyzed hydrolytic transformation, yielding predominantly isomeric and other products. Toxicity evaluation of the transformation products showed that the products retained some antimicrobial properties. The occurrence of IPAs and isomeric transformation products was also observed in poultry litter and agricultural runoff samples. Considering the common presence of mildly acidic environments (pH 4 – 7) in soils and waters, the acid-catalyzed transformation identified in this study likely plays an important role in the environmental fate of IPAs.

Chapter 5 investigated the degradation of IPAs due to photolytic reactions under UV and solar irradiation. Efforts were also made to calculate the quantum yield, predict photodegradation kinetics, elucidate transformation products and mechanisms, and evaluate toxicity of the transformation products of IPAs. The results showed that MON was persistent in deionized (DI) water, whereas SAL and NAR could undergo direct photolysis when exposed to UV and sunlight. The quantum yield of SAL was found to be considerably higher than those of other common veterinary pharmaceuticals including tetracyclines and sulfamethoxazole. Water components, such as nitrate and dissolved organic matter (DOM), had a great impact on the photolytic degradation of IPAs. A pseudo-steady state model was applied to quantify the influence of water components, which yielded satisfactory prediction of IPAs' photodegradation rates in real water matrices. Applying LC/MS/MS, multiple photolytic transformation products of SAL and NAR were observed, and tentative molecular structures were proposed. Two major transformation mechanisms were proposed for the direct photolysis of SAL and NAR, yielding (i) lower molecular weight products than the parent IPAs via cleavage on the ketone moiety; and (ii) oxyl-SAL or oxyl-NAR product via self-sensitized photolysis. With the presence of nitrate, photolysis of MON primarily occurred via reaction with hydroxyl radicals produced by photo-

excited nitrate, whereas SAL showed reactivity toward both hydroxyl and nitrogen-dioxide radicals. Additionally, toxicity tests showed that photolysis of IPAs eliminated their antibiotic properties against target microorganisms.

Chapters 6 and 7 assessed the inhibition and biotransformation of IPAs under conditions related to water-litter-soil systems. Specifically, Chapter 6 tested biodegradation of IPAs in PL and soil microcosms under varied temperature and water content conditions. Factor analysis was conducted to delineate the interaction of water and temperature on SAL and NAR degradation in the PL. Degradation of IPAs was also assessed in soil microcosms set up with PL-fertilized and non-fertilized soil samples, in which the effects of water content, carbon source amendment, and initial IPA concentration were investigated. Several primary biotransformation products of IPAs were detected. Additionally, PL and soil samples from a field study were analyzed to assess the fate and potential degradation of IPAs during litter stacking and subsequent application of the PL to agricultural fields, and the results were compared with those obtained in the laboratory study.

Chapter 7 assessed the inhibition and biotransformation potential of IPAs with different electron acceptors. Inhibition tests focused on examining IPAs' impact on microbial processes, including denitrification, sulfate-reduction, and methane production. Biodegradation tests were conducted with different electron acceptors, including oxygen, nitrate, sulfate, and organic carbons, with efforts to elucidate primary biotransformation products.

Chapter 8 presents the conclusions based on the results from this study. An overall environmental transformation of IPAs was delineated. Recommendations on IPA selection were made based on their environmental persistence. Furthermore, an improved animal waste management strategy was suggested with the purpose to reduce the amount of IPAs released from animal farms. Potential future research directions in this area are also discussed.

## CHAPTER 2

### DETECTION AND QUANTIFICATION OF IONOPHORE ANTIBIOTICS IN STANDARD MATRIX, RUNOFF, SOIL AND POULTRY LITTER

#### 2.1 Introduction

In order to investigate the occurrence and transformation reactions of IPAs in the soil-water-litter systems, a reliable analytical method capable of quantifying parent IPAs in various sample matrices efficiently and accurately must first be established. A number of analytical methods have been developed to detect IPAs in animal tissues (e.g. (Blanchflower and Kennedy, 1996; Matabudul *et al.*, 2001; Mortier *et al.*, 2005)), manure (e.g. (Blackwell *et al.*, 2004; Schlusener *et al.*, 2003a)), soil (e.g. (Furtula *et al.*, 2009; Schlusener *et al.*, 2003b; Watanabe *et al.*, 2008)), surface water (e.g. (Cha *et al.*, 2005; Dolliver *et al.*, 2008b; Hao *et al.*, 2006; Kim and Carlson, 2007a)) and wastewater (e.g. (Herrero *et al.*, 2013; Herrero *et al.*, 2012)). Commonly, IPAs in water were extracted using Oasis HLB cartridges followed by methanol as elution solvent (Hansen *et al.*, 2009a; Hao *et al.*, 2006; Kim and Carlson, 2007a). Novel extraction methods, such as single-drop micro-extraction (Sekar and Wu, 2006) and supercritical fluid extraction (Ramsey *et al.*, 2010), were also tested for quantification of IPAs in water matrix. Recoveries reported in these studies were in the range of 80 – 115%. IPAs in solid samples were extracted by organic solvents such as ethyl acetate and methanol and then diluted into water followed by a similar solid-phase extraction (SPE) procedure as a second clean-up and extraction step (Carlson and Kim, 2006; Schlusener *et al.*, 2003a; Schlusener *et al.*, 2003b). Quantification of IPAs typically requires LC/MS with electrospray ionization at positive mode (ESI(+)). In some studies, LC/MS/MS was applied for confirmatory purposes (Cha *et al.*, 2005; Kim and Carlson, 2007a). With the reported analytical methods, the presence of IPAs in soil, sediments,

sewage, surface water and groundwater has been reported by several studies (Carlson and Kim, 2006; Hao *et al.*, 2006; Kim and Carlson, 2007a; Watanabe *et al.*, 2008; Watkinson *et al.*, 2009). For example, IPAs were detected in surface waters, groundwater, and river sediments at concentrations up to 0.22 µg/L (Hao *et al.*, 2006), 0.39 µg/L (Watanabe *et al.*, 2008), and 30 µg/kg (Kim and Carlson, 2007b), respectively. Watkinson *et al.* reported that MON and SAL were detected in 94% and 21% of all samples analyzed, respectively, in surface waters and occasionally in municipal wastewater treatment plant effluent (Watkinson *et al.*, 2009).

Only a limited number of studies have thus far focused on detecting IPAs in poultry litter (Furtula *et al.*, 2009) and surface runoff from agricultural fields, which are expected to be among the primary sources of IPAs introduced to the environment. Thus, to better understand the occurrence, fate and transport of IPAs in the environment, the research described in this chapter aimed to develop a robust analytical method that can quantify IPAs in various environmental compartments, especially in high-organic matrices such as poultry litter, and soil and runoff from litter-applied lands. Specifically, efforts were made to optimize the analytical method for the three most widely used IPAs (MON, SAL and NAR) with respect to improving extraction recovery and reducing matrix effects. Nigericin (NIG), another IPA not commercially applied to livestock, was evaluated as a surrogate standard for the other IPAs.

## **2.2 Materials and Methods**

### ***2.2.1 Chemicals and reagents***

MON sodium salt (purity, 97%) and NAR sodium salt (purity, 97%) were purchased from Sigma-Aldrich (St. Louis, MO). SAL (purity, 96%) and NIG (purity, 99%) in the form of sodium salt were purchased from Fisher Scientific (Pittsburgh, PA). HPLC-grade methanol (purity, 99.9%) and acetonitrile (ACN) (purity, 99.9%) and analytical-grade formic acid (purity, 99%), ethyl acetate (purity, 99.8%), and hexane (purity, 95%) were obtained from Sigma-Aldrich. All other reagents used were at analytical grade obtained from Fisher Scientific. Reagent-grade deionized (DI) water (resistivity > 18 mΩ·cm) was obtained from a Millipore nanopure water purification system (Billerica, MA). Individual IPA stock solutions (50 mg/L) were prepared in methanol and stored at 4°C before use.

### ***2.2.2 Sample collection and pre-treatment***

#### ***2.2.2.1 Water samples***

Simulated rainfall at 75 mm/h was applied to tall fescue/bermuda grassplots (0.75 m × 2 m) with or without poultry litter application at 5,000 kg/ha. Runoff was collected for 30 min at the downstream end of each plot in 1-liter glass jars with Teflon-lined caps. The samples were stored on ice in cooler boxes, and immediately transported to the labs for analysis. Two hundred milliliters of each runoff sample was filtered through a 0.45-μm glass-fiber filter (Millipore, Billerica, MA) and then transferred to an amber bottle. Water pH was adjusted to 7.0 - 7.5 by addition of either HCl or NaOH solution. When samples could not be analyzed within the same day of collection, 100 mg/L of sodium azide was added to inhibit microbial activity. Preliminary experiments confirmed that IPAs did not react with sodium azide (data not shown).

### *2.2.2.2 Soil and poultry litter samples*

Soil samples for method development were collected from the top 0 – 10 cm of two experimental grass plots, one that had received poultry litter applications for more than 10 years, and one that had received inorganic fertilizers but no poultry litter. These plots are located at the Central Research and Education Center of the University of Georgia, Eatonton, GA (33° 24' N, 83° 29' W, elevation 150 m). The soil in the area is dominated by Cecil series (fine, kaolinitic, thermic Typic Kanhapludults). Poultry litter samples were collected from broiler farms in Georgia, USA. All solid samples were kept at 4 °C prior to analysis.

### *2.2.3 Water sample analysis - solid phase extraction (SPE)*

The filtered runoff sample (200 mL) was spiked with the surrogate standard NIG (50 µg/L) and extracted through a 500 mg, 6 mL hydrophilic–lipophilic balance (HLB) cartridge (Waters, Taunton, MA). Before SPE, the HLB cartridges were pre-conditioned with 5 mL methanol followed by 5 mL DI water. The runoff sample was extracted at approximately 2 mL/min under vacuum using a Visiprep apparatus (Supelco, Bellefonte, PA). Afterwards, the cartridge was rinsed with 5 mL DI water, and then dried for 10 min under vacuum. Three milliliter of methanol was applied twice to elute IPAs from the HLB cartridges to an amber bottle. The collected methanol extract was evaporated to dryness under vacuum at room temperature (20 – 22 °C) and then analytes were reconstituted by adding 0.5 mL of a buffer solution containing 10 mM Na<sub>2</sub>HPO<sub>4</sub> and 5 mL ethyl acetate. The mixture was shaken for 30 min at 120 rpm and then the buffer layer was discarded using a Pasteur pipette. The remaining ethyl acetate layer was evaporated to dryness under vacuum and then analytes were finally

reconstituted in 1 mL mixture of methanol and 10 mM Na<sub>2</sub>HPO<sub>4</sub> solution (50/50 v/v). The final sample was transferred to a HPLC amber vial for LC/MS analysis.

#### ***2.2.4 Solid sample analysis - solvent extraction***

One gram of freeze-dried and ground solid sample was spiked with NIG at 0.5 µg/kg and then transferred to a 50-mL centrifuge tube. Then, 7.5 mL of McIlvaine's buffer containing 10 mM EDTA, Na<sub>2</sub>HPO<sub>4</sub> and citric acid (pH 7) was added, followed by 2.5 mL methanol and 5 mL hexane. The sample was then shaken for 30 min at 300 rpm. After centrifugation for 5 min at 3000 rpm, the hexane layer was transferred to an amber bottle with a pipette. The extraction was repeated by adding another 5 mL hexane to the sample following the same procedures described above. The combined 10 mL of hexane extract was then evaporated to dryness under vacuum at room temperature, and then analytes were finally reconstituted with 1 mL mixture of methanol and 10 mM Na<sub>2</sub>HPO<sub>4</sub> solution (50/50 v/v). The final sample was transferred to a HPLC amber vial for LC/MS analysis.

#### ***2.2.5 LC-MS analysis***

IPAs were detected by an Agilent 1100 Series LC/MSD system (Agilent, Palo Alto, CA) equipped with a reversed-phase column (2.1×150 mm, 3 µm Ascentis RP-amide column, Supelco, Bellefonte, PA). The column was maintained at 40°C with a flow rate of 0.30 mL/min. Mobile phase consisted of (A) a mixture of HPLC-grade water and formic acid (99.9:0.1 v/v) with 25% ACN; and (B) HPLC-grade methanol and ACN (50/50 v/v). The gradient consisted of mobile phase B being ramped from 50% to 90% in the first 8 min and then to 100% at 12 min. Then, the system ran at 100% B for 3 min. The injection volume was 10 µL. A 5-min post-run

period was allowed between each analysis to re-equilibrate the column with the mobile phase (50% A and 50% B). The mass spectrometer was set at positive electrospray ionization mode (ESI+) with 190 V fragmentation voltage and +4500 V capillary voltage (mass resolution 0.1 m/z). Nitrogen was used both as a nebulizer gas (35 psi) and a drying gas at 350°C (6.0 L/min). Selected ion monitoring (SIM) mode was applied for quantification of IPAs. The sodium adducts of IPAs with m/z of [M+23] were used for quantification (Table 2.1).

**Table 2.1** LC/MS parameters of IPAs

<b>IPAs</b>	<b>Molecular weight [g/mol]</b>	<b>Molecular ion (m/z) [M+Na]<sup>+</sup></b>	<b>Confirming ion (m/z)</b>	<b>Retention time (min)</b>
<b>MON</b>	670.9	693	635	8.7
<b>SAL</b>	751.0	773	733	9.4
<b>NAR</b>	765.0	787	747	10.5
<b>NIG</b>	725.0	747	730	11.5

### 2.2.6 Calibration and method validation

The calibration standards were prepared by spiking 20  $\mu\text{L}$  of each IPA stock solution into 1 mL mixture of methanol and 10 mM  $\text{Na}_2\text{HPO}_4$  solution (50/50 v/v) to achieve 1000 ng/mL. The other concentrations were made by serial dilution of the 1000 ng/mL standard using the same methanol/buffer mixture.

Recoveries of IPAs were determined by the standard addition method. IPAs were spiked into runoff, soil and poultry litter samples at multiple concentration levels (100 – 3000 ng/L for runoff, 50–1500  $\mu\text{g}/\text{kg}$  for soil and litter samples). The recovery of each individual spiking was calculated according to Equation 2.1:

$$\text{Recovery}(\%) = \frac{[\text{IPA}]_{\text{spiked}} - [\text{IPA}]_{\text{unspiked}}}{[\text{S}]} \times 100 \quad (2.1)$$

where  $[\text{IPA}]_{\text{spiked}}$  and  $[\text{IPA}]_{\text{unspiked}}$  are the IPA concentrations detected in the sample with and without spiking with IPA, respectively, and  $[\text{S}]$  is the amount of IPA spiked into the samples. The average recovery from multiple spiking experiments in each matrix is reported.

The recovery calculated by Equation 2.1 is influenced by both extraction efficiency and matrix effects. To quantify the signal suppression impact from sample matrix, Equation 2.2 was applied.

$$\text{Signal Suppression}(\%) = \left( 1 - \frac{I_s - I_x}{I_{\text{Std}}} \right) \times 100 \quad (2.2)$$

where  $I_s$  is the IPA signal intensity in a sample extract after S amount of IPAs was spiked after extraction,  $I_x$  is the IPA signal intensity in the unspiked sample extract, and  $I_{\text{Std}}$  is the IPA signal intensity in standard solution matrix (50% MeOH/50% 10 mM  $\text{NaH}_2\text{PO}_4$ ) spiked with S amount of IPAs.

Thus, the extraction efficiency was obtained by dividing recovery by signal suppression

(Equation 2.3)

$$\text{Extraction Efficiency (\%)} = \frac{\text{Recovery}}{1 - \text{Signal Suppression}} \times 100 \quad (2.3)$$

The method detection limit (MDL) was determined by the procedures reported by Gros et al. (Gros *et al.*, 2006). The MDL was defined as the minimum detectable amount of IPAs with signal-to-noise (S/N) ratios of 3. To determine MDL, all IPAs were spiked (n = 3) into water or solid samples and processed by the entire extraction procedures described above.

## 2.3 Results and Discussion

### 2.3.1 Optimization of standard matrix and LC conditions

Experiments were first conducted to optimize the standard matrix and LC/MS conditions that will yield the best sensitivity and analytical accuracy for IPAs. Several factors in the standard matrix including the presence of methanol co-solvent, counter cations and pH level were evaluated. MON calibration standards were prepared in different matrix compositions. Solution pH (3, 5 or 8) was adjusted by NaOH or HCl. The counter cations included sodium, potassium and ammonium ions. As shown in Figure 2.1, MON's signal intensity was consistently the highest at pH 8 and when methanol was added. The much lower signal intensity at pH 3 was likely due to instability of IPAs under acidic conditions. Our recent work (Sun *et al.*, 2013b) has demonstrated that IPAs are prone to acid-catalyzed hydrolysis under acidic conditions. Since IPA analysis was based on their sodium adducts by LC/MS, other cations such as potassium and ammonium could compete with sodium to complex with MON and thus decrease its signal intensity (Figure 2.1). Although the above tests were conducted with MON only, the results are likely applicable to other IPAs due to their very similar structures. Thus, the standard matrix of MeOH/10 mM Na<sub>2</sub>HPO<sub>4</sub> solution (50/50 v/v), which provides methanol co-solvent, neutral pH and excess sodium conditions, was deemed optimal.

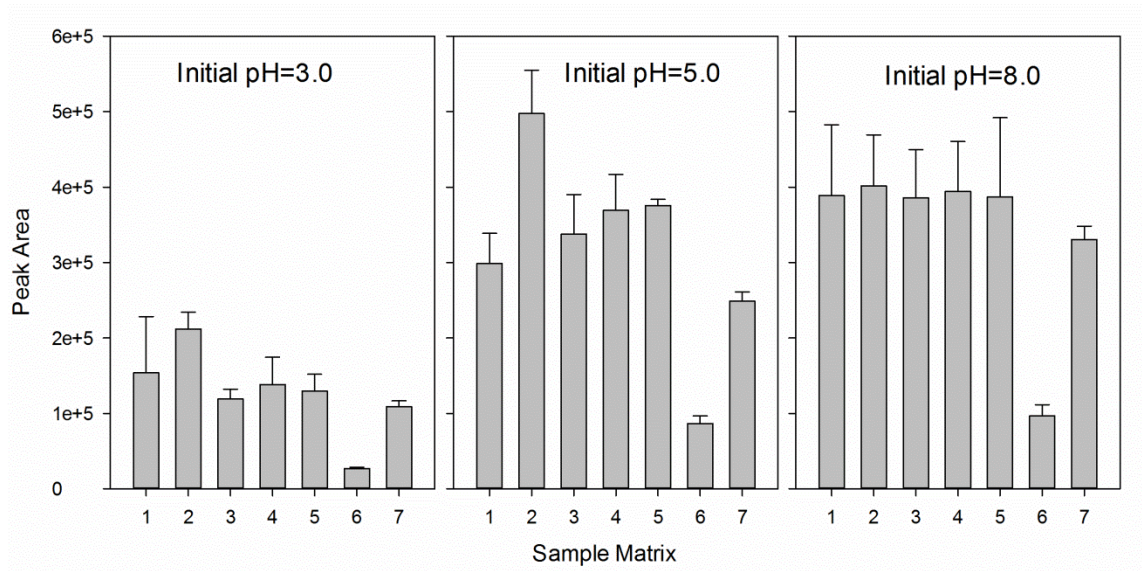


**Figure 2.1** MON signal intensity in different standard sample matrices buffered with phosphate: (1) deionized water; (2) methanol:water = 50:50 (v:v); (3) deionized water with 1 mM NaCl; (4) deionized water with 10 mM NaCl; (5) deionized water with 100 mM NaCl; (6) deionized water with 10 mM NaCl and 90 mM KCl; (7) deionized water with 10 mM NaCl and 90 mM NH<sub>4</sub>Cl. Error bars represent standard deviation from triplicate samples.

Previous studies showed that mobile phases of water with formic acid and methanol were effective for detection of IPAs by LC/MS (Kim and Carlson, 2007a). However, NAR and NIG could not be separated by such a mobile phase combination using the Ascentis RP-amide column. Because the major daughter ion of NAR and the parent NIG share the same  $m/z$  value ( $m/z$  747), it is necessary to separate these two compounds completely. Replacing methanol by ACN yielded satisfactory separation between NAR and NIG. However, there were two drawbacks of using ACN: (1) overlapping peaks of MON and SAL; and (2) decreased sensitivity for all IPAs. Thus, an optimal mobile phase combination was determined to be: (A) 0.1% formic acid in water with 25% ACN; and (B) 50% ACN with 50% MeOH. The gradient elution of the above mobile phase is described in Section 2.2.5 above. The separation of IPAs and their retention times are shown in Figure 2.2 and Table 2.1.

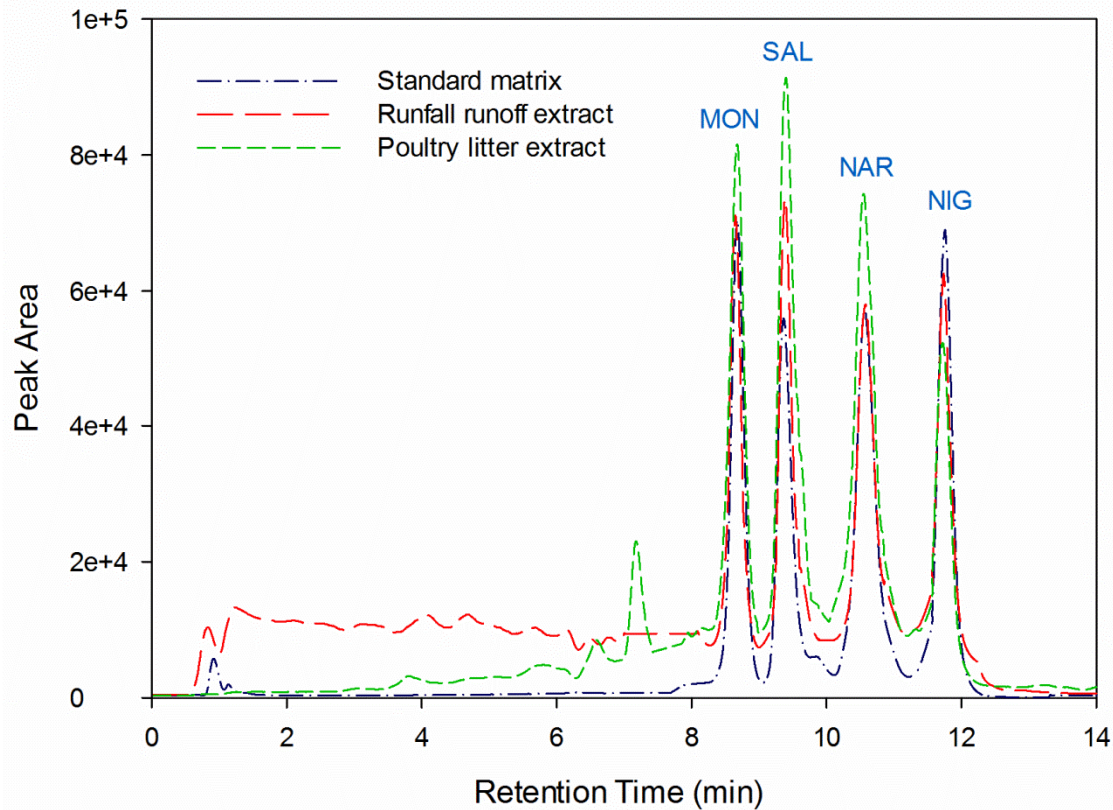


**Figure 2.2** Example of total ion chromatograms of IPA in a standard mixture, an extract of runoff from PL-fertilized plots, or an extract of PL. IPAs were spiked at 500  $\mu\text{g/L}$  into final extracts and analyzed by ESI(+) with selected ion monitoring mode.

### ***2.3.2 Water sample extraction and clean-up***

The HLB SPE cartridges have been shown to have high extraction recoveries for a variety of pharmaceutical compounds (Gros *et al.*, 2006; Hu *et al.*, 2008; Kim and Carlson, 2007a). Previously, the HLB cartridges were used by Kim *et al.* (Kim and Carlson, 2007a) to extract IPAs from surface water with satisfactory recoveries and thus were selected to extract IPAs in surface runoff from litter-fertilized grasslands. To avoid degradation of IPAs by acid-catalyzed hydrolysis as shown by our recent work (Sun *et al.*, 2013b), water samples were adjusted to pH 7 - 8 by adding NaOH or HCl before extraction in this study. However, due to the unselective adsorption properties of HLB resins, both IPAs and dissolved organic matter (DOM) are retained. The UV absorbance at 254 nm of surface runoff samples from litter-fertilized lands were above 3.2, indicating extremely high DOM content. High DOM content in the samples poses risks of clogging the HPLC column and significantly interfering with the detection of IPAs by MS via signal suppression (e.g., decrease in the ionization efficiency of IPAs). Thus, a suitable clean-up procedure was needed to remove DOM from the extracted samples before LC/MS analysis. Several sample clean-up methods have been developed by other researchers. Some studies applied an anion-exchange cartridge (e.g., Supelco SAX cartridges, Bellefonte, PA) on top of the HLB cartridge during SPE (Renew and Huang, 2004). Owing to DOM's predominantly negative charge in water matrices, much of the DOM was retained by the anion-exchange cartridge before being in contact with the HLB cartridge. Other studies proposed using less polar elution solvents than methanol, such as acetone, because DOM has lower solubility in apolar solvents.

In this study, several different clean-up methods were tested. Recovery, signal suppression and extraction efficiency were compared and shown in Figure 2.3. Results indicated

that methanol was an effective solvent to elute IPAs from the HLB cartridges but a significant amount of DOM also ended up in the final extract resulting in strong signal suppression. The signal suppression was reduced when a SAX cartridge was applied in SPE as discussed above; however, only a limited amount of IPAs was extracted as evidenced by the lower extraction efficiency, possibly due to adsorption of IPAs to the SAX cartridge. A possible way to avoid adsorption of IPAs to the SAX cartridge is to acidify samples to below the pKa values (4.3-4.4) of IPAs to protonate IPAs' anionic carboxylic group. However, such an approach cannot be used because IPAs undergo rapid acid-catalyzed hydrolysis at pH below 5 (Sun *et al.*, 2013b).

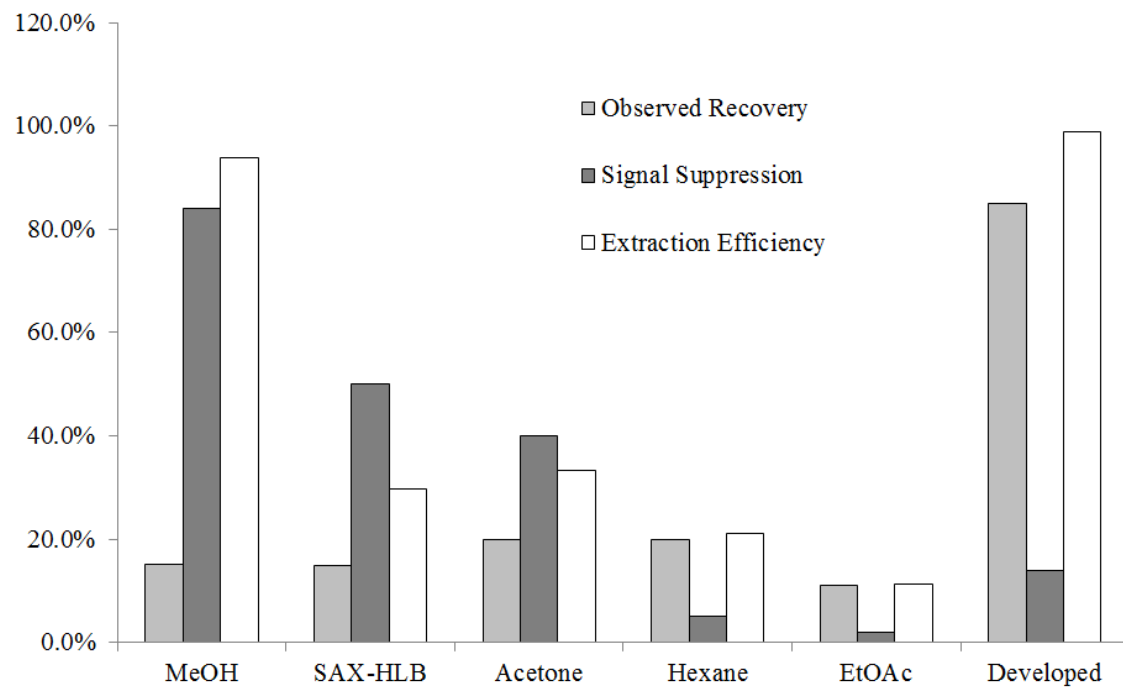


**Figure 2.3** Recovery, signal suppression and extraction efficiency of MON with different clean-up methods after HLB SPE. SAX-HLB represents tandem SPE by both types of cartridges. The sample matrix was rainfall runoff from PL-fertilized plots. MON was spiked at 2.5 $\mu$ g/L.

Acetone, ethyl acetate and hexane eluted significantly less DOM from the HLB cartridges, leading to lower signal suppression. However, the extraction efficiency was poor because all three solvents were not strong enough to elute IPAs from the HLB cartridges. Indeed, for samples of high organic content, the significant amount of DOM adsorbed on the HLB resins is likely to retain a certain amount of IPAs. If a solvent, such as acetone, does not dissolve DOM, the retained IPAs are unlikely to be recovered during elution. Thus, a new clean-up method was needed to specifically target the separation of IPAs from the high DOM content in the runoff samples.

A new clean-up method was developed in this study on the basis of the high lipophilicity of IPAs and low solubility of DOM in the ethyl acetate solvent. First, methanol was applied to elute adsorbates from the HLB cartridge after SPE since methanol has a strong capacity to dissolve IPAs along with DOM. Because IPAs have extremely low vapor pressure ( $<10^{-28}$  Pa), the sample was then evaporated to complete dryness under vacuum at room temperature. After evaporation, a dried DOM cake was left as a coating on the interior surfaces of the container. A  $\text{Na}_2\text{HPO}_4$  aqueous solution was added to dissolve the DOM cake followed by adding ethyl acetate; this procedure increased the contact with the IPAs and helped transfer to the ethyl acetate layer. Adding  $\text{Na}_2\text{HPO}_4$  in the aqueous solution was able to (i) maintain a mildly basic condition and thus prevent hydrolysis of IPAs, (ii) increase IPAs' lipophilicity by complexation with sodium ions, and (iii) increase signal intensity since IPAs are detected as sodium adducts. Given sufficient agitation and contact time, most IPAs were effectively transferred into the ethyl acetate layer, leaving DOM in the buffer phase. Compared with other clean-up methods, the developed clean-up method showed lower signal suppression and significantly higher recovery (Figure 2.3).

### ***2.3.3 Soil/litter sample extraction and clean-up***

Since poultry litter contains around 45% organic matter (weight/litter dry weight), which is considerably higher than typically found in soils, the method development for extraction of IPAs from solids was focused on the litter matrix. Similarly, the extraction procedure should be applied under neutral to mildly basic conditions to prevent acid-catalyzed transformation of IPAs, and aimed at separating IPAs from the organic matter in the litter. Different organic solvents including methanol, hexane and ethyl acetate were tested to extract IPAs from poultry litter and soil matrices. As shown in Figure 2.4, methanol exhibited the highest extraction efficiency but also the strongest signal suppression on LC/MS, whereas less polar solvents (i.e., hexane and ethyl acetate) yielded the cleanest extract but poor extraction efficiency for IPAs. None of the above solvents achieved satisfactory recovery. Methanol is a strong enough solvent to dissolve IPAs from the litter matrix but a significant amount of organic matter also was dissolved in the methanol phase, leading to strong matrix effects on the ionization on LC/MS. Hexane and ethyl acetate did a great job to minimize organic content in the final extract; however, due to the hydrophilic property of litter solids, apolar solvents have insufficient contact with litter particles, resulting in poor extraction efficiency.

Based on the above observations, a combination of aqueous buffer and an apolar solvent may be able to achieve high extraction efficiency and low signal suppression simultaneously. A combination of McIlvaine's buffer, methanol and hexane as the extraction liquid was developed and shown to be effective. The McIlvaine's buffer (a mixture of 0.1 M citric acid and 0.2 M  $\text{Na}_2\text{HPO}_4$ ) at pH 7 was used because (1) it has a strong buffer capacity at neutral pH, and (2) citric acid can compete with IPAs in adsorption with alkaline metals on the solid surfaces. The aqueous buffer was amended with 25% (v/v) methanol because of three reasons. First, due to the

lipophilic nature of IPAs, desorption of IPAs from litter to the aqueous buffer may be slow and difficult and can be facilitated by methanol. Furthermore, the IPA's concentration in the aqueous buffer is a driving force for its transfer to the hexane phase, and thus a low solubility in the aqueous buffer will be unfavorable for extraction efficiency. Second, methanol is expected to increase the solubility of organic matter in the aqueous buffer, resulting in less organic matter in the hexane phase. Third, methanol content higher than 25% will lead to a considerable amount of IPAs staying in the buffer instead of transferring into the hexane phase (data not shown). In addition to methanol, 10 mM EDTA was added into the McIlvaine's buffer. Poultry litter is commonly amended with alum ( $\text{Al}_2(\text{SO}_4)_3 \cdot 12\text{H}_2\text{O}$ ) to reduce odor and inhibit pathogens (Moore *et al.*, 2000a; b; Moore *et al.*, 1995). However, alum dissolved in the aqueous buffer can greatly lower pH (e.g., 20% (w/w) alum lowered the pH from 7 to 4) even at buffer concentration as high as 0.1 M. Thus, EDTA as a chelating ligand with aluminum ions was applied to reduce the pH impact from alum in poultry litter.

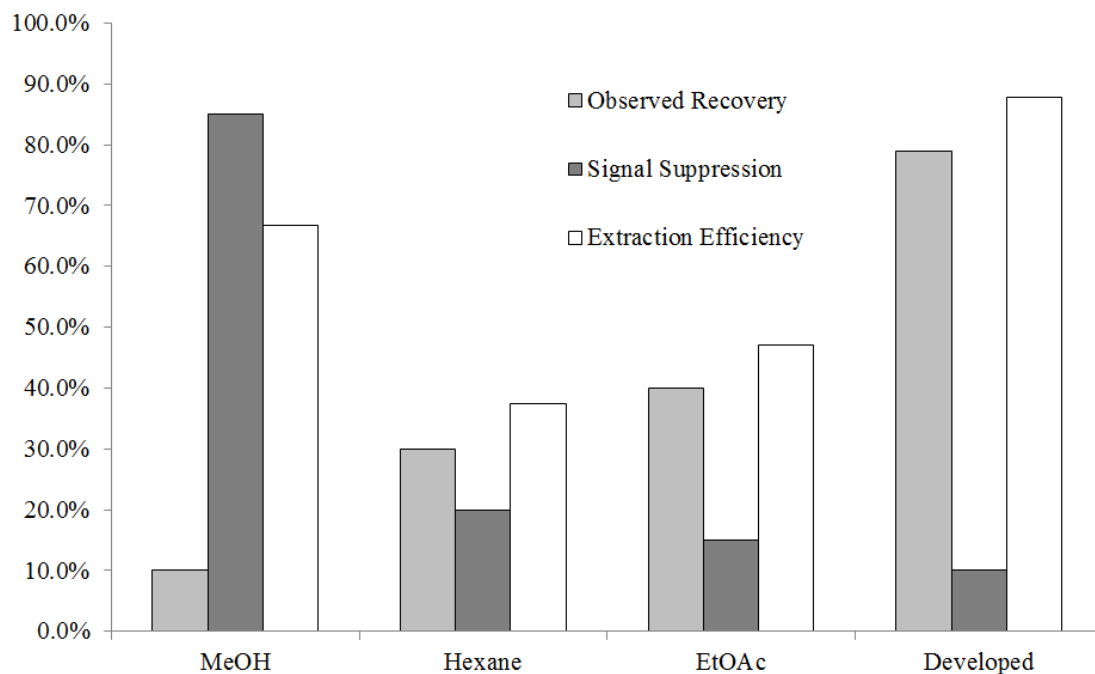


**Figure 2.4** Recovery, signal suppression and extraction efficiency of MON in poultry litter extract by different extraction solvents. MON was spiked at 0.5 mg/kg.

### **2.3.4 Method validation**

#### *2.3.4.1 Linearity, MDL, MQL and recovery*

As shown in Table 2.2, the average recoveries achieved for all IPAs ranged from 79% to 99% for all matrices. For each matrix, all four IPAs have comparable recoveries, indicating similar behavior during the extraction process. Better recoveries were obtained in the matrix containing less organic matter, such as runoff samples from unfertilized field and soil samples without application of poultry litter.

Calibration linearity, instrument detection limit (IDL), and method detection limit (MDL) are shown in Table 2.3. Calibration curves were generated using linear regression, which yielded a good fit ( $r^2 > 0.999$ ) in the range from 30 to 1000  $\mu\text{g/L}$ . The IDL values of all IPAs were at the pg level. Similar to recoveries, lower MDLs were achieved in the samples with lower organic content.

**Table 2.2** Recovery of IPAs.

	Runoff <sup>a</sup> (n=3)	Runoff <sup>b</sup> (n=7)	Soil (n=7)	PL (n=7)
MON	95±3	82±19	98±4	79±11
SAL	94±9	85±13	99±2	82±15
NAR	92±7	83±11	93±6	83±12
NIG	95±6	81±17	96±4	80±16

<sup>a</sup> rainfall runoff from plots without litter application

<sup>b</sup> rainfall runoff from plots with litter application

**Table 2.3** Calibration linearity, instrument detection limit (IDL), and method detection limit (MDL) in runoff samples from unfertilized field<sup>a</sup>, poultry litter fertilized field<sup>b</sup> soil and poultry litter.

	Linearity (30- 1000 µg/L) (r <sup>2</sup> )	IDL (pg injected)	MDL (ng/L)		MDL (µg/kg)	
			Runoff <sup>a</sup>	Runoff <sup>b</sup>	soil	PL
MON	0.9996	28	18.0	22.0	7.6	18.6
SAL	0.9994	38	18.5	38.8	9.0	25.1
NAR	0.9992	45	15.5	26.2	11.6	16.8
NIG	0.9997	57	17.1	24.0	12.5	16.5

<sup>a</sup> rainfall runoff from plots without litter application; <sup>b</sup> rainfall runoff from plots with litter application

**Table 2.4** Signal suppression (%) of IPAs in the final extracts.

Compound	Runoff (unfertilized plots)	Runoff (PL-fertilized plots)	Soil extracts	Poultry litter extracts
MON	3	14	8	9
SAL	5	19	8	12
NAR	6	17	7	9
NIG	4	18	5	11

#### 2.3.4.2 Validation of surrogate standard NIG

Due to the lack of synthetic isotopic standards of the commercially used IPAs, a surrogate standard is necessary to account for and quantify the variability during extraction and detection. NIG was suggested to be a candidate by other researchers (Dubois *et al.*, 2004; Vincent *et al.*, 2008). However, a systematic validation of NIG as a suitable surrogate for IPAs was not previously performed and thus was addressed in this study. As shown in Tables 2.3 and 2.4, for both recovery and signal suppression, NIG showed similar values as the other IPAs tested in this study, indicating that NIG likely behaves similarly during both extraction and ionization processes.

To further assess if NIG can represent the recoveries of other IPAs over a wide range of concentrations and sample matrices, MON and SAL standards were spiked at various concentrations in runoff and litter samples. As shown in Figure 2.5A and 2.5C, without correction by the recoveries of NIG, the concentrations of MON and SAL detected in the spiked samples were below the standard curves, indicating loss during extraction and/or signal suppression during ionization. In Figure 2.5B and 2.5D, the overlapping with the standard curves suggested that the recoveries of the other IPAs were successfully corrected by NIG used as a surrogate standard.

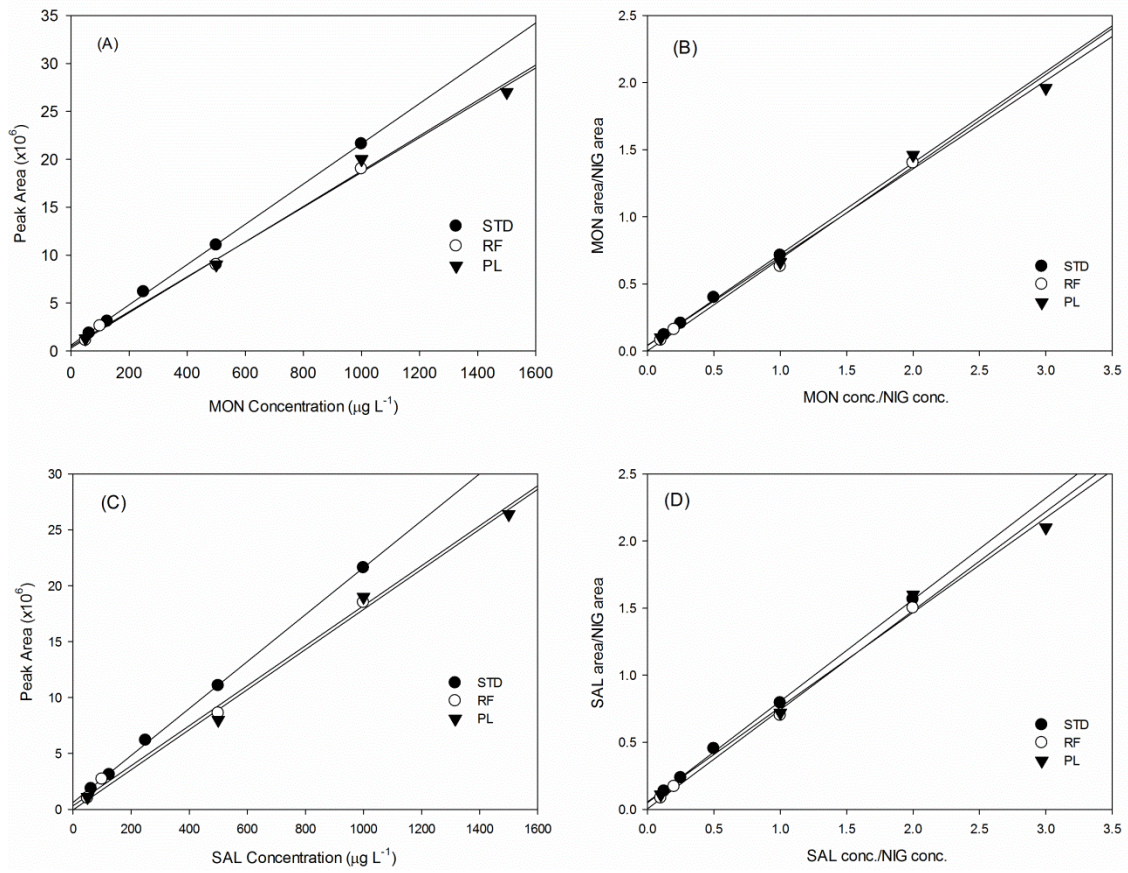


**Figure 2.5** Peak areas of MON (A) and SAL (C) obtained in standard matrix (STD), rainfall runoff (RF) and poultry litter (PL). Peak areas of MON (B) and SAL (D) normalized by the NIG peak area in each sample matrix.

### ***2.3.5 Occurrence of IPAs in the environment***

The developed method was further applied to assess the occurrence of IPAs in a range of environmental samples. Poultry litter samples were collected from several broiler farms in Georgia, U.S. Total 13 soil samples were collected from agricultural lands in Georgia, Arkansas and Iowa, U.S.. Water samples were rainfall runoff collected from grass fields with and without applications of poultry litter. NIG was spiked to each sample at 500 µg/L or µg/kg before performing extraction. IPAs were quantified based on the recovery of NIG.

As shown in Table 2.5, IPAs were not detected in the samples that were not in contact with poultry litter (i.e., unfertilized soils and the rainfall runoff from them). However, in the poultry litter-fertilized fields and rainfall runoff from them, IPAs were detected at a wide range of concentrations, indicating that poultry litter is contributing to the release of IPAs into the environment. Although the water solubility of IPAs is low due to their high  $K_{ow}$  values (EFSA., 2004; 2005; Thiele-Bruhn, 2003), the detection of high concentrations of IPAs in the runoff samples suggested that IPAs can be transported via runoff in the environment. This observation may be partly due to the fact that a significant amount of DOM was also eluted with rainfall runoff, to which IPAs have strong potential to partition. Among the poultry litter samples tested in this study, at least one type of IPAs was detected in each litter sample at high concentrations, which agrees with previously published reports that considerable amounts of IPAs are consumed in poultry production industry.

**Table 2.5** The environmental occurrence of IPAs

IPAs	Runoff from unfertilized lands (ng/L)	Runoff from litter-fertilized lands (ng/L)			Top soil from unfertilized lands (µg/kg)	Top soil from litter-fertilized lands (µg/kg)			Poultry litter (µg/kg)		
	n	Min.	Med.	Max.	n	Min.	Med.	Max.	Min.	Med.	Max.
MON	17	ND	572	2389	3	5	101	183	ND	291	4057
SAL	ND	ND	ND	9022	ND		ND		ND	4607	21878
NAR		ND	ND	348			ND		ND	237	3310

ND, not detected. IPA concentration is lower than minimum detection limit

## **2.4 Conclusions**

This study has established reliable detection methods for widely used IPAs, including MON, SAL and NAR, in rainfall runoff, soil, and poultry litter. The clean-up methods were particularly optimized to achieve high recovery of IPAs in high organic matrices, such as poultry litter. NIG was validated as a suitable surrogate standard for use in the extraction of IPAs. The developed methods were successfully applied to detect IPAs in a wide range of environmental samples. The results showed that poultry litter contained considerable amounts of IPAs, which can be transported with rainfall runoff from poultry litter-fertilized fields to other environmental compartments.

## CHAPTER 3

### ESTIMATION OF ACIDITY CONSTANTS, METAL COMPLEXATION CONSTANTS AND AQUEOUS SOLUBILITY OF IPAS

#### 3.1 Introduction

Due to the low solubility of IPAs in water, the environmentally relevant chemical properties of IPAs, such as acidity constant ( $pK_a$ ) and IPA-metal complex dissociation constant ( $K_{diss}$ ), in the aqueous phase are difficult to obtain and limited in the literature. In addition, the literature reported water solubility limits of IPAs spanned a large range (0.85 – 905 mg/L, Table 1.1 in Chapter 1), which has not been explained in the previous studies and casts doubts on the accuracy of the data.

According to the literature, IPAs differ in their tendency to complex with alkali metal ions. For example, MON more favorably complexes with  $Na^+$  than with  $K^+$ , whereas SAL favors the opposite. However, it should be noted that, while many studies have reported the relative tendency of certain IPAs to complex with cations such as  $H^+$ ,  $Na^+$ ,  $K^+$  and  $NH_4^+$  (Cox *et al.*, 1984a; b; Degani, 1977; Duax *et al.*, 1980; Lutz *et al.*, 1970; Morf and Simon, 1971; Steinrau.Lk *et al.*, 1971), all of these experiments were conducted in organic solvents or water/solvent mixture, and thus the associated results may not be directly applicable to the aqueous environment. The  $pK_a$  values of IPAs were also previously measured in organic solvents, which were significantly different from the predicted values by the chemical properties estimation computer program SPARC (<https://archemcalc.com/sparc>) (Table 1.1 in Chapter 1).

Therefore, the aim of the research described in this chapter was to estimate the chemical properties of IPAs in aqueous phase, including acidity constant ( $pK_a$ ), metal-complex dissociation constant ( $K_{diss}$ ), and aqueous solubility of each IPA species.

## 3.2 Materials and Methods

### 3.2.1 General Methodology

The general methodology to estimate the  $K_a$ ,  $K_{diss}$ , and aqueous solubility of each IPA species was by measuring the total dissolved IPA under different pH and metal ion concentration conditions.

MON and SAL are carboxylic acids, which have strong affinity to complex with monovalent metal ions (e.g.,  $Na^+$  and  $K^+$ ) to form pseudo-cyclic conformation. Therefore, the total dissolved IPA ( $[IPA]_T$ ), in aqueous phase in the presence of metal ions, is the sum of three species: protonated IPA ( $[IPA-H]$ ), deprotonated IPA ( $[IPA^-]$ ), and metal-complexed IPA ( $[IPA-Me]$ ) (Equation 3.1). The aqueous concentrations of the three species are correlated by  $K_a$  and  $K_{diss}$  (Equations 3.2 and 3.3), where  $\gamma_{\pm 1}$  is the activity coefficient for metal ions, estimated by the extended Debye-Hückel equation.  $\gamma_{IPA^-}$ ,  $\gamma_{IPA-H}$  and  $\gamma_{IPA-Me}$  are the corresponding activity coefficients, which are assumed to be close to unity in this study.

$$[IPA]_T = [IPA-H] + [IPA^-] + [IPA-Na] \quad (3.1)$$

$$K_a = \frac{\{H^+\} \{IPA^-\}}{\{IPA-H\}} = \frac{\{H^+\} \cdot \gamma_{IPA^-} [IPA^-]}{\gamma_{IPA-H} [IPA-H]} = \frac{\{H^+\} [IPA^-]}{[IPA-H]} \quad (3.2)$$

$$K_{diss} = \frac{\{Me^+\} \{IPA^-\}}{\{IPA-Me\}} = \frac{\gamma_{\pm 1} [Me^+] \cdot \gamma_{IPA^-} [IPA^-]}{\gamma_{IPA-Me} [IPA-Me]} = \frac{\gamma_{\pm 1} [Me^+] [IPA^-]}{[IPA-Me]} \quad (3.3)$$

Therefore,  $[IPA]_T$  can be expressed by either Equation 3.4 or Equation 3.5.

$$[IPA]_T = \left( 1 + \frac{K_a}{\{H^+\}} + \frac{\gamma_{\pm 1} [Me^+]}{K_{di}} \cdot \frac{K_a}{\{H^+\}} \right) \cdot [IPA-H] \quad (3.4)$$

$$[IPA]_T = \left( 1 + \frac{K_{diss}}{\gamma_{\pm 1} [Me^+]} + \frac{\{H^+\}}{K_a} \cdot \frac{K_{diss}}{\gamma_{\pm 1} [Me^+]} \right) \cdot [IPA-Me] \quad (3.5)$$

Compared to the deprotonated IPAs, the protonated and metal complexed IPAs are

expected much less soluble in aqueous phase, because they are neutrally-charged apolar complexes (Schwarzenbach *et al.*, 2005). Therefore, the saturated concentration of total dissolved IPA in water ( $[IPA]_{T,sat}$ ) is either governed by the intrinsic solubility of IPA-H ( $[IPA-H]_{sat}$ ) or IPA-Me ( $[IPA-Me]_{sat}$ ).

### **3.2.2 Chemicals**

MON (97%) in the form of sodium salt from Sigma-Aldrich Co. (St. Louis, MO) and SAL sodium salt (96%) from MP Biomedicals Inc. (Solon, OH) were used without further purification. HPLC-grade methanol and chloroform, and analytical-grade formic acid (99%) were obtained from Sigma-Aldrich. Acetic acid, NaOH, KOH, HCl, Na<sub>2</sub>HPO<sub>4</sub>, and KH<sub>2</sub>PO<sub>4</sub> from Fisher Scientific were used to prepare pH buffer solutions. NaCl, KCl, and Ca(OH)<sub>2</sub> were purchased from Fisher Scientific. Reagent-grade water (resistivity 18 mΩ-cm) was produced by a nanopure Millipore water purification system (Millipore, Billerica, MA).

### **3.2.3 Experimental set-up**

The acid form of IPAs was prepared from sodium IPAs as previously reported (Gertenbach and Popov, 1975). Briefly, IPA-Na powder was first dissolved in chloroform at 5 g/L. This chloroform liquid was then mixed with 0.1 M HCl aqueous solution at 1:1 v/v ratio and shaken for 10 min. Then the aqueous phase was replaced by an equal volume of fresh 0.1 M HCl aqueous solution, followed by similar shaking. These steps were repeated three times in order to let the sodium that was complexed with IPAs fully exchange with proton. Then, an aliquot of the chloroform that contained mostly IPA-H was transferred to a 2 mL autosampler vial, followed by evaporation to dryness under vacuum. Finally, the IPA-H solid coated vials were spiked with 0.5

mL of aqueous solutions at different pH and metal ion conditions (see preparations detailed below) to reach saturation amount. All experiments were conducted at lab room temperature (~22°C).

To prepare aqueous solutions at low pH and low metal ( $\text{Na}^+$  and  $\text{K}^+$ ) ion conditions, an aqueous solution was made with 1 mM acetic acid and adjusted with pH by using calcium hydroxide. Because neither MON nor SAL are expected to have high affinity to complex with  $\text{Ca}^{2+}$  at acidic conditions, the concentration of IPA-Ca complex is expected to be negligible. To prepare aqueous solutions with conditions at high pH and varying metal ion concentrations, NaCl or KCl solution was added into sodium or potassium phosphate buffer at around pH 8.5.

#### ***3.2.4 IPA analysis***

The total dissolved IPA concentrations at the saturation level in the final samples were determined using an Agilent 1100 Series LC/MSD system (Agilent Technologies, Palo Alto, CA). The HPLC set-up was previously described in Sun et al. 2013 (Chapter 2). The mass spectrometer was set at positive electron-spray ionization mode (ESI+) with selective ion monitoring (SIM). The sum of peak areas of IPA-ion adducts with sodium, potassium, and ammonium ( $m/z$  of  $[\text{M}+23]$ ,  $[\text{M}+39]$ , and  $[\text{M}+18]$ , respectively) was used for quantification.

### 3.3 Experimental Results

#### 3.3.1 $pK_a$ determination

At low pH (i.e., < pH 5) with low sodium and potassium concentration (i.e., < 0.001 M) conditions, the dominant species of dissolved IPA were IPA-H and  $\text{IPA}^-$ . Under such conditions, Equation 3.4 can be simplified as Equation 3.6.

$$[\text{IPA}]_{\text{T,sat}} = [\text{IPA-H}]_{\text{sat}} + [\text{IPA}^-] = [\text{IPA-H}]_{\text{sat}} + K_a \cdot [\text{IPA-H}]_{\text{sat}} \cdot \frac{1}{\{\text{H}^+\}} \quad (3.6)$$

By varying the pH (within low pH conditions), a linear correlation was obtained between  $[\text{IPA}]_{\text{T,sat}}$  and  $1/\{\text{H}^+\}$  (Figure 3.1). From the linear correlation, the intercept represented  $[\text{IPA-H}]_{\text{sat}}$  and the slope represented  $K_a \cdot [\text{IPA-H}]_{\text{sat}}$ . The results are summarized in Table 3.1.

#### 3.3.2 $K_{\text{diss}}$ determination

Similarly, at high pH (i.e., pH 8.5) with increasing metal ion concentrations (i.e., 0.01 – 1 M), the dominant species of dissolved IPA were IPA-Me and  $\text{IPA}^-$ . Thus, Equation 3.5 can be simplified as Equation 3.7. By varying the metal ion concentrations, a linear correlation was obtained between  $[\text{IPA}]_{\text{T,sat}}$  and  $1/\{\text{Me}^+\}$ , with intercept as  $[\text{IPA-Me}]_{\text{sat}}$  and slope as  $K_{\text{diss}} \cdot [\text{IPA-Me}]_{\text{sat}}$  (Figures 3.2 – 3.4). Therefore, the intrinsic solubility of IPA-Me and  $K_{\text{diss}}$  could be obtained and the results summarized in Tables 3.1 and 3.2.

$$[\text{IPA}]_{\text{T,sat}} = [\text{IPA-Me}]_{\text{sat}} + [\text{IPA}^-] = [\text{IPA-Me}]_{\text{sat}} + K_{\text{diss}} \cdot [\text{IPA-Me}]_{\text{sat}} \cdot \frac{1}{\{\text{Me}^+\}} \quad (3.7)$$

**Table 3.1** Acidity constant ( $pK_a$ ), dissociation constant ( $K_{diss}$ ), and intrinsic solubility of different forms of IPAs in water (at 22°C)

	MON	SAL
$pK_a$	4.50±0.05	4.37 <sup>a</sup>
$K_{diss}$ (Na <sup>+</sup> ) (M)	0.058±0.008	1.31±0.25
$K_{diss}$ (K <sup>+</sup> ) (M)	0.573±0.072	NA <sup>b</sup>
[IPA-H] <sub>sat</sub>	76.6±7.5 μM	NA
[IPA-Na] <sub>sat</sub>	2.67±0.35 μM	108.1±19.9 μM
[IPA-K] <sub>sat</sub>	199.6±24.3 μM	NA
[IPA <sup>-</sup> ] <sub>sat</sub>	> 1200 μM	> 500 μM

<sup>a</sup> values predicted by SPARC; <sup>b</sup> NA, not analyzed

**Table 3.2** Dissociation constant ( $\text{Log}(K_{diss})$  (M)) of IPAs in different solvents

	MON		SAL	
	Na <sup>+</sup>	K <sup>+</sup>	Na <sup>+</sup>	K <sup>+</sup>
Water	-1.24 <sup>a</sup>	-0.24 <sup>a</sup>	0.12 <sup>a</sup>	NA
Methanol	-6.4 <sup>c</sup>	-4.9 <sup>c</sup>	-3.64 <sup>b</sup>	-5.52 <sup>b</sup>
Ethanol	-8.8 <sup>c</sup>	-7.2 <sup>c</sup>	NA <sup>e</sup>	NA
Bilayer lipid vesicle	NA	NA	-0.78 <sup>d</sup>	-1.31 <sup>d</sup>

<sup>a</sup> Measured in this study

<sup>b</sup> Narasin dissociation constants (Caughey *et al.*, 1986)

<sup>c</sup> (Cox *et al.*, 1984a)

<sup>d</sup> (Riddell and Tompsett, 1990)

<sup>e</sup> NA, not available

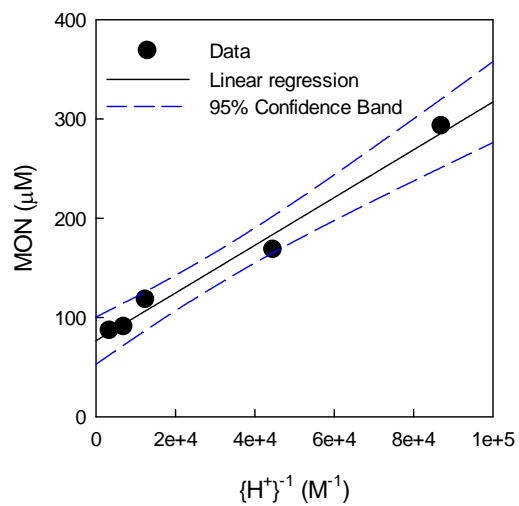


**Figure 3.1** Total dissolved MON in water at pH 3.55 – 4.94.

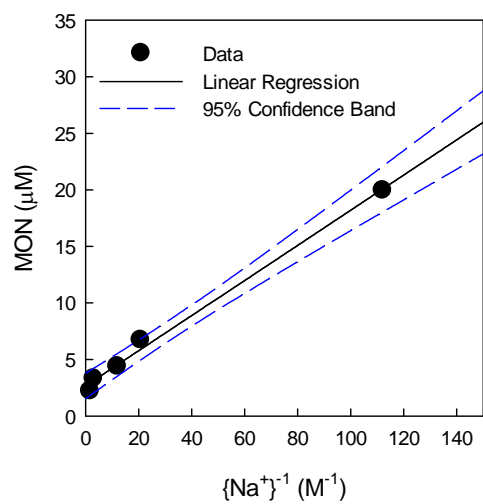


**Figure 3.2** Total dissolved MON in water at pH 8.5 with sodium concentration 0.01 – 1.0 M.

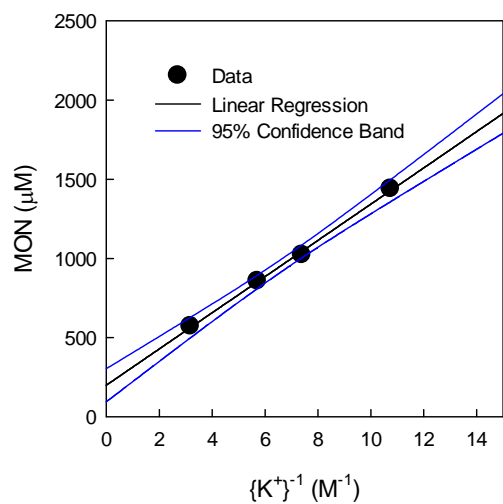


**Figure 3.3** Total dissolved MON in water at pH 8.5 with potassium concentration 0.15 – 0.4 M.

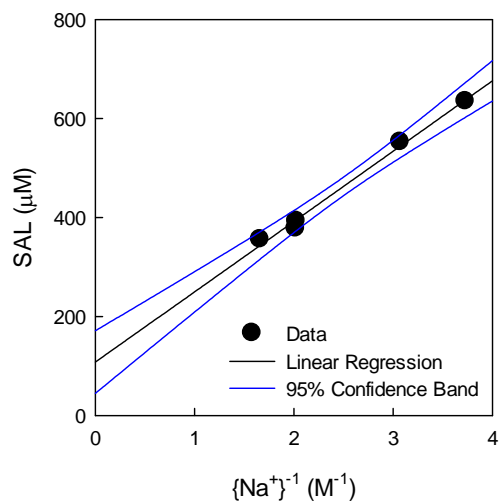


**Figure 3.4** Total dissolved SAL in water at pH 8.5 with sodium concentration 0.3 – 1.0 M.

## 3.4 Discussion

### 3.4.1 Justifications of assumptions

There are several key assumptions used to simplify the expression of total dissolved IPAs.

(1) Hydrolysis of MON. Because MON are not stable under acidic conditions, it is possible that the concentration measured after 12 hours may be lower than the true saturated concentration of total dissolved MON, if degradation of MON in the aqueous phase was at a comparable rate as the solvation rate of MON-H solid. According to our recent study, the half-lives of acid-catalyzed hydrolysis of MON at pH 3-5 were longer than 40 hours, which is expected to be substantially slower than MON-H solvation rate. The hypothesis that the hydrolysis of MON could be neglected is also supported by the observation that excess MON solid was observed after 12 h of solvation process. Therefore, it is reasonable to assume that the measured concentration was close to the saturated concentration of total dissolved MON at pH 3-5.

(2) Ionic strength estimation. In order to correct the activity of sodium and potassium ions, the extended Debye-Hückel equation for aqueous solution (Equation 3.8) was applied.

$$\log \gamma_{\pm 1} = -\frac{0.509\sqrt{I}}{1 + 3.29 \cdot \alpha_i \cdot \sqrt{I}} \quad (3.8)$$

where,  $\gamma_{\pm 1}$  is the activity coefficient for monovalent ions;  $I$  is the solution ionic strength; and  $\alpha_i$  is the diameter of sodium or potassium hydronium ions. However, cautions should be exercised on the results because the extended Debye-Hückel equation is usually used for solutions with ionic strength lower than 0.1 M, whereas the NaCl or KCl concentrations ranged from 0.01 to 1.0 M in this study. The Davies equation was not used in this study because (1) it does not distinguish sodium and potassium ions, and (2) activity coefficients obtained from the Davies equation

increase drastically with the increase of ionic strength from 0.8 to 1 M.

(3) Background concentrations of sodium and potassium ions. Glass containers are known to release sodium ions when soaked in water solution. Because the [IPA-H]-containing chloroform was evaporated in glass vials, which may introduce sodium ions during the process of re-dissolving IPA-H in sample solutions. However, a preliminary study using ICP-MS showed that the background sodium concentration in sample solution was lower than 1 mM. Considering the sodium concentrations (0.01 to 1 M) used in this study, the background sodium was negligible. For potassium ions, it is expected that glass vials release a lesser amount of potassium than sodium. Therefore, the background potassium can also be assumed negligible.

(4) Salting-out effect. The salting-out effect is known as that dissolved salt will lower water availability, which results in a decrease of total solubility of organic compounds (Schwarzenbach *et al.*, 2005). Therefore, it is expected that the total dissolved IPAs will decrease with the increase of NaCl or KCl concentrations. Because the hydrated sodium and potassium ions have comparable radius, the salting-out effect from NaCl and KCl is expected to be similar. However, the measured total dissolved IPA showed very different concentrations when exposed to the same amount of NaCl and KCl (Figures 3.2 and 3.3), which indicates the salting-out effect was unlikely responsible for the difference. Therefore, the salting-out effect was not considered in the simplified model (Equations 3.6 and 3.7)

### **3.4.2 $pK_a$ of IPAs**

As shown in Table 3.1, the experimentally determined  $pK_a$  of MON is  $4.50 \pm 0.05$  in this study, which is close to the value of 4.25 predicted by SPARC, but significantly lower than the  $pK_a$  values (6.65 - 6.7) determined in solvent/water mixtures (Table 1.1). The difference between

the  $pK_a$  values determined in water versus in solvent/water is expected because the neutrally-charged protonated form of IPAs (IPA-H) is likely much more soluble than  $IPA^-$  in organic solvent, resulting a higher percentage of IPA-H. Therefore, IPAs, like other carboxylic acid compounds, tend to form neutrally-charged protonated form (IPA-H) in organic solvents, resulting a much higher  $pK_a$ . Moreover, the  $pK_a$  value around 4.5 was also supported by the adsorption behavior of MON to different soil matrices (Sassman and Lee, 2007).

The  $[IPA-H]_{sat}$  and  $K_a$  values were only measured for MON, because the degradation of SAL was fast at pH lower than 5 (Sun *et al.*, 2013b). However, the predicted  $pK_a$  value, 4.37, of SAL by SPARC was expected to be a reasonable estimation based on the satisfactory agreement between the experimentally determined  $pK_a$  of MON and the value predicted by SPARC.

### 3.4.3 $K_{diss}$ of IPAs

The dissociation constants of MON with sodium and potassium ions were 0.058 and 0.573, respectively (Table 3.1). The values estimated in this study were significantly higher than the previous reported values measured in methanol (i.e.,  $\text{Log}(K_{diss, Na^+}) = -6.3$ ;  $\text{Log}(K_{diss, K^+}) = -4.9$ ) (Cox *et al.*, 1984b), and the values measured in ethanol (i.e.,  $\text{Log}(K_{diss, Na^+}) = -8.8$ ;  $\text{Log}(K_{diss, K^+}) = -7.3$ ) (Cox *et al.*, 1984a) (Table 3.2). As for SAL, the  $K_{diss}$  value of SAL with sodium ions was determined to be 1.31. Although the  $K_{diss}$  values of SAL in organic solvent are not available, it is expected that SAL has similar  $K_{diss}$  values in methanol as NAR (i.e.,  $\text{Log}(K_{diss, Na^+}) = -3.64$ ). Therefore, the  $K_{diss}$  value of SAL estimated in this study was also significantly higher than the values in methanol. However, the  $K_{diss}$  values in this study are in comparable range as other polyether compounds previously measured in water (e.g.,  $\text{Log}(K_{diss}(\text{Dicyclohexyl-18-crown-6}, Na^+)) = -1.85 - -1.2$  (M),  $\text{Log}(K_{diss}(\text{Cyclohexyl-18-crown-6}, Na^+)) = -0.8$  (M), and

$\text{Log}(K_{\text{diss}}(\text{Cyclohexyl-18-crown-6}, \text{K}^+)) = -1.9 \text{ (M)} \text{ (Frensdor.Hk, 1971)}$ .

Such a difference between  $K_{\text{diss}}$  values of IPAs determined in this study and the reported values, however, is expected because of the very different polarity of solvents employed. Indeed, the metal-complex neutral form, IPA-Me, is likely more soluble in less polar organic solvents, whereas deprotonated IPA is likely to dissolve more easily in more polar water. In particular, the polarity of solvents ranks in the order water > methanol > ethanol. Therefore,  $K_{\text{diss}}$  follows the same trend with decreasing value in water > methanol (> ethanol).

It is also interesting to note that, although the absolute difference of  $K_{\text{diss}}$  values was significant in different solvents, the relative difference of affinity to complex with sodium and potassium was small with respect to each solvent. Equation 3.9 expresses the relative affinity of IPAs to complex with potassium over sodium ions. The complexation constant,  $K_c$ , is expressed in Equation 3.10.



$$K_c = \frac{\{\text{IPA} - \text{K}\} \{\text{Na}^+\}}{\{\text{IPA} - \text{Na}\} \{\text{K}^+\}} = \frac{K_{\text{diss,Na}}}{K_{\text{diss,K}}} \quad (3.10)$$

where,  $K_{\text{diss,Na}}$  and  $K_{\text{diss,K}}$  are the dissociation constants with respect to each solvent. Therefore,  $\log(K_c)$  of MON were calculated to be -1.0, -1.4, and -1.5 in water, methanol and ethanol, respectively. The similar complexation constants indicate that the complexation of MON with sodium ions is around one magnitude more favorable than with potassium ions in all three solvents.

#### ***3.4.4 Intrinsic water solubility of IPA species***

As shown in Table 3.1, the intrinsic solubility of IPA species varied in the order  $[\text{MON-Na}]_{\text{sat}} < [\text{MON-H}]_{\text{sat}} < [\text{SAL-Na}]_{\text{sat}} < [\text{MON-K}]_{\text{sat}} \ll [\text{IPA}^-]_{\text{sat}}$ . The determined values supported

the assumption that the deprotonated form of IPAs are much more water soluble than the neutrally-charged forms. A previous study indicated that water molecule can interact with MON-H to form multiple hydrogen bonds with oxygen atoms on the cyclic-ether or alcohol moieties, whereas a sodium ion can fill in the MON cavity (Figure 1.2 in Chapter 1), eliminating interactions between MON and water. Therefore, it is expected the intrinsic water solubility of MON-H is higher than MON-Na (Gertenbach and Popov, 1975). The solid-state conformation of SAL with sodium was reported previously, which showed that the SAL-complexed sodium ion can coordinate with two water molecules as well (Paulus *et al.*, 1998). This result suggests that SAL-Na likely has stronger interaction with water, thus has higher water solubility than MON-H and MON-Na.

### 3.5 Conclusions

Determination of the chemical properties of IPAs, including acidity constant ( $K_a$ ), metal-complex dissociation constant ( $K_{diss}$ ), and water solubility of IPA species, was carried out in aqueous phase by measuring the total dissolved IPAs at saturation level under different conditions. The  $pK_a$  value of MON was found to be close to other aliphatic carboxylic acids (Schwarzenbach *et al.*, 2005), and the predicted value by SPARC. The  $K_{diss}$  values of IPAs were found to be significantly higher than the previously determined values in organic solvents. However, the relative selectivity of metal ions ( $Na^+$  versus  $K^+$ ) of IPAs was in the same order as that in organic solvents. Results from this study can be applied to predict speciation of IPAs and water solubility limits under different pH conditions with varying sodium and potassium concentrations.

## CHAPTER 4

# ACID-CATALYZED TRANSFORMATION OF IONOPHORE VETERINARY ANTIBIOTICS: REACTION MECHANISM AND PRODUCT IMPLICATIONS

### 4.1 Introduction

The acid- or base-catalyzed hydrolysis is among the most common transformation pathways of organic contaminants in the aquatic environment. Previous studies indicate that IPAs may be unstable under acidic conditions (Agtarap *et al.*, 1967; EFSA., 2004; Wells *et al.*, 1988). Agtarap *et al.* showed MON transformed to yield an amorphous solid when treated in acetic anhydride-pyridine (Agtarap *et al.*, 1967). Wells *et al.* detected degradation products of SAL and NAR after treating them with high concentrations of formic acid in tetrahydrofuran solvent (Wells *et al.*, 1988). IPAs' instability in acidic conditions was also documented in two scientific reports of coccidiostats by the European Food Safety Authority (EFSA) (EFSA., 2004; 2005). However, the studies cited above employed experimental conditions that were poorly defined or not applicable to the environment. Furthermore, little information exists regarding degradation kinetics, transformation mechanisms or products for IPAs. Therefore, the objectives of this study were to assess different IPAs' hydrolytic transformation potential, characterize the reactions' pH dependence and kinetics, elucidate transformation products and mechanisms, and evaluate toxicity of the transformation products. Preliminary analysis was also conducted to assess the occurrence of IPAs and transformation products in environmental samples. To the authors' best knowledge, this study is among the first to report and elucidate acid-catalyzed transformation of IPAs under environmentally relevant aquatic conditions.

## 4.2 Materials and Methods

### 4.2.1 Chemicals

MON (97%) and NAR (97%) in the form of sodium salt from Sigma-Aldrich Co. (St. Louis, MO) and SAL sodium salt (96%) from MP Biomedicals Inc. (Solon, OH) were used without further purification. HPLC-grade methanol (99.9%), and analytical-grade formic acid (99%) were obtained from Sigma-Aldrich. Acetic acid, NaOH, HCl, Na<sub>2</sub>HPO<sub>4</sub>, NaH<sub>2</sub>PO<sub>4</sub> and sodium borate from Fisher Scientific were used to prepare pH buffer solutions. NaCl, KCl, NH<sub>4</sub>Cl and Ca(OH)<sub>2</sub> were purchased from Fisher Scientific. Reagent-grade water (resistivity 18 mΩ-cm) was produced by a nanopure Millipore water purification system (Millipore, Billerica, MA). IPA stock solutions (50 mg/L) were prepared in methanol and stored at 4°C prior to use.

### 4.2.2 Hydrolysis experiment

All glassware was rinsed several times with reagent-grade water and methanol, and dried at 105°C. Reaction solutions were maintained at desired pH using 5 mM buffer: acetic acid plus HCl or NaOH for pH 3.0 - 5.0, mono- and di-sodium phosphates for pH 6.0 - 8.0, and sodium borate plus HCl for pH 9.0 - 10.0. Ionic strength was fixed at 0.1 M by addition of NaCl. Hydrolysis experiments were conducted in amber borosilicate bottles to minimize any potential photolytic reactions and were initiated by spiking an appropriate amount of individual IPA methanolic stock solution into the buffered solution. The methanol content of reaction solution was below 2% (v/v). Reaction solution was continuously stirred using a Teflon-coated stir bar at 22°C and aliquots were periodically taken for analysis.

### **4.2.3 Analytical methods**

#### **4.2.3.1 Chemical analysis**

The concentrations of IPAs were monitored by an Agilent 1100 Series LC/MSD system (Agilent, Palo Alto, CA) equipped with a reversed-phase column (2.1×150 mm, 3 μm Ascentis RP-amide column, Supelco, Bellefonte, PA). The column was maintained at 40°C with a flow rate of 0.30 mL/min. Mobile phase consisted of (A) a mixture of HPLC-grade water and formic acid (99.9:0.1 v/v) to maintain around pH 2.2, and (B) HPLC-grade methanol. The gradient of mobile phase B was ramped from 50% to 90% in the first 8 minutes and to 100% at 12 minutes. Then, the system was running at 100% methanol for 3 minutes. The injection volume was 25 μL. A five minute post-run period was allowed between each analysis to re-equilibrate the column with mobile phase (50% A and 50% B). The mass spectrometer was set at positive electrospray ionization mode (ESI+) with a 70 V fragmentation voltage and +4500 V for the capillary voltage. Nitrogen was used both as nebulizer gas (35 psi) and drying gas at 350°C (6.0 L/min). A full-scan mode from 100 to 1700 m/z was applied for detecting the parent IPAs as well as searching for transformation products. The sodium adducts of IPAs with a m/z of [M+23] were used in quantification of parent IPAs.

An Agilent 1100 HPLC system with a diode-array (DAD) UV detector was also used to analyze the transformation products. The HPLC conditions including column, mobile phase composition and flow rate were the same as those described above for LC/MS, with only small changes in the eluent gradient program. To characterize transformation products, the UV detector was set at scan mode from 190 nm to 400 nm.

A Shimadzu (Columbia, MD) HPLC and Applied Biosystems (Foster City, CA) 4000 Q-Trap Model HPLC-tandem MS system was also used to examine the structures of IPAs'

transformation products. The HPLC parameters were set at the same conditions as those for LC/MSD. The tandem mass spectrometer was set at product-full-scan mode for the purpose of obtaining sufficient fragment information for structure elucidation. The MS parameters for MON products were  $m/z$  693.4 for selected ion, declustering potential (DP) = 60 eV, entrance potential (EP) = 10 eV, collision energy (CE) = 75 eV, and cell exit potential (CXP) = 21 eV. The MS parameters for SAL products were selected ion =  $m/z$  773.4, DP = 60 eV, EP = 10 eV, CE = 85 eV, and CXP = 10 eV.

#### *4.2.3.2 Protocols for detection of IPAs in field samples*

To detect IPAs and their transformation products in field samples, sample preparation was conducted following the developed analytical method in Chapter 2. Briefly, solid phase extraction (SPE) was applied to extract IPAs from rainfall runoff samples. Nigericin (NIG) was spiked into the runoff sample before performing SPE. For poultry litter samples, bi-phase solvent extraction was applied to extract IPAs using NIG as the surrogate standard. The final extract was transferred into a HPLC amber vial for LC/MS analysis.

#### *4.2.4 Toxicity tests for transformation products*

The antimicrobial property of MON and its transformation products was tested against Gram(+) bacteria *Bacillus subtilis* (ATCC 6633). Since standards of transformation products are not commercially available, it is difficult to assess the toxicity of the products individually. Instead, a sample aliquot was taken at each selected time interval from a hydrolytic reaction of MON at pH 3.0, neutralized to pH 7 by a small amount of concentrated NaOH solution, mixed

with culture medium, and the combined mixture was spiked with pre-cultured *Bacillus subtilis* to achieve OD600 (i.e. optical density measured at 600 nm wavelength) around 0.1 units. The culture medium including carbon sources was Mueller Hinton Broth from Fluka (St. Louis, MO). Control experiments were performed by replacing hydrolysis samples with reagent water. Reference tests were also performed by replacing hydrolysis samples with a standard solution of MON at a concentration identical to that of the remaining MON in the hydrolysis reaction at each time point. Experiments were conducted in triplicates for each condition. Cultures were incubated under aerobic conditions at 22°C with continuously shaking for 12 hours. OD600 of each culture was then measured as an indication of bacteria growth.

## 4.3 Results and Discussion

### 4.3.1 Hydrolysis of IPAs under acidic conditions

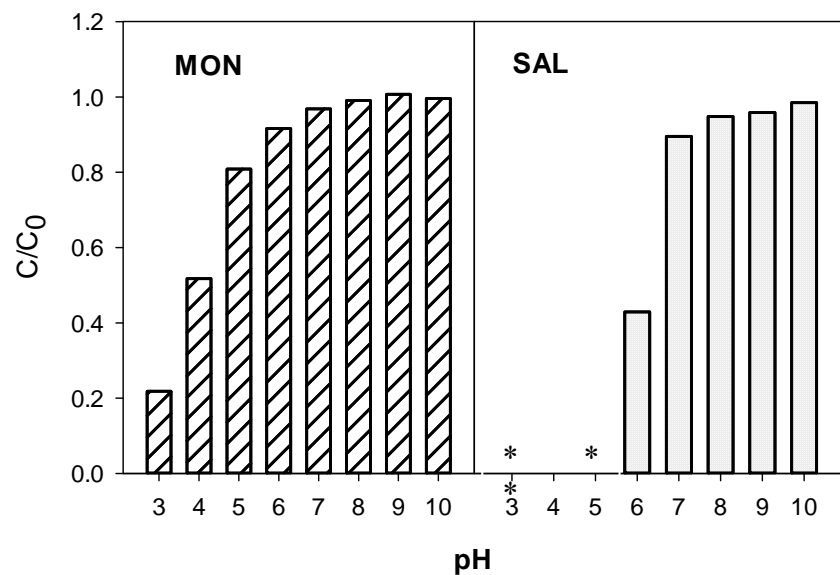
Preliminary experiments that examined the stability of MON and SAL in aqueous solutions at pH 3.0 to 10.0 showed that the parent IPAs were stable at pH above 7.0 over an one-week period (Figure 4.1). However, significant degradation of parent IPAs was observed at acidic conditions. After 7 days, 78, 48, 19, and 8% of parent MON degraded at pH 3, 4, 5 and 6, respectively. For SAL, the parent compound was not observed at the end of 7 days of reaction at pH 3, 4 and 5, whereas 43% of SAL remained at pH 6.

Results from further experiments to investigate the reaction kinetics of IPA's hydrolytic transformation at pH 3.0 to 7.0 are shown in Figure 4.2. The reaction was faster at lower pH. The logarithm of the concentration ratio ( $\ln(C_t/C_0)$ ) versus time plots were linear ( $R^2 > 0.98$ ) for SAL and NAR, from which the first-order decay rate constants and the corresponding half-lives were calculated and listed in Table 4.1. However, MON's  $\ln(C_t/C_0)$  vs. time curve was non-linear,

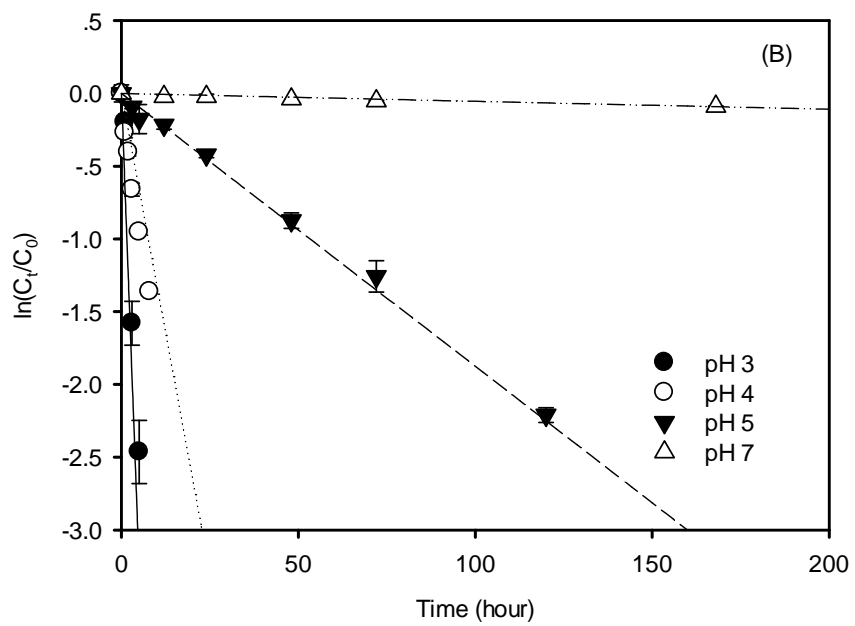
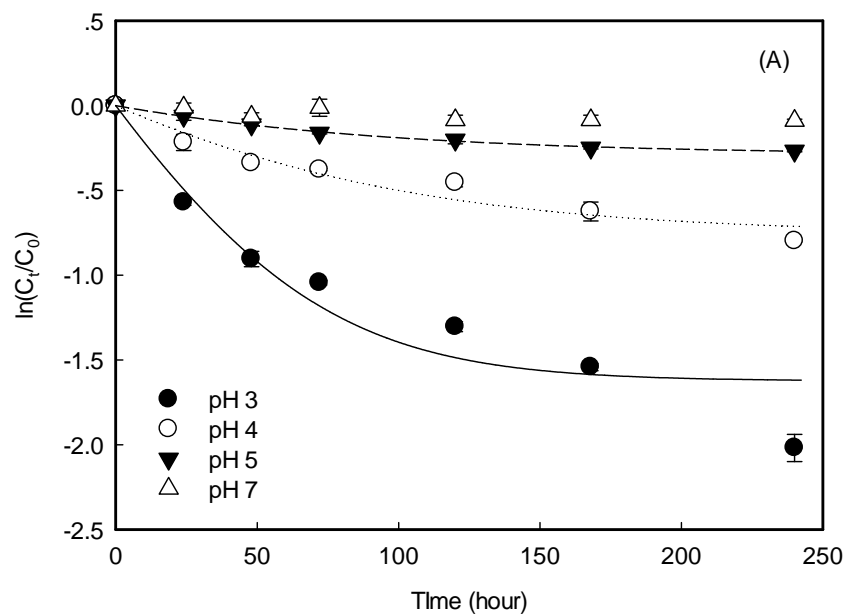
suggesting the decay of MON does not follow first-order kinetics. The half-lives of MON at different pH values estimated from the decay plots are also listed in Table 4.1. Evidently, SAL and NAR exhibited comparable instability at each pH, whereas MON took approximately 40 times longer than SAL and NAR to degrade to half of its initial concentration under the same conditions.

The similar transformation kinetics of SAL and NAR may be expected because their structures closely resemble each other with only one difference by a methyl substituent on the A ring (NAR has one additional methyl group, see Figure 1.1). However, it is somewhat surprising that MON exhibited a much slower degradation rate and much different kinetic behavior compared to SAL and NAR, since overall MON's structure also contains several similar moieties to those in SAL and NAR such as the A, D and E rings, and the end carboxylate group (see Figure 1.1).

Extensive literature review found an early study which reported isomerization of the spiro-ketal group of steroidal sapogenins with acids in heated alcoholic solutions (Callow and Massyberesford, 1958). Two other studies that treated IPAs with high concentrations of organic acids such as formic acid also reported alteration of the spiro-ketal moiety of MON, SAL and NAR (Agtarap *et al.*, 1967; Wells *et al.*, 1988). Thus, the IPA transformation at pH 3-6 observed in this study is likely related to their spiro-ketal groups (i.e. the A-B ring system in MON and the B-C-D ring system in SAL and NAR). Also, the faster degradation rate of SAL and NAR than MON suggests that the three-ring spiro-ketal structure in SAL and NAR is more susceptible to this acid-catalyzed transformation than the two-ring spiro-ketal structure in MON. The above hypotheses are further supported by the identified transformation products that will be discussed in detail later.



**Figure 4.1** The ratio of IPA concentration after 7 days of reaction to the initial IPA concentration at different pH values. \*No parent SAL was observed in pH 3–5 samples after 7 days of reaction. Initial concentration of IPA was 500  $\mu\text{g/L}$ .



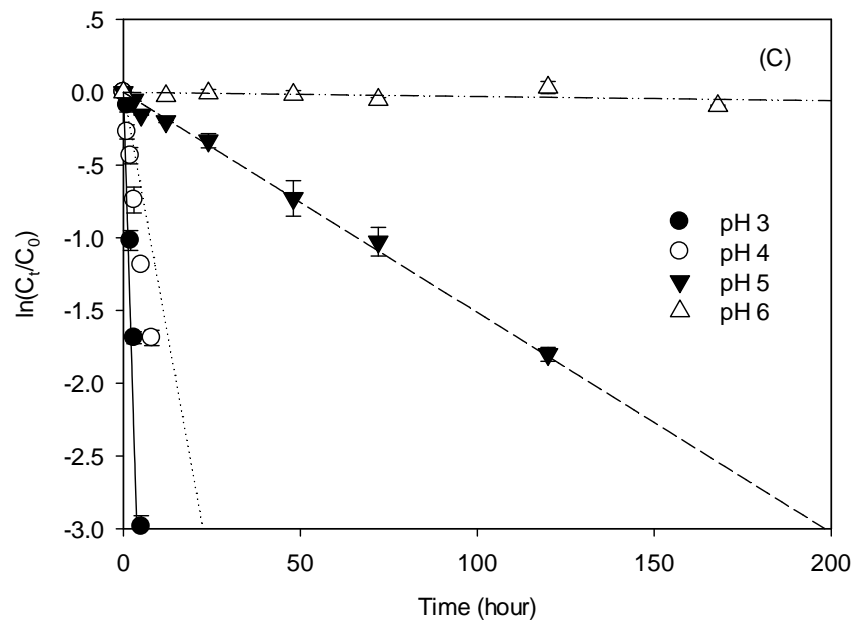


**Figure 4.2** Hydrolysis of (A) MON, (B) SAL and (C) NAR at acidic conditions. Initial concentration of IPA was 1  $\mu\text{M}$ .  $C_0$  and  $C_t$  are IPA concentration at time 0 and  $t$ , respectively. Error bars represent standard deviations of data from triplicate samples. Lines are model fits (see text).

### 4.3.2 Kinetic modeling of IPA transformation

According to Figures 4.2B and 4.2C, degradation of SAL and NAR follows first-order kinetics and can be expressed using Equation 4.1 with the observed first-order rate constant,  $k_{obs}$  ( $\text{h}^{-1}$ ).

$$\frac{d[IPA]}{dt} = -k_{obs} \cdot [IPA] \quad (4.1)$$

Because SAL and NAR are expected to only react with protons,  $k_{obs}$  can be further expressed by the rate constant  $k_{IPA/H^+}$  ( $\text{M}^{-n} \cdot \text{h}^{-1}$ ) multiplied by proton activity with its proper reaction order  $n$  (Equation 4.2).

$$k_{obs} = k_{IPA/H^+} \cdot \{H^+\}^n \quad (4.2)$$

By plotting  $\log(k_{obs})$  versus pH (Figure 4.3),  $k_{IPA/H^+}$  was found to be 132.8 and 302.0, and  $n$  was 0.77 and 0.86, for SAL and NAR, respectively. Thus, the hydrolysis of SAL and NAR in the presence of protons can be expressed by Equation 4.3, which can be used to predict the hydrolysis rate at any given pH.

$$\frac{d[SAL]}{dt} = -132.8 \cdot \{H^+\}^{0.77} \cdot [SAL], \text{ and } \frac{d[NAR]}{dt} = -302.0 \cdot \{H^+\}^{0.86} \cdot [NAR] \quad (4.3)$$

The proton order  $n$  values are considered close to 1 within the uncertainty of experimental data, implying that the hydrolytic transformation of SAL and NAR is likely initiated by one molecule of IPA reacting with one proton. The good correlations between the first-order rate constant and proton concentration also indicate that the initial reaction with proton is likely the rate-determining step for the hydrolysis of SAL and NAR.

In contrast, transformation of MON (Figure 4.2A) shows non-first-order kinetics, suggesting the overall hydrolysis rate is not only determined by the initial reaction with protons, but also related to the transformation kinetics of intermediates. A preliminary hydrolysis

experiment showed the peak area of MON could partially be recovered after adjusting the solution pH from 3 to 9 (data not shown). Hence, it is reasonable to consider a backward reaction from MON's hydrolysis products ( $MP_t$ ) to parent MON simultaneously with the forward reaction. Thus, the overall hydrolysis of MON is expressed as:



where  $k_1$  is MON hydrolysis forward reaction rate constant and  $k_{-1}$  is the backward reaction rate constant of  $MP_t$  to MON.

Based on reaction 4.4, the kinetics of MON hydrolysis can be expressed by Equation 4.5:

$$\frac{d[\text{MON}]}{dt} = -k_1[\text{MON}] + k_{-1}[\text{MP}_t] \quad (4.5)$$

At any given time,  $[\text{MON}]_0 = [\text{MON}] + [\text{MP}_t]$ , where  $[\text{MON}]_0$  is the initial concentration of MON. Hence,

$$[\text{MON}] = [\text{MON}]_0 \frac{(k_1)\exp(-(k_1 + k_{-1})t) + k_{-1}}{(k_1 + k_{-1})} \quad (4.6)$$

Fitting Equation 4.6 to the experimental data using Matlab yielded  $k_1$  and  $k_{-1}$  values at different pH ( $R^2 = 0.95 - 0.99$ ) as listed in Table 4.1. As shown in Figure 4.2A, this model successfully described the kinetics of MON transformation at pH 4 and 5. At pH 3, although the overall fitting  $R^2$  value was 0.98, the model represented only the initial reaction stage (up to 70 hours) consistently but did not capture the later decay trend well. The different kinetic behavior of MON at pH 3 suggests that MON may transform via different pathways at the stronger acidic conditions, leading to both reversible and irreversible formation of transformation products. At pH 4 and above, the proposed mechanism (Equation 4.4) predominates and thus the proposed model is adequate. These kinetic features are further supported by MON's transformation products analysis as discussed below.

**Table 4.1** Hydrolysis rate constants and half-lives of IPAs at pH 3-5

IPA	$k$ ( $\text{h}^{-1}$ )			$t_{1/2}$ (h)		
	pH 3	pH 4	pH 5	pH 3	pH 4	pH 5
MON	0.0222* (0.0054) <sup>†</sup>	0.0072* (0.0064) <sup>†</sup>	0.0029* (0.0088) <sup>†</sup>	40.0	159.8	N.A.
SAL	0.522	0.167	0.017	1.3	4.2	40.8
NAR	0.634	0.212	0.014	1.1	3.3	49.5

\*The first-order decay constants ( $k$ ) of MON shown in this table without parentheses are for the forward reaction.

<sup>†</sup> Data in parentheses are the backward reaction rate constants ( $k_{-1}$ ) of MON.

N.A. = not available

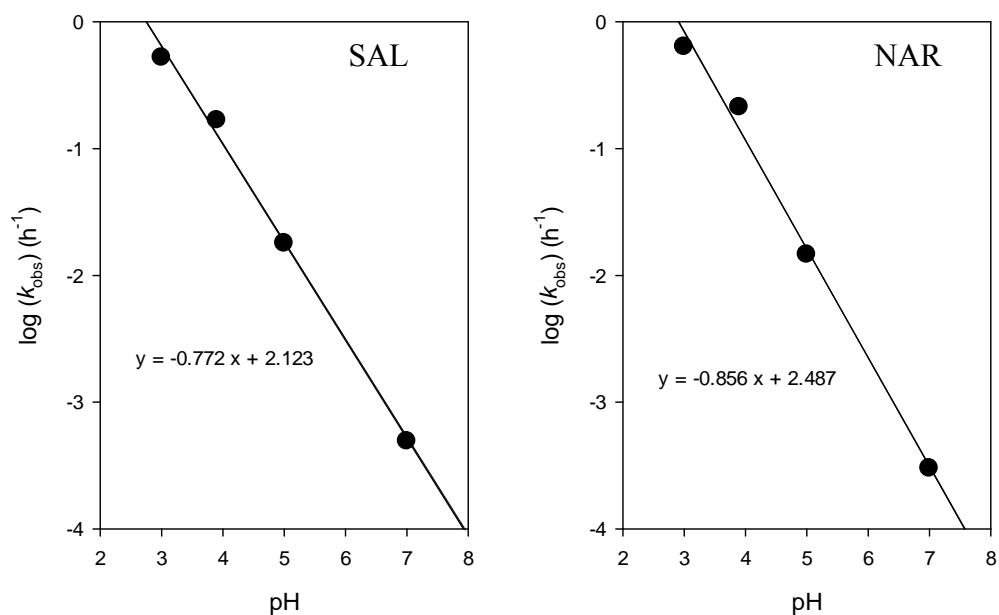


**Figure 4.3** Regression of the log of first-order rate constant  $k_{\text{obs}}$  versus pH plot for SAL and NAR. The 95% confidence interval for the regression slope is 0.624 – 0.921 for SAL and 0.633-1.079 for NAR.

### 4.3.3 Transformation products and pathways

The IPAs' transformation products were first analyzed by LC/MS, which was set at the same operational conditions for detecting parent IPAs. Multiple new peaks representing products of IPAs were observed after hydrolysis. LC/MS/MS and LC/UV analyses were further conducted to provide additional structural information for product identification. Finally, experiments were conducted in D<sub>2</sub>O with DCI to confirm the proposed transformation pathways and the role of protons. In the following section, the transformation pathways of MON and SAL will be discussed in detail. NAR was not investigated in depth because it is expected to undergo similar hydrolysis pathways as SAL on the basis of their identical structural moiety that is susceptible to hydrolysis.

**Monensin.** In all experiments, one major hydrolysis product of MON (named MP1) was observed at pH 4 and 5 by LC/MS (Figure 4.4B), and two other hydrolysis products in addition to MP1 were observed at pH 3 (named MP2 and MP3) (Figure 4.4A). MP1 and MP2 have the same molecular weight (MW) of parent MON ( $m/z$  693,  $[M+Na]^+$ ), indicating they are isomers of MON. MP3 has  $m/z$  of 675, 18 Da lower than MON, suggesting one water molecule was eliminated from parent MON or from the isomeric hydrolysis products. Note that all hydrolysis products were eluted before parent MON (LC retention time was 9.3, 8.9, 9.6, 10.0 min for MP1, MP2, MP3 and MON, respectively). Because reverse-phase liquid chromatography was used, this observation indicates the isomeric products are less lipophilic than the parent MON. The peak area of MP1 increased at first but gradually decreased after 24 hours of reaction, suggesting MP1 could be a product which could transform back to parent MON or an intermediate between MON and other products.

LC/MS/MS was employed to obtain more structural information of the isomeric transformation products. The  $m/z$  693.4 ions were selected from the full-scan analysis of products and subjected to collision activated dissociation (CAD) using MS<sup>2</sup> set-up identical to that for parent MON. The mass spectrum of MP1 was nearly identical to that of MON, with common base peaks at  $m/z$  461.4, 479.3 and 501.3 (Figure 4.5). The mass spectrum of MP2, while sharing similar base peaks as that of MON, exhibited a more different fragmentation pattern and a new base peak at  $m/z$  519 that MON and MP1 did not have (Figure 4.5C). LC/UV analysis at 200-400 nm showed little significant absorbance by the hydrolysis products at pH 3 and above.

On the basis of the above observations and the mechanism proposed by Perron and Albizati (Perron and Albizati, 1989), a plausible transformation pathway of MON is proposed in Figure 4.6. The acid-catalyzed transformation of MON is initiated by protonation of one of the spiro-ketal's oxygen atoms (the A-B ring) to yield intermediate 1 (MI1). The resulted positive charge facilitates O(+)-C5 bond breakage and C=O bond formation involving the other spiro-ketal oxygen atom, leading to intermediate 2 (MI2). C5 then picks up the hydrogen atom on C1, yielding intermediate 3 (MI3), which is the central intermediate of MON hydrolysis pathways. The above transformation is likely reversible, and the reverse reaction of MI3 may generate MON or the diastereomer MP1 via racimization of C1 and C5 (from MI3 to MI5). Hence, MP1 is a reversible transformation product of MON, which supports the reversible reaction kinetic model (Equation 4.4) proposed for MON transformation earlier.

Alternative to the reverse reaction to MON or MP1, MI3 may transform into MP2 (Figure 4.6). MP2 is the result of a permanent ring breakage and thus is not a reversible transformation product. The unique fragment of  $m/z$  519 from MP2 in the LC/MS/MS spectrum

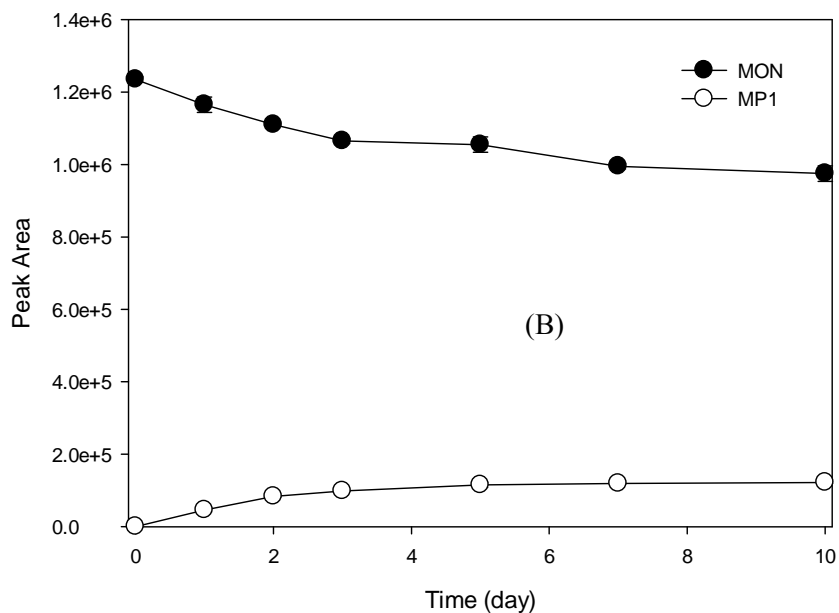
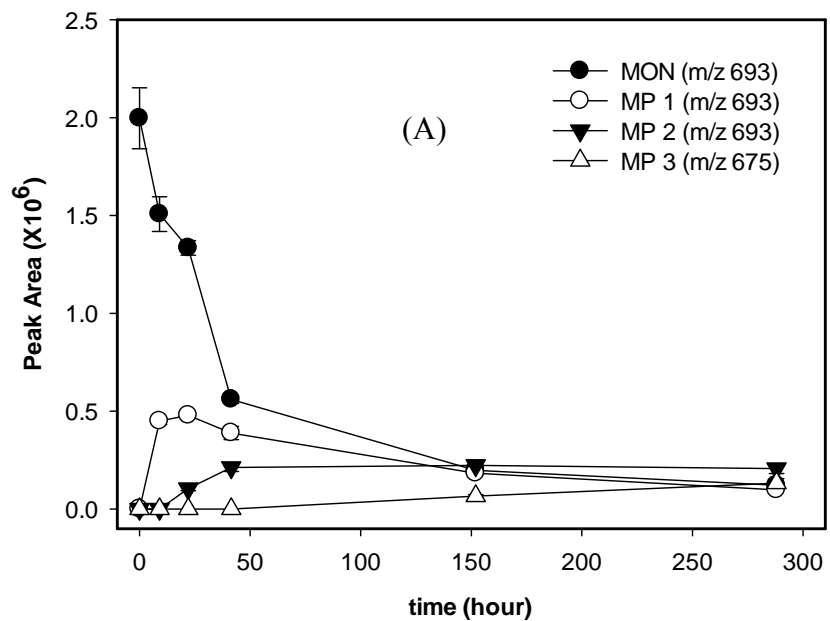
can be explained by cleavage from its C1-C2 ketone-carbon bond in the opened ring (see Figure 4.5C), whereas the structure of MON and MP1 is much less likely to generate  $m/z$  519 fragment. Further elimination of a water molecule from MP2 (possibly also facilitated by  $H^+$ ) then yields MP3 (Figure 4.6). MP2 and MP3 products were observed only at pH 3, not at pH 4 and 5; this result is consistent with the lesser agreement between the reversible kinetic model and experimental data at pH 3 (Figure 4.2A).

According to the proposed mechanism, proton only acts as a catalyst in the reactions. A separate experiment using DCl (instead of HCl) was performed in  $D_2O$  (instead of  $H_2O$ ). Results indicated no change in the  $m/z$  of the transformation products, meaning that deuterium atom was not incorporated into the products, and thus confirmed the catalytic role of proton.

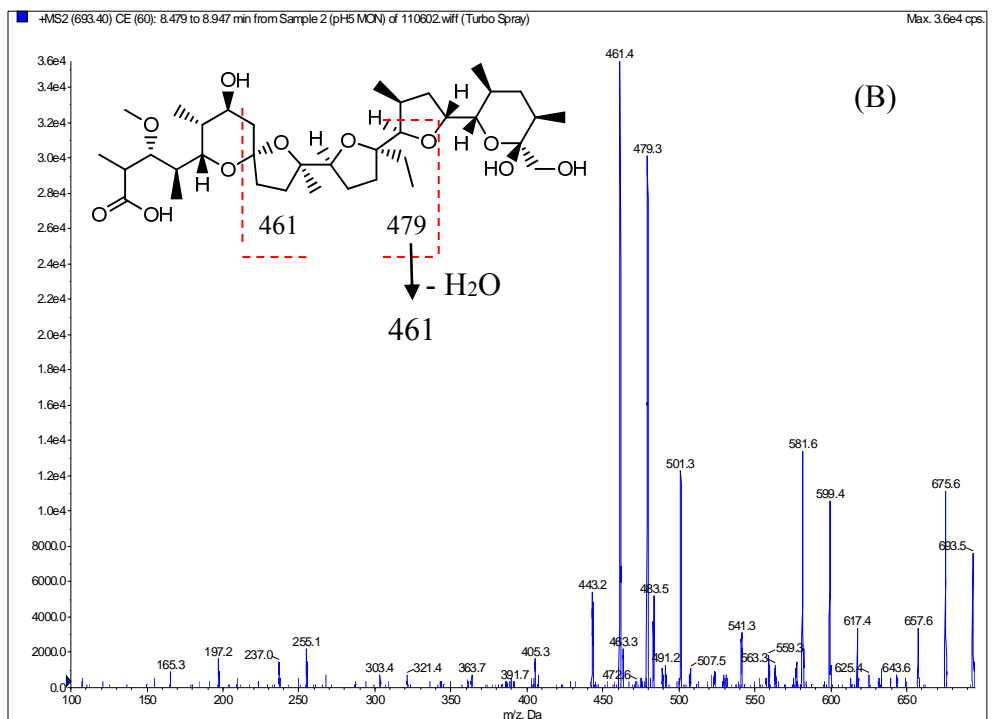
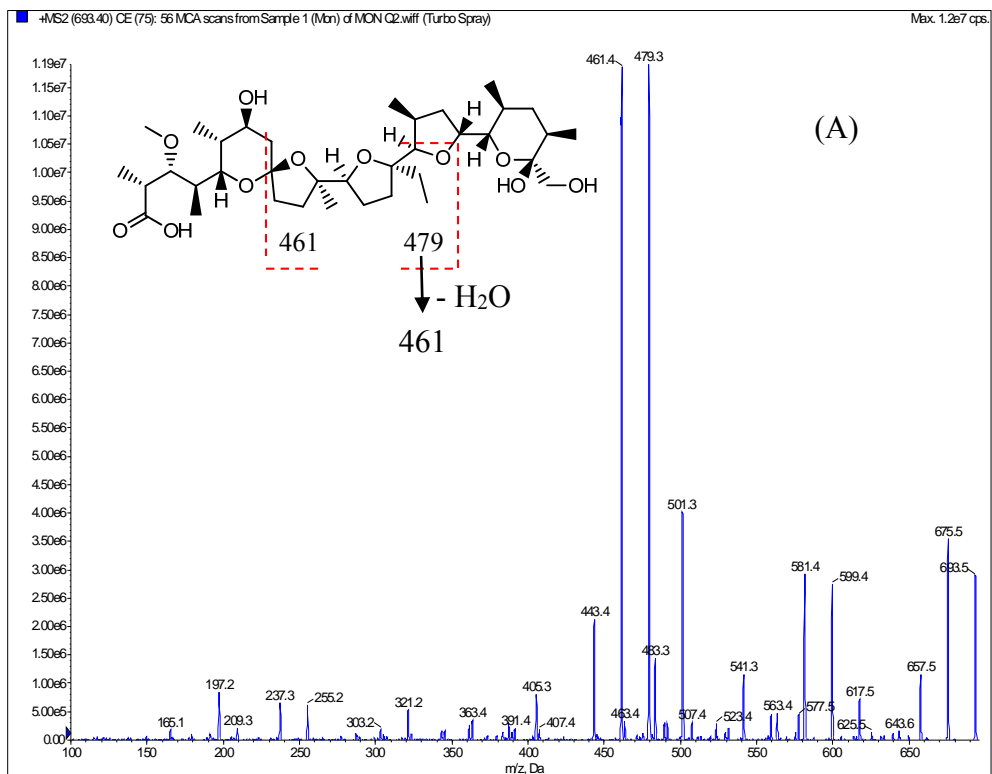
Note that select hydrolysis experiments of MON were conducted at pH 2.0 for 12 hours, which yielded two products (named MP4 and MP5) that exhibited distinct UV absorbance at 235 nm and 290 nm, respectively (Figure 4.7). UV absorption at above 200 nm may indicate presence of conjugated  $\pi$  bonds. It is hypothesized that MP4 may be the same as MP3, since MP3 possesses two conjugated double bonds and may absorb light at around 235 nm. At pH 3, the amount of this product was very low and thus no significant UV absorbance could be detected. A significant amount of this product was formed at pH 2 and thus yielded a detectable UV absorbance.

In the earlier study by Agtarap *et al.*, 1967, MON was treated with strong acid to yield a product (proposed structure shown in Figure 4.8) with three conjugated double bonds. Since typically absorption at a higher wavelength represents a higher order of  $\pi$  bond conjugation, MP5 (UV absorption at 290 nm) is considered to correspond to the product proposed by Agtarap

*et al.*, 1967. Both products (MP4 and MP5) are unlikely important in most environmental conditions owing to their generation only under strongly acidic conditions.



**Figure 4.4** MON hydrolysis products at pH 3 (A) and pH 5 (B) buffered by acetic acid and HCl. Ionic strength was fixed with 0.1 M NaCl. The m/z values represent sodium adducts of parent MON and its products (i.e.  $[M + 23]^+$ ).



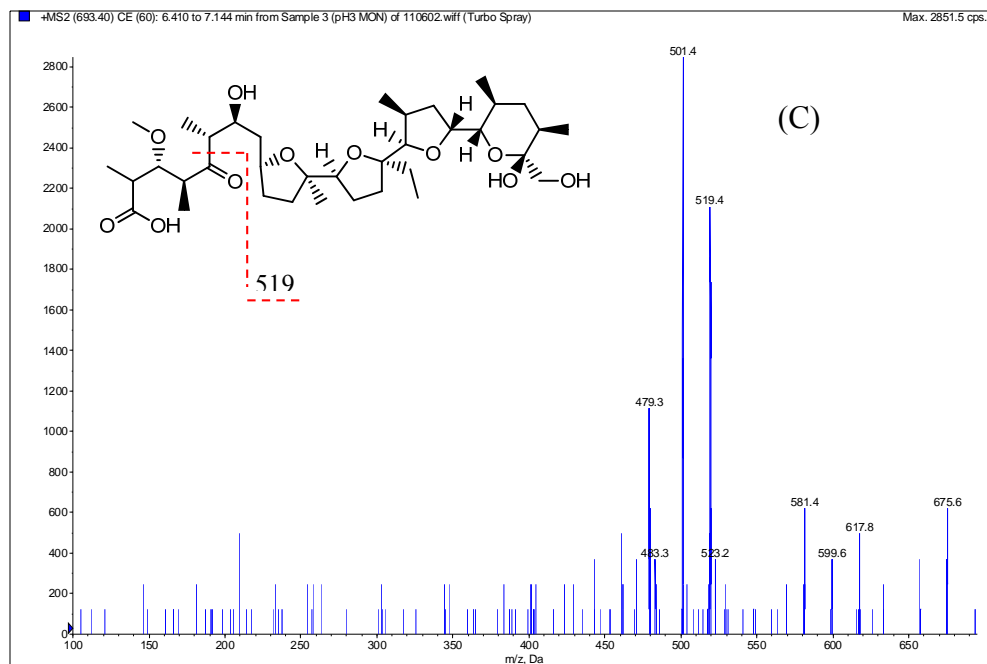


**Figure 4.5** LC/MS/MS spectra of (A) MON, (B) MP1 and (C) MP2.

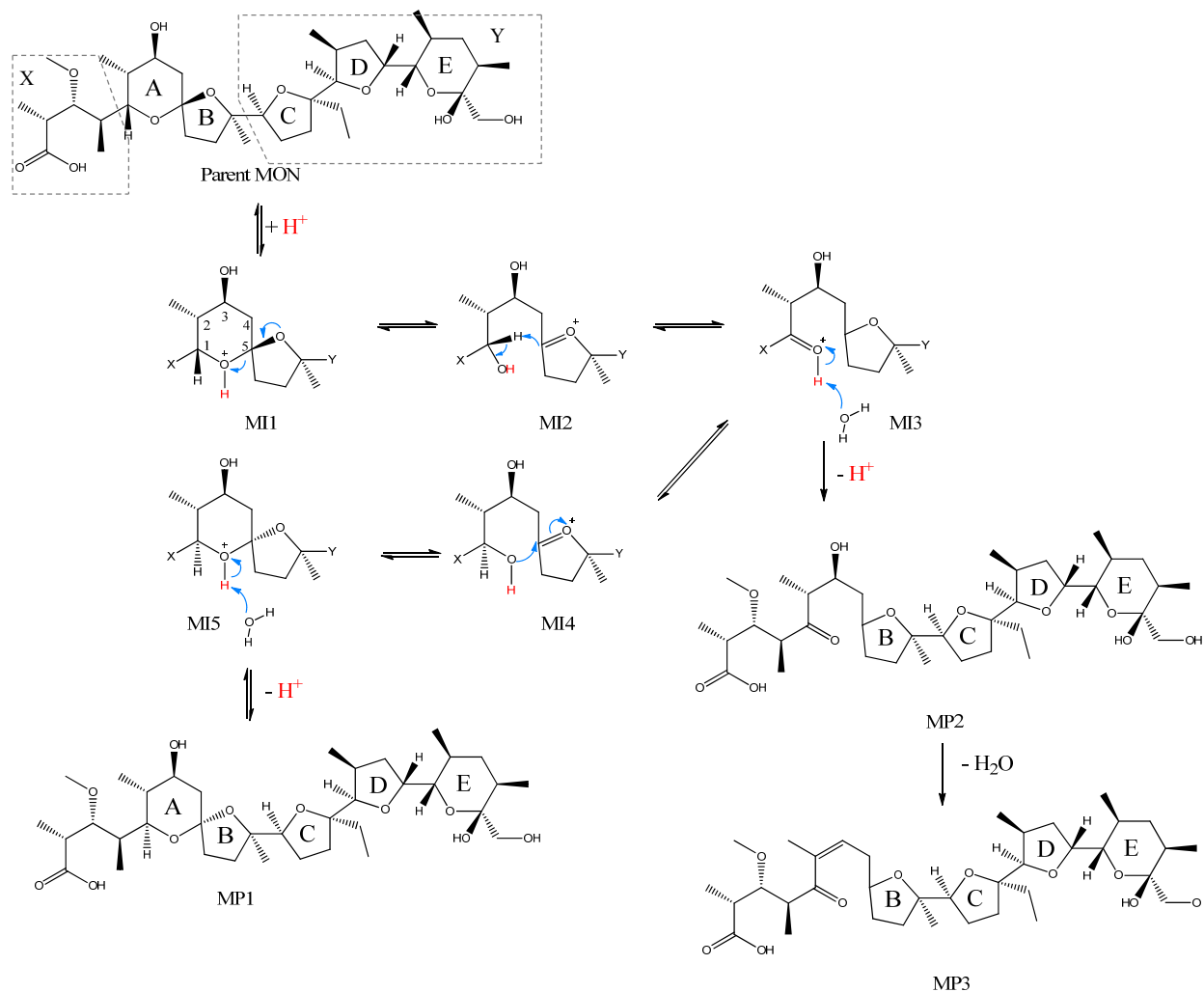


**Figure 4.6** Proposed acid-catalyzed transformation pathways of MON with mechanism of reactions from parent MON to MP1 and MP2. Note: MP represents products and MI represents intermediates of MON transformation. Hydrogen atoms in red represent protons from aqueous solution.

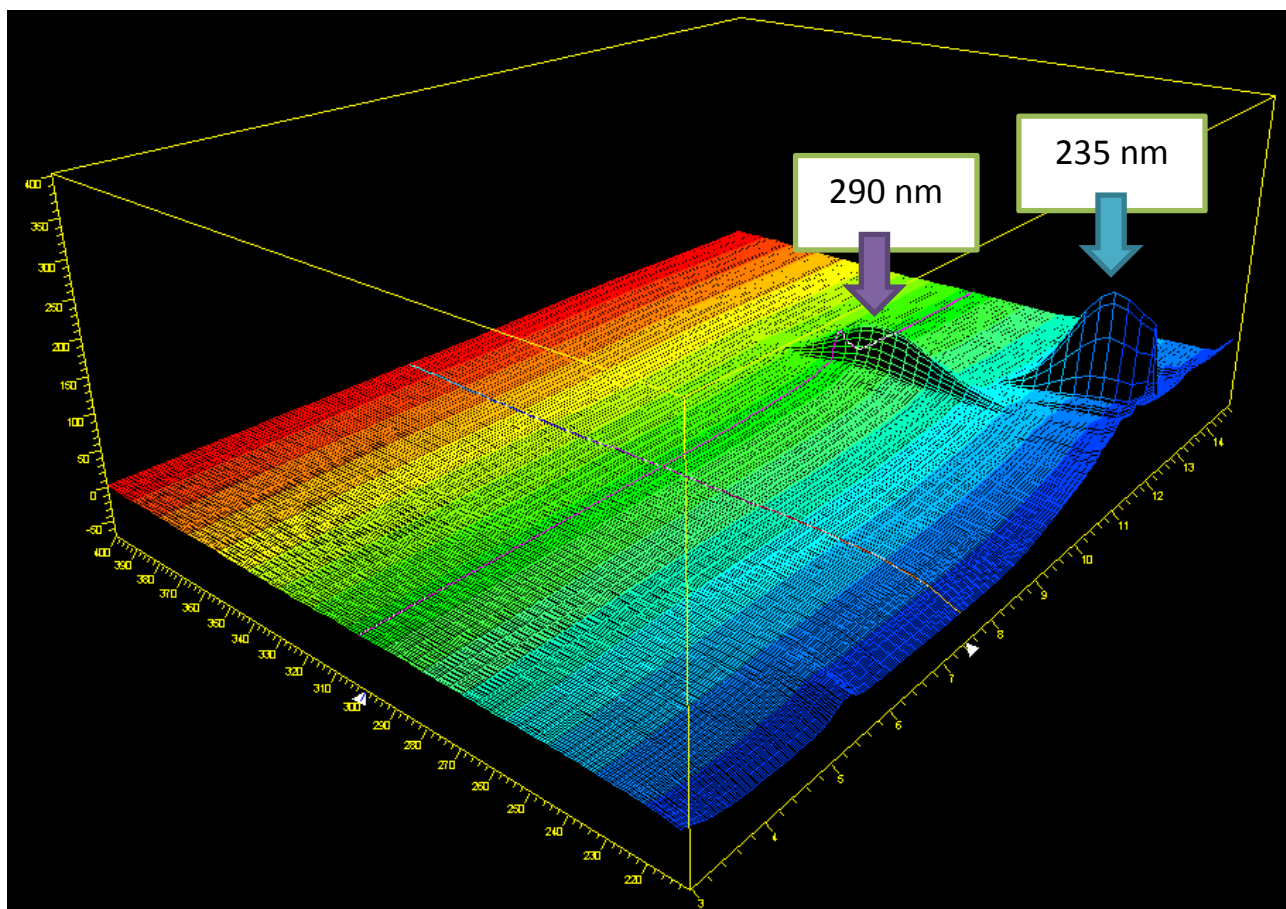


**Figure 4.7** MON hydrolyzed at pH 2.0, yielding two new transformation products (MP4 and MP5) with strong UV absorption at 235 nm and 290 nm, respectively.

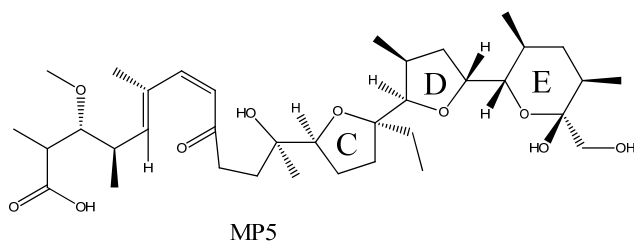


**Figure 4.8** Structure of MP5 (proposed by Agtarap *et al.*, 1967)

**Salinomycin.** Hydrolysis of SAL at pH 3 produced three products (named SP1, SP2 and SP3), with SP1 at a much higher amount (on the basis of peak area) (Figure 4.9A). At pH 5, SP1 was the only product observed over the time of reaction (Figure 4.9B). SP1 has the same MW as SAL (m/z 773), suggesting an isomeric transformation product. SP2 and SP3 showed m/z of 531 and 265, respectively, which match with the two products of SAL when it is treated with formic acid (Wells *et al.*, 1988). The formation of SP1 from the hydrolysis of SAL has not been reported in the literature. The hydrolysis products were eluted earlier than SAL (LC retention time: SP1 = 9.5 min, SP2 = 9.9 min, SP3 = 3.3 min, and SAL = 10.4 min), indicating lower hydrophobicity. The product evolution trend (Figure 4.9A) showed that the hydrolysis products remained stable after generation (i.e. little peak area change from 5 to 50 hours), and that SP1, SP2 and SP3 were generated simultaneously.

When analyzed by LC/UV, SP1 showed a strong absorbance at 285 nm (Figure 4.10), indicating existence of conjugated  $\pi$  bonds. In LC/MS/MS spectra, SP1 differed from SAL for lacking the m/z 403 fragment (Figure 4.11). Because the MS/MS spectrum was still insufficient to identify the structure of SP1 that corresponded to the strong absorbance at 285 nm, computational chemistry tools were employed to simulate UV spectra of the proposed structure for SP1 (structure shown in Figure 4.12) and identify the functional group that contributes to the peak at 285 nm (Note: the computational calculations were conducted by Dr. Daisuke Minakata). Aqueous phase molecular structure of SAL hydrolysis byproduct, SP1, was first optimized at level of B3LYP/6-31G+(d) with SMD solvation model. The optimized structure of SP1 is shown in Figure 4.13. Then, time-dependent density functional theory (TD-DFT) calculation is performed to obtain UV-VIS spectrum at level of B3LYP+G(d,p) with SMD solvation model

(nstates = 20). The obtained spectrum in the aqueous phase is shown in Figure 4.14. All calculations were performed using Gaussian09 Rev. E01 software.<sup>2</sup>

Consistent with the results observed by HPLC-UV analysis, TD-DFT calculations also revealed a strong peak of absorbance at 283.446 nm of wavelength. Molecular orbital distribution analysis indicates larger contribution of 199alpha and beta orbitals to the observed peak. Other orbitals that also have significant contribution to this absorbance peak are 206, 203, 207 and 200 molecular orbitals. Figure 4.15 shows molecular orbitals distribution at 199alpha orbital. Further quantitative analysis of the 200 molecular orbitals shows the largest contribution of [C(71)=O(73)] moiety of SP1 structure in Figure 4.16. Accordingly, application of computational chemistry confirms that the strong absorption at 285 nm from the HPLC-UV analysis results from the C=O moiety (next nearest to the D ring) as shown in Figure 4.16. The computational chemistry analysis supports the proposed SP1 structure by the strong agreement between the structure and the 285 nm absorbance band.

Based on the above results, hydrolysis of SAL under acidic conditions is likely to proceed via two pathways as proposed in Figure 4.12. The initial step of pathway I is via a similar mechanism as that proposed for MON transformation, in which protonation of SAL's spiro-ketal ring (the B-C-D ring) oxygen facilitates opening of the ring. The following steps involve all oxygen atoms on the B-C-D ring in rearrangement to yield SP1. Proton's role is a catalyst in this transformation with no net proton gains by the product. Hydrolysis experiments conducted in D<sub>2</sub>O with DCl yielded SP1 with the same MW as SAL ( $m/z = 773$ ), confirming no permanent incorporation of deuterium into the product. Furthermore, formation of SP1 involves substantial transformation of B and C rings, which renders reverse reaction of SP1 to SAL much less likely in contrast to MP1 of MON.

Pathway II is according to the proposed transformation of SAL promoted by formic acid by Wells et al (Wells *et al.*, 1988). Concerted fragmentation within the spiro-ketal C ring (Figure 4.12) leads to breakage of SAL into two fragments: one is SP3 that possesses a furanone moiety and the other undergoes further rearrangement to SP2. Both reactions are facilitated by protons. Pathway II becomes significant only when pH is much lower (3 and below).

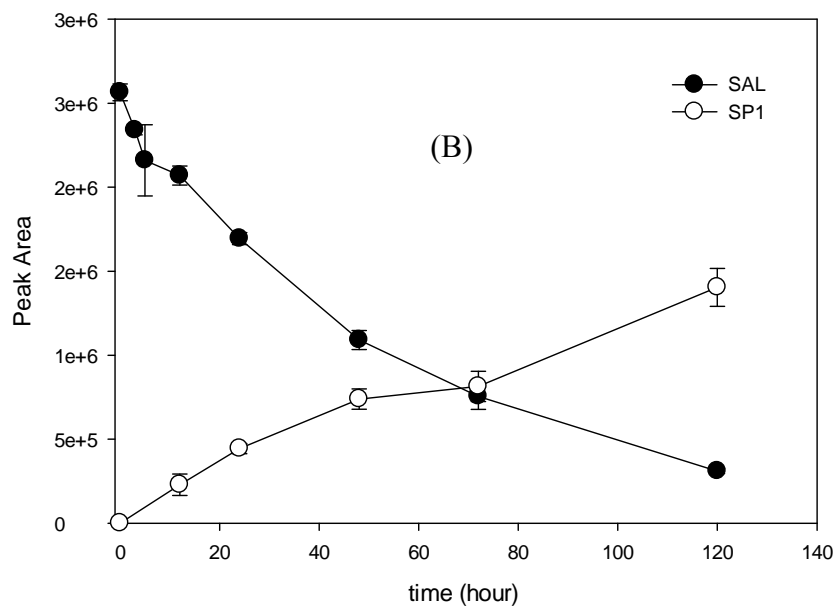
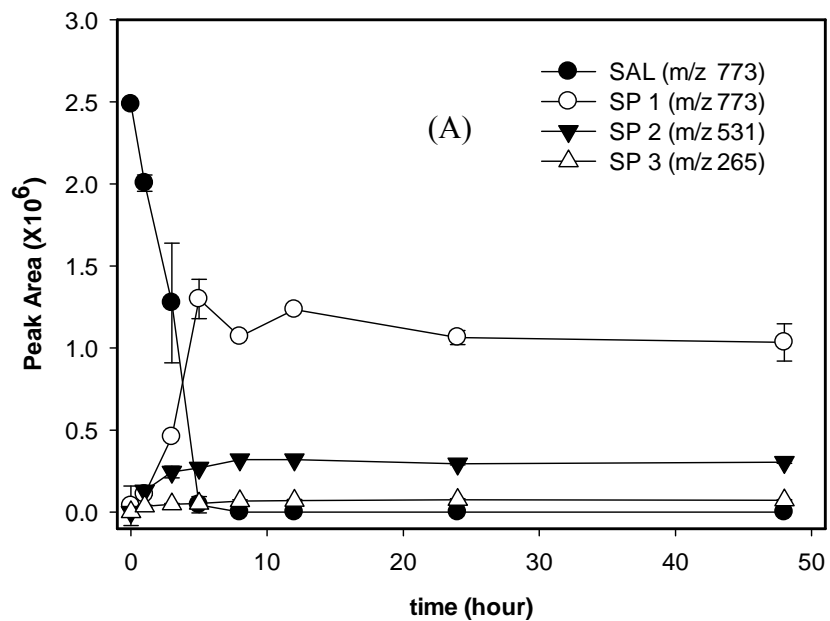


**Figure 4.9** SAL hydrolysis products at pH 3 (A) and pH 5 (B) buffered by acetic acid and HCl. Ionic strength was fixed with 0.1 M NaCl. The m/z values represent sodium adducts of parent SAL and its products (i.e.  $[M + 23]^+$ ).

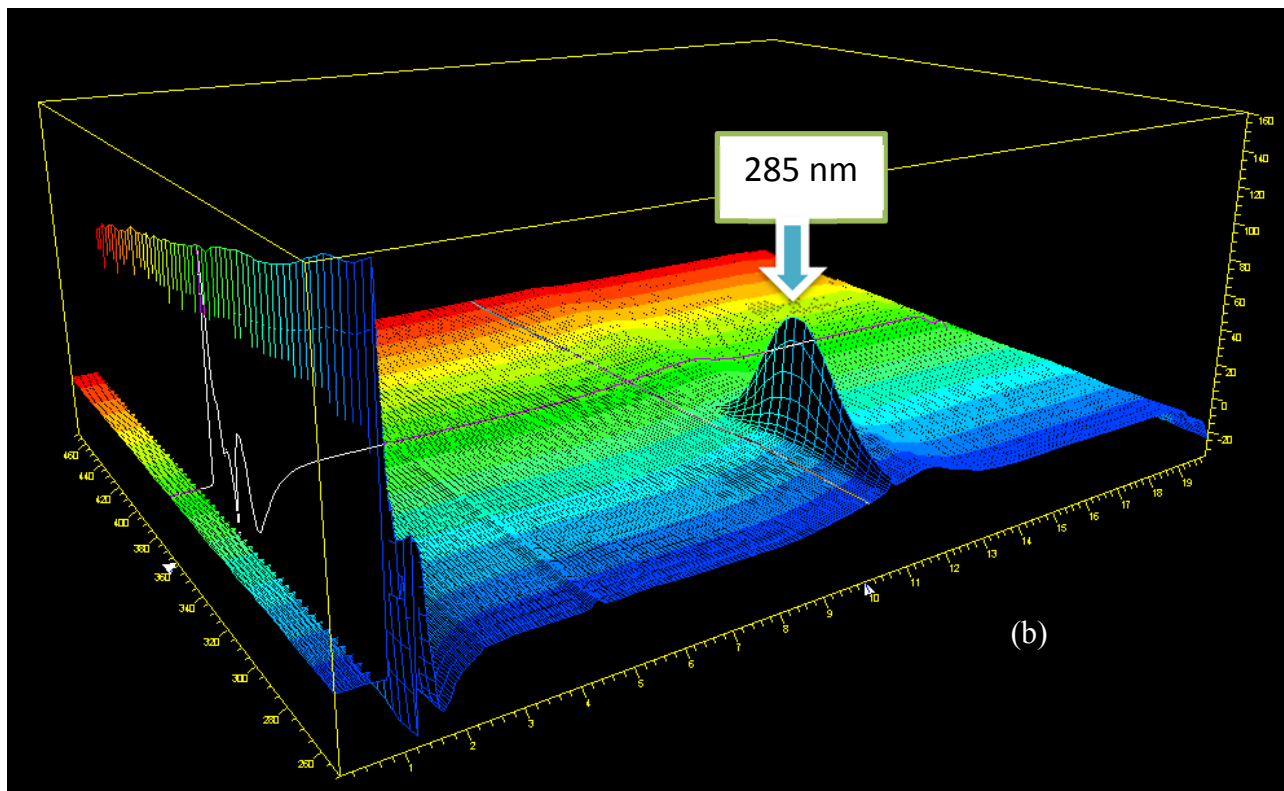


**Figure 4.10** SAL hydrolyzed at pH 3.0, yielding SP1 with UV absorption peaked at 285 nm.

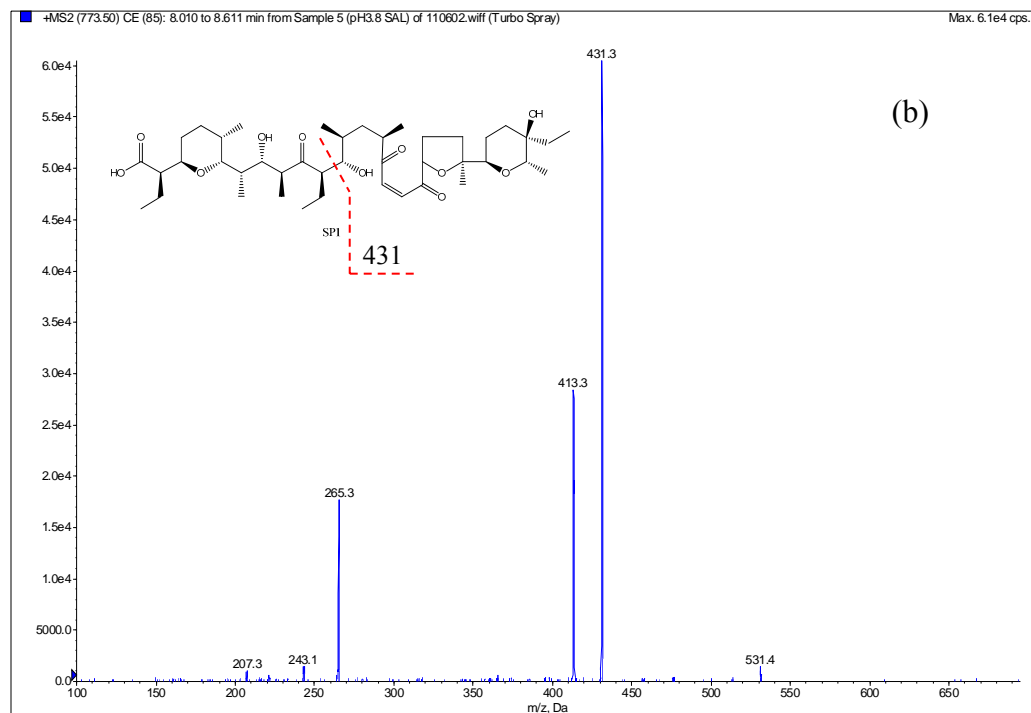
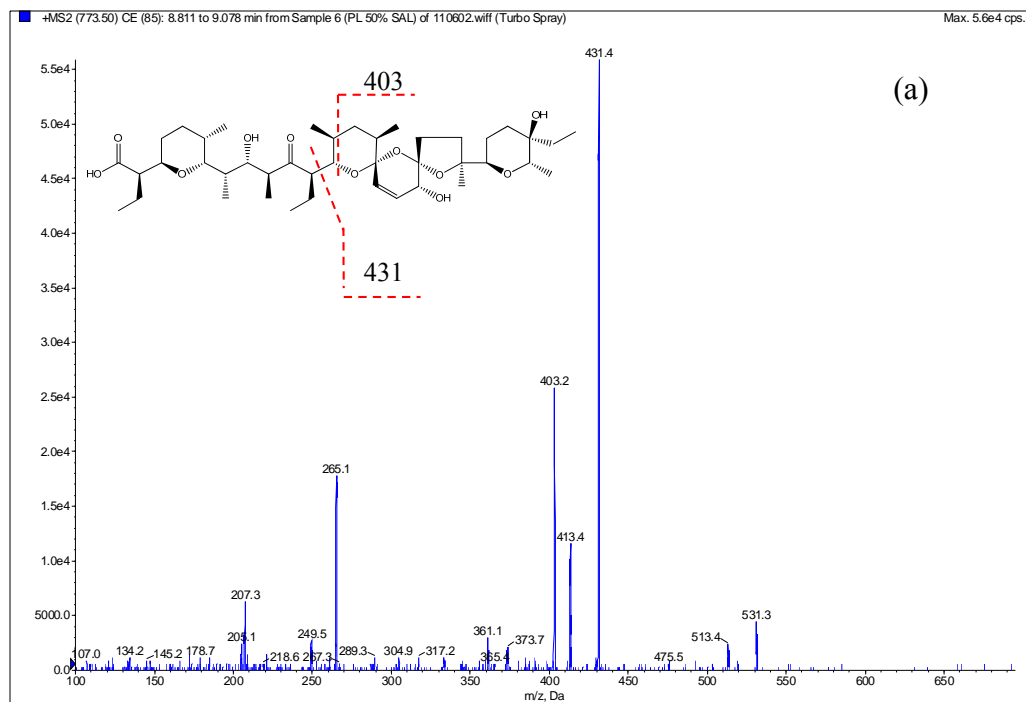


**Figure 4.11** LC/MS/MS spectra of (a) SAL and (b) SP1.

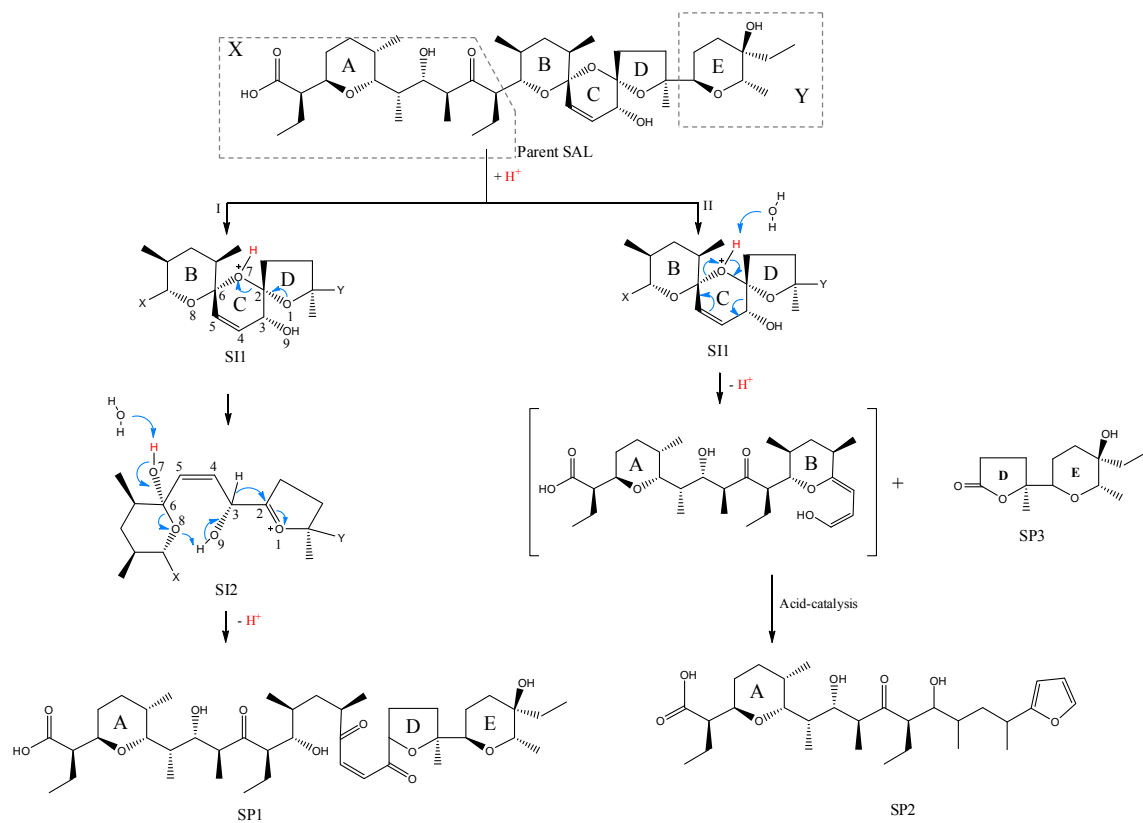


**Figure 4.12** Proposed acid-catalyzed transformation pathways and mechanism of SAL. Note: SP represents products and SI represents intermediates of SAL transformation. Hydrogen atoms in red represent protons from aqueous solution.

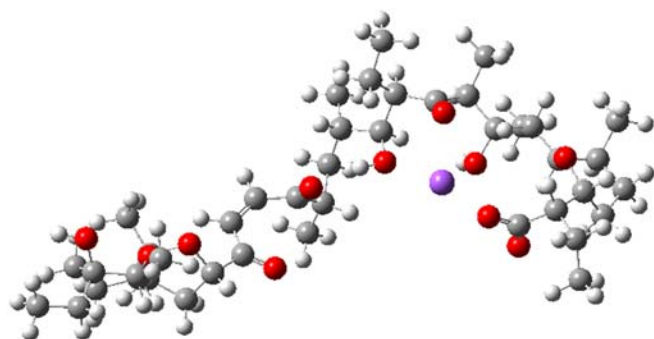


**Figure 4.13** Aqueous phase optimized structure of SP1 sodium form.

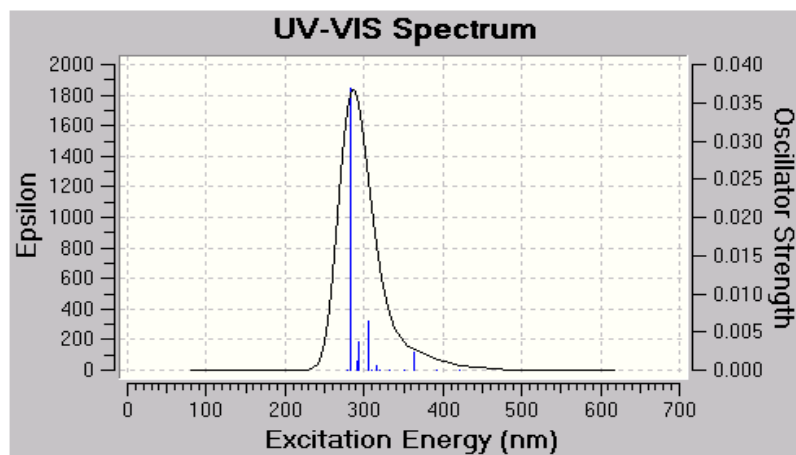


**Figure 4.14** Aqueous phase UV-VIS spectrum of SP1.

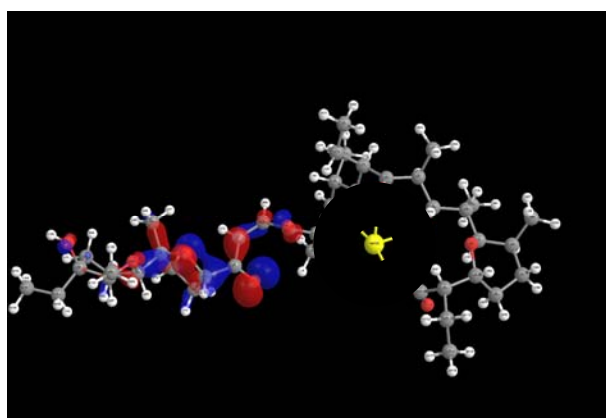


**Figure 4.15** Molecular orbital of 199alpha.

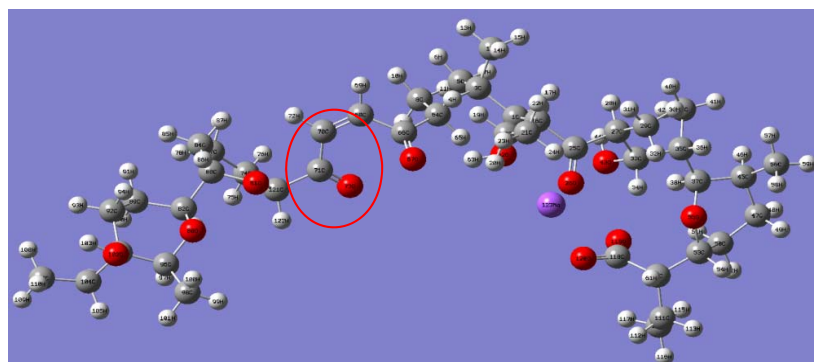


**Figure 4.16** [C(71)=O(73)] moiety of SP1 structure.

#### 4.3.4 Toxicity of transformation products

Evidently, isomerization is the dominant transformation of IPAs under mildly acidic conditions. Isomers of IPAs (i.e. MP1 and MP2 for MON, and SP1 for SAL) likely exist and may persist in the environment. The isomers have only minor alterations in the structures of IPAs and thus may still retain some antimicrobial property. Therefore, it is necessary to evaluate the toxicity of the hydrolytic transformation products of IPAs.

Gram(+) bacteria *Bacillus subtilis* (ATCC 6633) was used to test the antimicrobial property of MON and its transformation products for two reasons. First, Gram(-) bacteria have MW cut-off around 600 Dalton for transport through cell membranes (O'Shea and Moser, 2008); thus, the commonly used IPAs (MW = 671-765, Table 1.1) likely have little adverse impact on Gram(-) bacteria. Second, studies have shown inhibitory effect on *Bacillus subtilis* growth was significant and thus this organism could serve as an indicator of MON toxicity (Dorkov *et al.*, 2008; Pantcheva *et al.*, 2009).

The growth inhibitory effect is expressed by Equation 4.7:

$$\text{Inhibition (\%)} = \left( 1 - \frac{OD_{600}(\text{Sample})}{OD_{600}(\text{Control})} \right) \times 100 \quad (4.7)$$

As shown in Figure 5, the inhibition varied significantly when different MON concentration was employed in the reference tests, suggesting this test is sensitive and proper to exhibit the toxicity of MON. The toxicity of hydrolysis samples decreased as the hydrolytic reaction progressed; however, the decrease in toxicity was not proportional to the decrease in MON concentration and the inhibitory effect of hydrolysis samples was always greater than that of the reference samples (Figure 4.17). For example, the inhibitory effect was 61.4% by the hydrolysis sample after 8 hours of hydrolysis, but only 45.5% by the reference sample that contained the same amount of MON, indicating the hydrolysis products retain some

antimicrobial properties. Since isomeric products (MP1 and MP2) are the main hydrolysis products of MON, they are likely responsible for the additional antimicrobial effect in the hydrolysis sample. A good correlation can be seen between the decrease of toxicity and the decrease in the sum of peak areas of MON and its isomers in hydrolysis samples (except for the last data point) (Figure 4.17); this observation supports the hypothesis that MON isomers contributed additional antimicrobial effect. While it remains a possibility that the toxicity might be amplified in the hydrolysis samples due to co-existence of MON and its products, it is considered not likely due to structural similarity of these compounds.

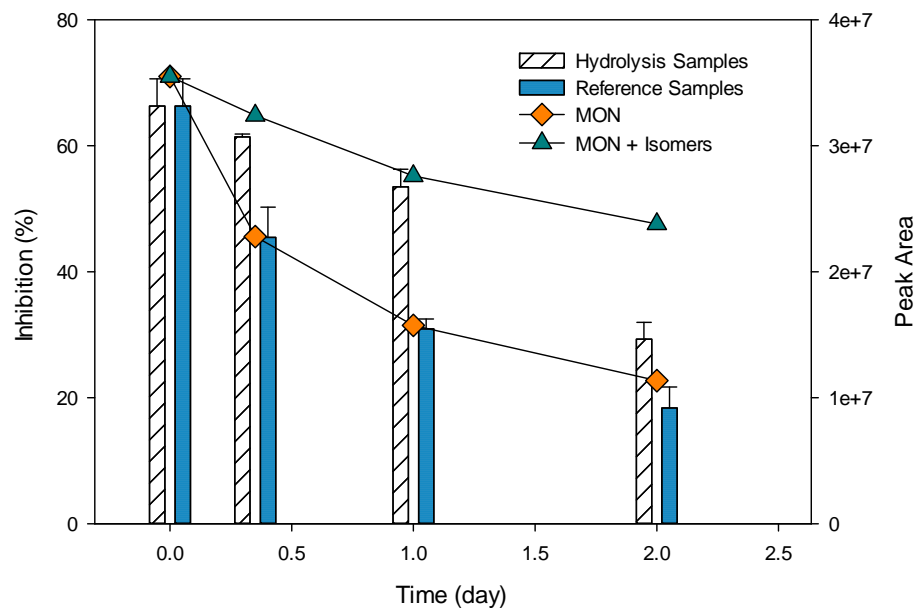


**Figure 4.17** Growth inhibition (represented by bars) by MON hydrolysis samples (obtained after different hydrolysis time) and by reference samples containing the same MON concentration as that remained in the hydrolysis samples at each time point. Data points represent MON peak area and sum of MON+isomeric product peak areas during hydrolysis. Hydrolysis was at pH 3.0 with initial MON at 1.08  $\mu\text{M}$ . The remaining MON concentration at the three subsequent sampling points was 0.70, 0.48 and 0.35  $\mu\text{M}$ , respectively. Error bars represent standard deviations of data from triplicate samples.

#### ***4.3.5 Preliminary study of environmental occurrence of IPAs and transformation products***

Preliminary analyses were conducted to detect the occurrence of MON and SAL and their transformation products in environmental samples. Fresh samples of poultry litter (PL) and rainfall runoff from PL-fertilized grassland were collected in Georgia and analyzed. PL is a mixture of animal excreta and materials such as wood shavings, peanut shells, wasted feed and feathers. PL likely contains IPAs since it's a common practice to add IPAs to the feed for broilers and chickens and PL is typically applied to land as fertilizer (Moore *et al.*, 1995).

MON and SAL were both detected in the PL and runoff samples (shown in Figure 4.18). MON and SAL were present, respectively, at 0.16 and 0.17 mg/kg in PL, and 657 and 125 ng/L in runoff. Although a significant amount of MON was present, its isomeric hydrolysis products were not detected. On the other hand, both PL and runoff samples contained SAL's isomeric product SP1 at a significant quantity (peak area larger than that of parent SAL). The presence of SP1 in these environmental samples was confirmed by both LC/MS and LC/MS/MS. As discussed earlier, MON undergoes the acid-catalyzed hydrolysis at a much slower rate than SAL, implying that MON will be more persistent in the environment than SAL. The preliminary results in detecting IPAs and transformation products in environmental samples corroborate with the above conclusion since MON was found at a higher concentration than SAL but more hydrolysis product of SAL was detected in the PL and runoff samples.

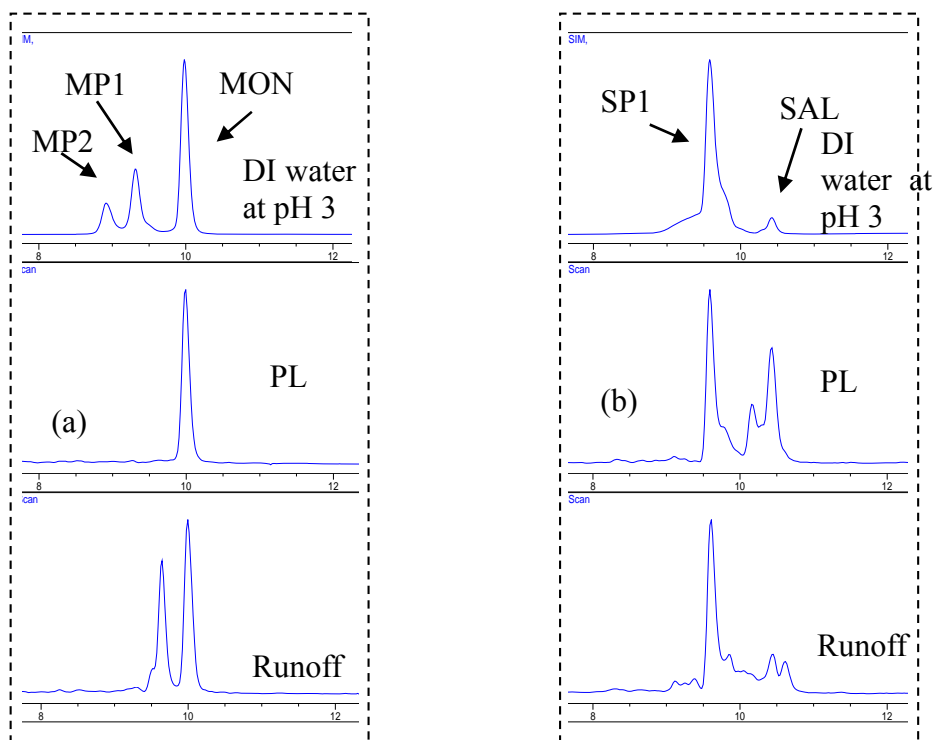


**Figure 4.18** Detection of (a)  $m/z$  693 and (b)  $m/z$  773 ions in samples of (i) hydrolysis experiments (DI water pH 3), (ii) poultry litter extract (PL) and (iii) extract of runoff from PL-fertilized grass plots. Note:  $m/z$  693 is related to parent MON and its isomeric hydrolysis products;  $m/z$  773 is related to parent SAL and its isomeric hydrolysis products.

#### 4.4 Environmental Implications

This study revealed that IPAs are prone to transformation in acidic environments, which are widely present in natural systems. For example, acidic soils are the predominant soil type in the Southeastern part of the U.S., where a significant amount of IPAs are being consumed and released due to active livestock husbandry. IPAs are also likely to undergo hydrolysis during animal waste processing. For example, PL is commonly amended with alum ( $\text{Al}_2(\text{SO}_4)_3 \cdot 18\text{H}_2\text{O}$ ) before land applications in order to reduce odor and volatile ammonia. Preliminary tests found that the pH of PL dropped from 7.0 to 4.3 (data not shown) after amendment with 20% alum (w/w). Furthermore, high concentrations of ammonium compounds in animal waste and/or fertilizers will stimulate microbial nitrification process, which consumes alkalinity and acidifies the micro-environment.

This study also delineated the different transformation kinetics of three common IPAs (MON, SAL and NAR) under acidic conditions and their transformation products. The improved understanding of the different environmental behavior of IPAs will aid in the proper selection of IPAs in future applications and better prediction of their environmental fate. The toxicity tests imply that potential adverse impacts from the transformation products may be as significant as those of the parent IPAs. Hence, more research should be conducted to obtain a comprehensive understanding of the IPA's transformation pathways under a wider range of environmental conditions, as well as the toxicological effects of both parent IPAs and their transformation products.

## CHAPTER 5

### PHOTODEGRADATION OF VETERINARY IONOPHORE ANTIBIOTICS UNDER UV AND SOLAR IRRADIATION

#### 5.1 Introduction

Although IPAs are hydrophobic compounds, significant amounts of IPAs can be transported with rainfall runoff from manure-fertilized lands (Davis *et al.*, 2006; Kim *et al.*, 2010) and eventually end up in receiving waters. The residual concentrations of IPAs in surface waters and wastewater treatment plants have been reported in a number of studies (Cha *et al.*, 2005; Hao *et al.*, 2006; Herrero *et al.*, 2012; Kim and Carlson, 2007b; Watanabe *et al.*, 2008; Watkinson *et al.*, 2009). For example, IPAs were found at up to 0.22 µg/L in surface water (Hao *et al.*, 2006), and at 0.03 – 0.06 µg/L in river water near agricultural fields (Cha *et al.*, 2005). Watkinson *et al.* examined the occurrence of antibiotics in different environmental waters, among which MON and SAL were detected at 94% and 21% of all collected samples (n > 84) in surface waters and occasionally in wastewater treatment plant effluent (Watkinson *et al.*, 2009).

Photolysis is known to affect the fate of various pharmaceutical contaminants in the aquatic environment. In surface or waste waters, degradation of IPAs many occur due to exposure to solar (in natural water systems) or UV (in treatment facilities) radiation and such photodegradation may play an important role in affecting the overall environmental fate of IPAs. To date, however, research has been scarce in evaluating the susceptibility of IPAs to photo-induced degradation. In comparison, the degradation of IPAs via other transformation mechanisms has been investigated in several previous studies. For example, biodegradation of IPAs was reported in several articles with half-lives of 3-5 days in soil (Carlson and Mabury, 2004; Sassman and Lee, 2007; Schlusener and Bester, 2006). IPAs' instability in acidic conditions was recognized in the reports by the European Food Safety Authority (EFSA)

(EFSA., 2004; 2005). In Chapter 4, the acid-catalyzed hydrolysis of IPAs was investigated in aqueous solutions with elucidation of transformation mechanisms and products (Sun *et al.*, 2013b). The degradation of IPAs under UV/H<sub>2</sub>O<sub>2</sub> advanced oxidation process (AOP) conditions was also examined recently (Yao *et al.*, 2013). Although few studies had focused on the photodegradation of IPAs in the literature, it can be expected that some IPAs (e.g., SAL) may undergo direct photolysis due to the presence of the carbonyl moiety in their structures (Bohn *et al.*, 2013).

Therefore, the objectives of this study were to investigate the direct and indirect photodegradation of IPAs under environmental conditions, measure the quantum yield values, elucidate associated transformation products and mechanisms, and evaluate the toxicity of the transformation products. To the authors' best knowledge, this study is among the first to report and elucidate photolytic transformation of IPAs under environmentally relevant aquatic conditions.

## 5.2 Materials and Methods

### 5.2.1 Chemicals, reagents and water samples

MON sodium salt (purity, 97%) and NAR sodium salt (purity, 97%) were purchased from Sigma-Aldrich (St. Louis, MO, USA). SAL sodium salt (purity, 96%) was purchased from Fisher Scientific (Pittsburgh, PA, USA). HPLC-grade methanol (purity, 99.9%), acetonitrile (purity, 99.9%), analytical-grade formic acid (purity, 99%) were obtained from Sigma-Aldrich. All other reagents used were of analytical grade obtained from Fisher Scientific. Suwannee River humic acid (SRHA) was purchased from the International Humic Substance Society (IHSS, St. Paul, MN, USA). Another type of humic acid (MPHA) was purchased from MP Biomedicals (Solon, OH, USA). Reagent-grade deionized (DI) water (resistance > 18 m $\Omega$ ·cm) was obtained from a Millipore nanopure water purification system (Billerica, MA, USA).

To prepare IPA stock solutions, individual IPA powder was weighted and pre-dissolved in methanol. Then, aliquots of methanolic IPA were evaporated to dryness under vacuum and re-dissolved into DI water at 5 mg/L, which was then stored at 4°C prior to use. To prepare dissolved organic matter (DOM) stock solutions, SRHA and MPHA were individually weighted and prepared in DI water. Water extracts from poultry litter (PL-extract) were obtained by mixing DI water and poultry litter (20/1 w/w) for 12 h, followed by centrifugation (3000 rpm, 10 min) and sterilization by passing through 0.2  $\mu$ m filters. All DOM stock solutions were kept at 4°C prior to use.

Rainfall runoff was simulated by soaking PL-fertilized soil with DI water for 30 min (w:w 2:100). The supernatant was then collected by passing through 0.2  $\mu$ m pore-size filters. Animal waste plume water was obtained by soaking poultry litter with DI water (w:w 2:100). The supernatant was then collected by passing through 0.2  $\mu$ m pore-size filters. Wastewater

samples from the secondary effluent after activated sludge and calcification processes were collected at a local municipal wastewater treatment plant (WWTP). Characteristics of the above real water matrices are listed in Table 5.1.

**Table 5.1** Characteristics of real water samples

	DOC (mg C/L)	Nitrate (mM)	pH	HCO <sub>3</sub> <sup>-</sup> (mM)	CO <sub>3</sub> <sup>2-</sup> (mM)
WWTP secondary effluent	0.435	1.45	7.4	1.20E-01	1.41E-04
Runoff from PL-fertilized land	60.55	0.71	6.5	1.51E-02	2.24E-06
Plume water	2074	0.01	7.2	7.59E-02	5.62E-05

## **5.2.2 Photolysis experimental set-up**

### *5.2.2.1 Sample preparation*

Reaction solutions were prepared with 0.5 – 2.5 mg/L IPA in DI water, rainfall runoff, animal waste plume or WWTP secondary effluent. The DI water matrix was buffered at pH 7.0 using 5 mM sodium phosphate, whereas the other water matrices were not adjusted for pH. In the experiments to investigate the effects of nitrate and DOM, aliquots of nitrate or DOM stock solutions were spiked into the DI water matrix to achieve the desired concentrations.

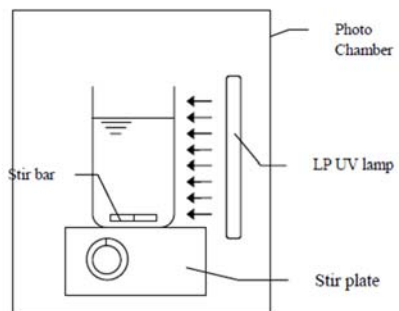
### *5.2.2.2 UV Photolysis*

Photolysis of IPAs under UV irradiation was studied using a similar set-up as previously described (Yao *et al.*, 2013), and shown in Figure 5.1. Experiments were conducted in a magnetically stirred 100-mL cylindrical quartz reactor kept in a photo-chamber equipped with a 4-W low pressure (LP) UV lamp (G4T5 Hg lamp, Philips TUV4W) peaking at 254 nm at ambient temperature (22°C). Reaction was initiated by exposing the solution to UV irradiation. A sample aliquot was taken at each time interval and injected into a 2-mL amber glass vial prior to LC/MS analysis.

### *5.2.2.3 Simulated and natural sunlight photolysis*

Simulated sunlight was generated by a 300-W Xenon lamp (PerkinElmer, PE300BF). Reaction solutions were kept in 10-mL quartz tubes, which were held perpendicular to the light source (illustrated in Figure 5.1). For natural sunlight experiments, the quartz tubes were kept vertically in a rack on the roof of a laboratory building in Atlanta, GA, USA (latitude 33.8° N). The sunlight photolysis experiments were conducted in April, 2013.

A. UV experimental set-up



B. Simulated / natural sunlight experimental set-up

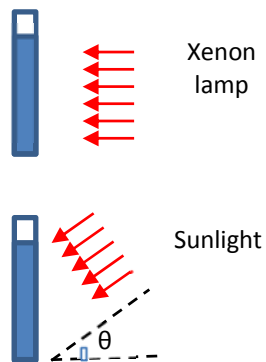


**Figure 5.1** Illustrations of photolysis experimental set-up

### ***5.2.3 Chemical and instrumental analysis***

The total dissolved organic carbon (TOC) of DOM stock solutions was analyzed by a Shimadzu TOC-V total organic carbon analyzer. Nitrate was measured by a Dionex DX-100 ion chromatography instrument with conductivity detection. The UV absorbance of IPAs and DOM was measured using an Agilent UV-Vis spectrophotometer. The light irradiance in the photolysis experiments was measured using a spectroradiometer (Spectral Evolution, SR-1100).

IPAs were analyzed by an Agilent 1100 Series high performance liquid chromatography mass spectrometry (HPLC/MS) system (Agilent, Palo Alto, CA) with a reversed-phase Ascentis RP-amide column (2.1 × 150 mm, 3 mm). The analytical methods were described in detail in our previous study (Sun *et al.*, 2013a, Chapter 2). For elucidation of transformation products, a LC/MS/MS unit (Agilent 1260 Infinity LC system, 6410 Triple Quad MSD, Agilent, Palo Alto, CA) was employed. The MS parameters were set up as fragmentation voltage of 135 V, and collision-activated-dissociation (CAD) energy of 50 eV.

## 5.3 Results and Discussion

The photo-induced degradation of MON and SAL was investigated extensively under LP UV, simulated sunlight, and natural sunlight irradiation. NAR was expected to behave similarly as SAL via photolysis, on the basis that its structure closely resembles that of SAL with only one difference of a methyl group on the A ring (Figure 1.1 in Chapter 1). Previously, NAR also behaves similarly as SAL in acid-catalyzed hydrolysis (Sun *et al.*, 2013b). Thus, NAR was investigated in this study primarily for the purpose of elucidation of transformation products of SAL.

### 5.3.1 Direct photolysis of IPAs with LP UV, simulated sunlight and natural sunlight

Photolysis of IPAs due to direct absorption of light was investigated in DI water buffered by 5 mM phosphate at pH 7. In all dark controls, no significant loss of IPAs was observed for over one week (data not shown). MON was resistant to photodegradation in DI water matrix under exposure to any light sources. In contrast, the degradation of SAL was observed, at the fastest rate under UV radiation, followed by simulated sunlight and then natural sunlight (Table 5.2, Figure 5.2). The kinetics of SAL degradation showed good linear relations ( $R^2 > 0.98$ ) between  $\ln([SAL]/[SAL]_0)$  and irradiation time (Figure 5.2), indicating pseudo-first-order kinetics. Thus, the first-order rate constants were calculated for SAL direct photolysis, shown in Table 5.2.

MON consists of mostly sigma bonds (C-H, C-C, C-O and O-H) except for a carboxylic carbonyl group at one end (Figure 1.1). These structural features result in its low absorption of light over 220 nm (Figure 5.3). However, the additional C=C bond (C18-C19) and carbonyl group (C11-O) of SAL (NAR) contribute to two significant absorbance ranges, which peak at

around 200 nm and 285 nm, respectively (Figure 5.3). The first-order rate constant of NAR under UV irradiation was  $0.47 \pm 0.01 \text{ h}^{-1}$ , which was close to that of SAL (Table 5.2) due to their similar molecular structures.

The half-life of SAL in DI water with sunlight radiation (in April) was  $53.3 \pm 4.1 \text{ h}$ , which is relatively long compared to other commonly used veterinary pharmaceuticals. For example, the half-life of tetracycline due to photolysis was around 44 min in July (Werner *et al.*, 2006), and that of sulfamethoxazole was around 10.4 h in summer time (Bonvin *et al.*, 2012). However, considering the extremely low molar extinction coefficient of SAL (Figure 5.3), the results suggest that SAL has a relatively high quantum yield compared to other veterinary pharmaceuticals.

*Apparent Quantum yield of SAL.* The first-order rate constant of direct photolysis,  $k$ , can be expressed using Equation 5.1 (Zepp, 1978).

$$\frac{dC}{dt} = k \cdot C = \int \Phi_{\text{SAL}/\lambda} \cdot 2.303 \cdot (1 - \exp(-A_\lambda)) \cdot f_\lambda \cdot I_\lambda \cdot l \quad (5.1)$$

where,

$\Phi_{\text{SAL}/\lambda}$  = quantum yield of SAL at  $\lambda$  wavelength, mole/Einstein;

$A_\lambda$  = Absorbance of reaction solution at  $\lambda$  wavelength;

$f_\lambda = \frac{\epsilon_{\text{SAL}/\lambda} \cdot [\text{SAL}]}{\epsilon_{\text{SAL}/\lambda} \cdot [\text{SAL}] + \sum \epsilon_{\text{Si}/\lambda} \cdot [\text{S}_i]}$ , the fraction of light absorbed by SAL at  $\lambda$  wavelength;

$I_\lambda$  = the irradiance received by the solution at given wavelength, Einstein/L/s;

$l$  = the light pathlength of the reactor, cm.

The term,  $(1 - \exp(-A_\lambda)) \cdot f_\lambda$ , can be simplified as  $\epsilon_\lambda \cdot C$ , because  $A_\lambda$  is lower than 0.1 for DI water matrix (Zepp, 1978). In addition, although the quantum yield of SAL may vary at different wavelengths, it is expected that the variation is small compared to the other parameters (i.e.,  $\epsilon_\lambda$

and  $I_\lambda$ ). Thus, we consider  $\Phi_{\text{SAL}/\lambda}$  to be a constant value with respect to wavelength. Based on the above assumptions, Equation 5.2 expresses the quantum yield of SAL.

$$\Phi_{\text{SAL}} = \frac{k}{2.303 \cdot I \cdot \int_{220}^{350} \epsilon_\lambda \cdot I_\lambda} \quad (4.2)$$

Since SAL only absorbs light at wavelengths shorter than 350 nm and all three light sources emit light at wavelengths longer than 220 nm (Figure 5.3), the term,  $\epsilon_\lambda \cdot I_\lambda$  was intergraded from 220 to 350 nm and plotted against the wavelength in Figure 5.4. As Figure 5.4 shows,  $\epsilon_\lambda \cdot I_\lambda$  peaked at around 254, 305 and 315 nm for UV, simulated sunlight and natural sunlight, respectively. Therefore, applying Equation 5.2 and assumptions above, the quantum yield of SAL was calculated and shown in Table 5.2.

The quantum yield values of SAL were similar for all three light sources, which suggests the assumption is valid that the quantum yield of SAL varies little with respect to wavelength. Comparing to other pharmaceuticals, the apparent quantum yield of SAL is considerably higher. For example, the quantum yield values of tetracycline (0.00024 – 0.002) (Werner *et al.*, 2006), naproxen (0.012) (Moore and Chappuis, 1988), diclofenac (0.031 – 0.22) (Buser *et al.*, 1998; Moore and Wilkins, 1990), carbamazepine (0.00013) (Lam and Mabury, 2005), levofloxacin (0.00008) (Andreozzi *et al.*, 2003), amoxicillin (0.0045 – 0.0060) (Andreozzi *et al.*, 2005), and sulfamethoxazole (0.02) (Lam and Mabury, 2005) are all in the range of 0.001 – 0.22 under simulated sunlight or natural sunlight, which are much lower than that of SAL. However, on the other hand, some ketone-containing compounds, such as penton-2-one, hexan-2-one, 2,2-dimethylheptan-3-one, 3,3-dimethylbutan-2-one, 2,2-dimethylhexan-3-one, and 2,2,4,4-tetramethylpentan-3-one have quantum yield values of 0.27 – 0.71 (Yang *et al.*, 1970; Yang and Feit, 1968). The similar range of quantum yields of SAL and the ketone-containing compounds

suggests that the photo-reactive part of SAL is likely the ketone moiety (C11-O).

**Table 5.2** Rate constants of MON and SAL (hour<sup>-1</sup>) (R<sup>2</sup>>0.98)

	UV		Xenon		Sunlight	
	MON	SAL	MON	SAL	MON	SAL
$\phi$	ND	0.66±0.05	ND	0.66±0.03	ND	0.70±0.03
----- <i>k</i> 's (hr <sup>-1</sup> )-----						
<b>DI water</b> <sup>a</sup>	ND	0.46±0.01	ND	0.24±0.01	ND	0.013±0.001
<b>DI +Nitrate</b> <sup>b</sup>	0.53±0.04	1.00±0.07	0.53±0.01	0.72±0.03		
<b>DI + SRHA</b>			0.20±0.04	0.27±0.01		
<b>DI + MPHA</b>			0.15±0.05	0.31±0.12		
<b>DI + PL extract</b>			ND	0.08±0.02		
<b>WWTP effluent</b>	0.56±0.07 (0.59) <sup>c</sup>	0.74±0.05 (1.10)				
<b>Plume</b>	ND	ND	ND	ND	ND (<0.001)	ND (<0.001)
<b>Surface runoff</b>					0.007±0.001 (0.007)	0.015±0.001 (0.016)

<sup>a</sup> DI water buffered with 5 mM phosphate buffer at pH 7; <sup>b</sup> DI water containing 5 mg/L NaNO<sub>3</sub>; <sup>c</sup> numbers in parenthesis are predicted values using Equation 5.4; ND, no degradation, *k*'s values were statistically zero.

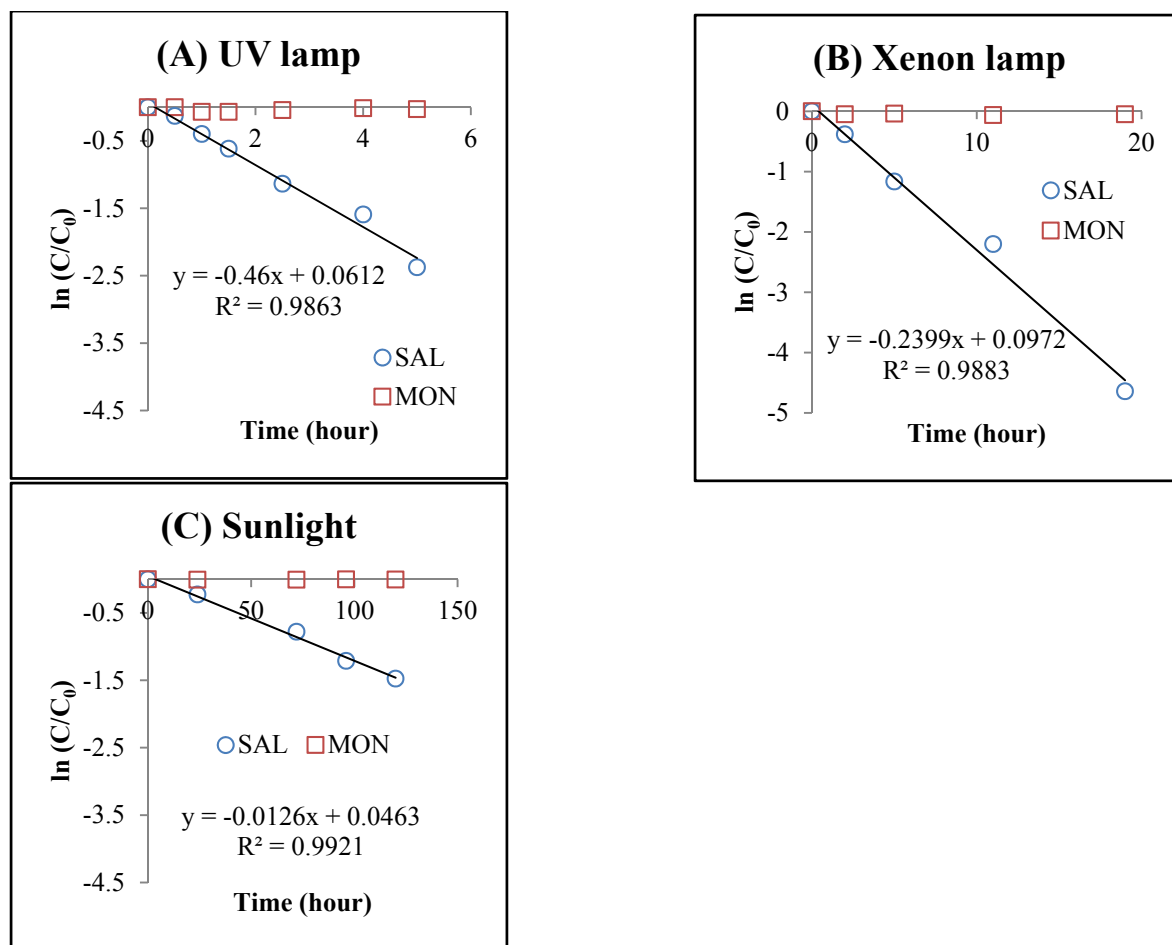


**Figure 5.2** Direct photolysis of IPAs under (A) LP UV, (B) simulated sunlight, and (C) natural sunlight.

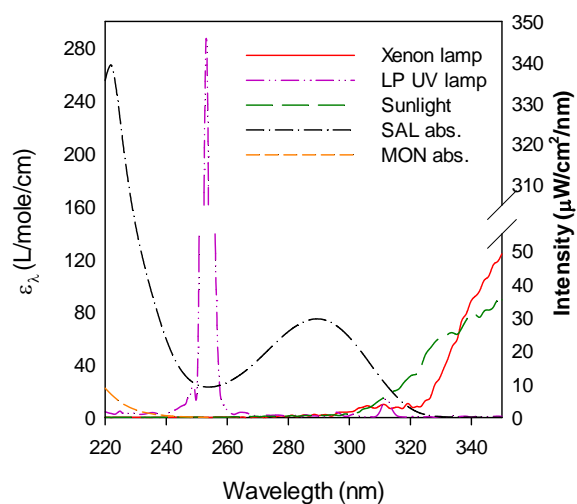


**Figure 5.3** Light emission spectra and UV absorbance of IPAs.

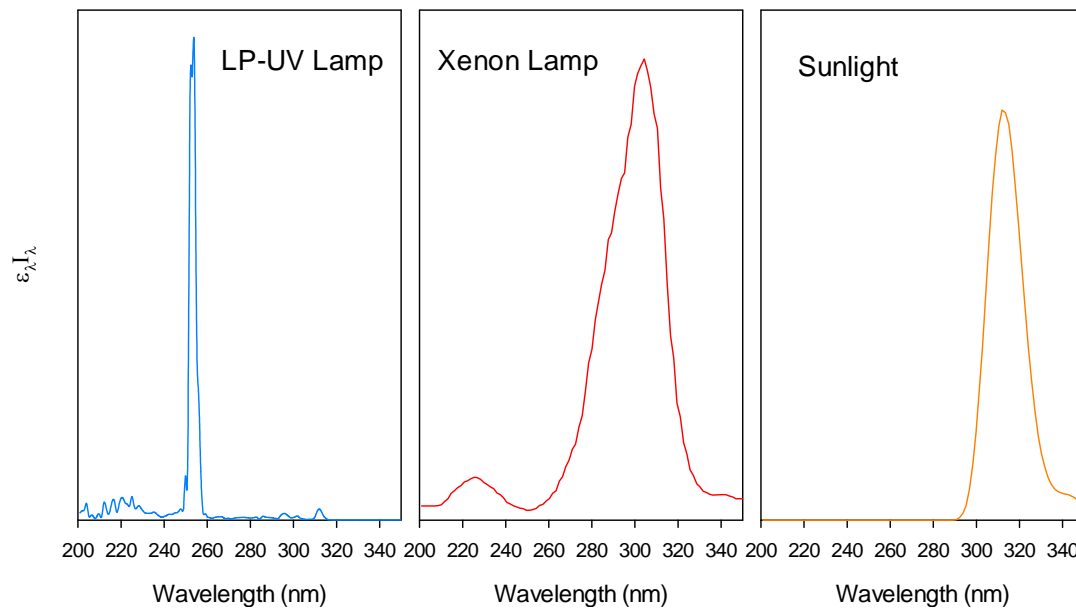


**Figure 5.4** Overlapping of SAL absorbance with light source spectra ( $\epsilon_{\lambda} \cdot I_{\lambda}$ ).  $\epsilon_{\lambda}$  is the extinction coefficient of SAL at given wavelength;  $I_{\lambda}$  is the irradiance received by the solution at given wavelength, Einstein/L/s.

### 5.3.2 Indirect photolysis of IPAs

Although MON is stable under all three light source exposures in DI matrix, the indirect photolysis of MON is expected in real water matrix via reacting with reactive species generated by natural photo-sensitizers. For SAL, the observed photolysis rate in real water matrix may also be influenced by different water components due to various mechanisms, such as light-shielding effects, energy transfer to/from photo-excited DOM, and/or reactions with reactive species generated by photo-sensitizers. Nitrate and DOM are real water components particularly considered in this study, because (1) they are known to have great impact on photolysis of micropollutants in water systems (Brezonik and Fulkerson-Brekken, 1998; Nelieu *et al.*, 2009; Vione *et al.*, 2005; Walse *et al.*, 2004); and (2) they are the major components in WWTP effluent, agricultural runoff and natural water bodies.

#### 5.3.2.1 Effect of nitrate

Nitrate concentrations in WWTP effluent and agricultural runoff could reach 10 mg/L as N or higher. In this study, 0 – 10 mg/L nitrate as sodium nitrate was spiked into DI water matrix under simulated sunlight exposure to investigate the influence of nitrate on IPA photolysis. As shown in Figure 5.5, the photodegradation of MON and SAL were both enhanced by the presence of nitrate. The first-order degradation rate constant of MON increased linearly with increasing nitrate concentration ( $R^2 > 0.990$ ). The presence of nitrate also enhanced the degradation of SAL under simulated sunlight irradiation; however, the first-order rate constant did not yield as a good linearity with nitrate concentration as that of MON. Indeed, increasing nitrate concentration resulted in diminished enhancement of the degradation rate of SAL. Because the presence of nitrate did not raise the light absorbance to greater than 0.1, light-

shielding effect was negligible (Zepp, 1978). The combined results suggest that the presence of nitrate enhanced the photolysis of both MON and SAL, but likely via different mechanisms.

Nitrate is well known to produce hydroxyl radicals under either UV or sunlight exposure (Mack and Bolton, 1999; Mostofa *et al.*, 2012; Sharpless and Linden, 2001; Zepp *et al.*, 1987). Therefore, attempts were made to apply an established numerical model which estimates the steady-state HO· concentration from nitrate photolysis (Equation 5.3) (Glaze *et al.*, 1995; Keen *et al.*, 2012), to predict the photolysis rates of IPAs with different nitrate concentrations.

$$[\text{HO}\cdot]_{\text{ss}} = \frac{\int I_{\lambda} \cdot l \cdot \epsilon_{\text{NO}_3^-, \lambda} \cdot [\text{NO}_3^-] \cdot \Phi_{\text{NO}_3^-}}{\sum k_{\text{S}_i} \cdot [\text{S}_i]} \quad (5.3)$$

where

$[\text{HO}\cdot]_{\text{ss}}$  = steady-state hydroxyl radical concentration, M

$I_{\lambda}$  = the irradiance received by the solution at given wavelength, Einstein·L<sup>-1</sup>·s<sup>-1</sup>

$\epsilon_{\text{NO}_3^-, \lambda}$  = molar absorption coefficient of nitrate at given wavelength, M<sup>-1</sup>·cm<sup>-1</sup>

$l$  = light pathlength of reactor, cm

$\Phi$  = quantum yield of HO· production from nitrate, M·Einstein<sup>-1</sup>

$k_{\text{S}_i}$  = second order rate constants of co-solutes (S<sub>i</sub>) with HO·, M<sup>-1</sup>·s<sup>-1</sup>

$[\text{S}_i]$  = concentrations of co-solutes (S<sub>i</sub>), M

After computing  $[\text{HO}\cdot]_{\text{ss}}$ , the photolysis rate constants of IPAs in the presence of simulated sunlight and nitrate were predicted by multiplying  $[\text{HO}\cdot]_{\text{ss}}$  with the known second-order rate constants of IPAs with hydroxyl radicals (Yao *et al.*, 2013). As shown in Figure 5.5, the predicted rate constants agreed well with the experimental data for MON, which suggests that indirect photolysis of MON with nitrate was primarily via the reaction with HO·. However, the model underestimated the degradation rates of SAL with 0.2 – 1 mg/L NaNO<sub>3</sub> (Figure 5.5),

which suggests reactive species other than HO· may play a part in the indirect photolysis of SAL. Indeed, besides generation of HO·, the photolysis of nitrate also produces several reactive nitrogen species (RNS), primarily NO<sub>2</sub>· (Keen *et al.*, 2012; Mack and Bolton, 1999; Vione *et al.*, 2005) (illustrated in Figure 5.6), which potentially reacted with SAL. Therefore, the photolysis of SAL in the presence of nitrate was likely partly contributed by reactions with RNS. Furthermore, at an increasing nitrate concentration, the RNS concentration does not necessarily increase proportionally due to the possibility of radical combining: NO· + HO· → HNO<sub>2</sub> ( $k = 1.0 \times 10^{10} \text{ M}^{-1} \cdot \text{s}^{-1}$ ), NO<sub>2</sub>· + HO· → HOONO ( $k = 1.3 \times 10^9 \text{ M}^{-1} \cdot \text{s}^{-1}$ ), and NO<sub>2</sub>· + NO<sub>2</sub>· → N<sub>2</sub>O<sub>4</sub> ( $k = 4.5 \times 10^8 \text{ M}^{-1} \cdot \text{s}^{-1}$ ) (Buxton *et al.*, 1988; Gratzel *et al.*, 1969). The above phenomena could explain the observed non-linear dependence of the rate constant with increasing nitrate concentration (Figure 5.5). Thus, it is hypothesized that, at a lower nitrate concentration, RNS contributed to degradation of SAL, resulting in underestimation of photolysis rate by the steady-state hydroxyl radical model. In contrast, at a higher nitrate concentration, RNS was self-quenched yielding a diminished increase in the photolysis rate of SAL. The reaction between SAL and RNS was further supported by elucidation of the transformation products (see section below).



### 5.3.2.2 Effect of DOM

The effects of DOM on IPA photolysis were tested under simulated sunlight irradiation. SRHA, MPHA, and PL-extract were selected because they represent commonly used model DOM (i.e., SRHA and MPHA) or NOM that IPAs will likely encounter in agricultural field (i.e., PL-extract). The UV-Vis spectra of DOM working solutions are shown in Figure 5.7. The degradation of IPAs was strongly influenced by the introduction of DOM (Table 5.2). Both MON and SAL degraded slightly faster with the presence of SRHA and MPHA, compared with the rates in DI water matrix. However, PL-extract exhibited significant inhibitory effects on the photolysis of SAL.

The effect of DOM on the photolytic transformation of organic compounds was studied extensively in the literature (Page *et al.*, 2011; Wenk *et al.*, 2011; Zafiriou *et al.*, 1984). In general, irradiation of DOM may produce light-excited DOM (DOM\*), singlet oxygen, and HO· species that can react with organic pollutants in water and lead to enhanced pollutant degradation (Dalrymple *et al.*, 2010; Wenk *et al.*, 2011). On the other hand, DOM may inhibit pollutants' photolysis by light-shielding and physical quenching effects, particularly at high DOM concentrations (Canonica and Laubscher, 2008; Westerhoff *et al.*, 2007; Young *et al.*, 2013).

In this study, both enhancement and inhibition of SAL photolysis by DOM were observed. All three types of DOM showed absorbance greater than 0.1 at around 285 nm (Figure 5.7), suggesting that light-shielding by DOM was not negligible under the experiments. The light-shielding effect was calculated to be around 14%, 21%, and 25% for SRHA, MPHA and PL-extract, respectively, under the employed experimental conditions. Even though light-shielding effects by the DOM were comparable, PL-extract exhibited strong inhibition while

SRHA and MPHA exhibited moderate enhancement on SAL photolysis. This difference was likely due to different properties of the tested DOM. For example, when normalizing the light absorbance of DOM from 220 to 400 nm by DOM's DOC content ( $A_{220-400}/\text{mg C/L}$ ), PL-extract had the lowest light absorbance per carbon basis. This result suggests that PL-extract contained a greater proportion of non-photo-reactive organic compounds which might lower PL-extract's potential to produce reactive species upon irradiation and could compete with IPAs to react with reactive species produced by photo-sensitive compounds. Furthermore, the inhibitory effect of PL-extract was considerably greater than that attributable to light shielding, suggesting that physical quenching by PL-extract might also be operative. Indeed, literature has shown that DOM that can interact with excited triplet states of ketones leads to inhibited photolytic transformation of the ketone moiety (Loutfy and Yip, 1973; Schuster, 1975). Based on the results with PL-extract, the organic matter in runoff from PL-fertilized lands is likely to exert mostly scavenging effects on IPAs' photo-degradation.

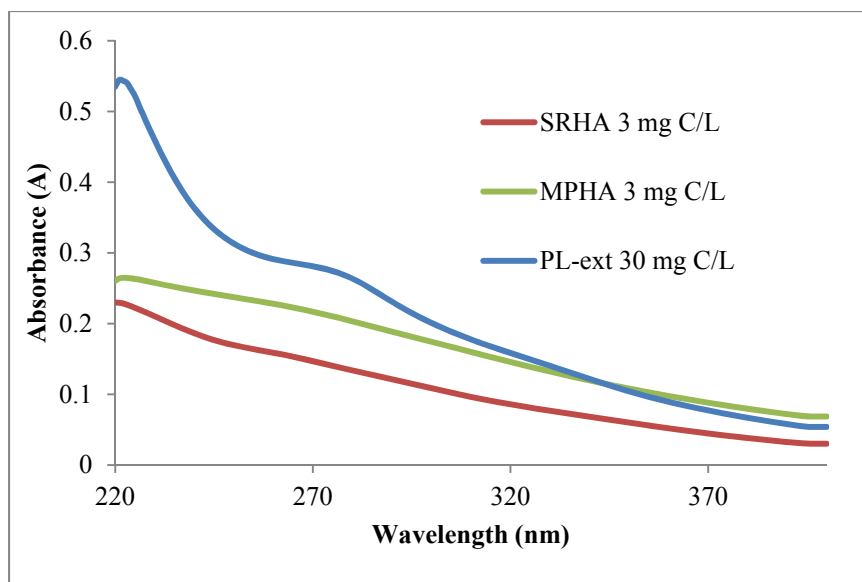


**Figure 5.7** UV-Vis absorbance of DOM working solutions.

### 5.3.2.3 Real water matrix

The photolysis of IPAs was examined in three real water samples with different light irradiations, including corrected WWTP secondary effluent (with UV), simulated plume water from a poultry farm (with sunlight), and simulated surface runoff from PL-fertilized land (with sunlight). Characteristics of the selected real water matrices are listed in Table 5.1.

Both MON and SAL were degraded in WWTP effluent and surface runoff, whereas no significant loss of IPAs was detected in the plume matrix for over 5 days under sunlight irradiation. Half-lives of MON and SAL were 1.2 and 0.95 hours in WWTP effluent, respectively. Considering a typical UV disinfection dosage of 100 mJ/cm<sup>2</sup> (i.e., around 2 min of UV irradiation in this study), neither MON nor SAL would be efficiently removed by UV treatment (less than 3% removal). Indeed, our previous study showed that, even at LP UV combined with 30 mg/L H<sub>2</sub>O<sub>2</sub> AOP conditions, it requires ~1000 mJ/cm<sup>2</sup> to remove over 90% of IPAs in WWTP effluent matrix (Yao *et al.*, 2013). In surface runoff, the rate constants of MON and SAL were 0.007 and 0.015 h<sup>-1</sup>, respectively, in the spring season. Comparing with the photolysis of IPAs in DI water matrix, the degradation of MON substantially increased, whereas the enhancement of the degradation of SAL was not significant.

The overall photodegradation of IPAs in real water matrices is a result of both direct and indirect photolysis. A steady-state model (Equation 5.4) was applied to predict IPA photolysis rates with the assumptions that (1) nitrate was the main photo-reactive constituent in the sample, and (2) DOM was considered for its scavenging effect on HO· reactions.

$$\begin{aligned}
 k_{\text{obs}} &= k_{\text{direct}} + k_{\text{indirect}} \\
 &= \int \Phi_{\text{IPA}/\lambda} \cdot 2.303 \cdot (1 - \exp(-A_{\lambda})) \cdot f_{\lambda} \cdot I_{\lambda} \cdot l \\
 &\quad + \frac{k_{\text{IPA}/\text{HO}\cdot} \int 2.303 \cdot I_{\lambda} \cdot l \cdot \epsilon_{\text{NO}_3^-/\lambda} \cdot [\text{NO}_3^-] \cdot \Phi_{\text{NO}_3^-}}{k_{\text{IPA}/\text{HO}\cdot} \cdot [\text{IPA}] + k_{\text{DOM}/\text{HO}\cdot} \cdot [\text{DOM}] + k_{\text{HCO}_3^-/\text{HO}\cdot} \cdot [\text{HCO}_3^-] + k_{\text{CO}_3^{2-}/\text{HO}\cdot} \cdot [\text{CO}_3^{2-}]}
 \end{aligned} \tag{5.4}$$

Applying this model, the observed rate constants of MON and SAL can be predicted in different water matrices. Shown in Table 5.2, the predicted values were close to the experimental rate constants for surface runoff and plume water matrices. However, although the prediction had a good agreement for MON in WWTP effluent, the model substantially overestimated the degradation of SAL, which may be caused by stronger interactions of DOM in WWTP effluent with photo-excited ketone moiety of SAL than the DOM in surface runoff and plume water.

### ***5.3.3 Product identification and photolytic transformation mechanism***

#### ***5.3.3.1 Products of SAL via direct photolysis***

Nine new significant peaks representing the major transformation products of SAL (SAL-TPs) were observed in the direct photolysis experiments (Figure 5.8), which had  $m/z$  (sodium adduct) of 265, 337, 447, 489, 491, 507, 519, 531, and 805. Although all nine SAL-TPs were detected in the samples under UV, simulated sunlight and natural sunlight irradiation, the most abundant products were different with respect to each light source when assuming similar MS signal response for each product (Figure 5.9). Under UV irradiation,  $m/z$  489 and 805 were the dominant SAL-TP species in the first 4 hours of irradiation and then were replaced by  $m/z$  265. SAL-TPs with  $m/z$  447, 265, and 507 were most abundant under simulated sunlight irradiation, whereas  $m/z$  447 was not among the major SAL-TPs in samples exposed to natural sunlight. This light-dependent generation of SAL-TPs may be resulted from two possible mechanisms. First, the absorbance of SAL overlapping with UV, simulated sunlight and natural sunlight at different wavelengths, may favor specific photolytic transformation pathways to yield certain dominant SAL-TPs (Figure 5.4). Indeed, dominant SAL-TPs were more similar under simulated and natural sunlight, than those under LP UV. Second, the photolytic stability of SAL-TPs may be different under each light source irradiation, which might also lead to different dominant SAL-TP species.

LC/MS/MS was employed to obtain more structural information of SAL-TPs. The mass spectra of parent SAL as well as selected SAL-TPs are shown in Figure 5.10. The SAL-TPs with  $m/z$  of 489, 491, 507, 519 and 531 were featured by almost identical fragmentation patterns below  $m/z$  of 500 with parent SAL. The common base peaks,  $m/z$  431(433) and 403, suggested that the products retained rings B-E, i.e., the right part of SAL molecule as shown Figure 1.1.

Fragment  $m/z$  433, instead of  $m/z$  431, was present in some of SAL-TPs, which may be due to an alcohol group addition onto C12, rendering the ring B more easily to obtain a hydrogen atom from the alcohol group during fragmentation, instead of forming a double bond between C13 and C14 (Volmer and Lock, 1998). It is also noteworthy that the identified SAL-TP  $m/z$  531 is the same as the major biotransformation product of SAL in poultry litter or in soil (Hansen *et al.*, 2012; Vertesy *et al.*, 1987).

Fragmentation of SAL-TPs  $m/z$  265, 337, and 447 were not successful using LC/MS/MS. However, the direct photolysis of NAR also yielded products  $m/z$  337 and 447, indicating that these products did not contain ring A. Additional to SAL-TP  $m/z$  265, the direct photolysis of NAR yielded a new product  $m/z$  279, which is 14 Da increased from 265. The presence of both  $m/z$  265 and 279 suggests photolysis of SAL yielded two SAL-TPs with  $m/z$  265, one with ring A and the other without ring A.

SAL-TP  $m/z$  805, along with 787 and 789 (observed, but not significant peaks), referred to as oxyl-SALs, were likely the parent SAL added with one or two oxygen atoms, forming additional ketone or alcohol groups. Multiple peaks of SAL-TP  $m/z$  805 were detected in the ion chromatogram (Figure 5.10), suggesting multiple sites of parent SAL were subjected to oxygen addition. It was also found that the oxyl-SALs were not photolytically stable and were degraded over time.

Based on the identification of major transformation products, the overall direct photolytic transformation of SAL was proposed in Figure 5.11. The molecular structures of SAL-TPs clearly indicated that direct photolysis of SAL occurred majorly on its ketone moiety. Ketone-containing compounds are subject to direct photolysis with UV or sunlight irradiation, whose mechanisms were detailed in Turro *et al.* 2012 (Turro *et al.*, 2012). Briefly, photo-excited ketone

group would form a diradical intermediate (i.e.,  $>C=O \rightarrow >C\cdot-O\cdot$ ), which further transforms via either  $\alpha$ -cleavage on the ketone carbon with the adjacent carbon, or hydrogen abstraction from suitable donors by the ketone oxygen atom. The latter mechanism could also lead to the formation of ROS, such as  $\cdot OOH$  and  $O_2^{\cdot-}$ , with the presence of dissolved oxygen. The generation of SAL-TPs with  $m/z$  less than parent SAL was likely due to the  $\alpha$ -cleavage pathway, whereas the formation of oxyl-SAL clearly suggests ROS generation during direct photolysis of SAL. Moreover, since direct photolysis experiments were performed in DI matrix without any organic compounds other than SAL, it indicates that ROS was produced via intramolecular hydrogen abstraction of photo-excited SAL. To further confirm the self-photosensitized reactions of SAL, 1% (v/v) *t*-butanol (a ROS scavenger) or MON was spiked into DI matrix with SAL under simulated sunlight irradiation. Results showed that the degradation rate of SAL decreased by about 27% in the samples with *t*-butanol, and degradation of MON was observed in the solution containing 2.5 mg/L SAL (Table 5.3). These observations confirmed that ROS were generated during the direct photolysis of SAL. However, we caution that, at the current stage, the role of impurities from SAL chemical was not able to be tested. Thus, the possibility that some reactive species were generated by impurities cannot be ruled out.

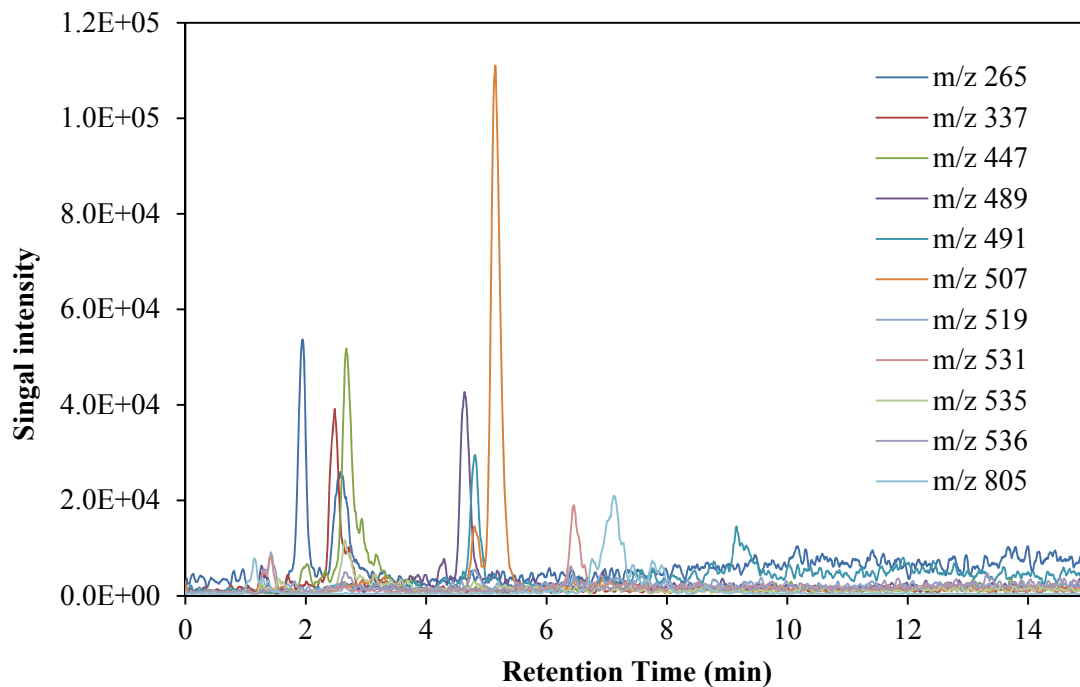


**Figure 5.8** Ion chromatograms of TP-SALs on LC/MS.

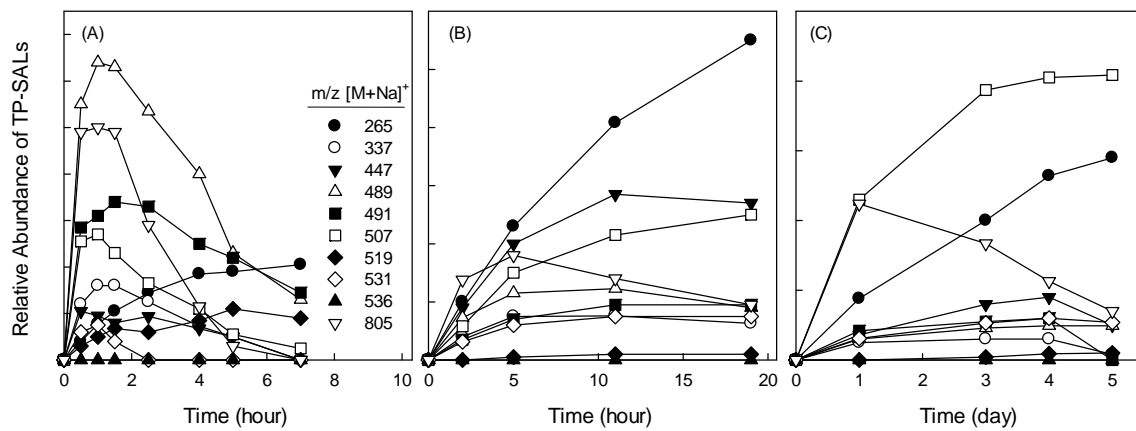
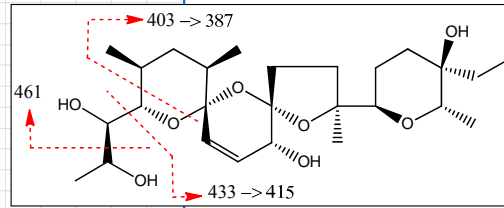
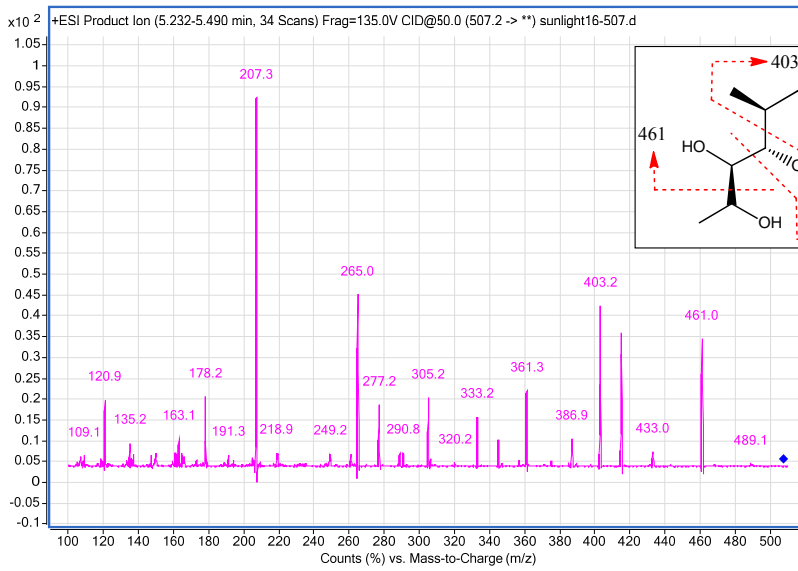
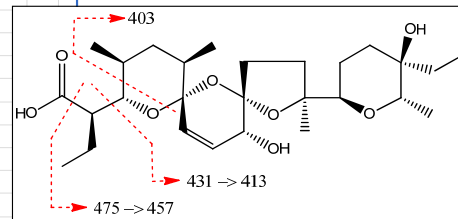
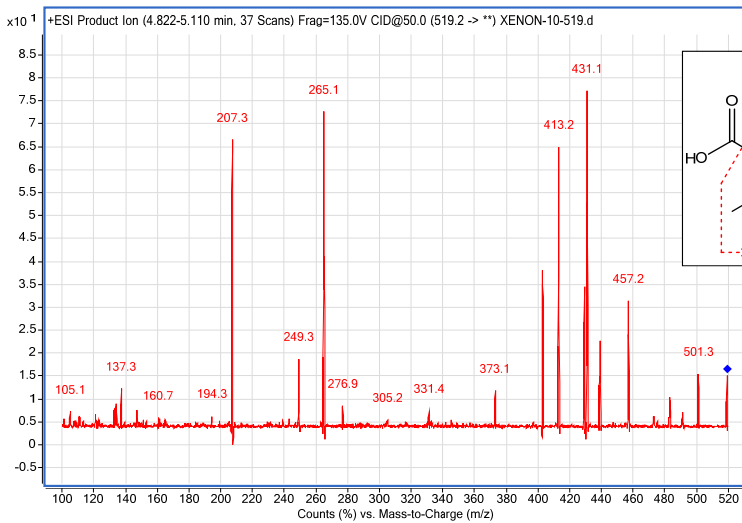


**Figure 5.9** SAL photolytic transformation products under LP UV (A), simulated sunlight (B), and natural sunlight (C) irradiation in DI water matrix.

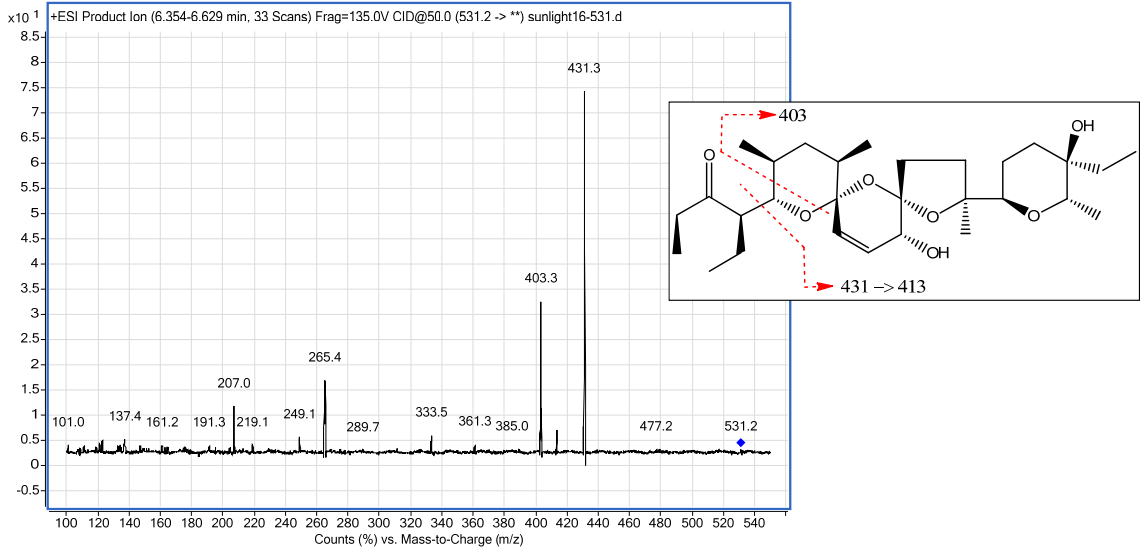
m/z = 507



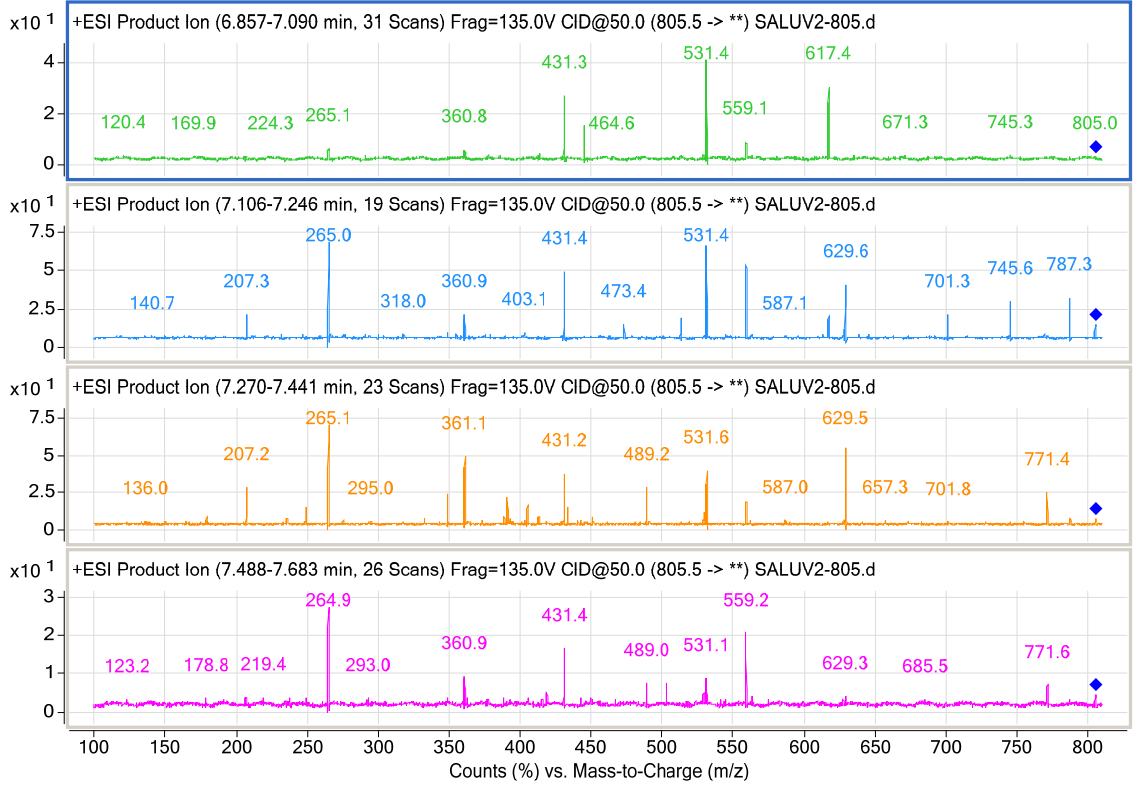
m/z = 519



m/z = 531



m/z = 805



$m/z = 536$

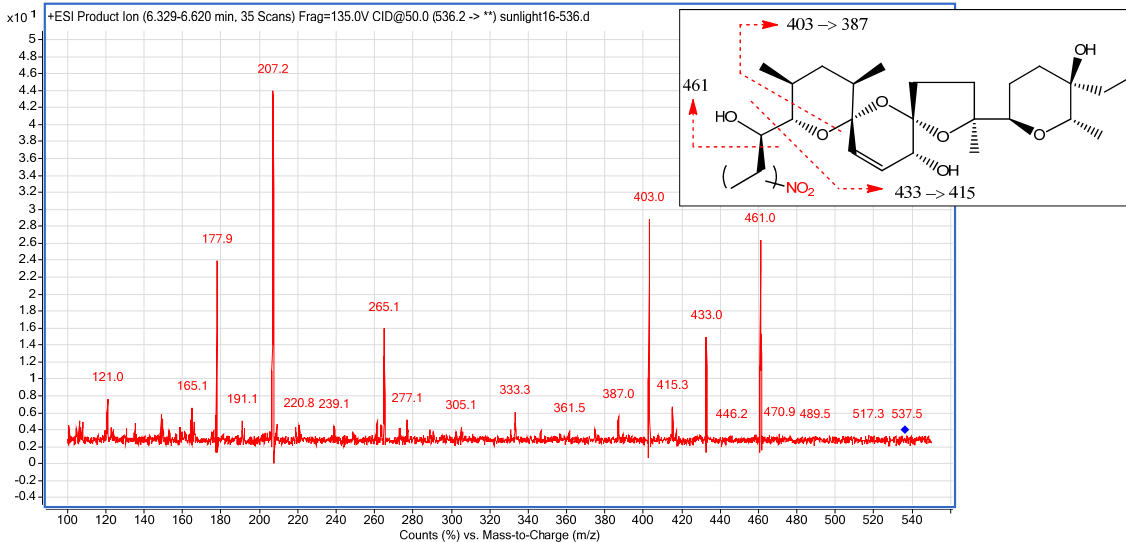


Figure 5.10 MS/MS fragmentation patterns of selected TP-SALs.

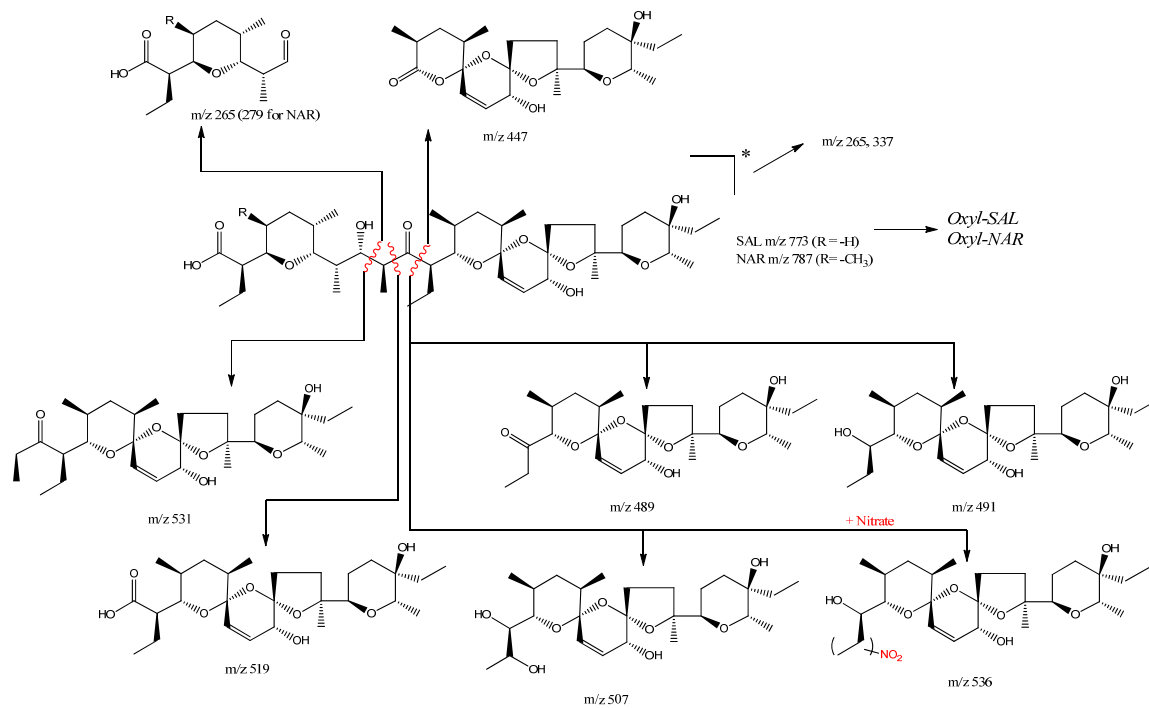


Figure 5.11 SAL photolytic transformation pathways

**Table 5.3** Direct photolysis of SAL under simulated sunlight: effects of the presence of *t*-butanol or MON

<b>Conditions</b>	<b><i>k</i> (hr<sup>-1</sup>)</b>	<b>Results</b>
SAL	0.22	Oxyl-SAL production
SAL + 1% <i>t</i> -butanol	0.16	No oxyl-SAL production
MON	<0.01	No degradation
SAL + MON	0.05 (for MON)	MON degraded; Oxyl-MON production

### 5.3.3.2 Photolysis products of IPAs with nitrate

Five major peaks were observed during the photolytic degradation of MON with the presence of nitrate under simulated sunlight. They were with  $m/z$  (sodium adduct) of 723, 709, 707, 691 and 549 (called MON-TPs, shown in Figure 5.12). The MON-TPs with  $m/z$  of 723, 709, 707 and 691 were observed in our previous study, which investigated MON degradation under UV/H<sub>2</sub>O<sub>2</sub> AOP conditions (Yao *et al.*, 2013). UV at 254 nm combined with H<sub>2</sub>O<sub>2</sub> is well known to produce hydroxyl radicals as primary reactive species. Therefore, the consistent  $m/z$  values of MON degradation products observed in this study confirmed that the major mechanism responsible for photolytic degradation of MON in the presence of sunlight and nitrate was due to reactions with hydroxyl radicals. MON-TP with  $m/z$  of 549 was believed to be a secondary transformation product yielded from other MON-TPs.

Indirect photolysis of SAL with nitrate yielded almost identical SAL-TPs with direct photolysis, except that a new dominant peak with  $m/z$  (sodium adduct) of 536 was observed. It is interesting to note that an even  $m/z$  (sodium adduct) value was observed on MS with ESI(+) mode, which suggested the molecule contains an odd number of nitrogen atoms. Because parent SAL only contains C, O, and H atoms, it is likely that the indirect photolysis of SAL involved in a reaction with RNS generated by photo-excited nitrate. To test this hypothesis, indirect photolysis of SAL was conducted with the presence of <sup>15</sup>N-nitrate. The new peak with  $m/z$  of 537 was observed on LC/MS, instead of  $m/z$  of 536, which confirmed that one nitrogen atom was incorporated into SAL-TP. MS/MS fragments (Figure 5.10) indicated that nitration of SAL likely occurred on C35 or C36, yielding the proposed molecular structure (Figure 5.11). It should be pointed out that while nitration of aromatic organic pollutants via photolysis of nitrate/nitrite was observed in a number of studies (Vione *et al.*, 2006; Vione *et al.*, 2003; Vione *et al.*, 2002;

2005; Vione *et al.*, 2001), the above finding is among the first to report photo-nitration of ketone-containing compounds.

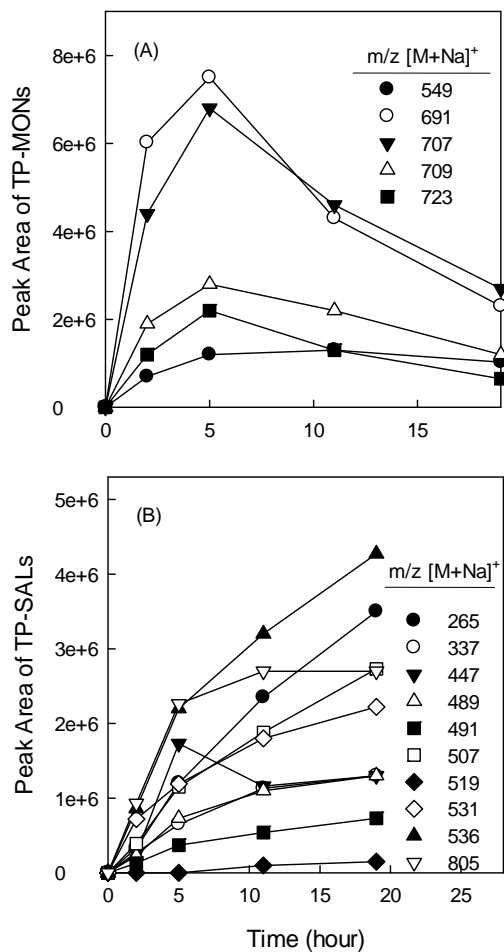


**Figure 5.12** MON (A) and SAL (B) photolytic transformation products under simulated sunlight irradiation with 5 mg/L NaNO<sub>3</sub>.

#### 5.3.4 Toxicity tests

MON was stable in water matrix without any photosensitizers. MON-TPs via indirect photolysis of MON, once generated, was quickly degraded by the same reactive species (e.g., HO·). In contrast, SAL-TPs via either direct or indirect photolysis showed relatively persistent in aqueous solutions. Therefore, toxicity tests were performed for SAL-TPs.

The growth of *Bacillus subtilis* was shown to be sensitive to IPA concentration and thus this microorganism was chosen for the toxicity tests (Dorkov *et al.*, 2008; Sun *et al.*, 2013b). The growth inhibition is expressed in Equation 5.5.

$$\text{Growth Inhibition (\%)} = \left( 1 - \frac{\text{OD}_{600}(\text{Sample})}{\text{OD}_{600}(\text{Control})} \right) \times 100 \quad (5.5)$$

As shown in Figure 5.13, the growth of the target microorganism was sensitive to the tested SAL concentration (i.e., 100 – 400 µg/L). A linear regression was obtained to correlate the inhibitory effect and the residual SAL concentration. The inhibitory effects of SAL photolysis samples via direct photolysis or indirect photolysis with NaNO<sub>3</sub> were almost identical to those of SAL standards, which indicated that the inhibitory effect of SAL photolysis samples was contributed by the residual parent SAL. Thus, SAL-TPs do not present apparent toxicity against the target microorganism.

Indeed, the antibiotic property of IPAs was known to relate to their ability to complex with metal cations (Chapman *et al.*, 2010; Westley, 1983). Multiple oxygen atoms on IPAs' cyclic ether moieties coordinate to the metal cation and the carboxylic and alcoholic end groups connected together to form a pseudo-cyclic conformation (Westley, 1983). However, the major SAL-TPs were produced via cleavage on the ketone moiety, yielding SAL-TPs with smaller molecular sizes. As a result, SAL-TPs contained fewer oxygen atoms, and the molecules were

more rigid, which decreased the affinity to complex with metal cations. Therefore, SAL-TPs did not present inhibitory effects in the toxicity assay.

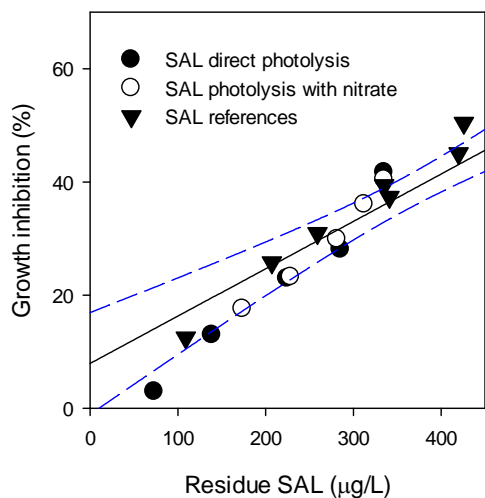


**Figure 5.13** Toxicity test of SAL photolytic transformation products. Dashed lines represent 95% confidence level.

## 5.4 Environmental Implications

Among the three commonly used IPAs, MON shows resistance to direct photolysis whereas SAL and NAR can be degraded via direct absorption of UV or sunlight. Environmental conditions can greatly affect IPAs' photodegradation. Water near agricultural fields contains significant amounts of nitrate, which will enhance the photo-degradation of IPAs. On the other hand, the DOM from poultry manure showed strong inhibition on the direct photolysis of SAL. More than one type of IPAs may co-exist in animal waste or agricultural runoff depending on feed composition. Interestingly, our results showed that MON's photolysis can be sensitized by SAL in DI water via reactive species production. However, such impact from SAL may be modest in the environment because SAL concentration in natural waters is expected to be low. Additionally, the toxicity tests showed that photolysis of IPAs eliminated their antibiotic properties against the target microorganism.

Because photodegradation strongly depends on light irradiance and water matrix, IPA photodegradation will be most important at summer time in shallow water containing low concentrations of DOM. The photolysis half-lives observed in this study were 4.1 and 1.9 days for MON and SAL, respectively, in agricultural runoff in April. These half-lives are relatively short compared to other degradation mechanisms of IPAs. For example, our previous study on the hydrolysis of IPAs showed that in mildly acidic water (pH 6 – 7), MON was stable and the half-lives of SAL were 9 – 53 days (Sun *et al.*, 2013b). The degradation of IPAs in the top soil fertilized with IPA-containing PL was also studied and showed that SAL was stable while the half-life of MON was around 10 days (Chapter 6, (Sun *et al.*, 2014)). However, considering that photodegradation primarily occurs in the top layer of water bodies, the IPA photodegradation rates in the environment are expected to be slower than the observed rates in this study.

Nevertheless, it is evident that photodegradation of IPAs is a competitive process compared to hydrolysis and biodegradation, which all contribute to influencing the environmental fate of IPAs.

## CHAPTER 6

### BIODEGRADATION OF VETERINARY IONOPHORE ANTIBIOTICS IN POULTRY LITTER AND SOIL MICROCOSMS

#### 6.1 Introduction

In broiler production, it is estimated that one kg of chicken feed contains around 300 mg of IPAs (MON, SAL and NAR combined, UCS, 2001). However, because IPAs are poorly absorbed and broken-down in the animals' gut, more than 80% of the administered IPAs may be excreted (EFSA., 2004), and found in the poultry litter (PL) at 0.2 – 20 mg/kg (Sun *et al.*, 2013a). After stacking (i.e., a process of stockpiling waste litter), the PL is almost always used to fertilize agricultural fields at a rate of at least 5 metric tons/hectare/application (Kuykendall *et al.*, 1999), which may result in 1-100 g of IPAs/hectare/application. Thus, PL is likely a major source of IPA release into the environment. Therefore, PL and soil are the two major components where IPAs would be subject to active biodegradation.

Although little information is available regarding the degradation of IPAs in the PL, several studies have investigated IPA degradation during animal manure composting. MON and SAL half-lives <5 days to > 10 weeks have been reported, depending on the type of animal manure and composting conditions (Dolliver *et al.*, 2008a; Donoho, 1984; Ramaswamy *et al.*, 2010; Schlusener *et al.*, 2006). Dolliver *et al.* reported a half-life of 17 days for MON in turkey litter composting (Dolliver *et al.*, 2008a). SAL in stored pig manure under anaerobic conditions at 20°C degraded with a half-life of 5 days (Schlusener *et al.*, 2006).

Decrease of IPAs in soil has also been reported. The half-life of MON applied to agricultural soil at 300 µg/kg was 3.3 and 3.8 days with and without manure amendment, respectively (Carlson and Mabury, 2006). MON decreased over 10 days in non-sterilized soils; in

contrast, after an initial decrease of 40% within 5 days, MON was stable for over 40 days in sterilized soil samples (Sassman and Lee, 2007). SAL-amended soil incubated under aerobic conditions resulted in its disappearance with a 5-day half-life (Schlusener and Bester, 2006).

Although half-lives of IPAs in animal waste and soil have been reported, information related to IPA degradation potential and biotransformation products is limited. The objective of this study was to investigate the biodegradation of IPAs under conditions typically encountered in PL and soil. Microcosms were set up to assess the effect of water content and temperature on the degradation of IPAs in PL, two parameters that are significant for the PL stacking process. Degradation of IPAs was also assessed in soil microcosms set up with PL-fertilized and non-fertilized soil samples, in which the effects of water content, carbon source amendment, and initial IPA concentration were investigated. Several primary biotransformation products of IPAs were detected. Additionally, PL and soil samples from a field study were analyzed to assess the fate and potential degradation of IPAs during litter stacking and subsequent application of the PL to agricultural fields, and the results were compared with those obtained in the laboratory study.

## **6.2 Materials and Methods**

### **6.2.1 Chemicals**

MON sodium salt (purity, 97%) and NAR sodium salt (purity, 97%) were purchased from Sigma-Aldrich (St. Louis, MO). SAL sodium salt (purity, 96%) was purchased from Fisher Scientific (Pittsburgh, PA). HPLC-grade methanol (purity, 99.9%), acetonitrile (ACN) (purity, 99.9%), analytical-grade formic acid (purity, 99%), and hexane (purity, 95%) were obtained from Sigma-Aldrich. All other reagents used were of analytical grade obtained from Fisher Scientific. Reagent-grade deionized (DI) water (resistance > 18 mΩ·cm) was obtained from a Millipore nanopure water purification system (Billerica, MA). Individual IPA stock solutions were prepared in methanol and stored at 4°C prior to use.

### **6.2.2 Poultry litter microcosms**

The PL used in this study was a mixture of litters obtained from several broiler farms across Georgia, U.S. The fresh litter was stored at 4°C without any treatment. The characteristics of PL and PL-water extract are shown in Table 6.1.

To assess the biodegradation potential of IPAs in PL, laboratory microcosms were established by adding 1 g of litter into 20-mL glass serum tubes, which were then sealed with rubber stoppers and aluminum caps in order to periodically monitor the headspace gas composition as an indicator of microbial activity. The tube headspace was refreshed every other day. Therefore, the PL microcosms were maintained under aerobic/microaerophilic conditions. IPAs were not added because the PL used contained a significant amount of IPAs (MON, SAL and NAR; Table 6.1). To distinguish biotic from abiotic degradation, autoclaved microcosms were set up and monitored in parallel with non-autoclaved ones. Preliminary tests showed that

IPAs were stable during autoclaving (21.5 psi, 121°C, 30 min).

The water content of fresh PL is typically 16 – 46% (water/wet litter, w/w) (Hartel *et al.*, 2000) and its water holding capacity is around 70%. In order to investigate the effect of water content on IPA degradation, water levels at 24, 40, 57 and 72% water/wet litter (i.e., 32, 67, 133, and 257% water/dry litter; translation between dry and wet weight basis is shown below) were tested. The 24 and 72% water content levels were chosen to represent PL in-situ and very high water content conditions, respectively. After addition of water, the tubes were vortexed to uniformly distribute water. All microcosms were kept in a 35°C constant temperature room.

The water content in litter and soil can be expressed either as water/dry litter or water/wet litter. The latter expression was used in this study as the degradation of IPAs was found to be more linearly correlated to water/wet litter as opposed to water/dry litter. The two expressions are related as shown in the equations below.

$$\text{water/wet litter} = \frac{\text{weight of water}}{\text{weight of water} + \text{weight of dry litter}} \quad (6.1)$$

$$\text{water/dry litter} = \frac{\text{weight of water}}{\text{weight of dry litter}} \quad (6.2)$$

$$\text{Therefore,} \quad \text{water/dry litter} = \frac{1}{\frac{1}{\text{water/wet litter}} - 1} \quad (6.3)$$

Temperature is another factor expected to significantly affect microbial activity and thus possible degradation of IPAs in PL. During stacking, the PL temperature gradually increases to above ambient temperature and ranges from 35 to 60°C, depending on aeration conditions and depth of the stacking piles (Kwak *et al.*, 2005). Thus, for this assay temperature values at 35, 45 and 60°C were selected to simulate conditions during litter stacking. In order to expand the temperature/water content combinations, assays were also conducted at 35°C with 64% water

content, and at 53°C with 64 and 72% water content.

### **6.2.3 Soil microcosms**

Surface soil samples (top 0-10 cm) were collected from an experimental plot with Bermuda grass/tall fescue that has been receiving PL for more than 10 years and from another plot that has not received PL or any organic fertilizer. The plots are located at the Central Research and Education Center of the University of Georgia (33° 24' N, 83° 29' W, elevation 150 m). The soil in the area is dominated by Cecil series (fine, kaolinitic, thermic Typic Kanhapludults). Soil characteristics are shown in Table 6.1. The soil microcosms were set up in a similar fashion as the PL microcosms. One gram of soil was transferred into glass serum tubes, which were then sealed with rubber stoppers and aluminum caps. Three microcosm series were prepared: soil, soil with sterilized water (1/1 w/w), and soil with sterilized PL water extract (1/1 w/w). The PL water extract was prepared by mixing water and PL (20/1 w/w) for 12 h, followed by centrifugation (3000 rpm, 10 min) and then filter-sterilized (0.2- $\mu$ m filters). Because the soil used in this study did not contain any measurable amounts of IPAs, MON and SAL at 1000  $\mu$ g/kg each were added to each soil tube. Control series were set up with autoclaved soil samples to distinguish between abiotic and biotic reaction(s). The tubes were incubated at room temperature (20-22°C).

### **6.2.4 Field study**

A field study was conducted in which fresh PL was spiked with MON and SAL at 1.5-2.0 mg IPAs/kg PL and then placed in a stacking bin (1.2 x 1.2 x 1.2 m) to a height of 1.2 m for 57 days. PL samples were collected at the center of the bin at 0, 14, 28, and 57 days. Samples were

homogenized for each sampling day, freeze-dried and ground, and then analyzed for MON and SAL. Temperature was measured at the center of each 0.3-m layer and recorded with data loggers.

A rainfall simulation study was also conducted in which PL samples from the stacking study were applied to a grassed plot (0.75 x 2 m, a Cecil soil) and rainfall was simulated at 75 mm h<sup>-1</sup> immediately after PL application until 30 min or runoff was generated. Top soil samples (0-5 cm) were collected at 0, 7, 14, and 21 days after rainwater was applied. During the study, the plot was covered with a clear polyethylene tarp, suspended 40-50 cm above ground, to prevent natural rainfall from reaching the plot.

#### ***6.2.5 Analytical methods***

The PL water content was measured gravimetrically after drying at 105°C for 12 h and its water potential was measured with a WP4C Dewpoint Potentiometer (Decagon Devices, Pullman, WA). The PL and soil organic carbon content was measured by dry combustion (Nelson and Sommers, 1982). Ammonia, nitrate, and phosphate in PL and soil extracts were measured following procedures outlined in Standard Methods (Association, 2012). Headspace gas composition (O<sub>2</sub>, CO<sub>2</sub>) was measured by gas chromatography (GC) with thermal conductivity detection.

Quantification of IPAs in PL and soil microcosms was achieved by extracting sacrificial tubes, followed by LC/MS analysis. Samples were spiked with nigericin, used as a surrogate standard, then extracted with a mixture of hexane and an aqueous buffer. After volume reduction of the solvent extract, the final analytes were reconstituted in 1 mL mixture of methanol and 10 mM Na<sub>2</sub>HPO<sub>4</sub> solution (50/50 v/v). Detailed sample preparation procedures have been shown in

Chapter 2 and in Sun *et al.*, 2013a. Extracted IPAs were routinely analyzed with an Agilent 1100 Series LC/MSD system (Agilent Technologies, Palo Alto, CA) equipped with a reversed-phase column (2.1×150 mm, 3 μm Ascentis RP-amide column; Supelco, Bellefonte, PA). The mass spectrometer was set at positive electron-spray ionization mode (ESI+). The sodium adducts of IPAs with m/z of [M+23] were used for quantification. A full-scan mode from 100 to 1700 m/z was applied for searching for transformation products. A LC/MS/MS unit (Agilent 1260 Infinity LC system, 6410 Triple Quad MSD, Agilent Technologies, Palo Alto, CA) was used for structural identification of IPA transformation products. The LC part was set at the same conditions as those stated above for the LC/MS. The MS parameters were fragmentation voltage 135 V, and collision-activated-dissociation (CAD) energy 70 eV.

**Table 6.1** Characteristics of Poultry Litter (PL), Non-fertilized Soil, and PL-fertilized Soil

Property	PL	Non-fertilized soil	PL-fertilized soil
	----- Solid -----		
$f_{oc}$ (kg OC/kg solid) <sup>a</sup>	0.275	0.024	0.030
MON (mg/kg)	0.2	<MDL <sup>b</sup>	0.005
SAL (mg/kg)	3.9	<MDL	<MDL
NAR (mg/kg)	0.18	<MDL	<MDL
	----- Water extract <sup>c</sup> -----		
pH (units)	7.2	5.7	6.3
NH <sub>4</sub> <sup>+</sup> (mM)	70	4.4	1.6
NO <sub>3</sub> <sup>-</sup> (mM)	0.01	12.3	13.0
PO <sub>4</sub> <sup>3-</sup> (mM)	4.72	0.3	4.6

<sup>a</sup> OC, organic carbon.

<sup>b</sup> MDL, method detection limit. MDL values are 0.001, 0.002, and 0.002 mg/kg for MON, SAL and NAR, respectively.

<sup>c</sup> Water extract prepared by mixing deionized water with solid at water to solid ratios (w/w) of 1/1 for soil, and 20/1 for PL. After shaking for 3 hours for soil, and 12 hours for PL, water extracts were passed through 0.2 µm filters.

## **6.3 Results and Discussion**

### ***6.3.1 Poultry litter and soil characteristics***

The PL was high in organic carbon and contained significant amounts of ammoniacal nitrogen and phosphate (Table 6.1). All three IPAs were detected in PL, and SAL was the highest at 3.9 mg/kg. Degradation of IPAs was not observed in PL kept at 4°C over the duration of the study. Nutrients were also available in the two soil samples used, with higher organic carbon and phosphate content in the PL-fertilized soil than in the non-fertilized soil. IPAs in both soil samples were below the method detection limits (MDLs; Table 6.1).

### ***6.3.2 IPA degradation in poultry litter microcosms***

#### ***6.3.2.1 Effect of water content on microbial activity***

The change of headspace O<sub>2</sub> and CO<sub>2</sub> content was used as an indicator of microbial activity in all PL microcosms incubated at 35°C. In all autoclaved PL microcosms, the headspace gas composition did not change over 14 days (data not shown). O<sub>2</sub> consumption and CO<sub>2</sub> production profiles suggest low microbial activity in PL microcosms with 24 and 40% water content, whereas active respiration occurred in the 57 and 72% series (Figure 6.1). The highest microbial activity was observed in litter with 72% water content, in which the headspace O<sub>2</sub> was completely consumed within 2 days initially, and within 1 day subsequently, suggesting increased microbial activity over time. In the 57% water content microcosms, O<sub>2</sub> was initially depleted in 4 days and then within 2 days. Overall, addition of water resulted in increased microbial activity in the PL microcosms incubated at 35°C.

It has been previously shown that microbial activity is strongly correlated with moisture content in animal waste and wood litters (Schimel *et al.*, 1999; Tiquia and Tam, 2002; Tiquia *et*

*al.*, 1996; Wagener and Schimel, 1998). Because PL is a mixture of chicken excreta and bedding materials, which usually contain wood shavings, the PL water content is expected to have a strong impact on microbial activity. The litter water content tested in this assay ranged from 24 to 72%, which corresponds to water potential values from -14.9 to -0.66 MPa (Figure 6.2). It was reported that water potential lower than -10 MPa greatly inhibited bacterial activity in soil (Parr *et al.*, 1981). Thus, microcosms with a water content of 24% represent a condition of severely limited water availability.

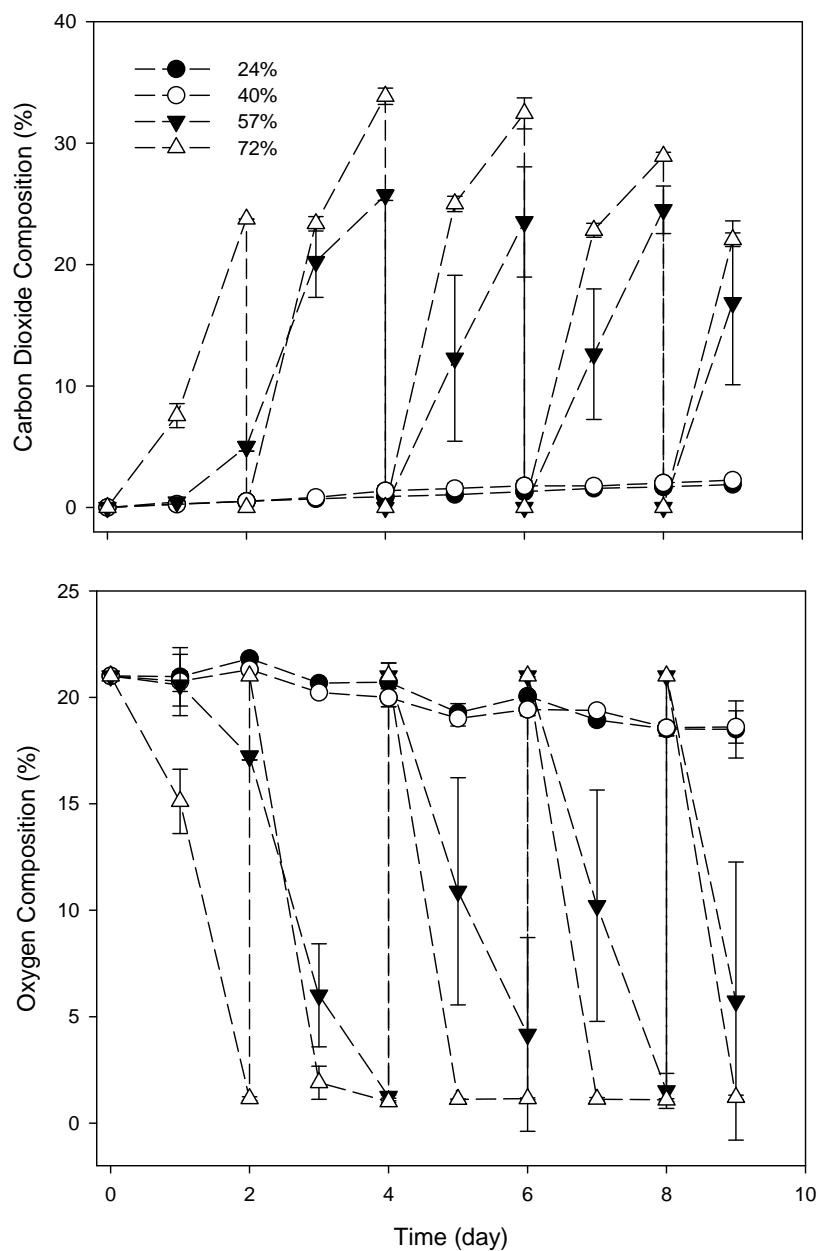


**Figure 6.1** Headspace gas composition of PL microcosms set-up with 24, 40, 57, and 72% water content and incubated at 35°C. Error bars represent one standard deviation of the means ( $n = 2$ ). The headspace was refreshed by opening the tubes every other day.

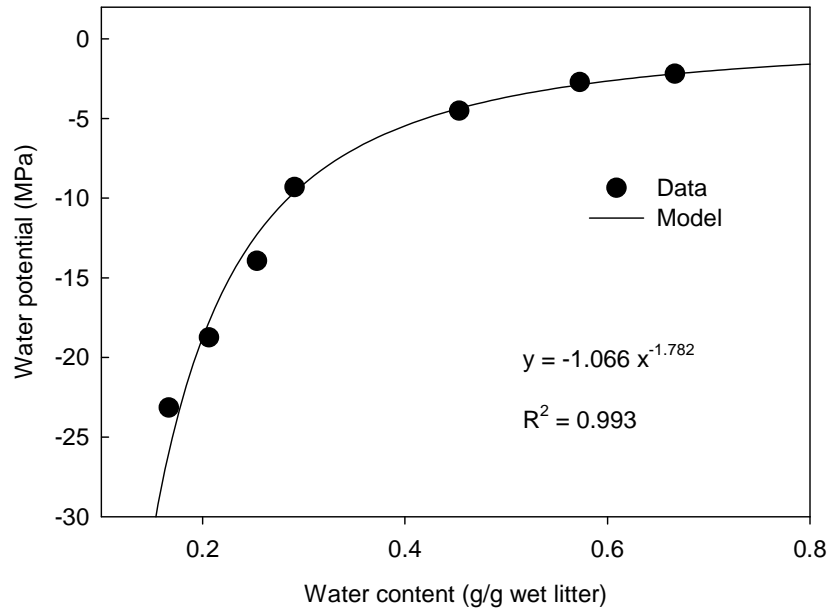


**Figure 6.2** Moisture release curve for poultry litter

### 6.3.2.2 Effect of water content on IPA degradation

Degradation of parent IPAs was not observed in PL microcosms with 24 and 40% water content over 14 days (Figure 6.3), which is consistent with the above-discussed low microbial activity (low O<sub>2</sub> consumption). However, SAL was almost depleted in PL microcosms with 57 and 72% water content, whereas NAR was depleted in microcosms with 72% water content after 14 days of incubation. MON, on the other hand, was stable in all PL microcosms over the 14-day incubation. The structures of SAL and NAR are very similar, except for a methyl group difference (see Figure 1.1 in Chapter 1). Thus, the degradation of SAL and NAR was expected to follow a similar trend. IPAs were not degraded in all autoclaved PL (data not shown), suggesting the loss of IPAs in non-autoclaved microcosms was due to biological activity. Overall, degradation of IPAs at 35°C was accelerated with an increase in the litter water content.

Our data clearly show that the water content is a limiting factor to microbial activity in PL at 35°C. Because the PL water content is typically 16-46% (Hartel *et al.*, 2000), the results of this study show that minimal biodegradation of IPAs is expected during the litter stacking process. However, after litter is applied to the field, its water content may increase (e.g., after rainfall), which will likely enhance microbial activity, thus creating conditions favorable for the degradation of IPAs.

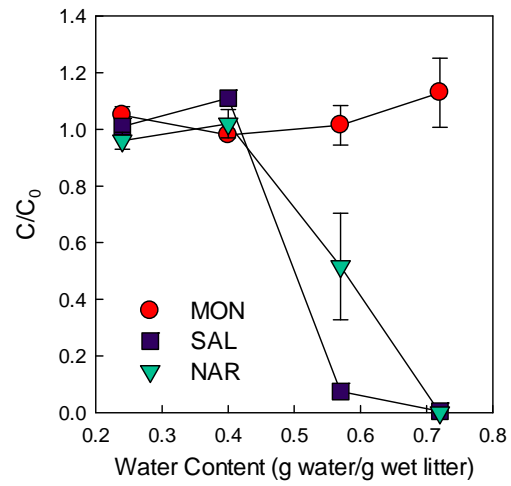


**Figure 6.3** Normalized IPA content in PL microcosms after 14-day incubation at 35°C and a range of PL water content. Error bars represent one standard deviation of the means ( $n = 2$ ).

### 6.3.2.3 *Effect of temperature on microbial activity and IPA degradation*

The O<sub>2</sub> consumption and CO<sub>2</sub> production in PL microcosms with 24% water content increased as the temperature increased from 35 to 60°C (Figure 6.4), indicating increased microbial activity with increasing temperature. However, the microbial activity in the PL microcosms with a water content of 72% was significantly lower at 60°C than at 35°C or 45°C. Correlated with microbial activity, SAL and NAR degraded faster in series with higher O<sub>2</sub> consumption and CO<sub>2</sub> production rates (Figure 6.4 and 6.5). However, MON was stable under all conditions tested. In all autoclaved PL microcosms, neither gas composition change in the headspace nor loss of IPAs was detected (data not shown), suggesting that SAL and NAR degradation in non-autoclaved microcosms was due to biological activity.

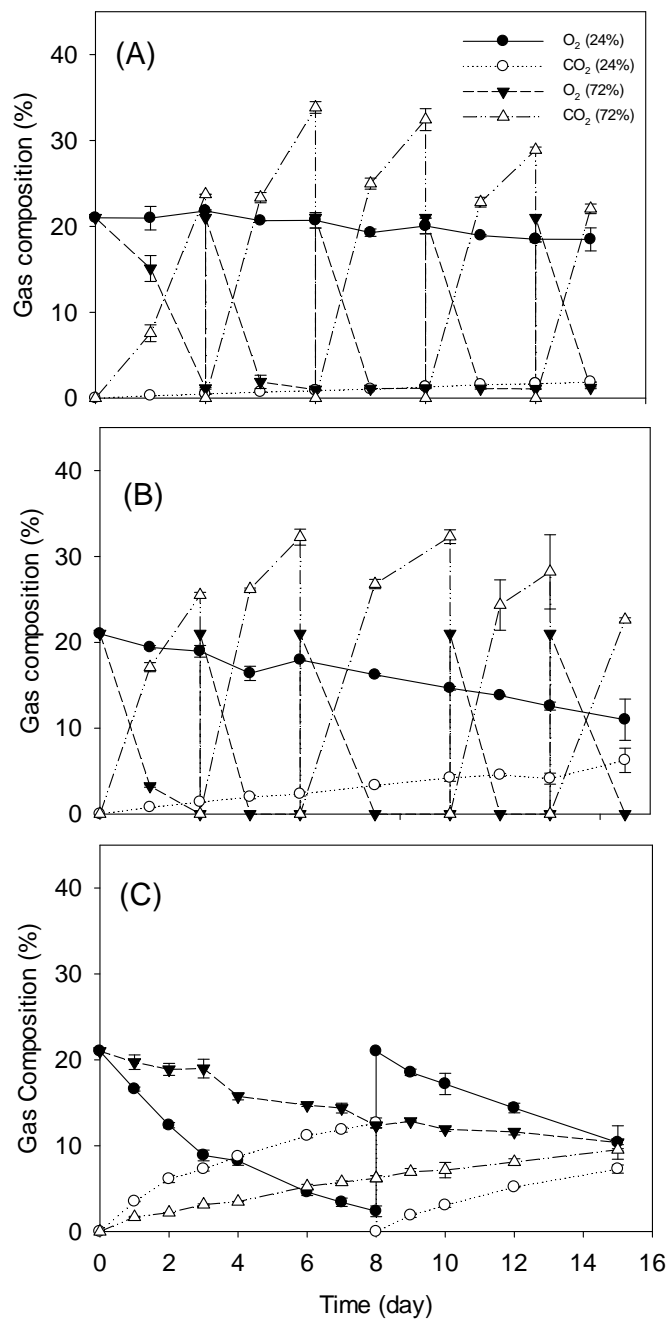


**Figure 6.4** Headspace gas composition of PL microcosms set-up with 24% and 72% water content and incubated at (A) 35°C, (B) 45°C and (C) 60°C. Error bars represent one standard deviation of the means ( $n = 2$ ).

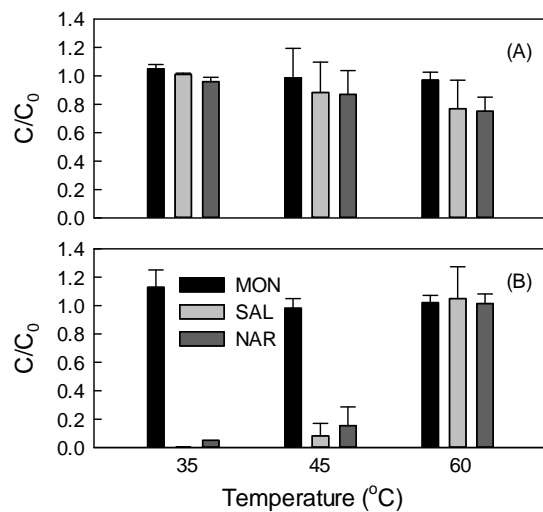


**Figure 6.5** Normalized IPA concentration in PL microcosms after 14-day incubation at 35, 45, and 60°C with 24% (A) and 72% (B) water content. Error bars represent one standard deviation of the means ( $n = 2$ ).

#### 6.3.2.4 Combined effect of water content-temperature on IPA degradation

Combining the results from water content and temperature effect assays, it is suggested that water content and temperature significantly affect both microbial activity and IPA removal in PL microcosms. Therefore, attempts were made to directly correlate IPA removal to microbial activity. Using CO<sub>2</sub> production as a measure of microbial activity in the PL microcosms, good linear correlations were obtained between the removal of both SAL and NAR and cumulative CO<sub>2</sub> production as shown in Figure 6.6, suggesting the increase in microbial activity led to a faster degradation of IPAs.

Our results also revealed that the effect of PL water content on IPA degradation depends on temperature and vice versa. Therefore, to quantitatively evaluate the effect of both water content and temperature on IPA degradation in PL microcosms, factor analysis was conducted to evaluate the water content and temperature interactive effects on the degradation of IPAs. Given the very low concentration of IPAs in the PL, the degradation of IPAs is assumed to follow non-growth, pseudo first-order kinetics as was previously reported for SAL.<sup>22</sup> Factor analysis was conducted based on the following equation:

$$k = \alpha_0 + \alpha_1 \cdot W + \alpha_2 \cdot T + \alpha_{1,2} \cdot W \cdot T \quad (6.4)$$

where  $k$  is the pseudo first-order IPA degradation rate constant (d<sup>-1</sup>);  $W$  is the water content (% water/wet PL, w/w);  $T$  is the incubation temperature (°C);  $\alpha_0$  (d<sup>-1</sup>) is a constant;  $\alpha_1$  (d<sup>-1</sup>),  $\alpha_2$  (°C<sup>-1</sup>·d<sup>-1</sup>) and  $\alpha_{1,2}$  (°C<sup>-1</sup>·d<sup>-1</sup>) are coefficients which evaluate the weighted effect from the change of  $W$ ,  $T$ , and the  $W$ - $T$  interaction, respectively, on the degradation of IPAs. Equation 6.4 is valid for  $W$  and  $T$  values at which  $k \geq 0$  (i.e.,  $k < 0$  means no degradation).

Applying Equation 6.4 for  $35 \leq T \leq 60^\circ\text{C}$  and  $24 \leq W \leq 72\%$  to SAL and NAR degradation rate data (Table 6.2) using the MatLab curve fitting toolbox (Figure 6.7), the

following expressions were obtained, respectively:

$$k_{\text{SAL}} = -0.864 + 0.023W + 0.0146T - 0.00039W \cdot T \quad (R^2 = 0.974) \quad (6.5)$$

$$k_{\text{NAR}} = -1.140 + 0.023W + 0.0193T - 0.00039W \cdot T \quad (R^2 = 0.867) \quad (6.6)$$

Analysis of variance (ANOVA, Table 6.3 and 6.4) shows  $p$ -value  $< 0.0001$ , which suggests Equation 6.4 captures the effects of water content and temperature on IPA degradation. Furthermore, the plot of estimated  $k$  values using Equation 6.5 and 6.6 versus those experimentally measured shows a very high correlation ( $R^2 > 0.943$ ; Figure 6.8). Therefore, Equation 2 and 3 are suitable in expressing IPA degradation in PL microcosms within the conditions examined in the present study.

Several IPAs degradation features could be obtained from the above expressions. Firstly, the coefficient values in Equation 6.5 and 6.6 are close, suggesting that the effect of water content and temperature on the degradation of SAL is similar to that of NAR. Secondly, the negative values of coefficient  $\alpha_{1,2}$  indicate that the interaction of water content and temperature have a negative effect on SAL and NAR degradation, which is mainly due to reduced oxygen solubility and transfer with increased temperature at a relatively high water content. In the case of PL with a water content of 72%, slurry was formed as it exceeded the water holding capacity of the PL and thus oxygen transfer to microorganisms through the aqueous phase was likely limited because of the lower oxygen solubility at a higher temperature (e.g., 60°C). In contrast, in PL microcosms with 24% water content, the litter interstitial spaces were filled with air, which allowed faster oxygen transfer. Thirdly, if  $k = 0$ , water content-temperature domains (Figure 6.9) are obtained for conditions under which SAL and NAR degradation did not occur. Therefore, in order to achieve degradation of IPAs in PLs, both water content and temperature should be adjusted and maintained at values outside these water content-temperature domains. Although

the domains may vary for different PLs, Equation 1 provides valuable insights into the management of PLs in order to reduce their IPA content. As previously mentioned, the litter temperature during stacking is typically in the range of 35-60°C (Kwak *et al.*, 2005), suggesting that addition of water up to PL water holding capacity (~70% water/wet litter) will result in enhanced IPA degradation.

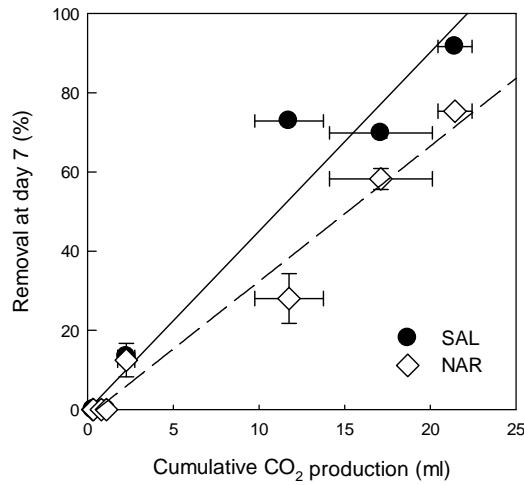


**Figure 6.6** Correlation of observed IPA removal with CO<sub>2</sub> production in PL microcosms set-up with water content from 24 to 72% and incubated at a temperature range from 35 to 60°C. Error bars represent one standard deviation of the means ( $n = 2$ ).

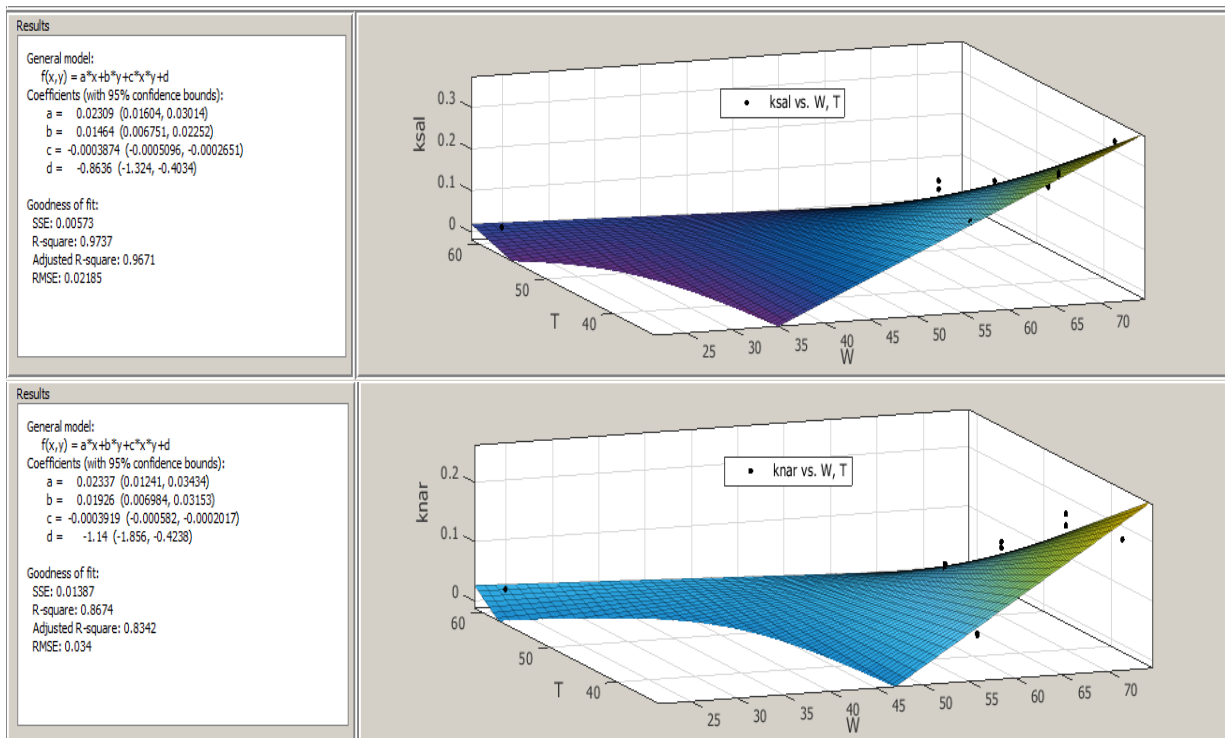


**Figure 6.7** Simulation of SAL and NAR degradation rates in PL microcosms using MatLab curve fitting toolbox.

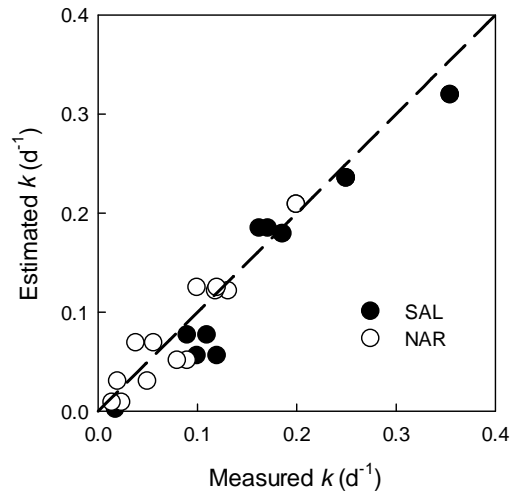


**Figure 6.8** Estimated values of IPA degradation rates versus experimentally measured values.

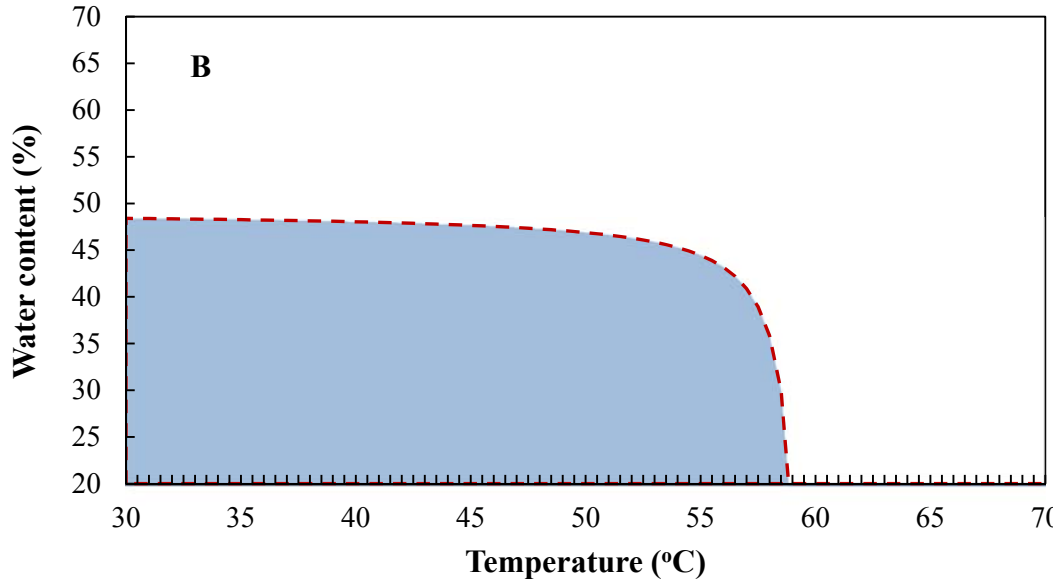
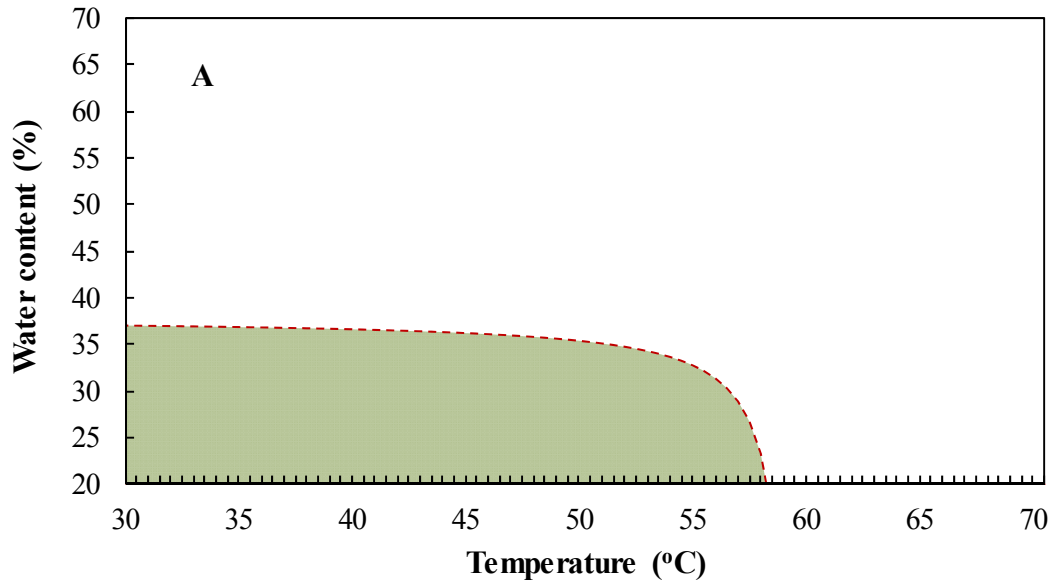


**Figure 6.9** Water content-temperature domain (shaded areas) where degradation of SAL (A) and NAR (B) in PL is not expected (i.e.,  $k = 0$ ).

**Table 6.2** Datasets for factor analysis

W (%)	T (°C)	$k_{SAL}$ (d <sup>-1</sup> )	$k_{NAR}$ (d <sup>-1</sup> )
24	60	0.02	0.02
24	60	0	0.01
57	35	0.19	0.06
57	35	0.19	0.04
63	35	0.25	0.12
63	35	0.25	0.1
63	53	0.1	0.05
63	53	0.12	0.02
72	35	0.36	0.2
72	35	0.35	0.2
72	45	0.17	0.13
72	45	0.16	0.12
72	53	0.11	0.09
72	53	0.09	0.08

**Table 6.3** ANOVA of SAL Data

Source	Sum of Squares	df	Mean Square	F Value	p-value Prob > F
Model	0.142	3	0.047	74.89	< 0.0001
W	0.023	1	0.023	36.95	0.0001
T	0.006	1	0.006	9.62	0.0112
WT	0.018	1	0.018	29.75	0.0003
Residual	0.006	10	0.001		

**Table 6.4** ANOVA of NAR Data

Source	Sum of Squares	df	Mean Square	F Value	p-value Prob > F
Model	0.046	3	0.015	97.55	< 0.0001
W	0.028	1	0.028	177.0	< 0.0001
T	0.003	1	0.003	20.15	0.0012
WT	0.020	1	0.020	131.4	< 0.0001
Residual	0.001	10	0.000		

#### 6.3.2.5 IPAs biotransformation products in poultry litter microcosms

One significant new peak was observed on LC/MS, with  $m/z$  of 531, named TP-SAL. Addition of SAL to PL microcosms on day 14 resulted in a sharp increase of TP-SAL production (Figure 6.10), confirming that TP-SAL was a SAL degradation product. Previous studies have shown products with  $m/z$  of 531 ( $[M+Na^+]$ ) formed as a result of either abiotic or biotic SAL transformation, albeit with different structures (Figure 6.11) (Hansen *et al.*, 2012; Schlusener *et al.*, 2006; Sun *et al.*, 2013b; Vertesy *et al.*, 1987; Wells *et al.*, 1988). In this study, LC/MS/MS was used to confirm the structure of TP-SAL. Compared to the SAL MS/MS spectrum, the fragmentation pattern of TP-SAL clearly shows that rings B, C, D and E are retained in the product (Figures 6.12, 6.13), which supports the structure of the previously identified product resulting from SAL biodegradation (Vertesy *et al.*, 1987). The structure of TP-SAL also implies that biodegradation of NAR yields the same product, because the difference between SAL and NAR occurs on the ring A moiety (Figure 1.1).

TP-SAL accumulated in PL microcosms during the 14-day incubation (Figure 6.10), showing that TP-SAL was stable under the conditions of the PL microcosm assay. To assess possible TP-SAL degradation in soil, selected samples were then mixed with non-fertilized soil at 1/1 PL/soil (w/w). After an incubation period of 10 days, no degradation of TP-SAL was observed, indicating that TP-SAL is not likely degraded after PL is applied to the field. Although TP-SAL may be persistent in the environment, a previous study showed that it does not form a complex with either sodium or potassium ions (Vertesy *et al.*, 1987). Thus, this product does not possess the antibiotic properties of ionophores which are associated with their capacity to form complexes with cations.

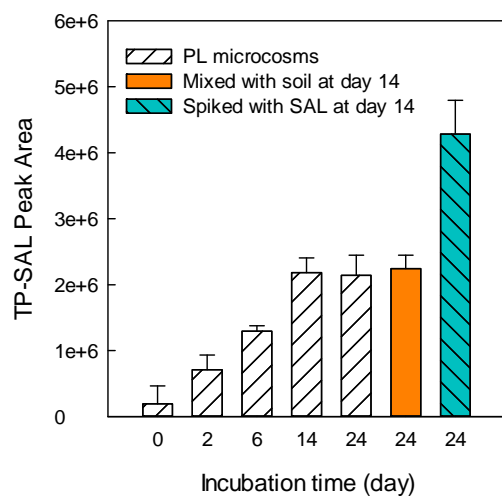


**Figure 6.10** Transformation product of SAL (TP-SAL) in the PL microcosms with 72% water content incubated at 35°C. At day 14, replicate microcosms were amended with non-fertilized soil (1/1, w/w) or 50 mg/kg SAL. Error bars represent one standard deviation of the means ( $n = 3$ ).

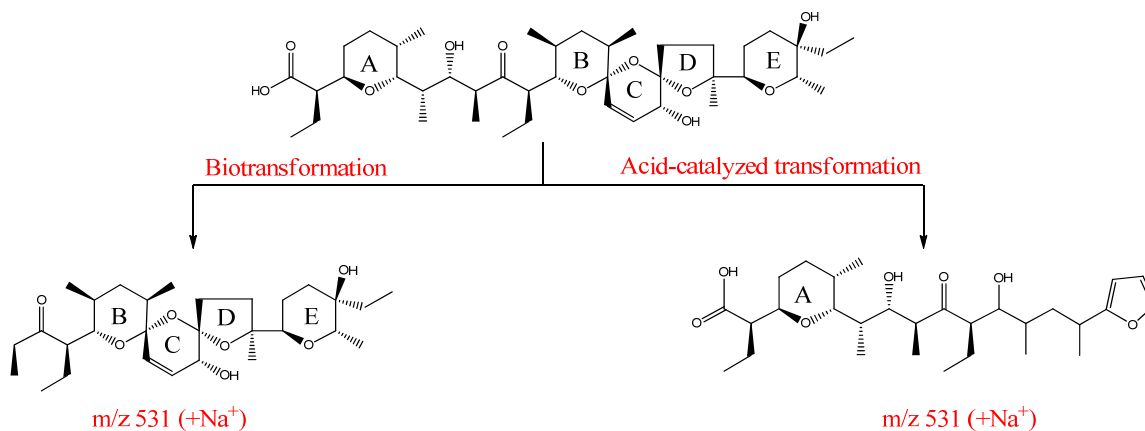


**Figure 6.11** Transformation of SAL yielding two products which have the same  $m/z$  of 531  $[M+Na]^+$  (Vertesy *et al.*, 1987; Wells *et al.*, 1988).

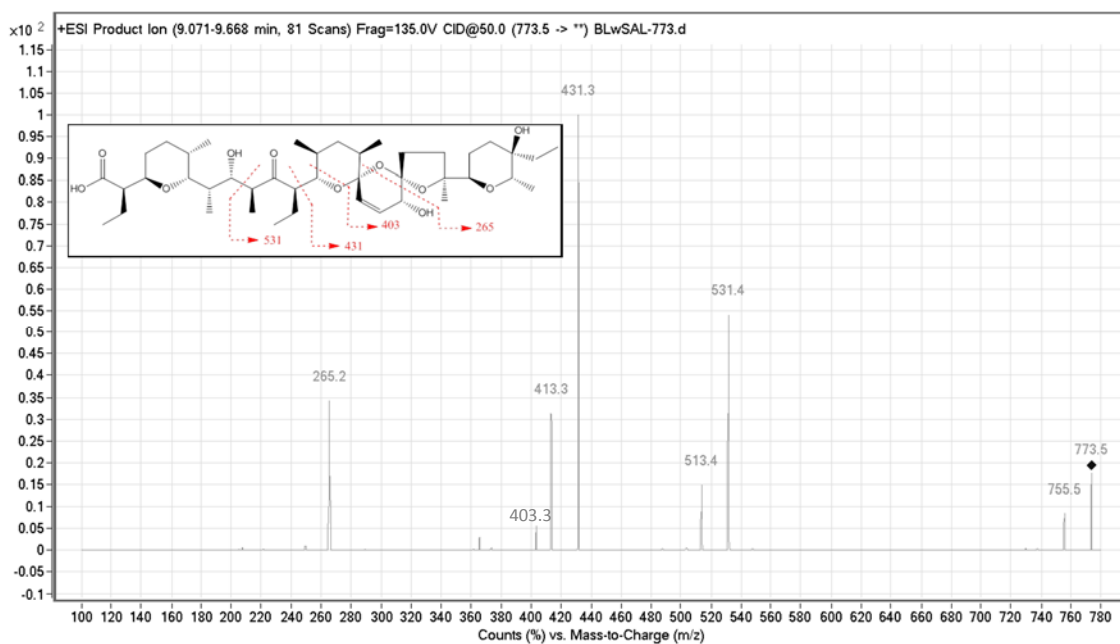


Figure 6.12. MS/MS spectrum of SAL.

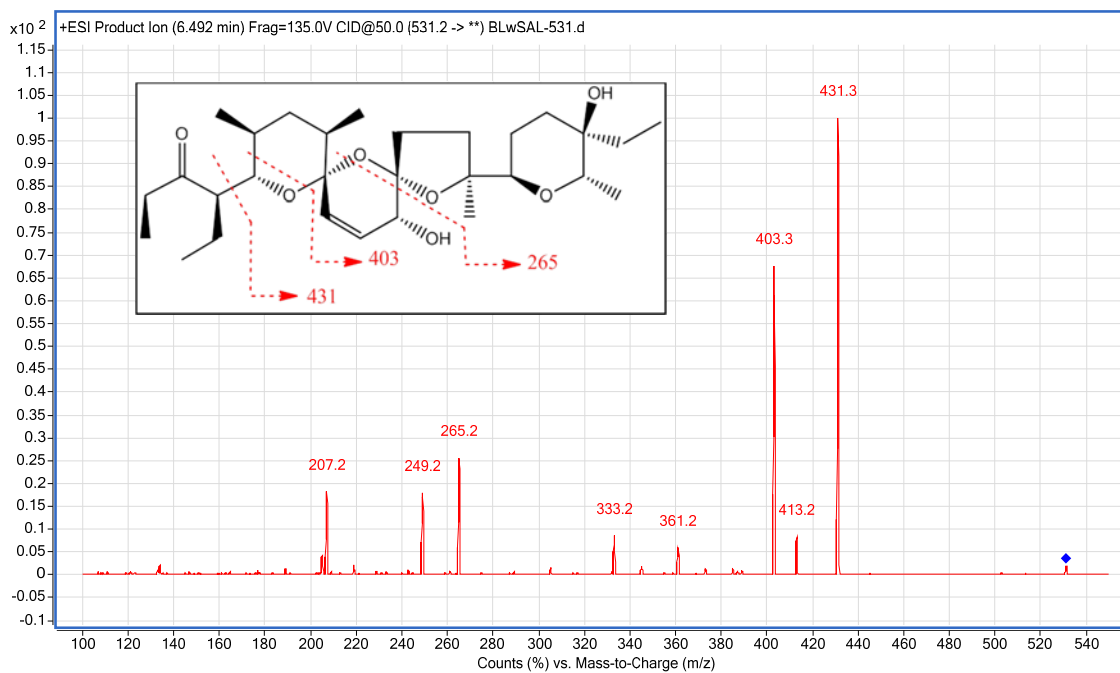


Figure 6.13 MS/MS spectrum of TP-SAL.

### **6.3.3 IPA degradation in soil microcosms**

#### **6.3.3.1 Degradation of parent IPAs in soil microcosms**

About 20% of MON was degraded in the control (i.e., autoclaved) non-fertilized soil microcosms under all three conditions (Figure 6.14 A-1), suggesting that abiotic degradation of MON occurred. Significant abiotic degradation (~20%) of MON was observed in the autoclaved PL-fertilized soil microcosms without water or filter-sterilized PL extract amendment (Figure 6.14 A-2). Degradation of MON was observed in non-autoclaved soil microcosms amended with water or PL extract regardless of whether the soil was fertilized or not. In contrast, minimal biodegradation of MON was observed in soil microcosms without water or PL extract amendment (Figure 6.14 A-1 and A-2).

Significant degradation (~80%) of SAL was observed in the non-fertilized soil microcosms without any amendment after a 7-day incubation period, whereas only 20-30% of SAL degraded in soil microcosms amended with water or PL extract (Figure 6.14 B-1). Unlike MON, the loss of SAL after a 7-day incubation period was comparable to that in the autoclaved soil microcosms under all three conditions (Figure 6.14 B-1), indicating that the decrease of SAL in non-fertilized soil microcosms was primarily due to abiotic reactions. About 25% SAL was degraded in autoclaved PL-fertilized soil microcosms under all three conditions (Figure 6.14 B-2). However, the loss of SAL was significant after a 7-day incubation period in non-autoclaved soil microcosms where 50 – 60% of SAL was biodegraded.

Assuming pseudo first-order kinetics, the half-lives of IPAs under the best conditions, i.e., soil with amendments, are comparable to previously reported values, between 3.3 and 5 days (Carlson and Mabury, 2006; Sassman and Lee, 2007; Schlusener and Bester, 2006). The observed degradation of MON and SAL in autoclaved soil microcosms suggests that abiotic

reactions contributed to the loss of the parent IPAs in the soil. However, caution is warranted when comparing autoclaved and non-autoclaved soil microcosms used in the present study as the soil structure and mineral properties may have been altered during autoclaving. Although no studies have directly investigated the abiotic transformation of IPAs in soil, one study indicated that abiotic degradation of MON in soil may be significant after observing a 40% loss of parent MON in  $^{60}\text{Co}$ -irradiated soil samples incubated for 30 days in the dark (Sassman and Lee, 2007). IPAs are known to undergo acid-catalyzed transformations (Sun *et al.*, 2013b). Given that the soil used in this study was slightly acidic (Table 6.1), IPAs likely underwent acid-catalyzed transformation. Though hydrolysis and some unknown products were observed in autoclaved soil samples, further identification of abiotic transformation products was beyond the scope of this study.

Compared to the autoclaved soil microcosms, MON was biodegraded in microcosms set up with both non-fertilized and PL-fertilized soil samples, which suggests MON degraders may be widely present in soil. Indeed, MON transformation by the soil bacterium *Sebekia benihana* has been reported (Vaufrey *et al.*, 1990). In contrast, SAL was only biodegraded in the PL-fertilized soil microcosms. Minimal SAL biodegradation observed in non-fertilized soil microcosms was not due to lack of nutrients because the PL extract is rich in carbon, nitrogen and phosphorus (Table 6.1). Therefore, microorganisms which can degrade SAL may not be widely present in the soil environment. In the PL microcosm assay, SAL readily degraded, whereas MON was persistent during the 14-day incubation. The above combined results imply that the microorganisms responsible for SAL degradation are likely introduced to soil with PL application.

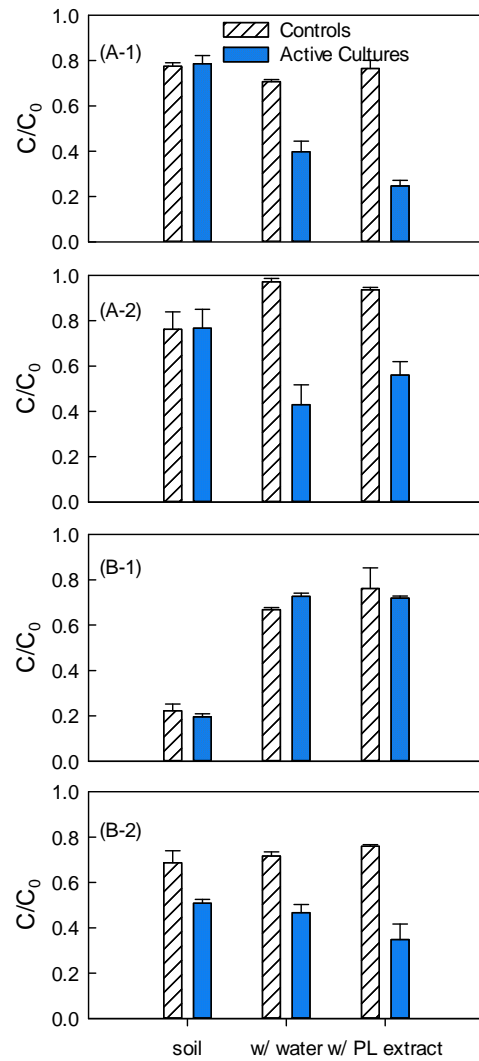


**Figure 6.14** MON (A) and SAL (B) normalized to initial IPA concentration (1 mg IPA/kg soil) in microcosms set up with non-fertilized (1) and PL-fertilized soil (2) after 7-day incubation. Abiotic controls were prepared with autoclaved soil. Error bars represent one standard deviation of the means ( $n = 3$ ).

### 6.3.3.2 IPAs biotransformation products in soil microcosms

Degradation of SAL in microcosms set up with PL-fertilized soil samples yielded one major product peak with  $m/z$  of 531 on LC/MS, which was identified by LC/MS/MS as the same biotransformation product as that observed in the PL microcosms (i.e., TP-SAL). Therefore, our efforts focused on the identification of MON biotransformation products in soil microcosms.

One product peak, named TP-MON ( $m/z$  707, an increase of 14  $m/z$  units compared to MON), was observed on LC/MS in soil samples incubated for 7 days. Analyses of autoclaved soil and reference soil (i.e., soil without MON amendment) confirmed that the new peak represented a product of MON biotransformation. To further investigate the biotransformation of MON by soil bacteria, assays were conducted with PL-fertilized soil samples at 50% water content with addition of MON at 0.2, 1 and 10 mg MON/kg soil. As shown in Figure 6.15 A, MON decreased over the incubation period with half-lives 4-6 days, which is consistent with previously reported half-lives of MON in soil (Carlson and Mabury, 2006; Sassman and Lee, 2007). It is noteworthy that MON degradation accelerated after the first two days, which may be due to an increase in the population size of MON degraders or the level of enzyme(s) involved in MON degradation in soil bacteria.

As MON decreased, the TP-MON peak area initially increased and then decreased (Figure 6.15 B), indicating TP-MON is likely biodegraded by soil bacteria. Assuming a similar MS signal response factor for MON and TP-MON, the sum of the peak areas of MON and TP-MON remained stable for the first 5 days in the samples with an initial 10 mg MON/kg soil, indicating that TP-MON is the major product resulting from the initial MON biotransformation (Figure 6.16). Indeed, about 40% of the parent MON was biotransformed to TP-MON in the first 5 days. However, samples amended with 0.2 and 1 mg MON/kg soil, the sum of peak areas

decreased overtime, which may be due to the fact that less TP-MON was generated and was efficiently removed by soil bacteria.

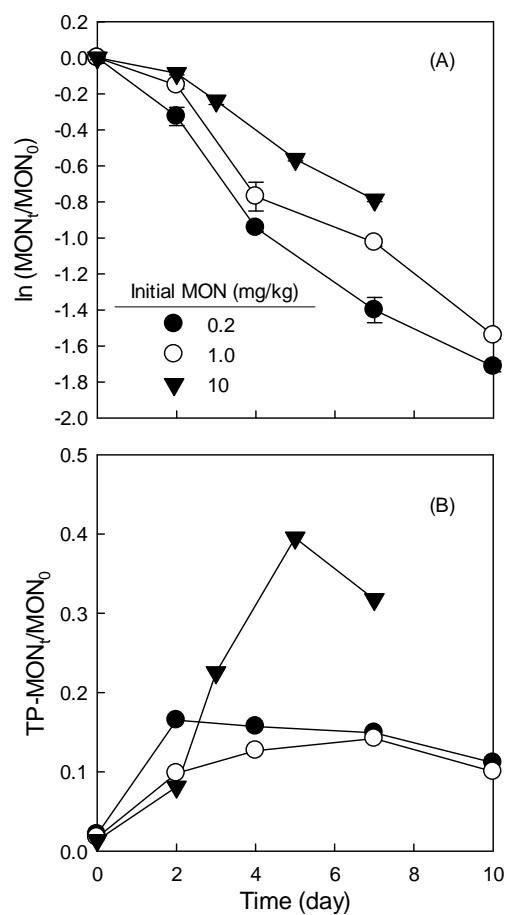


**Figure 6.15** Normalized MON (A) and MON product (TP-MON) (B) in PL-fertilized soil microcosms set up at a range of initial MON concentration (0.2 – 10 mg MON/kg soil). Error bars represent one standard deviation of the means ( $n = 2$ ).

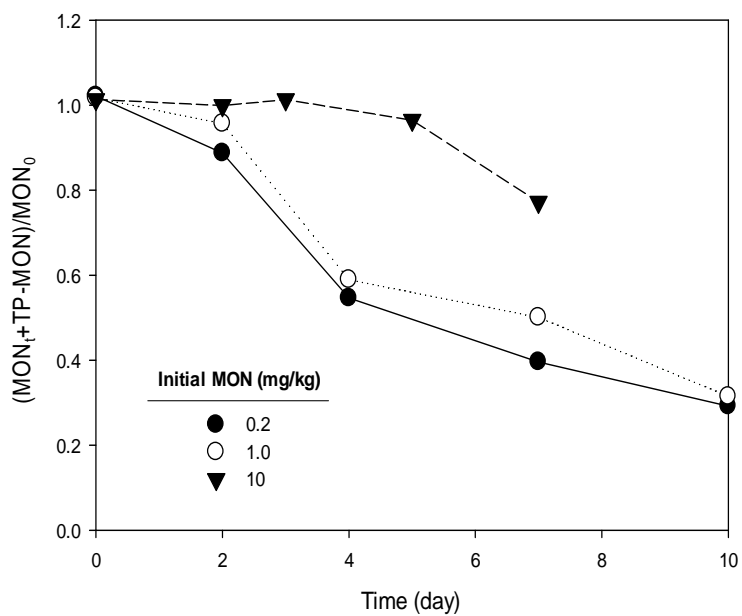


**Figure 6.16** Sum of peak areas of parent MON and TP-MON normalized to the initial MON peak area, over a 10-day incubation of soil microcosms amended with different initial MON.

### 6.3.3.3 Product structural identification

Molecular weight increase by 14 is common in biotransformation of organic substances, such as bioconversion of primary carbon of a hydrocarbon to an aldehyde, and oxidation of a –OH to –COOH. Based on the University of Minnesota-Biocatalyst/Biodegradation Database (UM-BBD), the ‘very-likely’ aerobic MON biotransformation pathway results in ring E opening and formation of a structure with a carboxyl group at the end (Figure 6.17 A). The molecular weight is increased by 14 due to the oxidation of the primary hydroxyl carbon. The first step in the biotransformation of ring E is a ring opening reaction possibly via acid-catalyzed hydrolysis of hemiacetal moiety. However, at pH above 5, the ring E moiety is stable under abiotic conditions (Sun *et al.*, 2013b), indicating that ring E is opened by an enzyme-facilitated hydrolysis. Indeed, hydrolysis of hemiacetal moiety was well studied in the biotransformation of other cyclic ethers (Bernhardt and Diekmann, 1991). Similarly, the spiral-ketal carbon connecting rings A and B is also known to undergo acid-catalyzed hydrolysis (Sun *et al.*, 2013b). Thus, it is possible that ring A and/or B

on TP-MON are also opened. Therefore, a TP-MON structure with both rings A and E open is proposed (Figure 6.17 B).

The proposed transformation product is supported by the LC/MS/MS results (Figures 6.18, 6.19). The  $m/z$  693.5 and 707.5 ions were selected for MON and TP-MON, respectively, from the full-scan analysis of products and subjected to collision activated dissociation. The mass spectrum of TP-MON was similar to that of MON, which confirmed that the  $m/z$  707.5 peak represents a MON transformation product. Based on a number of studies which have proposed the MS/MS fragmentation pattern of MON, interpretation of MS/MS results was made to further elucidate the molecular structure of TP-MON. The common base peaks at  $m/z$  443.3,

461.3, 479.3, and 501.3 suggest that oxygen was added on the right-hand part of the molecule (Volmer and Lock, 1998) (i.e., ring E and right-hand part of ring D). Elimination of  $m/z$  617.3 in TP-MON suggests that the C-O bond was opened on ring E. The new peak at  $m/z$  605.3 resulted from a cleavage on the opened ring E moiety. The new peak at  $m/z$  506.3 confirmed that ring A was also opened. Other fragment structures are also proposed and shown in Table 6.5. Therefore, based on the UM-BBD prediction and MS/MS results, the molecular structure of TP-MON was tentatively proposed as shown in Figure 6.17. However, use of analytical techniques, such as NMR, is required in order to further confirm the TP-MON structure.

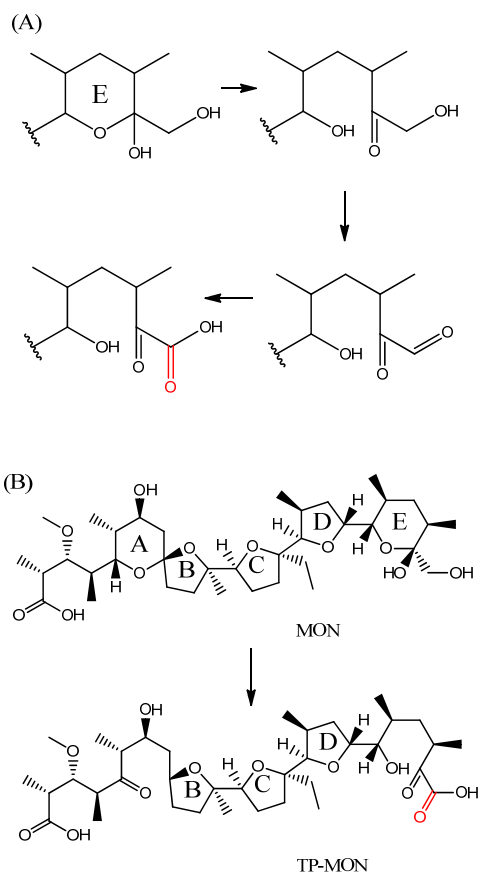


**Figure 6.17** (A) Initial steps of MON biotransformation predicted by UM-BBD. (B) Proposed molecular structure of MON product (TP-MON).

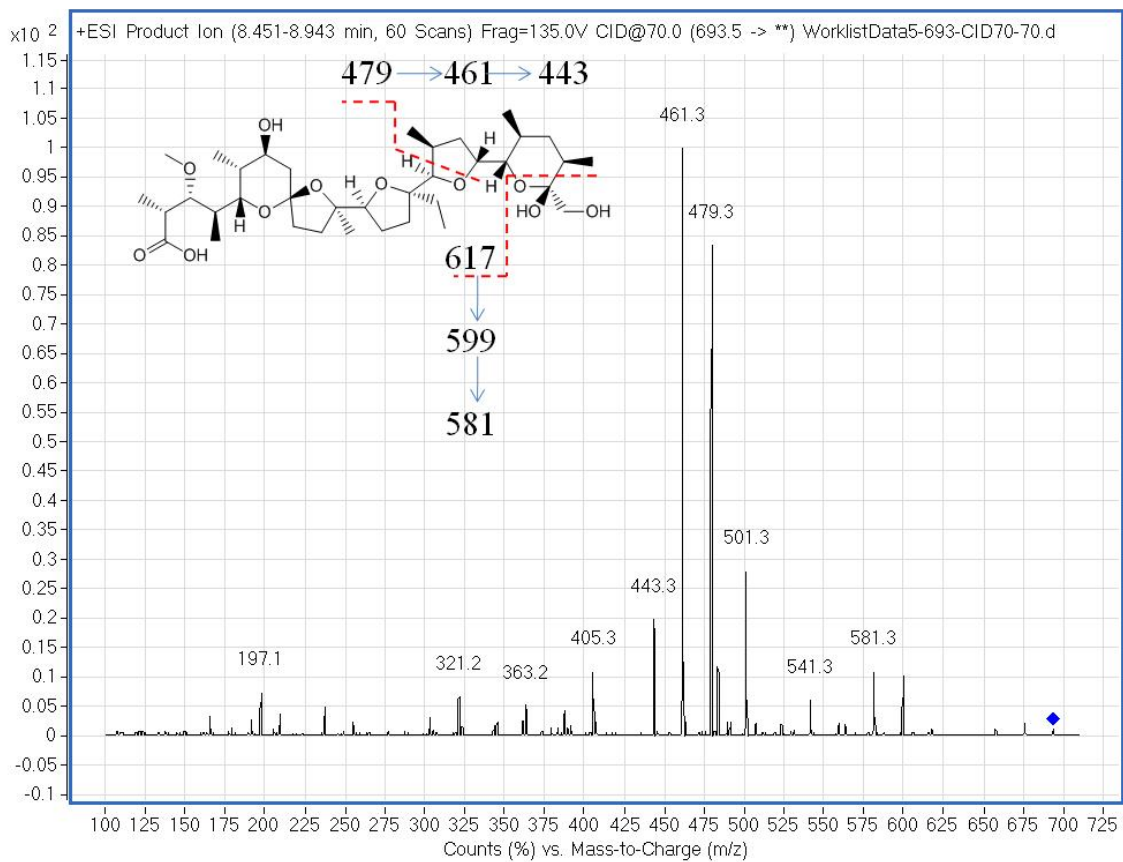


**Figure 6.18** MS/MS spectrum of MON. The arrows represent elimination of a water molecule.

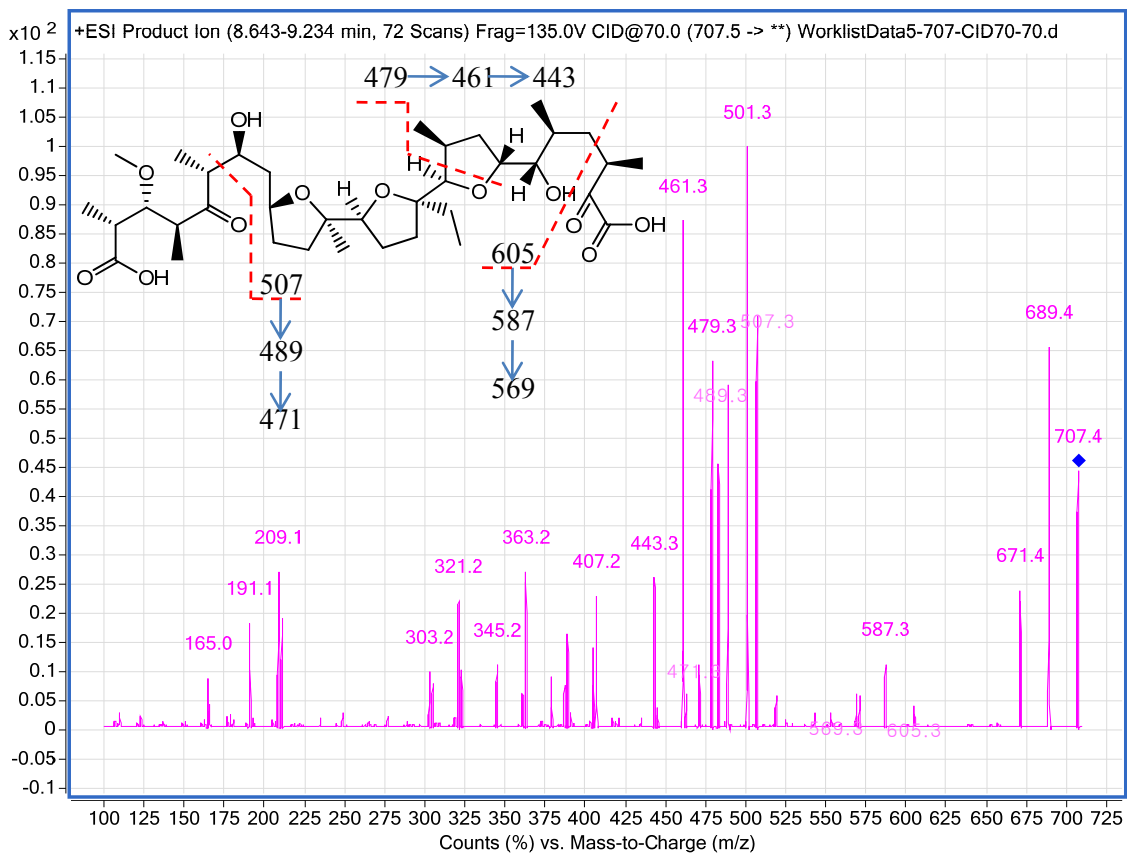


**Figure 6.19** MS/MS spectrum of TP-MON. The arrows represent elimination of a water molecule.

**Table 6.5** Proposed fragment structures of MON and its biotransformation product (TP-MON)

	MON	TP-MON
Cleavage sites		
Base peaks ( $m/z = [M+Na]^+$ )		
617 (599 = 617 - H <sub>2</sub> O) (581 = 617 - 2H <sub>2</sub> O)		ND#
605 (587 = 605 - H <sub>2</sub> O) (569 = 605 - 2H <sub>2</sub> O)	ND	
507 (589 = 507 - H <sub>2</sub> O) (571 = 507 - 2H <sub>2</sub> O)	ND	
479 (461 = 479 - H <sub>2</sub> O) (443 = 479 - 2H <sub>2</sub> O)		
407	ND	
405		
463		

ND, not detected.

#### **6.3.4 Field study**

Significant degradation of MON and SAL was not observed over 57 days during PL stacking (Figure 6.20). Based on the results of the PL microcosm assay, MON is expected to be stable during the stacking process. The PL used in the stacking study had an initial water content of 33% and decreased to 29% by day 57. At these water content values, based on Eqn. 2, SAL can only be degraded when the temperature is above 57°C (Figure 6.6). The litter stack temperature ranged from 30 to 50°C depending on the stack depth, and remained at 45°C in the center of the stack pile (data not shown). Thus, it is expected that SAL would remain stable during the PL stacking process.

After stacking, the litter was applied to an experimental field. IPAs were stable over four weeks under dry conditions (i.e., before the simulated rainfall; data not shown). Degradation of MON occurred after the simulated rainfall (Figure 6.21). MON degradation and TP-MON production was observed in the top soil in the first week after rainfall application, followed by a decrease of both MON and TP-MON in the subsequent two weeks resulting in a MON half-life of 1.5 weeks. SAL was stable in the top soil over three weeks. These observations are consistent with the results obtained with the soil microcosm assays, which suggests that MON degraders are likely widely present in soils.

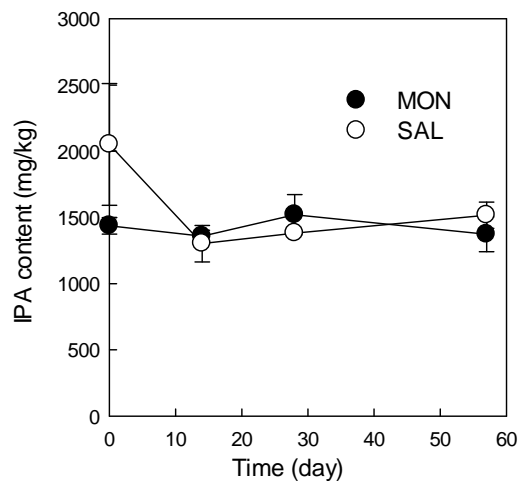


**Figure 6.20** IPA concentration during the PL stacking process. IPAs were spiked into PL at 1500 – 2000 mg/kg. Error bars represent one standard deviation of the means ( $n = 2$ ).

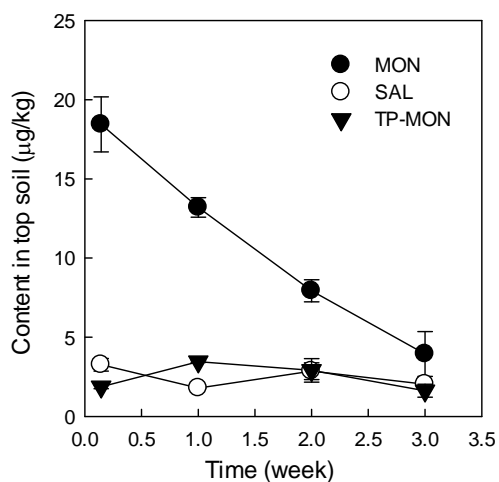


**Figure 6.21** IPA concentration in upper layer soil fertilized with PL containing MON and SAL, subjected to simulated rainfall right after PL application. Samples were collected at 0, 7, 14, and 21 days after rainfall. Error bars represent one standard deviation of the means ( $n = 2$ ).

#### **6.4 Environmental Implications**

This study assessed the degradation potential of MON, SAL and NAR in PL and soil microcosms under various water content and temperature conditions. Degradation of IPAs does not likely occur during the PL stacking process due to low water availability, though SAL and NAR degraders are present in PL. Because temperature is not usually controlled during the litter stacking process, in order to enhance IPAs degradation, water may be added to reach an optimal litter water content. From the standpoint of the fate and degradation of IPAs, SAL and NAR are recommended over MON as veterinary IPAs, because they can be degraded during litter stacking under optimal temperature and water content conditions, thus minimizing the release of IPAs into the environment. After PL is applied to the field, IPAs can potentially be degraded in the soil, although biodegradation of SAL was only observed in soil which had been receiving PL for years. A new primary product of MON biotransformation in soil identified in this study is not likely to persist in the environment and does not exhibit antibiotic properties of ionophores which are associated with their capacity to form complexes with cations.

## CHAPTER 7

### INHIBITION AND BIOTRANSFORMATION POTENTIAL OF VETERINARY IONOPHORE ANTIBIOTICS UNDER DIFFERENT REDOX CONDITIONS

#### 7.1 Introduction

In the previous chapter, the biodegradation of IPAs were investigated in PL and soil microcosms. In this chapter, cultures were enriched from PL and soil, and maintained with PL-extract, in order to study both the inhibition and biodegradation potential of IPAs under different redox conditions related to water-litter-soil systems.

Biodegradation of IPAs is expected to occur in soil and sediments near agricultural fields, because microbes are enriched in such systems which contain nutrients from manure application. Animal manure commonly contains significant levels of organic matter, ammoniacal nitrogen and sulfate. Table 7.1 lists the major components of PL water extract (PL-extract) from broiler production. Therefore, microbial activities in PL-fertilized soils may include (1) a heterotrophic/nitrifying zone in the top soil layer; (2) a denitrification zone after ammoniacal nitrogen is transformed to nitrate; and (3) a fermentative/sulfate-reducing zone, deeper, where oxygen is depleted. Moreover, fermentative/methanogenic conditions occur in anaerobic digesters and animal manure composting processes.

To date, however, the inhibition and biodegradation potential of IPAs have been scarcely investigated under the above stated environmental relevant conditions, though a number of studies have examined IPA degradation in animal waste storage processes and agricultural soil. For example, disappearance of MON from MON-fed cow fresh feces and a cattle manure pile was attributed to biodegradation, with faster degradation under aerobic conditions (Donoho, 1984; Schlusener *et al.*, 2006). The disappearance of MON was also observed in the upper soil

layer, with a half-life of 3.8 days (Carlson and Mabury, 2006). SAL-amended soil (2 mg/kg) incubated under aerobic conditions resulted in its disappearance with a 5-day half-life (Schlusener and Bester, 2006). SAL was biodegraded under aerobic conditions with bacteria extracted from soil; however, it was more persistent under anaerobic conditions (Hansen *et al.*, 2012). These findings could be explained by the fact that IPAs can be degraded by aerobic bacteria and mammalian enzymes via oxygen-dependent pathways, which are not functional in anaerobic environments (Russell and Houlihan, 2003). However, another study observed that SAL was readily biodegraded in stored pig manure under anaerobic conditions (Schlusener *et al.*, 2006). MON has been known to inhibit methanogenesis in animal manure fermentation and ruminal bacteria (Russell and Strobel, 1989; Wildenauer *et al.*, 1984). The inhibitory effect of IPAs on nitrification and aerobic respiration was examined with soil microorganisms, which showed NOEC (no observed effect concentration) values of IPAs were significantly higher than environmental relevant concentrations (Hansen *et al.*, 2009b). However, neither inhibition nor biodegradation of IPAs has been studied under denitrifying or sulfate-reducing conditions, and their impact on the anaerobic wastewater treatment processes has not been examined.

This study aimed at assessing the inhibition and biodegradation potential of IPAs under different redox conditions to provide a comprehensive evaluation of IPA bioreactivity after they are released from animal operations. The inhibition tests examined included microbial processes such as denitrification, sulfate-reduction, and methanogenesis. Biodegradation tests were conducted with different electron acceptors and efforts focused on identifying primary biotransformation products.

**Table 7.1** Characteristics of water extract from poultry litter (PL)

sCOD (g/L)	NH <sub>4</sub> <sup>+</sup> (mM)	NO <sub>3</sub> <sup>-</sup> (mM)	PO <sub>4</sub> <sup>3-</sup> (mM)	SO <sub>4</sub> <sup>2-</sup> (mM)
8.7	70	0.01	4.72	6.17

Water extract from PL was prepared by mixing deionized water with PL at water to solid ratios (w/w) of 20/1. After shaking for 12 hours, water extracts were passed through 0.2 µm filters.

## **7.2 Materials and Methods**

### **7.2.1 Chemicals**

MON sodium salt (purity, 97%) and NAR sodium salt (purity, 97%) were purchased from Sigma-Aldrich (St. Louis, MO). SAL sodium salt (purity, 96%) was purchased from Fisher Scientific (Pittsburgh, PA). HPLC-grade methanol (purity, 99.9%), acetonitrile (ACN) (purity, 99.9%), analytical-grade formic acid (purity, 99%), and hexane (purity, 95%) were obtained from Sigma-Aldrich. All other reagents used were of analytical grade obtained from Fisher Scientific. Reagent-grade deionized (DI) water (resistance > 18 mΩ·cm) was obtained from a Millipore nanopure water purification system (Billerica, MA). Individual IPA stock solutions were prepared in methanol and stored at 4°C prior to use.

### **7.2.2 Culture development and maintenance**

Three mixed stock cultures were developed and utilized to evaluate the biotransformation potential of IPAs under aerobic/anoxic, fermentative/sulfate-reducing, and fermentative/methanogenic conditions, respectively. Specifics for each culture are summarized in Table 7.2. Detail information on culture development and maintenance is provided below.

#### **7.2.2.1 Aerobic/anoxic culture development**

A suspended growth mixed culture was developed under alternating aerobic and denitrifying conditions using poultry litter (PL) and PL-fertilized soils as inoculum. The poultry litter was collected from several broiler farms across Georgia. The soil was collected from an agricultural site located at Central Research and Education Center of the University of Georgia (33° 24' N, 83° 29' W, elevation 150 m), to which PL has been applied as fertilizer for more than

10 years. Both the PL and soil were stored at 4°C constant temperature room prior to be used as inoculum.

Initially, a mixture of 5 grams of poultry litter and soil (1:1 w:w) was soaked in 100 ml inorganic culture media buffered at pH 7.0 for incubation of bacteria from poultry litter and soil. The culture medium was prepared with the following composition (in g/L): K<sub>2</sub>HPO<sub>4</sub>, 1.07; KH<sub>2</sub>PO<sub>4</sub>, 0.524; CaCl<sub>2</sub>·2H<sub>2</sub>O, 0.068; MgCl<sub>2</sub>·2H<sub>2</sub>O, 0.135; MgSO<sub>4</sub>·7H<sub>2</sub>O, 0.268; FeCl<sub>2</sub>·4H<sub>2</sub>O, 0.068; and 0.67 mL/L trace metal stock solution. Incubation was performed in a 250-mL Erlenmeyer flask on a horizontal shaker with a feeding cycle of one week. Two thirds of the suspension were discarded every week and replaced by water extract from 5% poultry litter as nutrient source. Several such transfers were made in the aim of eliminating solids coming from poultry litter and soil.

The culture was then transferred into a 5-L Pyrex® reactor and scaled up to a total liquid volume of 4 L. To achieve alternating aerobic and anoxic conditions, the culture has been aerated for 4 days, followed by an anoxic stage (by sealing the reactor with a rubber stopper) for the rest 3 days of each 7-day feeding cycle. Poultry litter extract equal to 500 ml and 300 ml was added to the culture on the initial day and the 5<sup>th</sup> day. The culture has been maintained with hydraulic residence time of 7 days, and a biomass retention time of 21 days.

#### *7.2.2.2 Fermentative/sulfate-reducing culture development*

A mixed fermentative/sulfate reducing culture was developed using the same poultry litter and soil described above as inoculum. Initially, the culture was started up by soaking 7.5 grams of solids in 1.5 L inorganic anaerobic culture media described above. One third of the suspension was discarded every two weeks for the initial three month and replaced by the same

volume of anaerobic culture media mixed with water extracts from poultry litter as carbon and nitrogen sources. The litter and soil particles were gradually removed from the culture after several feeding cycles. The culture has been maintained in a 2.6-L Pyrex® reactor with a liquid volume of 1.5 L, a biomass residence time of 70 days, fed once a week with 1 g/L dextrin and 150 ml poultry litter extract.

### *7.2.2.3 Fermentative/methanogenic culture development*

A mixed fermentative/methanogenic culture was developed with inoculum obtained from a municipal anaerobic digester. The feeding-cycle was 7 days with a loading of 1.2 g/L dextrin and 0.6 g/L peptone per week. One fifth of the suspension was discarded every week and replaced by the same volume of anaerobic culture media, corresponding to a biomass retention time of 35 days. The culture was maintained in a 10-L Pyrex® reactor with a total volume of 8 L in a 35°C laboratory room. The culture medium contained (in g/L): K<sub>2</sub>HPO<sub>4</sub>, 0.9; KH<sub>2</sub>PO<sub>4</sub>, 0.5; NH<sub>4</sub>Cl, 0.5; CaCl<sub>2</sub>·2H<sub>2</sub>O, 0.10; MgCl<sub>2</sub>·6H<sub>2</sub>O, 0.20; FeCl<sub>2</sub>·4H<sub>2</sub>O, 0.10; Na<sub>2</sub>S·9H<sub>2</sub>O, 0.5; NaHCO<sub>3</sub>, 6.7; and 1 mL/L trace metal and vitamin stock solutions (Tugtas and Pavlostathis, 2007). Resazurin was added as a redox indicator at 2 mg/L ( $E_h < -100$  mV). The steady-state methane, carbon dioxide, and biomass concentrations were 60.7±0.5%, 39.2±0.4%, 2.2±0.1 g VS/L (mean ± standard deviation), respectively (Misiti, 2013).

**Table 7.2** Stock cultures used to test inhibition and biotransformation assays

	PL-enriched aerobic/anoxic culture	Fermentative/ sulfate reducing culture	Fermentative/ methanogenic culture
Inoculum	Soil, PL	Soil, PL	Anaerobic digester sludge
Electron-acceptor	O <sub>2</sub> , NO <sub>3</sub> <sup>-</sup>	OC, SO <sub>4</sub> <sup>2-</sup>	OC, CO <sub>2</sub>
Primary carbon source	PL-extract	Dextrin, PL-extract	Dextrin, peptone
Feeding cycle (d)	7	7	7
Biomass retention time (d)	21	70	35

---

OC, organic carbon

### ***7.2.3 Inhibition and biotransformation assays***

A summary of conditions tested in this study are shown in Table 7.3. The highest IPA concentration tested in this study was 1 mg/L, which is expected to represent the maximum IPA concentration in the environment. Details on each assay set-up are provided below.

#### ***7.2.3.1 Aerobic conditions***

A batch assay was performed to investigate the biodegradation potential as well as identify biotransformation products of IPAs under aerobic conditions. The assay was performed in 250-ml Erlenmeyer flasks. A sample of 100 ml aerobic/anoxic culture, collected at the fourth day of a feeding cycle (i.e., at the end of the aerobic stage), was centrifuged at 3,000 rpm. The pellet was washed with 10 mM phosphate buffer at pH 7 to remove residual PL extracts, and resuspended in 30 ml inorganic culture medium.

Two series of cultures were set up, at initial pH 7.1 with 1 mM phosphate buffer and 10 mM phosphate buffer, respectively, to simulated low and high buffer capacity conditions. Culture samples were prepared by transferring 2 ml resuspended culture along with 50 ml of 2 mg/L stock solution of individual IPA into each flask. Reference samples were prepared with 50 ml DI water instead. In order to evaluate biodegradation of IPAs with different carbon sources, aliquots of dextrin solution or PL extracts were added to achieve a biodegradable chemical oxygen demand (COD) concentration of 250 mg/L. The culture was finally amended with concentrated inorganic culture media to reach a total volume of 100 ml. The initial concentrations were: individual IPAs, 1 mg/L; biomass (VSS), 0.1 g/L; ammoniacal nitrogen, 1 mM. Carbon sources included IPAs, IPA and dextrin, or IPA and PL-extracts. Abiotic controls were also set up by adding 200 mg/L sodium azide. The cultures were agitated at 200 rpm on a rotary shaker and

incubated at room temperature (22-23°C) over 7 days. The time course concentration of each IPA was monitored.

#### *7.2.3.2 Nitrate-reducing conditions*

This assay was conducted in 60-ml serum bottles (30 ml liquid volume) sealed with rubber stoppers and aluminum crimps, and then flushed with helium gas for 20 min. A sample of PL-enriched aerobic/anoxic culture suspension, collected at the 7<sup>th</sup> day of the feeding cycle, was prepared as describe above for the aerobic biotransformation assay, and 2 ml of culture suspension was then transferred into each bottle along with 6 ml of 5 mg/L stock solution of individual IPAs. The initial concentration of IPA was 1 mg/L. Bottles were either amended with external carbon source from 1 g/L dextrin or PL-extract, or set up without any external carbon source. Nitrate was added at 11 mM. The cultures were incubated at room temperature (20-22°C) over 20 days. The time course concentration of each IPA, CO<sub>2</sub> and N<sub>2</sub> production were monitored.

#### *7.2.3.3 Fermentative/sulfate-reducing conditions*

The assay to investigate the inhibition and biodegradation potential of IPAs under fermentative/sulfate-reducing conditions was conducted in 160-ml serum bottles (100 ml liquid volume) sealed with rubber stoppers and aluminum crimps and flushed with helium gas for 20 min. A sample of 79 ml PL-enriched fermentative/sulfate-reducing culture, collected at the end of the 7-day feeding cycle, was anaerobically transferred into each bottle along with 20 ml of 5 mg/L stock solution of individual IPA and 1 ml of 100 g/L dextrin suspension. The initial concentration of IPA was 1 mg/L. The cultures were incubated at room temperature (20-22°C)

over 14 days. The time course concentration of each IPA, CO<sub>2</sub> and H<sub>2</sub>S in the head space were monitored.

#### *7.2.3.4 Fermentative/methanogenic conditions*

This assay was conducted in serum bottles set up following the above-described procedure for the sulfate-reducing assay. A sample of 50 ml fermentative/methanogenic culture, collected at the end of the 7-day feeding cycle, was anaerobically transferred into each bottle along with 49 ml of IPA stock solution and 1 ml of 100 g/L dextrin suspension. The cultures were incubated at room temperature (20-22°C) over 21 days. The IPA concentration, total gas, CO<sub>2</sub> and CH<sub>4</sub> produced were monitored.

**Table 7.3** Experimental set-up and conditions for the inhibition and biotransformation assays

Conditions	Aerobic	Nitrate-reducing	Fermentative/ sulfate-reducing	Fermentative/ methanogenic
Seed culture	Aerobic/anoxic culture	Aerobic/anoxic culture	PL-enriched anaerobic culture	Anaerobic stock culture developed from anaerobic digester sludge
Electron- acceptor	O <sub>2</sub>	NO <sub>3</sub> <sup>-</sup>	OC, SO <sub>4</sub> <sup>2-</sup>	OC, CO <sub>2</sub>
Carbon source	Dextrin, PL- extract, IPAs, CO <sub>2</sub>	Dextrin, PL- extract, IPAs	Dextrin, PL- extract, IPAs	Dextrin, IPAs
Parameter monitored	IPAs, pH	IPAs, N <sub>2</sub>	IPAs, total gas, CO <sub>2</sub> , H <sub>2</sub> S, SO <sub>4</sub> <sup>2-</sup>	IPAs, total gas, CO <sub>2</sub> , CH <sub>4</sub> , VFAs

---

OC, organic carbon

#### **7.2.4 Analytical methods**

To measure the total concentration of IPAs in the culture samples, aliquots were mixed with methanol at 1:1 (v/v) ratio before centrifugation to remove biomass. Preliminary results showed that the method extraction efficiency was 90-110%. Extracted IPAs were routinely analyzed with an Agilent 1100 Series LC/MSD system (Agilent Technologies, Palo Alto, CA). The LC/MS set-up was previously described in Sun *et al.*, 2013a (Chapter 2). A full-scan mode from 100 to 1700 m/z was applied to search for transformation products. A LC/MS/MS unit (Agilent 1260 Infinity LC system, 6410 Triple Quad MSD, Agilent Technologies, Palo Alto, CA) was used for structural identification of IPA transformation products. The LC unit was set at the same conditions as those stated above for the LC/MS. The MS parameters were 135 V fragmentation voltage with collision-activated-dissociation (CAD) energy of 70 eV for MON and its products, and 50 eV for SAL and its products, respectively.

Ammonia, nitrate, phosphate, and chemical oxidation demand (COD) were measured following procedures outlined in Standard Methods (APHA, 2012). Total gas production was measured with a digital pressure/vacuum transducer. Gas composition (N<sub>2</sub>, O<sub>2</sub>, CO<sub>2</sub>, CH<sub>4</sub>, H<sub>2</sub>S) was measured by gas chromatography (GC) with thermal conductivity detection. Volatile fatty acids (VFAs), including acetic acid, propionic acid and butyric acid, were measured by a HPLC equipped with a diode-array detector (Agilent 1100 LC system, Agilent Technologies, Palo Alto, CA).

### **7.3 Results and Discussion**

#### **7.3.1 Energetics of IPA biodegradation**

The standard Gibbs free energies of formation ( $\Delta G_f^{0'}$ ) of IPAs have not been published.

Therefore, this study applied a group contribution method developed by Mavrovouniotis (1990) to calculate  $\Delta G_f^{0'}$  of IPAs using Equation 7.1.

$$\Delta G_f^{0'} = \sum_1^i a_i \Delta G_{f,i}^{0'} \quad (7.1)$$

where,  $a$  is the number of occurrences of group  $i$  and  $\Delta G_f^{0'}$  is the standard Gibbs free energy of formation of group  $i$ . The calculations are detailed in Appendix A.

The  $\Delta G_r^{0'}$  values for the complete degradation of MON and SAL are 29.92 and 29.23 kJ/eq, respectively, which are close because of similar molecular structures. Recalling that the  $\Delta G_r^{0'}$  values of the half reactions for the reduction of oxygen, nitrate, and sulfate and methanogenesis are -78.72, -72.20, 20.85, and 23.53 kJ/eq (Rittmann and McCarty, 2001), respectively, oxidation reactions of MON and SAL for their complete mineralization have negative  $\Delta G_r^{0'}$  values, which implies that their degradation is thermodynamically favorable under all three conditions (Appendix A).

### ***7.3.2 Characterization of PL-enriched aerobic/anoxic culture***

The performance of the anaerobic/anoxic culture was characterized by measuring ammoniacal nitrogen, nitrate, soluble COD (sCOD), total COD (tCOD), DO and pH in a typical feeding cycle. pH was stable at  $7.1 \pm 0.1$  over the entire feeding cycle. As shown in Figure 7.1, both sCOD and tCOD rapidly decreased within a day after feeding, then were stable for the subsequent three days. Ammoniacal nitrogen was depleted by the end of the aerobic stage (i.e., day 4), resulting in an increase of nitrate concentration, which reached the same nitrogen concentration as the initial ammonium, indicating that the culture carried out a complete nitrification within the aerobic stage. At the anoxic stage (i.e., day 4-7), both sCOD and tCOD decreased slowly. Nitrate produced in the aerobic stage was completely removed in the anoxic

stage. The DO was 8.4 mg/L in the aerobic stage, and quickly dropped to below 0.1 mg/L on day 6-7. Overall, the culture showed active heterotrophic/nitrifying/denitrifying activity.

IPAs were introduced to the PL-enriched culture through the feed (i.e., PL-extract). The concentrations of MON and SAL were around 0.15 and 6.4  $\mu\text{g/L}$  at the first day of each feeding cycle and 0.09 and 3.8  $\mu\text{g/L}$  was fed with PL-extract added at the fourth day, respectively. As shown in Figure 7.1D, both MON and SAL were degraded to below measurable concentrations within the aerobic stage. However, their degradation rates were significantly lower during the anoxic stage. By the last day of the feeding cycle, the degradation of MON and SAL stopped.

Recalling that the stock culture was maintained with a four-day aeration followed by three-day closed-cap condition, the redox environment during one feeding cycle was aerobic (0<sup>th</sup> – 4<sup>th</sup> day), microaerophilic (4<sup>th</sup> - ~6<sup>th</sup> day) and strict-anoxic (~6<sup>th</sup> – 7<sup>th</sup> day). Therefore, the concentration profile of IPAs suggests that IPAs were biodegraded by the PL-enriched culture in the presence of oxygen, but not under strict anoxic conditions when nitrate was the electron acceptor. To test this hypothesis, two batch assays were conducted under well-defined conditions to assess the IPA biodegradation potential under aerobic and anoxic (i.e., nitrate reducing) conditions, respectively.

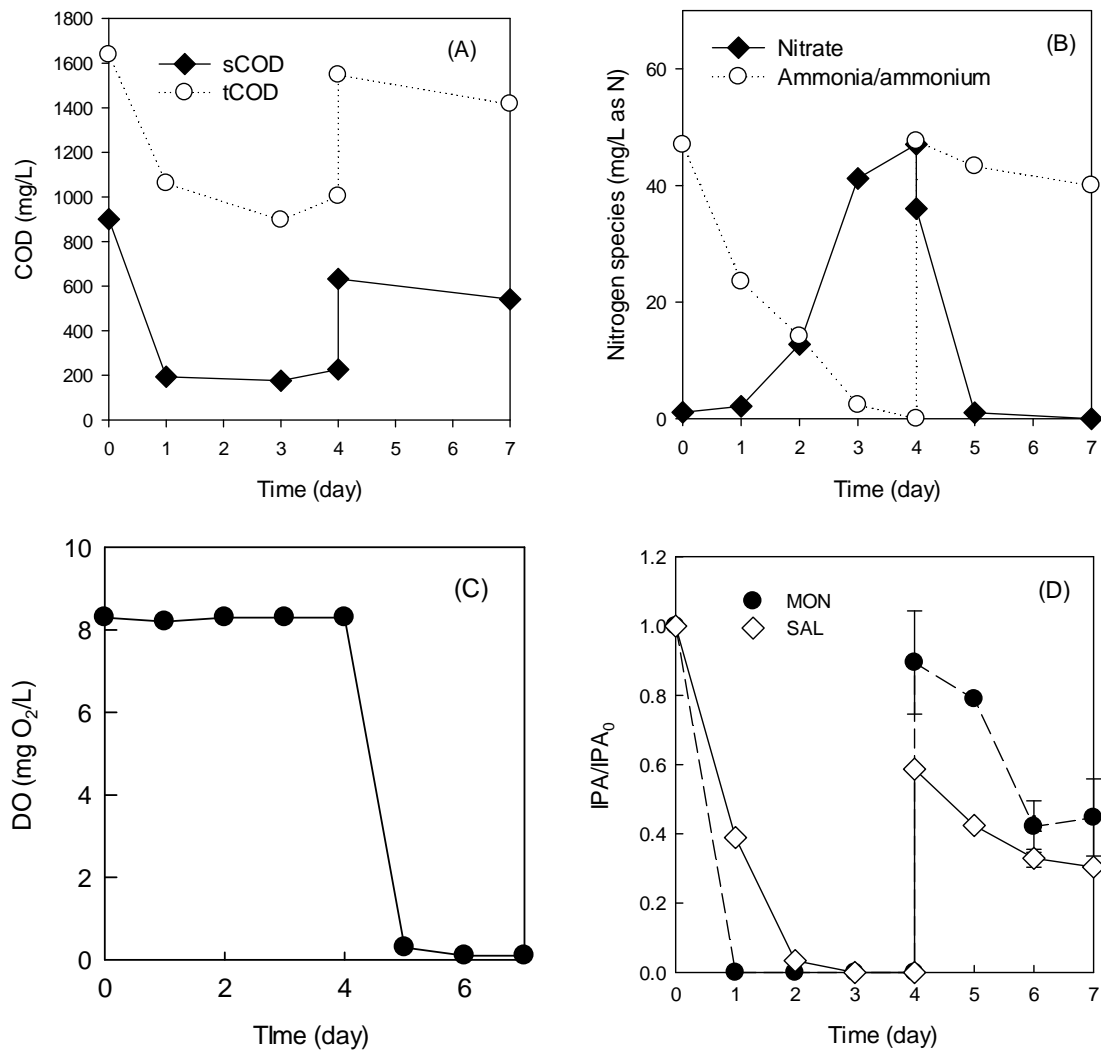


**Figure 7.1** Performance of the PL-enriched aerobic/anoxic culture during a typical feeding cycle. (A) soluble COD (sCOD) and total COD (tCOD); (B) nitrogen species; (C) dissolved oxygen (DO); (D) IPA concentration.

### **7.3.3 Biodegradation of IPAs under aerobic conditions**

The aerobic biodegradation potential of IPAs was first evaluated at a low buffer capacity, with 1 mM phosphate at pH 7.1 and the aerobic/anoxic culture. As shown in Figure 7.2, degradation of IPAs was not observed in medium controls or azide-amended culture series, which indicates that IPAs were stable in the absence of microbial activity. In contrast, significant degradation of IPAs was observed in the cultures set up with or without PL-extract as external carbon source. SAL was completely degraded after 5 days of incubation and around 30 – 40% of the initial MON remained at day 7. Although IPAs were stable in the controls, the loss of the parent IPAs in nonsterilized cultures was mainly due to abiotic reactions. Indeed, the pH of nonsterilized cultures dropped to 4.2 – 4.5 at day 7, under which pH MON and SAL are known to be subject to fast acid-catalyzed hydrolytic transformation with half-lives of ~160 and ~5 hours for MON and SAL, respectively (Sun *et al.*, 2013b). Moreover, the observation of abiotic hydrolysis products of IPAs on LC/MS further supports that hydrolysis of IPAs occurred (data not shown). According to our previous study (Sun *et al.*, 2013b), MON will be at equilibrium with its hydrolysis products resulting in residual MON in acidic solution, whereas SAL will be completely hydrolyzed if given enough time. These kinetic features agree with the concentration profiles of MON and SAL shown in Figure 7.2.

The acidification of the aerobic culture series likely resulted from active nitrification, which is known to consume solution alkalinity (Rittmann and McCarty, 2001). Consequently, IPAs degraded slightly faster in culture series amended with PL-extract due to additional ammoniacal nitrogen from the extract. Additionally, a preliminary test showed that the pH remained at 6.5-7.1 for one week incubation of the culture series with a lower initial ammonia concentration (i.e., 0.1 mg/L as N). Therefore, the degradation of IPAs in the weakly-buffered

culture series was primarily the result of nitrification-induced abiotic acid degradation.

To distinguish abiotic and biotic transformation of IPAs, a second assay was conducted by increasing the phosphate buffer concentration to 10 mM (at pH 7.1). Culture series seeded with the PL-enriched culture with/without external carbon source, were continuously aerated for 7 days. The pH was stable at 7.1 during this assay in all culture series. Therefore, degradation due to hydrolysis was excluded. No decline in IPA concentration was observed in the azide-amended series over 7 days (data not shown). As shown in Figure 7.3, MON and SAL were both degraded under aerobic conditions by the PL-enriched culture at pH 7.1. Addition of external carbon source enhanced the degradation rate of IPAs. Indeed, MON degraded significantly faster with the addition of dextrin and the degradation of SAL was enhanced with the addition of PL-extract.

In the culture series amended with external carbon source, IPAs readily degraded (i.e., no lag phase was observed), which suggests that IPA might serve as either primary carbon/energy source or be co-metabolized. On the other hand, degradation of IPAs was also observed in the culture series set up with IPA as the only external carbon source, suggesting that IPAs can be utilized as a carbon/energy source. The combined results suggest that IPAs might serve as primary carbon/energy source for microorganisms in the PL-enriched culture under aerobic conditions. However, due to the solubility limits of IPAs, measurable increase of biomass was difficult to obtain in such culture series. More evidence is needed to determine whether IPAs could support microbial growth.

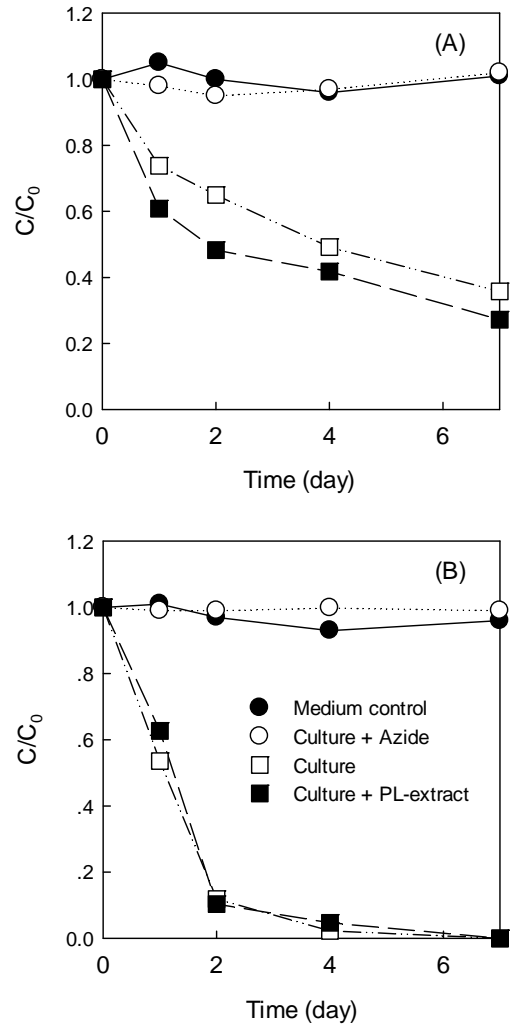


**Figure 7.2** MON (A) and SAL (B) degradation under aerobic conditions at a low buffer capacity medium.

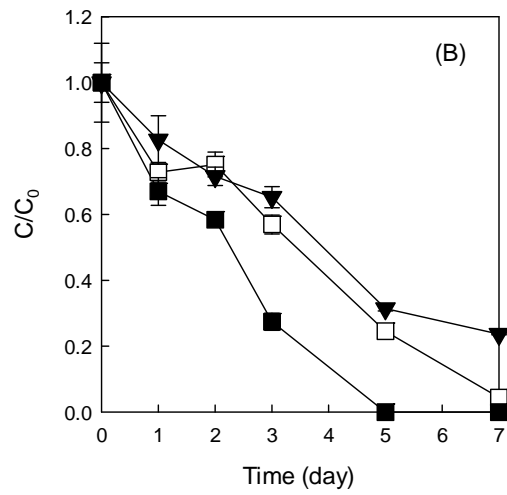
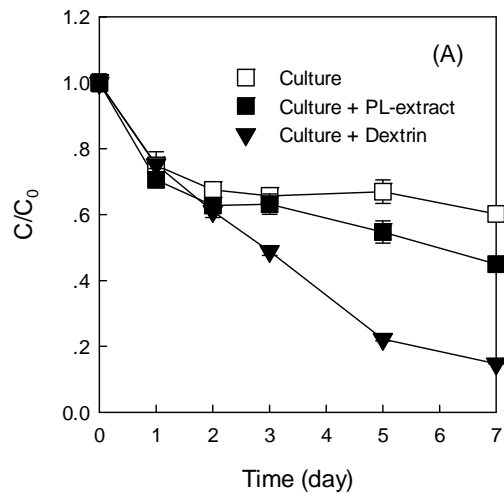


**Figure 7.3** MON (A) and SAL (B) degradation under aerobic conditions at a high buffer capacity medium.



### ***7.3.5 Inhibition and biodegradation of IPAs under fermentative/sulfate-reducing conditions***

Two culture series were set up with the PL-enriched fermentative/sulfate-reducing culture to examine IPA inhibition and biodegradation potential, respectively. The first culture series investigated IPA inhibition on fermentation/sulfate-reduction. The total gas, carbon dioxide, and hydrogen sulfide production in cultures with or without IPAs are shown in Figures 7.5-7.6. The cultures were active and produced significant volume of CO<sub>2</sub> and H<sub>2</sub>S. The total gas production decreased over time and stopped at around day 3. A second addition of dextrin on day 4 resulted in increased gas production, indicating that the initial slow-down was due to lack of carbon source. Compared to reference culture series, IPAs did not affect either total gas production or gas composition (Figure 7.6). Thus, IPAs, at 1 mg/L, do not inhibit the fermentation/sulfate-reduction processes of the PL-enriched culture.

The second culture series was set up to investigate the biodegradation potential of IPAs under fermentative/sulfate-reducing conditions. The initial and final pH values were 7.2, indicating a well buffered condition, and thus no acid hydrolysis of IPAs occurred during the incubation. As shown in Figure 7.7, MON was stable during the two-week incubation period, whereas SAL degraded after an initial lag of 4 days. Over 80% removal of initial SAL was achieved by day 7. An additional 0.5 mg/L of SAL was added on day 7.5, which was degraded in the subsequent 7 days. Recalling that the culture was amended with dextrin as the primary external carbon source along with sulfate, both fermentation and sulfate-reduction were active under such conditions. Therefore, it was interesting to examine which metabolic process was responsible for the observed SAL biodegradation.

In order to distinguish fermentation from sulfate reduction, sodium molybdate, a known inhibitor of sulfate reduction (Banat *et al.*, 1981), was added to select culture series of the second

culture group on day 7.5. As shown in Figure 7.8, removal of sulfate stopped upon the addition of molybdate, indicating a complete inhibition of sulfate reduction. However, SAL continued to be degraded in the culture series amended with molybdate. The final concentration of SAL at day 14 was the same in the culture series with or without molybdate addition. Therefore, this result suggests that SAL was biodegraded by fermentative microorganisms, not by sulfate-reducers.

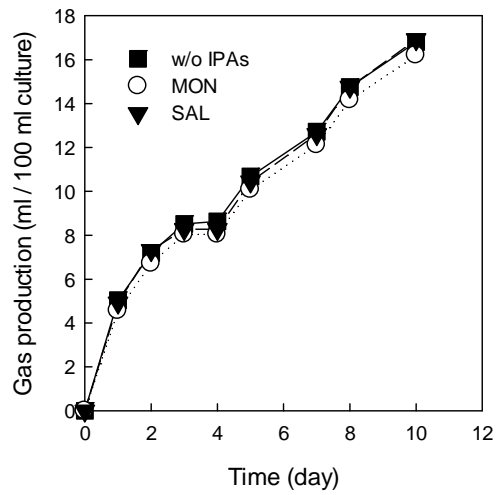


**Figure 7.5** Cumulative total gas production in culture series under fermentative/sulfate reducing conditions with or without IPAs. (1 atm and 25°C).

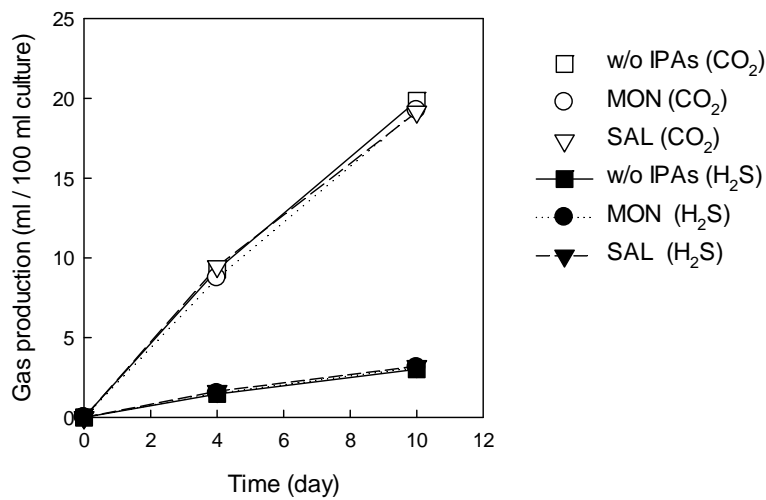


**Figure 7.6** Cumulative CO<sub>2</sub> and H<sub>2</sub>S production in culture series under fermentative/sulfate reducing conditions with or without IPAs. (1 atm and 25°C).

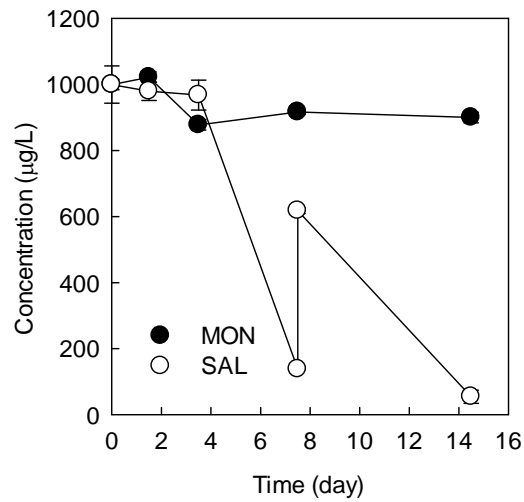


**Figure 7.7** Degradation of IPAs under fermentative/sulfate-reducing conditions. Initial concentrations of IPAs were 1 mg/L; an additional 0.5 mg/L SAL was added on day 7.5.

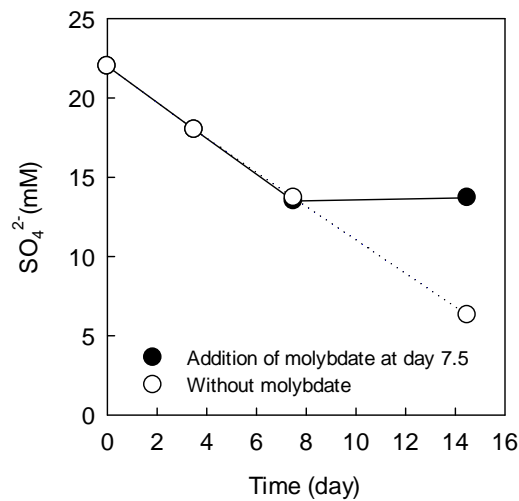


**Figure 7.8** Sulfate concentration in culture series under fermentative/sulfate-reducing conditions, without or with molybdate added on day 7.5.

### 7.3.6 Inhibition and biodegradation of IPAs under fermentative/methanogenic conditions

Total gas, methane and carbon dioxide production were measured on day 14 and used as indicators to assess potential inhibition of fermentation/methanogenesis by IPAs. The inhibitory effect was expressed by comparing the gas production in the culture series amended with IPAs with that in the reference culture series (Equation 7.2).

$$\text{Inhibition (\%)} = \frac{V_{\text{IPAs}} - V_{\text{reference}}}{V_{\text{reference}}} \times 100 \quad (7.2)$$

where,  $V_{\text{IPAs}}$  is the cumulative total gas (or methane) production in the culture series amended with IPAs on day 14, mL;  $V_{\text{reference}}$  is the cumulative total gas (or methane) production in the reference culture series on day 14, mL. For the IPA concentration range tested (0 – 1000  $\mu\text{g/L}$ ), addition of SAL did not inhibit methanogenesis (data not shown). In contrast, MON, at concentrations above 500  $\mu\text{g/L}$ , significantly inhibited methanogenesis by over 50% based on the total gas and cumulative methane production (Figure 7.9), whereas cumulative  $\text{CO}_2$  production was not affected at all MON concentrations tested in this study (data not shown). Degradation of MON or SAL was not observed in any culture series over 21 days of incubation (data not shown).

To further elucidate the inhibitory effect of MON on methanogenesis, time-course cumulative total gas, methane, carbon dioxide, and VFA production were measured in culture series with or without 1000  $\mu\text{g/L}$  MON over a 14-day incubation period. Figure 7.10A shows that gas production stopped after 14 days, and no recovery was observed in the culture series amended with MON over 30 days. Cumulative methane production (Figure 7.10B) was affected by MON. However, carbon dioxide production profiles were almost identical in the culture series with or without MON, indicating fermentation was not affected by MON (Figure 7.10C). A continuous increase of acetate concentration was observed in the MON-amended culture

compared to a transient accumulation of acetate in the MON-free reference culture series (Figure 7.10D). Propionate accumulated transiently in both MON-amended and reference culture series, whereas residual propionate was observed in the MON-amended series (Figure 7.10E). Butyric acid was also monitored in all cultures, but concentrations were below the detection limit.

These findings are consistent with previous studies which investigated the inhibitory effect of IPAs on methane production by ruminal bacteria and cultures developed from animal waste under fermentative/methanogenic conditions (Chen and Wolin, 1979; Russell and Martin, 1984; Russell, 1987; Varel and Hashimoto, 1982; Wildenauer *et al.*, 1984). MON inhibited the growth of and methane production by *Methanobacterium ruminantium* PS, *Methanosarcina barkeri* MS (Chen and Wolin, 1979). SAL had minimal effects on the methane production rate from cattle waste, whereas MON completely stopped methane production after a 3-week incubation (Varel and Hashimoto, 1982). Accumulation of acetate was also reported in a cattle manure fermentation process when treated with MON (Wildenauer *et al.*, 1984). The present study showed that MON had a similar inhibitory effect on the fermentation and methanogenesis of a mixed culture developed with inoculum from a wastewater anaerobic digester.

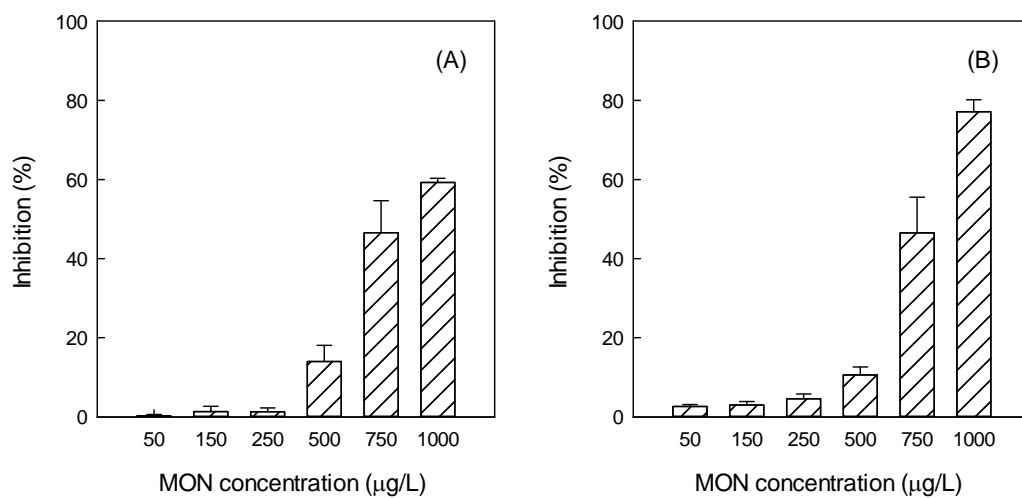


**Figure 7.9** Inhibitory effect of MON under fermentative/methanogenic conditions, based on total gas production (A), and cumulative methane production (B).

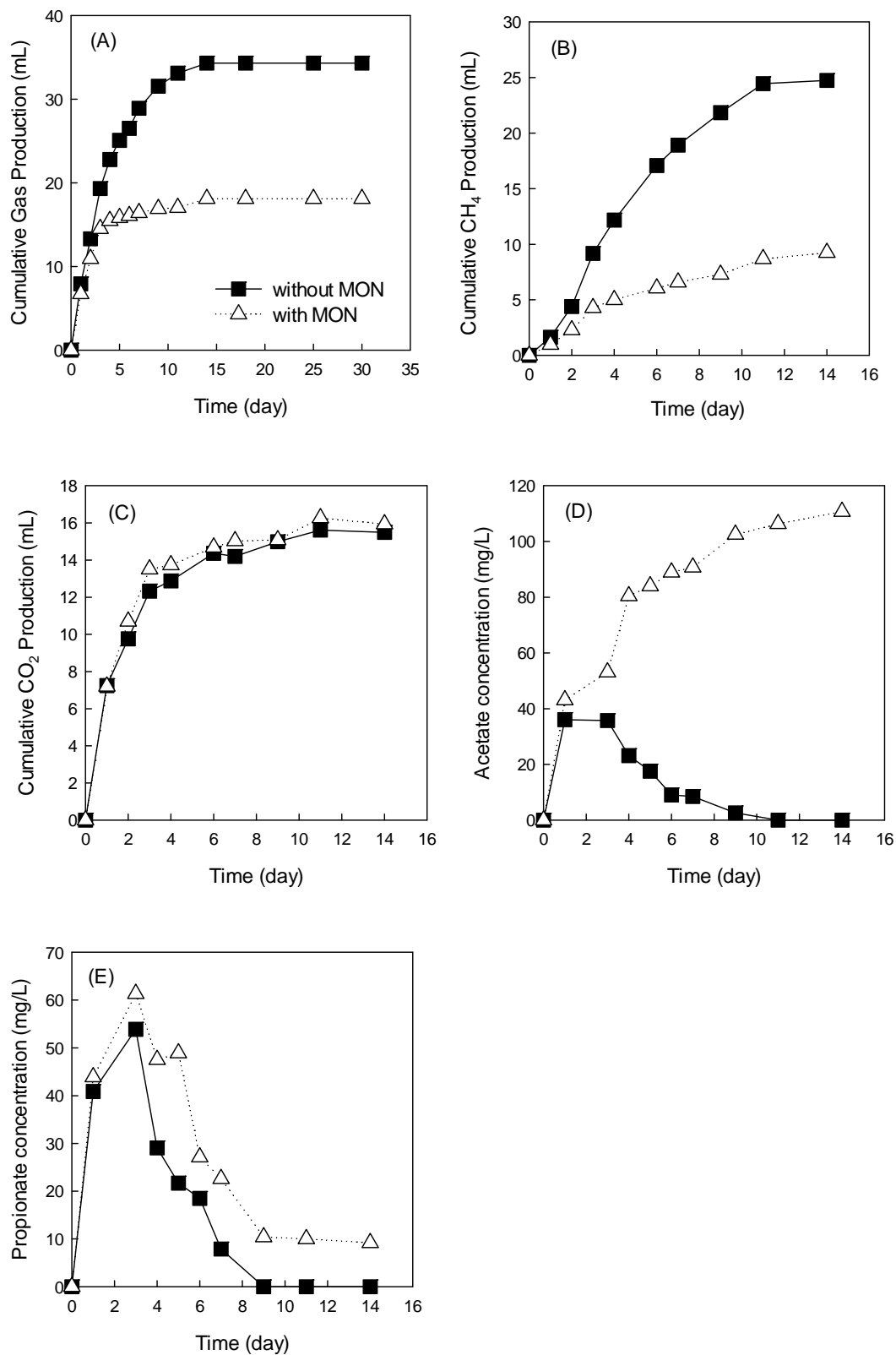


**Figure 7.10** Performance of the cultures with and without MON amendment. (A) Cumulative gas production; (B) Cumulative CH<sub>4</sub> production; (C) Cumulative CO<sub>2</sub> production; (D) Acetate concentration; (E) Propionate concentration (All gas data are at 1 atm and 25°C).

### 7.3.7 Biotransformation products of IPAs

#### 7.3.7.1 Biotransformation products under aerobic conditions

Several new peaks were detected on LC/MS in samples from the culture series with high buffer capacity, and their peak areas increased over time concomitantly with the decrease of the parent IPAs (Figure 7.11). Moreover, these new peaks were not observed in the IPA-free, reference culture series, indicating they were not metabolites from the degradation of other organic compounds (i.e., dextrin and PL-extract). Therefore, the new peaks represented transformation products of IPAs.

For MON, three major products (called MON-TPs) were observed with  $m/z$  ( $[M+Na]^+$ ) of 707 (MON-TP707) and 709 (MON-TP709-1 and MON-TP709-2). The molecular weight of MON-TPs suggest that an oxygen atom was added on the parent MON, forming a hydroxyl ( $m/z$  709) or ketone ( $m/z$  707) moiety. To further elucidate the structure of MON-TPs, LC/MS/MS was used to provide more structural information from collision-induced-dissociation (CID) fragments. MON-TP707 appeared to be the same product as one of the biotransformation products of MON previously identified in soil microcosms on the basis of identical fragmentation patterns (Figure 7.12) (Sun *et al.*, 2014). Therefore, one of the major pathways of MON degradation under aerobic conditions with the PL-enriched culture was the same as that found in soil microcosms. Because the PL-enriched culture was developed with PL and PL-fertilized soil as inoculum, and was fed over time with PL-extract, it is expected that the culture retained most of the metabolic capabilities of the microbial communities found in PL and soil.

The other two biotransformation products, both with  $m/z$  709, were not previously observed in soil microcosms. Based on their MS/MS fragmentation (Figure 7.12) and the fragmentation pattern of the parent MON (Figure 7.13), MON-TP709-1 and MON-TP709-2

were likely transformation products with oxygen addition to the MON moiety between C8 and C17 (Figure 7.13). The common peaks at  $m/z$  237 and 197 indicate that no alteration occurred at the carboxylic end of ring A (Figures 7.12 and 7.13). The base peak on the parent MON,  $m/z$  479, was replaced by  $m/z$  477, which was a result of elimination of a  $H_2O$  from the oxidized fragment  $m/z$  479 (i.e.,  $479+16-18$ ). For MON-TP709-2, the fragments of  $m/z$  495 and 465 were from the oxidized fragment  $m/z$  479 and from the elimination of  $-CH_2-OH$  from the oxidized fragment  $m/z$  479 (Figures 7.12 and 7.13), respectively. Therefore, oxidation of MON occurred on the moiety between C8 and C17 to yield MON-TP709-1 and MON-TP709-2. Although, it was not possible to identify the exact structure of MON-TP709-1 based on the MS/MS fragments, the elimination of  $-CH_2-OH$  strongly suggests that MON-TP709-2 was the result of oxidation on a primary carbon. Given that there are only two primary carbons (C30 and C32) in the MON middle moiety, which are subject to oxygen addition, the possible structures of MON-TP709-2 are proposed in Table 7.4.

For SAL, two major products (called SAL-TPs) were observed with  $m/z$  ( $[M+Na]^+$ ) of 531 and 633 by LC/MS. LC/MS/MS was used to provide additional structural information of SAL-TPs. The product with  $m/z$  of 531 (called SAL-TP531) was also identified from the biodegradation of SAL in soil and PL microcosms (Figure 7.12) (Sun *et al.*, 2014). Several previous studies also have reported that biodegradation of SAL in soil or by soil bacteria under aerobic conditions yielded a major product with  $m/z$  of 531 (sodium adduct) (Hansen *et al.*, 2012; Sun *et al.*, 2014). Therefore, the molecular structure of SAL-TP531 is as shown in Table 7.5. The product with  $m/z$  of 633 (called SAL-TP633) is a newly identified product. The MS/MS fragmentation pattern clearly shows that SAL-TP633 retained rings B-E from the parent SAL, resulting in fragments with  $m/z$  of 531.2, 431.2, 413.2, and 403.2 (Figures 7.12 and 7.13). Based

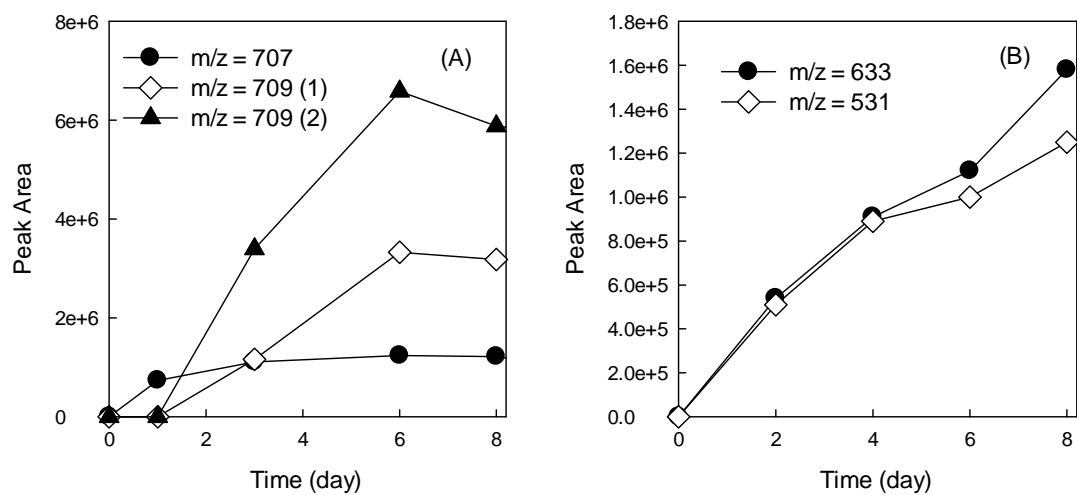
on its molecular weight, the structure of SAL-TP633 is tentatively proposed and shown in Table 7.5. However, more advanced instrumental analysis is needed in order to confirm the exact molecular structure of SAL-TP633.

#### *7.3.7.2 IPA biotransformation products under fermentative/sulfate-reducing conditions*

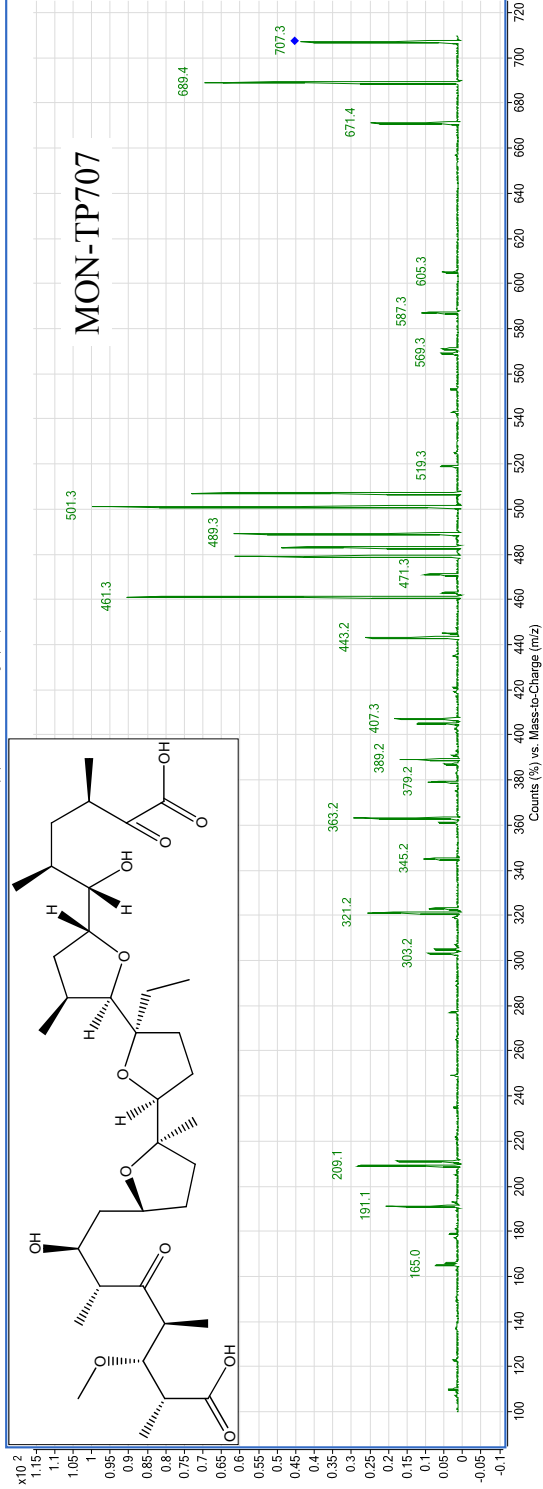
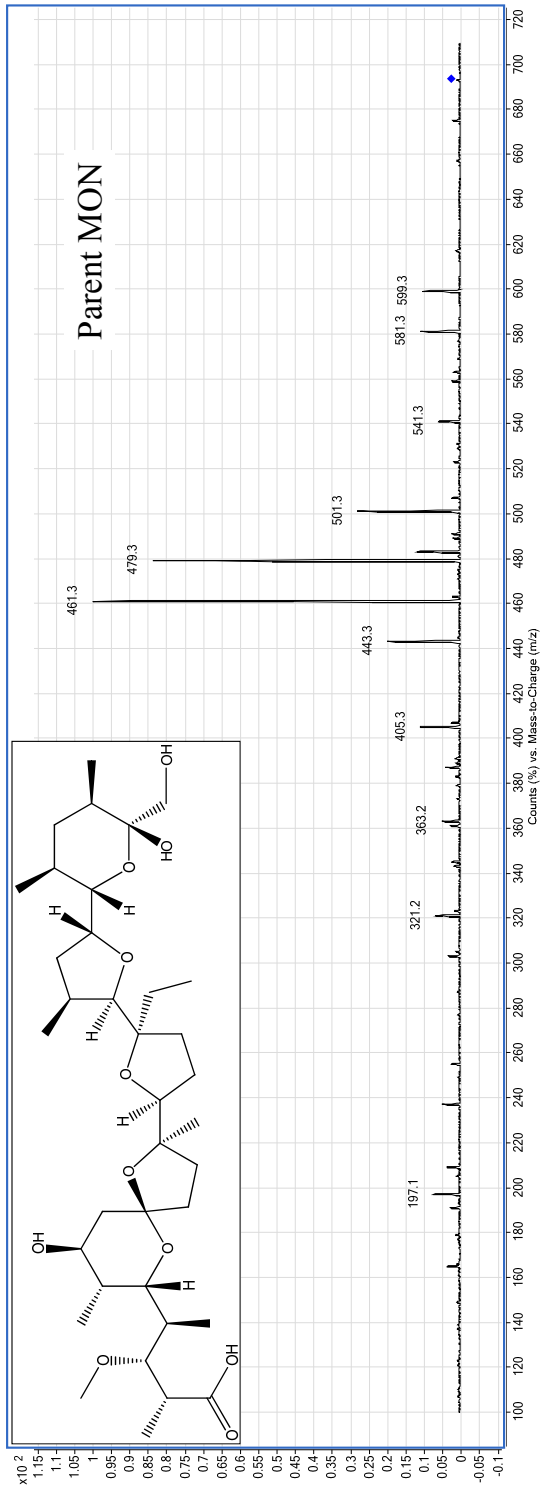
One new peak,  $m/z$  of 755 (called SAL-TP755), was detected by LC/MS in the culture series amended with SAL. This peak was neither observed in the IPA-free, reference series, nor in the MON-amended culture series (without SAL), indicating that the new peak represents the transformation product of SAL under fermentative/sulfate-reducing conditions.

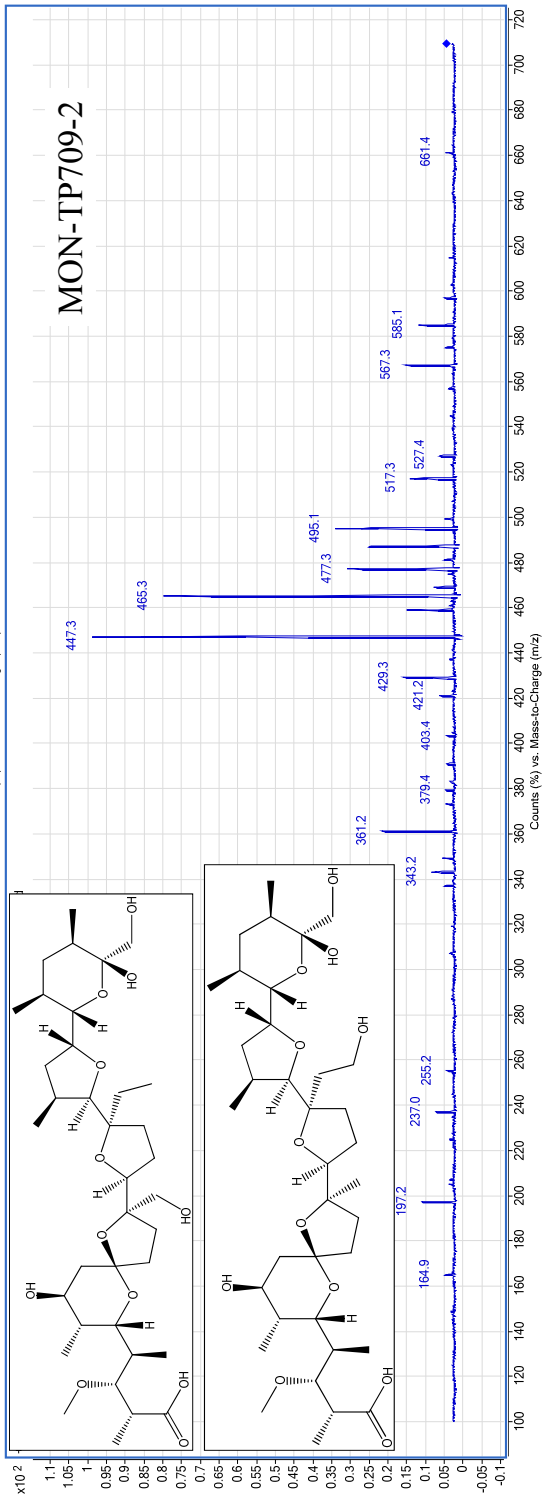
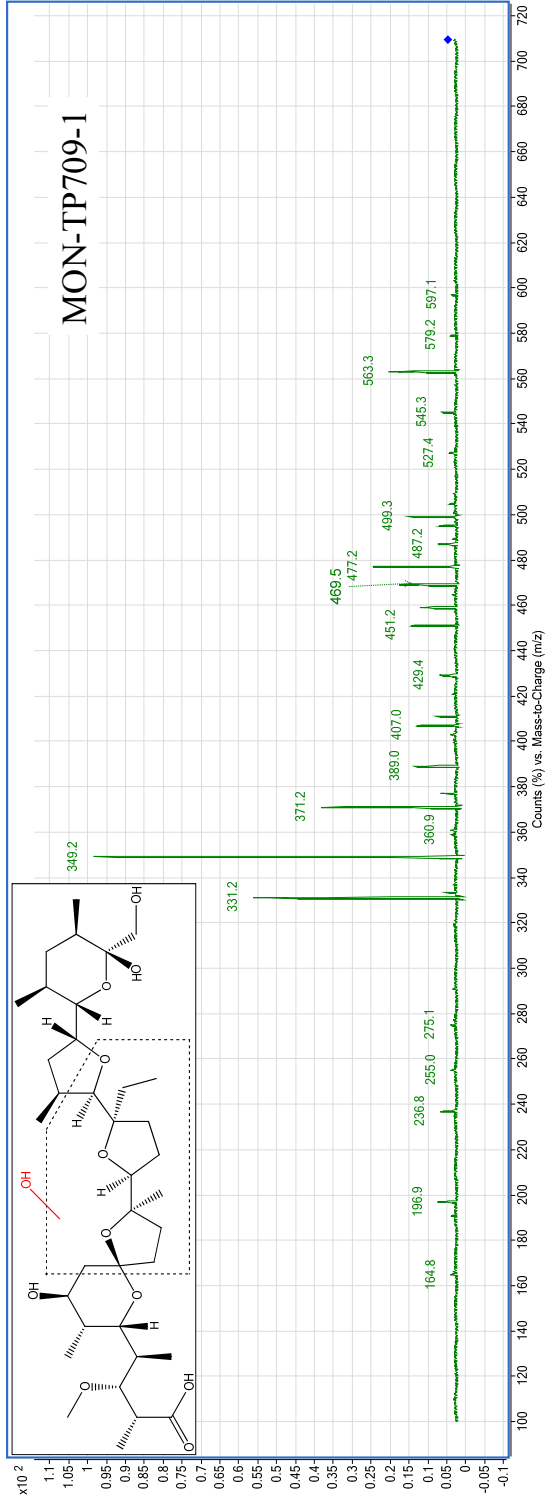
An  $m/z$  value of 755, an 18 Da lower than the parent SAL, suggests that SAL-TP755 was produced by elimination of an H<sub>2</sub>O molecule from the parent SAL. SAL bears multiple oxygen-containing groups which are all possibly be eliminated by a H<sub>2</sub>O molecule. In order to further elucidate the structure of SAL-TP755, LC/MS/MS was applied using the same CAD set-up as for the parent SAL. The MS/MS results (Figure 7.12) showed three main fragments,  $m/z$  of 513, 495, and 265. Compared with the MS/MS fragments of SAL (Figure 7.12), the common peak at  $m/z$  265 suggests SAL-TP755 retained rings C and D. The fragment of  $m/z$  531 of SAL was replaced by  $m/z$  513 in SAL-TP755. The difference of 18 Da between these two fragments suggests that the elimination occurred on the substructure of SAL fragment  $m/z$  531. Combined with the result of  $m/z$  265, the H<sub>2</sub>O elimination was likely associated with either the oxygen atom on ring B or with the -OH of ring C. Furthermore, the evidence that fragment of  $m/z$  431 (nor 413) was not observed for SAL-TP755 indicates that moieties around C12-C13 were altered which made C12-C13 difficult to cleave and yield the  $m/z$  431 fragment during CID. This observation suggests that the oxygen atom on ring B is likely to be eliminated, leading to two

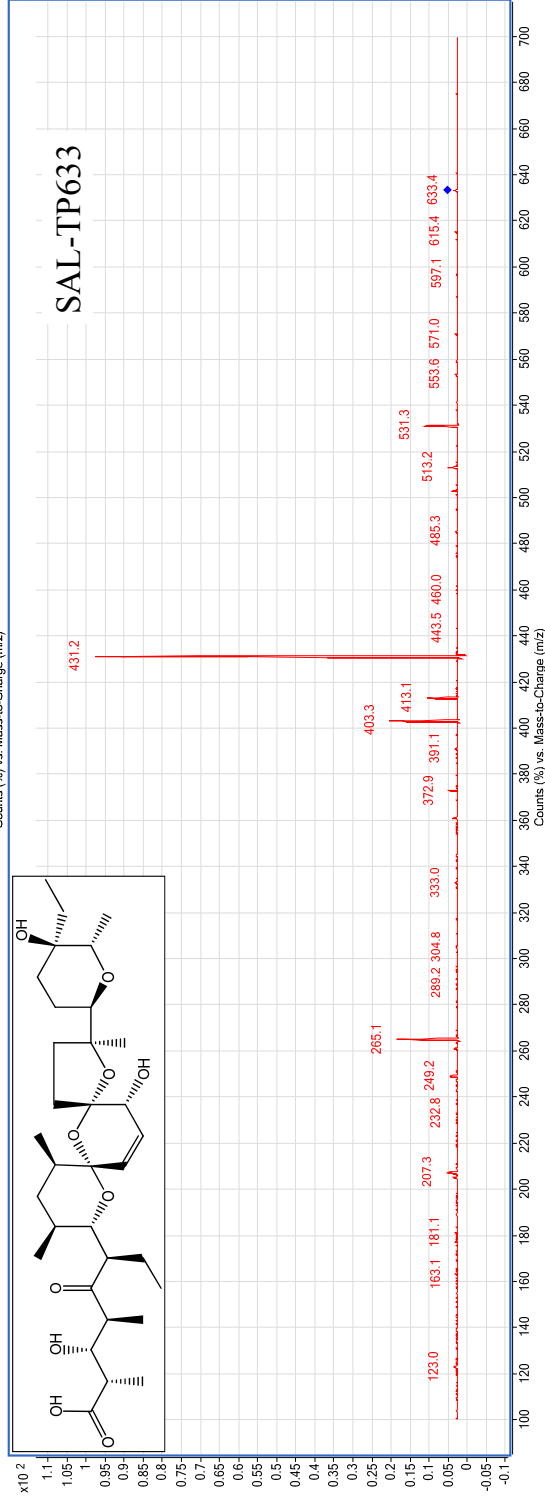
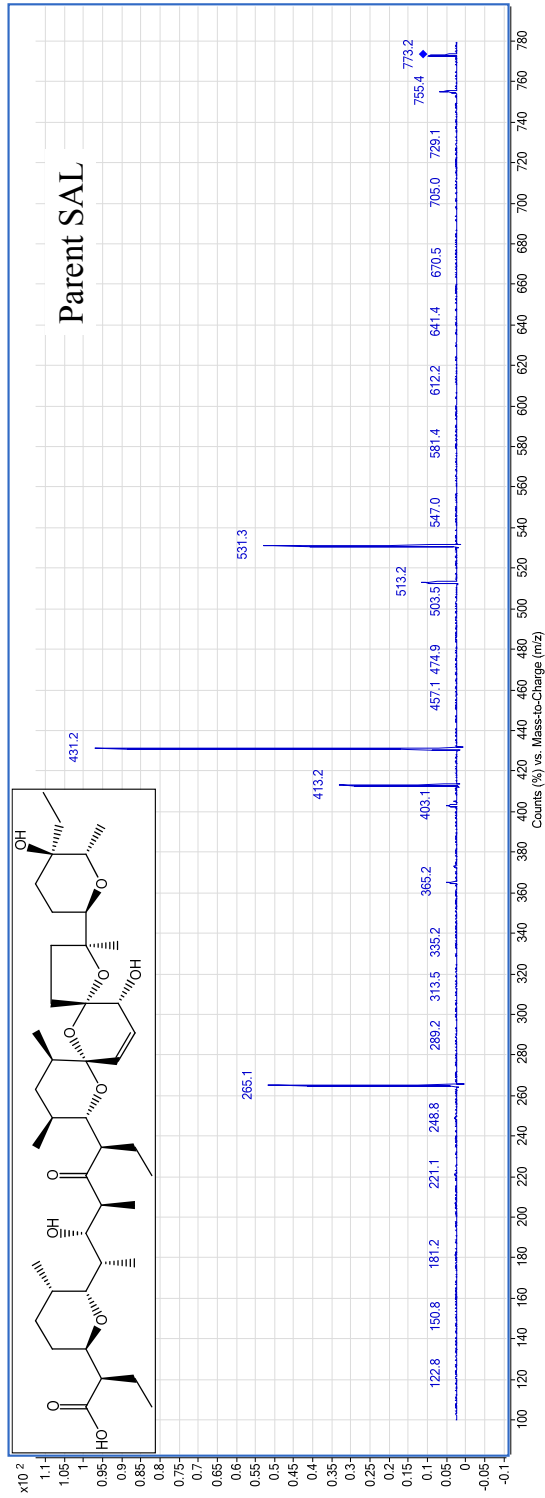
C=C bonds. Therefore, we tentatively propose the structure shown in Table 7.5 for the SAL-TP755 product.



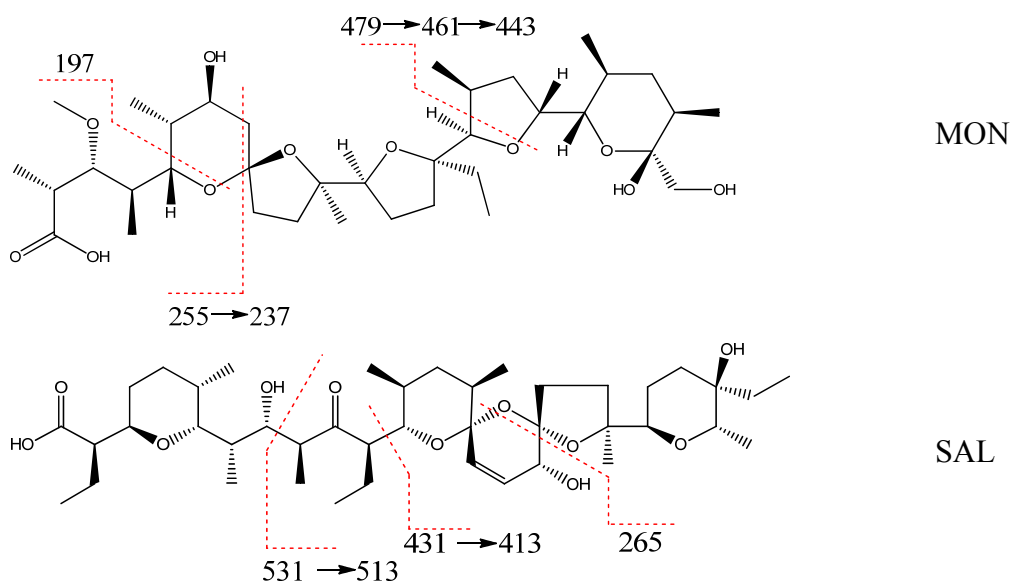
**Figure 7.11** Primary biotransformation products of MON (A) and SAL (B) in dextrin-amended culture series incubated under aerobic conditions.





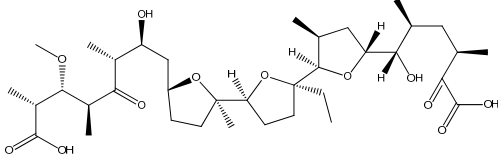
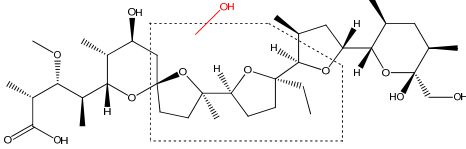
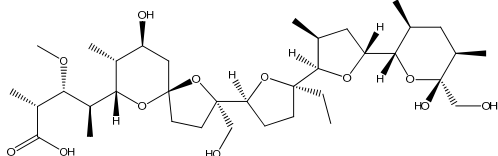
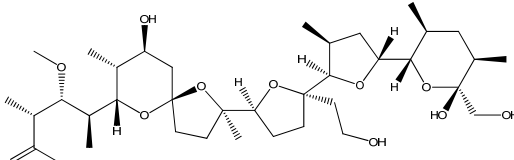




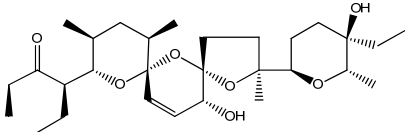
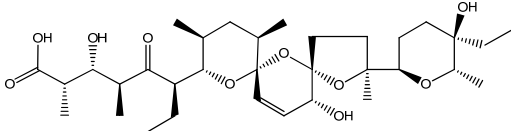
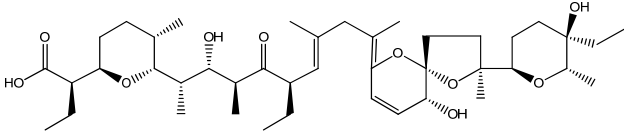


**Figure 7.13** CAD fragmentation sites of the parent IPAs. Arrows represent elimination of water.

**Table 7.4** Proposed structures of primary biotransformation products of MON

Conditions	Biotransformation products
Aerobic	 <p style="text-align: center;">MON-TP707</p>
Aerobic	 <p style="text-align: center;">MON-TP709-1</p>
Aerobic	 <p style="text-align: center;">MON-TP709-2</p> <p style="text-align: center;">or</p>  <p style="text-align: center;">MON-TP709-2</p>

**Table 7.5** Proposed structures of primary biotransformation products of SAL

Conditions	Biotransformation products
Aerobic	 <p>SAL-TP531</p>
Aerobic	 <p>SAL-TP633</p>
Fermentative/ sulfate reducing	 <p>SAL-TP755</p>

#### 7.4 Environmental Implications

IPAs are usually introduced into the environment by land application of animal waste used as fertilizer, which could encounter different redox conditions. Results from this study have several important implications related to the environmental fate of IPAs.

In top soil, both aerobic biodegradation and hydrolysis of IPAs could occur, depending on the buffer capacity of soil, as well as ammonia concentrations. Animal waste, such as fresh PL, is rich in ammoniacal nitrogen produced as a result of uric acid breakdown. When applied to agricultural fields, PL will stimulate nitrification, which consumes alkalinity, possibly resulting in acid-catalyzed hydrolysis of IPAs. The hydrolysis products of MON were previously studied by our group, showing that they retained some antibiotic properties of ionophores, and thus may pose a potential risk to local soil microbial community (Sun *et al.*, 2013b). In contrast, biodegradation of IPAs occurred relatively slowly compared to their hydrolysis at pH below 5. In river sediment or in deeper soil layers, denitrification will be predominant when oxygen supply is limited. However, our results showed that IPAs were persistent under strict denitrifying conditions, though the presence of IPAs up to 1 mg/L did not inhibit denitrification. In PL-fertilized soil, fermentation/sulfate-reduction is likely to occur in anoxic soil layers because significant amounts of organic matter and sulfate are introduced with PL. MON was found to be persistent under such conditions, but SAL was degraded by fermentative bacteria. Under methanogenic conditions, minimal inhibition was observed at a MON concentration as high as 250 µg/L, which suggests that the performance of municipal anaerobic digesters is not likely to be affected given the typical IPA concentrations in wastewater influent (less than 0.3 µg/L) (Watkinson *et al.*, 2009). In the case of anaerobic treatment of wastewater generated in the production of veterinary antibiotics, MON is expected to exceed 500 µg/L, and thus might

negatively affect methanogenesis in anaerobic digesters.

## CHAPTER 8

### CONCLUSIONS AND RECOMMENDATIONS

Antimicrobial agents released from agricultural activities into the environment have raised worldwide concerns because of their potential impact on ecological systems and the evolution of antibiotic resistant microorganisms. However, IPAs, the second top-selling antibiotic group in the U.S., have been scarcely investigated for their environmental fate and impact. This thesis aimed at conducting a systematic study on IPAs' environmental behavior after their release from litter related to poultry production. By simulating the conditions related to the water-soil-litter systems, the overall environmental transformation potential of IPAs has been delineated in this thesis. Based on the improved knowledge of IPAs' transformation mechanisms in the environment, recommendations for better IPA selection and agricultural waste management are made to reduce the environmental risks of IPAs.

#### 8.1 Quantification of IPAs in Environmental Matrices

Due to the increasing amount of IPAs used in livestock production, the necessity to monitor residual IPAs in the environment becomes more urgent. Especially, the sources of IPAs released to the environment should be particularly identified.

Research results of this thesis provided reliable detection methods for monitoring IPAs, including MON, SAL and NAR, in rainfall runoff, soil and poultry litter. Compared to the methods previously developed, the analytical method developed in this study focused on environmental matrices with high organic content. Efforts were especially made to separate IPAs from co-existing dissolved organic matter in order to achieve minimal signal suppression on LC/MS analysis.

The developed methods were successfully applied to detect IPAs in a wide range of environmental samples. The results showed that IPAs were only detected in the environmental compartments in contact with poultry litter, including soil and runoff from poultry litter-fertilized field, which suggests poultry litter is likely one of the major sources of IPAs in the environment. In addition, poultry litter contained considerable amounts of IPAs, which can be transported with rainfall runoff from poultry litter-fertilized fields to other environmental compartments.

## **8.2 Abiotic Transformation of IPAs**

Because IPAs could be transported with runoff, they likely end up in the aqueous environment. Therefore, transformation reactions, including hydrolysis and photolysis, play an important role in the environmental abiotic degradation of IPAs.

Previous research reported that IPAs were unstable in organic solvents when treated with acids, which imply that IPA may undergo acid-promoted reactions. However, the stability of IPAs in aqueous systems was unclear. Research in this thesis has identified the propensity of IPAs to undergo acid-catalyzed transformation in mildly acidic aquatic systems and characterized the reactions in depth. Considering the common presence of mildly acidic environments (pH 4 – 7) in soils and waters, the acid-catalyzed transformation identified in this study likely plays an important role in the environmental fate of IPAs.

Regarding photodegradation, to the authors' best knowledge, this research is among the first to investigate IPA transformation reactions under light irradiation. Environmental conditions can greatly affect IPAs' photodegradation. IPAs in shallow water likely undergo rapid photolysis when exposed to sunlight. Water near agricultural fields contains significant amounts of nitrate, which will enhance the photodegradation of IPAs. On the other hand, the photodegradation of IPAs could be inhibited in agricultural runoff because significant amounts of dissolved organic

matter likely co-exist with IPAs and the organic matter appeared to hinder photolysis of IPAs. Additionally, the toxicity tests showed that photolysis of IPAs eliminates its antibiotic properties against target microorganism.

### **8.3 Biotransformation of IPAs**

Microbial activity is expected to be one of the major processes of degradation of IPAs in the environment. Considering the compartments where IPAs would end up in, this thesis investigated the biotransformation potential and inhibition effect of IPAs in poultry litter, soil, and with litter/soil enriched cultures under different conditions.

The observation of degradation of IPAs in soil and animal waste was previously reported; however, conditions affecting the degradation rates were not investigated in detail. Moreover, information remained largely unknown about IPAs' biodegradation potential and biotransformation products under different redox conditions. This dissertation investigated IPA biodegradation in PL and soil microcosms as a process affecting the fate of IPAs in the environment. Water content and temperature have both shown significant influence on the biodegradation of IPAs in PL and soil microcosms. The major biotransformation product of MON was yielded as a result of oxidation of primary alcohol group with enzyme-facilitated hydrolysis, whereas SAL biodegraded via a cleavage on ketone moiety. A field study shows that MON and SAL are stable during poultry litter stacking, whereas MON degrades after poultry litter is applied to grassland. The biotransformation product of MON was also detected in the top soil layer where poultry litter was applied.

The inhibition and biodegradation potential of IPAs were performed with the enriched cultures under aerobic, denitrification, fermentation, sulfate-reduction, and methanogenesis

conditions, to provide a comprehensive evaluation of IPA bioreactivity after they are released from animal operations. The inhibition tests indicate that only methanogenesis would be affected by IPAs at environmentally relevant concentrations. Results also suggest that biodegradation of IPAs likely occurs under conditions in poultry litter-fertilized soil.

#### 8.4 Implications of IPA Transformation Reactions in the Environment

This study delineates the propensity of IPAs to undergo various transformation reactions under environmental conditions. Based on the findings from this research, Table 8.1 lists the transformation reactions most likely to occur under conditions related to the water-soil-litter systems.

**Table 8.1** IPA transformation reactions under conditions related to the water-soil-litter systems

Transformations	Matrix			Transformation products
	Poultry litter	Soil	Water system	
Hydrolysis	<ul style="list-style-type: none"> <li>• PL amended with alum</li> </ul>	<ul style="list-style-type: none"> <li>• Acidic soil</li> <li>• Soil fertilized with alum-amended PL</li> <li>• Soil with active nitrification</li> </ul>	<ul style="list-style-type: none"> <li>• Acidic surface water</li> <li>• Lagoon with active nitrification</li> </ul>	<ul style="list-style-type: none"> <li>• Isomers of IPAs (major)</li> <li>• Toxic against target bacteria</li> </ul>
Photolysis	<ul style="list-style-type: none"> <li>• Not significant</li> </ul>	<ul style="list-style-type: none"> <li>• Photolysis on soil surface under sunlight irradiation</li> </ul>	<ul style="list-style-type: none"> <li>• Surface water under sunlight irradiation</li> <li>• WWTP equipped with UV facility</li> </ul>	<ul style="list-style-type: none"> <li>• Products with smaller molecular weight</li> <li>• No ionophore property</li> </ul>
Biodegradation	<ul style="list-style-type: none"> <li>• SAL/NAR biodegradation in PL</li> </ul>	<ul style="list-style-type: none"> <li>• Biodegradation in top soil</li> <li>• Anaerobic</li> </ul>	<ul style="list-style-type: none"> <li>• Biodegradation in agricultural influenced</li> </ul>	<ul style="list-style-type: none"> <li>• The major MON products are</li> </ul>

---

stacking • Anaerobic biodegradation of SAL under fermentation conditions	biodegradation of SAL under fermentation conditions	water body • Anaerobic biodegradation of SAL in river sediment under fermentation conditions	biodegradable • The major SAL product is not biodegradable
---	---	---	---

---

## 8.5 Recommendations

Based on the findings in this thesis, several recommendations are made in order to mitigate the environmental impact of IPAs.

As discussed in Chapters 2 and 6, poultry litter is likely the major source of IPAs released into the aquatic environment. Therefore, the degradation of IPAs during poultry litter stacking process would help to reduce the quantity of IPAs in poultry litter before poultry litter is applied to agricultural field. Although abiotic degradation of IPAs in the poultry litter matrix was not specifically studied in this research, it is expected that the chemical amendment of alum will lower the pH of poultry litter, thus trigger the acid-catalyzed hydrolysis of IPAs. The degradation of IPAs can also be enhanced by adjusting stacking conditions. In Chapter 6, it was shown that the water content and temperature have a great impact on the biodegradation of IPAs in poultry litter microcosms. Because temperature is not easily controlled during poultry litter stacking process, addition of water is recommended to achieve optimal conditions for the biodegradation of IPAs.

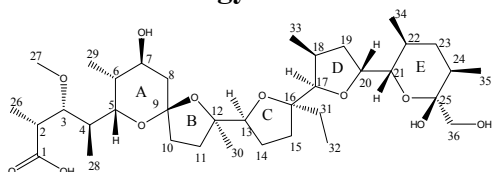
Among commonly used IPAs, SAL and NAR are more prone to degradation in the environment than MON, thus are more advantageous than MON from the environmental risk perspective. Indeed, the results from this study showed that SAL and NAR have faster hydrolysis and photolysis rates than MON under the same pH or illumination conditions. Moreover, complete degradation of SAL and NAR was observed in poultry litter microcosms, which indicates that elimination of SAL and NAR could be achieved during the poultry litter stacking process. Therefore, SAL and NAR are more advantageous than MON in mitigating the environmental impact of IPAs.

## **8.6 Future Work**

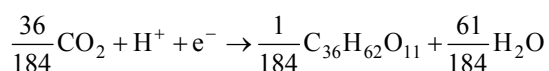
More extensive investigation on the environmental occurrence of IPAs as well as their major transformation products is a priority in near-future research, which will provide valuable information for a comprehensive assessment of the environmental risks of residual IPAs. For the long-term research, three major areas are recommended: (1) comprehensive evaluation of toxicity of IPA transformation products, (2) elucidation of the metabolic pathways which are responsible for IPA biotransformation, and (3) investigation of possible induction and evolution of antibiotic-resistant microorganisms with the co-presence of IPAs and/or their major transformation products.

## APPENDIX A GIBBS FREE ENERGY ESTIMATIONS OF IPAS

### Gibbs free energy calculation of MON



Group/Correction	# of occurrence	Contribution (kcal/mol)	Total contribution (kcal/mol)
Origin	1	-23.6	-23.6
-CH3	9	7.9	71.1
-OH (primary)	1	-29.3	-29.3
-OH (secondary)	1	-32.0	-32
-OH (tertiary)	1	-30.5	-30.5
-COO <sup>-</sup>	1	-72.0	-72
>CH-	3	-4.8	-14.4
>CH2	2	1.7	3.4
-O-	1	-22.5	-22.5
>CH2 (participating in a non-benzene ring)	7	6.1	42.7
>CH- (participating in a non-benzene ring)	10	-2.2	-22
>C< (participating in a non-benzene ring)	3	-12.8	-38.4
-O- (participating in a ring)	5	-24.3	-121.5
>C< (participating in two non-benzene rings)	1	-12.0	-12
$\Delta G_r^{0'}$			-301 kcal/mol -1259.4 kJ/mol



$$\Delta G_r^{0'} = 1/184 * (-1259.4) + 61/184 * (-237.18) - 36/184 * (-386.02) - 1 * (-39.87) = 29.92 \text{ kJ/eq}$$

$$E_0' = -\Delta G_r^{0'} / nF = 29.92 / 96.485 = -0.310 \text{ volts}$$

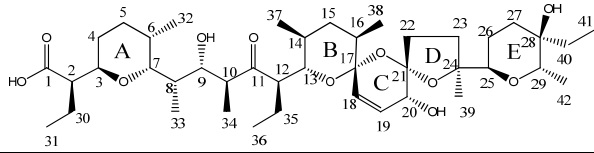
$$\text{Aerobic: } \Delta G_r^{0'} = -78.72 - 29.92 = -108.64 \text{ kJ/eq}$$

$$\text{Nitrate reducing (to N}_2\text{): } \Delta G_r^{0'} = -72.20 - 29.92 = -102.12 \text{ kJ/eq}$$

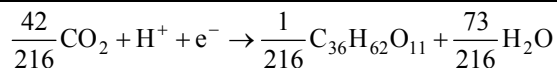
$$\text{Sulfate reducing (to sulfide): } \Delta G_r^{0'} = 20.85 - 29.92 = -9.07 \text{ kJ/eq}$$

$$\text{Methanogenic: } \Delta G_r^{0'} = 23.53 - 29.92 = -6.39 \text{ kJ/eq}$$

## Gibbs free energy calculation of SAL



Group/Correction	# of occurrence	Contribution (kcal/mol)	Total contribution (kcal/mol)
Origin	1	-23.6	-23.6
-CH3	10	7.9	79
-OH (primary)	0	-29.3	0
-OH (secondary)	2	-32.0	-64
-OH (tertiary)	1	-30.5	-30.5
-COO <sup>-</sup>	1	-72.0	-72
>CH-	5	-4.8	-24
>CH2	3	1.7	5.1
-O-	0	-22.5	0
>CO	1	-27.2	-27.2
>CH2 (participating in a non-benzene ring)	7	6.1	42.7
>CH- (participating in a non-benzene ring)	9	-2.2	-19.8
-CH= (participating in a non-benzene ring)	2	9.6	19.2
>C< (participating in a non-benzene ring)	2	-12.8	-25.6
-O- (participating in a ring)	5	-24.3	-121.5
>C< (participating in two non-benzene rings)	2	-12.0	-24
$\Delta G_f^{0'}$			-286.2 kcal/mol -1197.5 kJ/mol



$$\Delta G_r^{0'} = 1/216*(-1197.5) + 73/216*(-237.18) - 42/216*(-386.02) - 1*(-39.87) = 29.23 \text{ kJ/eq}$$

$$E_0' = -\Delta G_r^{0'}/nF = 29.23/96.485 = -0.303 \text{ volts}$$

$$\text{Aerobic: } \Delta G_r^{0'} = -78.72 - 29.23 = -107.95 \text{ kJ/eq}$$

$$\text{Nitrate reducing (to N}_2\text{): } \Delta G_r^{0'} = -72.20 - 29.23 = -101.43 \text{ kJ/eq}$$

$$\text{Sulfate reducing (to sulfide): } \Delta G_r^{0'} = 20.85 - 29.23 = -8.38 \text{ kJ/eq}$$

$$\text{Methanogenic: } \Delta G_r^{0'} = 23.53 - 29.23 = -5.70 \text{ kJ/eq}$$

## REFERENCES

- Agtarap, A., Chamberlin, J.W., Pinkerton, M., Steinrauf, L., 1967. The structure of monensic acid, a new biologically active compound. *Journal of the American Chemical Society* 89(22), 5737-5739.
- Alexy, R., Kumpel, T., Kummerer, K., 2004. Assessment of degradation of 18 antibiotics in the Closed Bottle Test. *Chemosphere* 57(6), 505-512.
- Andreozzi, R., Caprio, V., Ciniglia, C., de Champdore, M., Lo Giudice, R., Marotta, R., Zuccato, E., 2005. Antibiotics in the environment: Occurrence in Italian STPs, fate, and preliminary assessment on algal toxicity of amoxicillin. *Environmental Science & Technology* 39(20), 8112-8112.
- Andreozzi, R., Marotta, R., Paxeus, N., 2003. Pharmaceuticals in STP effluents and their solar photodegradation in aquatic environment. *Chemosphere* 50(10), 1319-1330.
- American Association of Public Health (APHA), 2012. Standard methods for the examination of water and wastewater, 22nd edition, APHA-AWWA-WEF, Washington, DC.
- Banat, I.M., Lindström, E.B., Nedwell, D.B., Balba, M.T., 1981. Evidence for coexistence of two distinct functional groups of sulfate-reducing bacteria in salt marsh sediment. *Applied and Environmental Microbiology* 42(6), 985-992.
- Bernhardt, D., Diekmann, H., 1991. Degradation of dioxane, tetrahydrofuran and other cyclic ethers by an environmental *Rhodococcus* strain. *Applied Microbiology and Biotechnology* 36(1), 120-123.
- Blackwell, P.A., Lutzhoft, H.C.H., Ma, H.P., Halling-Sorensen, B., Boxall, A.B.A., Kay, P., 2004. Ultrasonic extraction of veterinary antibiotics from soils and pig slurry with SPE clean-up and LC-UV and fluorescence detection. *Talanta* 64(4), 1058-1064.
- Blanchflower, W.J., Kennedy, D.G., 1996. Determination of monensin, salinomycin and narasin in muscle, liver and eggs from domestic fowl using liquid chromatography electrospray mass spectrometry. *Journal of Chromatography B-Biomedical Applications* 675(2), 225-233.
- Bohn, P., Bak, S.A., Björklund, E., Krogh, K.A., Hansen, M., 2013. Abiotic degradation of antibiotic ionophores. *Environmental Pollution* 182, 177-183.
- Bonvin, F., Omlin, J., Rutler, R., Schweizer, W.B., Alaimo, P.J., Strathmann, T.J., McNeill, K., Kohn, T., 2012. Direct photolysis of human metabolites of the antibiotic sulfamethoxazole: evidence for abiotic back-transformation. *Environmental Science & Technology* 47(13), 6746-6755.
- Brain, R.A., Johnson, D.J., Richards, S.M., Sanderson, H., Sibley, P.K., Solomon, K.R., 2004. Effects of 25 pharmaceutical compounds to *Lemna gibba* using a seven-day static-

- renewal test. *Environmental Toxicology and Chemistry* 23(2), 371-382.
- Brezonik, P.L., Fulkerson-Brekken, J., 1998. Nitrate-induced photolysis in natural waters: Controls on concentrations of hydroxyl radical photo-intermediates by natural scavenging agents. *Environmental Science & Technology* 32(19), 3004-3010.
- Buser, H.R., Poiger, T., Muller, M.D., 1998. Occurrence and fate of the pharmaceutical drug diclofenac in surface waters: Rapid photodegradation in a lake. *Environmental Science & Technology* 32(22), 3449-3456.
- Buxton, G.V., Greenstock, C.L., Helman, W.P., Ross, A.B., 1988. Critical-review of rate constants for reactions of hydrated electrons, hydrogen-atoms and hydroxyl radicals (.OH/.O-) in aqueous-solution. *Journal of Physical and Chemical Reference Data* 17(2), 513-886.
- Callow, R.K., Massyberesford, P.N., 1958. Steroidal sapogenins - the isomerisation of normal to iso-sapogenins. *Journal of the Chemical Society (Aug)*, 2645-2653.
- Canonica, S., Laubscher, H.-U., 2008. Inhibitory effect of dissolved organic matter on triplet-induced oxidation of aquatic contaminants. *Photochemical & Photobiological Sciences* 7(5), 547-551.
- Capleton, A.C., Courage, C., Rumsby, P., Holmes, P., Stutt, E., Boxall, A.B.A., Levy, L.S., 2006. Prioritising veterinary medicines according to their potential indirect human exposure and toxicity profile. *Toxicology Letters* 163(3), 213-223.
- Carlson, J.C., Mabury, S.A., 2004. Degradation kinetics and mobility of chlortetracycline, tylosin and monensin in an agricultural soil. *Abstracts of Papers of the American Chemical Society* 228, U629-U629.
- Carlson, J.C., Mabury, S.A., 2006. Dissipation kinetics and mobility of chlortetracycline, tylosin, and monensin in an agricultural soil in Northumberland County, Ontario, Canada. *Environmental Toxicology and Chemistry* 25(1), 1-10.
- Carlson, K., Kim, S.C., 2006. Occurrence of ionophore antibiotics in water and sediments of a mixed-landscape watershed. *Water Research* 40(13), 2549-2560.
- Carson, J., Statham, P., 1993. The inhibition by ionophores in-vitro of an enterococcus-like pathogen of rainbow-trout, *oncorhynchus-mykiss*. *Veterinary Microbiology* 36(3-4), 253-259.
- Cha, J.M., Yang, S., Carlson, K.H., 2005. Rapid analysis of trace levels of antibiotic polyether ionophores in surface water by solid-phase extraction and liquid chromatography with ion trap tandem mass spectrometric detection. *Journal of Chromatography A* 1065(2), 187-198.
- Chapman, H.D., Jeffers, T.K., Williams, R.B., 2010. Forty years of monensin for the control of coccidiosis in poultry. *Poultry Science* 89(9), 1788-1801.

- Chen, M., Wolin, M., 1979. Effect of monensin and lasalocid-sodium on the growth of methanogenic and rumen saccharolytic bacteria. *Applied and Environmental Microbiology* 38(1), 72-77.
- Chen, W.R., Ding, Y., Johnston, C.T., Teppen, B.J., Boyd, S.A., Li, H., 2010. Reaction of lincosamide antibiotics with manganese oxide in aqueous solution. *Environmental Science & Technology* 44(12), 4486-4492.
- Chen, W.R., Huang, C.H., 2010. Adsorption and transformation of tetracycline antibiotics with aluminum oxide. *Chemosphere* 79(8), 779-785.
- Cox, B.G., Vantruong, N., Rzeszotarska, J., Schneider, H., 1984. Rates and equilibria of alkali-metal and silver ion complex-formation with monensin in ethanol. *Journal of the American Chemical Society* 106(20), 5965-5969.
- Cox, B.G., Vantruong, N., Rzeszotarska, J., Schneider, H., 1984. Stability-constants of complexes of monensin and lasalocid with alkali-metal and alkaline-earth-metal ions in protic and polar aprotic-solvents. *Journal of the Chemical Society-Faraday Transactions I* 80, 3275-3284.
- Dalrymple, R.M., Carfagno, A.K., Sharpless, C.M., 2010. Correlations between dissolved organic matter optical properties and quantum yields of singlet oxygen and hydrogen peroxide. *Environmental Science & Technology* 44(15), 5824-5829.
- Davis, J.G., Truman, C.C., Kim, S.C., Ascough, J.C., Carlson, K., 2006. Antibiotic transport via runoff and soil loss. *Journal of environmental quality* 35(6), 2250-2260.
- Degani, H., 1977. Kinetics of monensin complexation with sodium ions by Na-23 NMR-spectroscopy. *Biophysical Chemistry* 6(3), 345-349.
- Dolliver, H., Gupta, S., Noll, S., 2008. Antibiotic degradation during manure composting. *Journal of environmental quality* 37(3), 1245-1253.
- Dolliver, H., Kumar, K., Gupta, S., Singh, A., 2008. Application of enzyme-linked immunosorbent assay analysis for determination of monensin in environmental samples. *Journal of environmental quality* 37(3), 1220-1226.
- Donoho, A.L., 1984. Biochemical-studies on the fate of monensin in animals and in the environment. *Journal of Animal Science* 58(6), 1528-1539.
- Dorkov, P., Pantcheva, I.N., Sheldrick, W.S., Mayer-Figge, H., Petrova, R., Mitewa, M., 2008. Synthesis, structure and antimicrobial activity of manganese(II) and cobalt(II) complexes of the polyether ionophore antibiotic Sodium Monensin A. *Journal of Inorganic Biochemistry* 102(1), 26-32.
- Duax, W.L., Smith, G.D., Strong, P.D., 1980. Complexation of metal-ions by monensin - crystal and molecular-structure of hydrated and anhydrous crystal forms of sodium monensin. *Journal of the American Chemical Society* 102(22), 6725-6729.

- Dubois, M., Pierret, G., Delahaut, P., 2004. Efficient and sensitive detection of residues of nine coccidiostats in egg and muscle by liquid chromatography-electrospray tandem mass spectrometry. *Journal of Chromatography B-Analytical Technologies in the Biomedical and Life Sciences* 813(1-2), 181-189.
- EFSA., 2004. Opinion of the scientific panel on additives and products or substances used in animal feed on a request from the commission on the safety and the efficacy of product "BIO-COX 120G" as feed additive in accordance with Council Directive 70/524/EEC, pp. 1-51, EFSA.
- EFSA., 2005. Opinion of the scientific panel on additives and products or substances used in animal feed on a request from the European Commission on the evaluation of the coccidiostat COXIDIN® (monensin sodium), pp. 1-53, EFSA.
- FDA, 2009. Summary Report on Antimicrobials Sold or Distributed for Use in Food-Producing Animals FDA (U.S. Food and Drug Administration).
- FDA, 2010. Summary Report on Antimicrobials Sold or Distributed for Use in Food-producing Animals, FDA (U.S. Food and Drug Administration).
- FDA, 2011. Summary Report on Antimicrobials Sold or Distributed for Use in Food-producing Animals, FDA (U.S. Food and Drug Administration).
- Franco, A., Fu, W.J., Trapp, S., 2009. Influence of soil pH on the sorption of ionizable chemicals: modeling advances. *Environmental Toxicology and Chemistry* 28(3), 458-464.
- Furtula, V., Huang, L., Chambers, P.A., 2009. Determination of veterinary pharmaceuticals in poultry litter and soil by methanol extraction and liquid chromatography-tandem mass spectrometry. *Journal of Environmental Science and Health Part B-Pesticides Food Contaminants and Agricultural Wastes* 44(7), 717-723.
- Glaze, W.H., Lay, Y., Kang, J.W., 1995. Advanced oxidation processes - a kinetic-model for the oxidation of 1,2-dibromo-3-chloropropane in water by the combination of hydrogen-peroxide and UV-radiation. *Industrial & Engineering Chemistry Research* 34(7), 2314-2323.
- Gratzel, M., Henglein, A., Lilie, J., Beck, G., 1969. Pulse radiolysis of some elementary oxidation-reduction processes of nitrite ion. *Berichte Der Bunsen-Gesellschaft Fur Physikalische Chemie* 73(7), 646.
- Gros, M., Petrovic, M., Barcelo, D., 2006. Development of a multi-residue analytical methodology based on liquid chromatography-tandem mass spectrometry (LC-MS/MS) for screening and trace level determination of pharmaceuticals in surface and wastewaters. *Talanta* 70(4), 678-690.
- Hansen, M., Bjorklund, E., Krogh, K.A., Brandt, A., Halling-Sorensen, B., 2012. Biotic transformation of anticoccidials in soil using a lab-scale bio-reactor as a precursor-tool. *Chemosphere* 86(2), 212-215.

- Hansen, M., Bjorklund, E., Krogh, K.A., Halling-Sorensen, B., 2009. Analytical strategies for assessing ionophores in the environment. *Trac-Trends in Analytical Chemistry* 28(5), 521-533.
- Hansen, M., Krogh, K.A., Bjorklund, E., Brandt, A., Halling-Sorensen, B., 2009. Environmental risk assessment of ionophores. *Trac-Trends in Analytical Chemistry* 28(5), 534-542.
- Hansen, M., Krogh, K.A., Brandt, A., Christensen, J.H., Halling-Sorensen, B., 2009. Fate and antibacterial potency of anticoccidial drugs and their main abiotic degradation products. *Environmental Pollution* 157(2), 474-480.
- Hanson, M.L., McGregor, E.B., Solomon, K.R., 2007. Monensin is not toxic to aquatic macrophytes at environmentally relevant concentrations. *Archives of Environmental Contamination and Toxicology* 53(4), 541-551.
- Hao, C.Y., Lissemore, L., Nguyen, B., Kleywegt, S., Yang, P., Solomon, K., 2006. Determination of pharmaceuticals in environmental waters by liquid chromatography/electrospray ionization/tandem mass spectrometry. *Analytical and Bioanalytical Chemistry* 384(2), 505-513.
- Hao, C.Y., Zhao, X.M., Tabe, S., Yang, P., 2008. Optimization of a multiresidual method for the determination of waterborne emerging organic pollutants using solid-phase extraction and liquid chromatography/tandem mass spectrometry and isotope dilution mass spectrometry. *Environmental Science & Technology* 42(11), 4068-4075.
- Hartel, P., Segars, W., Summer, J., Collins, J., Phillips, A., Whittle, E., 2000. Survival of fecal coliforms in fresh and stacked broiler litter. *The Journal of Applied Poultry Research* 9(4), 505-512.
- Herrero, P., Borrull, F., Marce, R.M., Pocurull, E., 2013. Determination of polyether ionophores in urban sewage sludge by pressurised liquid extraction and liquid chromatography-tandem mass spectrometry: Study of different clean-up strategies. *Journal of Chromatography A* 1285, 31-39.
- Herrero, P., Borrull, F., Pocurull, E., Marce, R.M., 2012. Novel amide polar-embedded reversed-phase column for the fast liquid chromatography-tandem mass spectrometry method to determine polyether ionophores in environmental waters. *Journal of Chromatography A* 1263, 7-13.
- Hillis, D.G., Lissemore, L., Sibley, P.K., Solomon, K.R., 2007. Effects of monensin on zooplankton communities in aquatic microcosms. *Environmental Science & Technology* 41(18), 6620-6626.
- Hu, X.G., Luo, Y., Zhou, Q.X., Xu, L., 2008. Determination of thirteen antibiotics residues in manure by solid phase extraction and high performance liquid chromatography. *Chinese Journal of Analytical Chemistry* 36(9), 1162-1166.
- Jensen, J., Diao, X.P., Hansen, A.D., 2009. Single- and two-species tests to study effects of the

- anthelmintics ivermectin and morantel and the coccidiostatic monensin on soil invertebrates. *Environmental Toxicology and Chemistry* 28(2), 316-323.
- Jiao, S.J., Zheng, S.R., Yin, D.Q., Wang, L.H., Chen, L.Y., 2008. Aqueous photolysis of tetracycline and toxicity of photolytic products to luminescent bacteria. *Chemosphere* 73(3), 377-382.
- Kart, A., Bilgili, A., 2008. Ionophore antibiotics: toxicity, mode of action and neurotoxic aspect of carboxylic ionophores. *Journal of Animal and Veterinary Advances* 7(6), 748-751.
- Keen, O.S., Love, N.G., Linden, K.G., 2012. The role of effluent nitrate in trace organic chemical oxidation during UV disinfection. *Water Research* 46(16), 5224-5234.
- Kim, S.C., Carlson, K., 2006. Occurrence of ionophore antibiotics in water and sediments of a mixed-landscape watershed. *Water Research* 40(13), 2549-2560.
- Kim, S.C., Carlson, K., 2007. Quantification of human and veterinary antibiotics in water and sediment using SPE/LC/MS/MS. *Analytical and Bioanalytical Chemistry* 387(4), 1301-1315.
- Kim, S.C., Carlson, K., 2007. Temporal and spatial trends in the occurrence of human and veterinary antibiotics in aqueous and river sediment matrices. *Environmental Science & Technology* 41(1), 50-57.
- Kim, S.C., Davis, J.G., Truman, C.C., Ascough, J.C., Carlson, K., 2010. Simulated rainfall study for transport of veterinary antibiotics - mass balance analysis. *Journal of Hazardous Materials* 175(1-3), 836-843.
- Kuykendall, H., Cabrera, M., Hoveland, C., McCann, M., West, L., 1999. Stocking method effects on nutrient runoff from pastures fertilized with broiler litter. *Journal of environmental quality* 28(6), 1886-1890.
- Kwak, W., Huh, J., McCaskey, T., 2005. Effect of processing time on enteric bacteria survival and on temperature and chemical composition of broiler poultry litter processed by two methods. *Bioresource Technology* 96(14), 1529-1536.
- Kyriakis, S.C., 1989. The effect of monensin against swine-dysentery. *British Veterinary Journal* 145(4), 373-377.
- Kyriakis, S.C., Sarris, K., Kritas, S.K., Saoulidis, K., Tsinas, A.C., Tsiloyiannis, V.K., 1995. The effect of salinomycin on the control of clostridium-perfringens type-a infection in growing pigs. *Journal of Veterinary Medicine Series B-Zentralblatt Fur Veterinarmedizin Reihe B-Infectious Diseases and Veterinary Public Health* 42(6), 355-359.
- Lam, M.W., Mabury, S.A., 2005. Photodegradation of the pharmaceuticals atorvastatin, carbamazepine, levofloxacin, and sulfamethoxazole in natural waters. *Aquatic Sciences* 67(2), 177-188.

- Loutfy, R.O., Yip, R.W., 1973. Triplet-state of ketones in solution - role of charge-transfer state in quenching of triplet acetone by aromatic molecules. *Canadian Journal of Chemistry- Revue Canadienne de Chimie* 51(11), 1881-1884.
- Lutz, W.K., Wipf, H.K., Simon, W., 1970. Alkali cation specificity and carrier properties of antibiotics nigericin and monensin. *Helvetica Chimica Acta* 53(7), 1741.
- Mack, J., Bolton, J.R., 1999. Photochemistry of nitrite and nitrate in aqueous solution: a review. *Journal of Photochemistry and Photobiology a-Chemistry* 128(1-3), 1-13.
- Matabudul, D.K., Conway, B., Lumley, I., Sumar, S., 2001. The simultaneous determination of the ionophore antibiotics in animal tissues and eggs by tandem electrospray LC-MS-MS. *Food Chemistry* 75(3), 345-354.
- McGregor, E.B., Solomon, K.R., Hanson, M.L., 2007. Monensin is not toxic to aquatic macrophytes at environmentally relevant concentrations. *Archives of Environmental Contamination and Toxicology* 53(4), 541-551.
- Mellon, M., Benbrook, C., K.L. Benbrook, 2001. Hogging it. Estimates of antimicrobial abuse in livestock. [http://www.ucsusa.org/assets/documents/food\\_and\\_agriculture/hog\\_front.pdf](http://www.ucsusa.org/assets/documents/food_and_agriculture/hog_front.pdf)
- Misiti, T., Tandukar, M., Tezel, U., Pavlostathis, S.G., 2013. Inhibition and biotransformation potential of naphthenic acids under different electron accepting conditions. *Water Research* 47(1), 406-418.
- Moore, D.E., Chappuis, P.P., 1988. A comparative-study of the photochemistry of the non-steroidal anti-inflammatory drugs, naproxen, benoxaprofen and indomethacin. *Photochemistry and Photobiology* 47(2), 173-180.
- Moore, D.E., Wilkins, B.J., 1990. Common products from gamma-radiolysis and ultraviolet photolysis of metronidazole. *Radiation Physics and Chemistry* 36(4), 547-550.
- Moore, P.A., Daniel, T.C., Edwards, D.R., 2000. Reducing nonpoint source phosphorus runoff from poultry manure with aluminum sulfate. *Biological Resource Management: Connecting Science and Policy*, 117-127
- Moore, P.A., Daniel, T.C., Edwards, D.R., 2000. Reducing phosphorus runoff and inhibiting ammonia loss from poultry manure with aluminum sulfate. *Journal of environmental quality* 29(1), 37-49.
- Moore, P.A., Daniel, T.C., Sharpley, A.N., Wood, C.W., 1995. Poultry manure management - environmentally sound options. *Journal of Soil and Water Conservation* 50(3), 321-327.
- Morf, W.E., Simon, W., 1971. Evaluation of alkali and alkaline earth ion selectivity of electrically neutral carrier antibiotics and model compounds. *Helvetica Chimica Acta* 54(8), 2683-2704.
- Mortier, L., Daeseleire, E., Van Peteghem, C., 2005. Determination of the ionophoric

- coccidiostats narasin, monensin/lasalocid and salinomycin in eggs by liquid chromatography/tandem mass spectrometry. *Rapid Communications in Mass Spectrometry* 19(4), 533-539.
- Mostofa, K.M.G., Yoshioka, T., Mottaleb, A., 2012. *Photobiogeochemistry of organic matter: principles and practices in water environments*, Springer, New York.
- Nelieu, S., Perreau, F., Bonnemoy, F., Ollitrault, M., Azam, D., Lagadic, L., Bohatier, J., Einhorn, J., 2009. Sunlight nitrate-induced photodegradation of chlorotoluron: evidence of the process in aquatic mesocosms. *Environmental Science & Technology* 43(9), 3148-3154.
- Nelson, D.W., Sommers, L.W., 1982. *Methods of soil analysis - Part 2*. Soil Science Society of America (SSSA), Madison, WI.
- O'Shea, R., Moser, H.E., 2008. Physicochemical properties of antibacterial compounds: Implications for drug discovery. *Journal of Medicinal Chemistry* 51(10), 2871-2878.
- Page, S.E., Arnold, W.A., McNeill, K., 2011. Assessing the contribution of free hydroxyl radical in organic matter-sensitized photohydroxylation reactions. *Environmental Science & Technology* 45(7), 2818-2825.
- Pangborn, W., Duax, W., Langs, D., 1987. The hydrated potassium complex of the ionophore monensin-A. *Journal of the American Chemical Society* 109(7), 2163-2165.
- Pantcheva, I.N., Dorkov, P., Atanasov, V.N., Mitewa, M., Shivachev, B.L., Nikolova, R.P., Mayer-Figge, H., Sheldrick, W.S., 2009. Crystal structure and properties of the copper(II) complex of sodium monensin A. *Journal of Inorganic Biochemistry* 103(10), 1419-1424.
- Parr, J.F., Gardner, W.R., Elliott, L.F., 1981. *Water potential relations in soil microbiology: proceedings of a symposium*, Soil Science Society of America (SSSA).
- Perron, F., Albizati, K.F., 1989. Chemistry of spiroketals. *Chemical Reviews* 89(7), 1617-1661.
- Ramaswamy, J., Prasher, S.O., Patel, R.M., Hussain, S.A., Barrington, S.F., 2010. The effect of composting on the degradation of a veterinary pharmaceutical. *Bioresource Technology* 101(7), 2294-2299.
- Ramsey, E.D., Rees, A.T., Wei, G., Liu, J.Y., Wu, X.H., 2010. Direct aqueous supercritical fluid extraction coupled on-line with liquid chromatography tandem mass spectrometry for the analysis of polyether ionophore antibiotics in water. *Journal of Chromatography A* 1217(20), 3348-3356.
- Renew, J.E., Huang, C.H., 2004. Simultaneous determination of fluoroquinolone, sulfonamide, and trimethoprim antibiotics in wastewater using tandem solid phase extraction and liquid chromatography-electrospray mass spectrometry. *Journal of Chromatography A* 1042(1-2), 113-121.
- Rittmann, B.E., McCarty, P.L., 2001. *Environmental Biotechnology: Principles and Applications*,

McGraw-Hill, New York.

- Russell, J., Martin, S., 1984. Effects of various methane inhibitors on the fermentation of amino acids by mixed rumen microorganisms in vitro. *Journal of Animal Science* 59(5), 1329-1338.
- Russell, J.B., 1987. A proposed mechanism of monensin action in inhibiting ruminal bacterial-growth - effects on ion flux and protonmotive force. *Journal of Animal Science* 64(5), 1519-1525.
- Russell, J.B., Houlihan, A.J., 2003. Ionophore resistance of ruminal bacteria and its potential impact on human health. *FEMS Microbiology Reviews* 27(1), 65-74.
- Russell, J.B., Strobel, H.J., 1989. Effect of ionophores on ruminal fermentation. *Applied and Environmental Microbiology* 55(1), 1-6.
- Sarmah, A.K., Meyer, M.T., Boxall, A.B.A., 2006. A global perspective on the use, sales, exposure pathways, occurrence, fate and effects of veterinary antibiotics (VAs) in the environment. *Chemosphere* 65(5), 725-759.
- Sassman, S.A., Lee, L.S., 2007. Sorption and degradation in soils of veterinary ionophore antibiotics: monensin and lasalocid. *Environmental Toxicology and Chemistry* 26(8), 1614-1621.
- Schimel, J.P., Gullledge, J.M., Clein-Curley, J.S., Lindstrom, J.E., Braddock, J.F., 1999. Moisture effects on microbial activity and community structure in decomposing birch litter in the Alaskan taiga. *Soil Biology & Biochemistry* 31(6), 831-838.
- Schlusener, M., von Arb, M.A., Bester, K., 2006. Elimination of macrolides, tiamulin, and salinomycin during manure storage. *Archives of Environmental Contamination and Toxicology* 51(1), 21-28.
- Schlusener, M.P., Bester, K., 2006. Persistence of antibiotics such as macrolides, tiamulin and salinomycin in soil. *Environmental Pollution* 143(3), 565-571.
- Schlusener, M.P., Bester, K., Spitteller, M., 2003. Determination of antibiotics such as macrolides, ionophores and tiamulin in liquid manure by HPLC-MS/MS. *Analytical and Bioanalytical Chemistry* 375(7), 942-947.
- Schlusener, M.P., Spitteller, M., Bester, K., 2003. Determination of antibiotics from soil by pressurized liquid extraction and liquid chromatography-tandem mass spectrometry. *Journal of Chromatography A* 1003(1-2), 21-28.
- Schuster, D.I., 1975. Energy wastage processes in ketone photochemistry. *Pure and Applied Chemistry* 41(4), 601-633.
- Sekar, R., Wu, H.F., 2006. Quantitative method for analysis of monensin in soil, water, and urine by direct combination of single-drop microextraction with atmospheric pressure matrix-

- assisted laser desorption/ionization mass spectrometry. *Analytical Chemistry* 78(18), 6306-6313.
- Sharpless, C.M., Linden, K.G., 2001. UV photolysis of nitrate: Effects of natural organic matter and dissolved inorganic carbon and implications for UV water disinfection. *Environmental Science & Technology* 35(14), 2949-2955.
- Song, W.L., Huang, M., Rumbelha, W., Li, H., 2007. Determination of amprolium, carbadox, monensin, and tylosin in surface water by liquid chromatography/tandem mass spectrometry. *Rapid Communications in Mass Spectrometry* 21(12), 1944-1950.
- Stackhouse, K.R., Rotz, C.A., Oltjen, J.W., Mitloehner, F.M., 2012. Growth-promoting technologies decrease the carbon footprint, ammonia emissions, and costs of California beef production systems. *Journal of Animal Science* 90(12), 4656-4665.
- Steinrau, Lk, Czerwinski, Ew, Pinkerton, M., 1971. Comparison of monovalent cation complexes of monensin, nigericin, and dianemycin. *Biochemical and Biophysical Research Communications* 45(5), 1279-1283.
- Sun, P., Barmaz, D., Cabrera, M.L., Pavlostathis, S.G., Huang, C.H., 2013. Detection and quantification of ionophore antibiotics in runoff, soil and poultry litter. *J Chromatogr A* 1312, 10-17.
- Sun, P., Cabrera, M., Huang, C.-H., Pavlostathis, S.G., 2014. Biodegradation of veterinary ionophore antibiotics in broiler litter and soil microcosms. *Environmental Science & Technology* 48(5), 2724-2731.
- Sun, P., Yao, H., Minakata, D., Crittenden, J.C., Pavlostathis, S.G., Huang, C.H., 2013. Acid-catalyzed transformation of ionophore veterinary antibiotics: reaction mechanism and product implications. *Environmental Science & Technology* 47(13), 6781-6789.
- Thiele-Bruhn, S., 2003. Pharmaceutical antibiotic compounds in soils - a review. *Journal of Plant Nutrition and Soil Science-Zeitschrift Fur Pflanzenernahrung Und Bodenkunde* 166(2), 145-167.
- Tiquia, S.M., Tam, N.F.Y., 2002. Characterization and composting of poultry litter in forced-aeration piles. *Process Biochemistry* 37(8), 869-880.
- Tiquia, S.M., Tam, N.F.Y., Hodgkiss, I.J., 1996. Microbial activities during composting of spent pig-manure sawdust litter at different moisture contents. *Bioresource Technology* 55(3), 201-206.
- Tugtas, A.E., Pavlostathis, S.G., 2007. Electron donor effect on reduction pathway and kinetics in a mixed methanogenic culture. *Biotechnology and Bioengineering* 98(4), 756-763.
- Turro, N.J., Ramamurthy, V., Scaiano, J.C., 2012. Modern molecular photochemistry of organic molecules. *Photochemistry and Photobiology* 88(4), 1033-1033.

- UCS, 2001. Hogging It: Appendices. [http://www.ucsusa.org/assets/documents/food\\_and\\_agriculture/hog\\_apps.pdf](http://www.ucsusa.org/assets/documents/food_and_agriculture/hog_apps.pdf). (UCS, Union of Concerned Scientists)
- Varel, V., Hashimoto, A., 1982. Methane production by fermentor cultures acclimated to waste from cattle fed monensin, lasalocid, salinomycin, or avoparcin. *Applied and Environmental Microbiology* 44(6), 1415-1420.
- Vaufrey, F., Delort, A.M., Jeminet, G., Dauphin, G., 1990. Bioconversion of monensin by a soil bacterium, *sebekia-benihana*. *Journal of Antibiotics* 43(9), 1189-1191.
- Vertesy, L., Heil, K., Fehlhaber, H.W., Ziegler, W., 1987. Microbial decomposition of salinomycin. *Journal of Antibiotics* 40(3), 388-390.
- Vincent, U., Chedin, M., Yasar, S., von Holst, C., 2008. Determination of ionophore coccidiostats in feedingstuffs by liquid chromatography-tandem mass spectrometry - Part I. Application to targeted feed. *Journal of Pharmaceutical and Biomedical Analysis* 47(4-5), 750-757.
- Vione, D., Falletti, G., Maurino, V., Minero, C., Pelizzetti, E., Malandrino, M., Ajassa, R., Olariu, R.I., Arsene, C., 2006. Sources and sinks of hydroxyl radicals upon irradiation of natural water samples. *Environmental Science & Technology* 40(12), 3775-3781.
- Vione, D., Maurino, V., Minero, C., Borghesi, D., Lucchiari, M., Pelizzetti, E., 2003. New processes in the environmental chemistry of nitrite. 2. The role of hydrogen peroxide. *Environmental Science & Technology* 37(20), 4635-4641.
- Vione, D., Maurino, V., Minero, C., Pelizzetti, E., 2002. New processes in the environmental chemistry of nitrite: Nitration of phenol upon nitrite photoinduced oxidation. *Environmental Science & Technology* 36(4), 669-676.
- Vione, D., Maurino, V., Minero, C., Pelizzetti, E., 2005. Nitration and photonitration of naphthalene in aqueous systems. *Environmental Science & Technology* 39(4), 1101-1110.
- Vione, D., Maurino, V., Minero, C., Vincenti, M., Pelizzetti, E., 2001. Formation of nitrophenols upon UV irradiation of phenol and nitrate in aqueous solutions and in TiO<sub>2</sub> aqueous suspensions. *Chemosphere* 44(2), 237-248.
- Volmer, D.A., Lock, C.M., 1998. Electrospray ionization and collision-induced dissociation of antibiotic polyether ionophores. *Rapid Communications in Mass Spectrometry* 12(4), 157-164.
- Wagener, S.M., Oswood, M.W., Schimel, J.P., 1998. Rivers and soils: Parallels in carbon and nutrient processing. *Bioscience* 48(2), 104-108.
- Wagener, S.M., Schimel, J.P., 1998. Stratification of soil ecological processes: a study of the birch forest floor in the Alaskan taiga. *Oikos* 81(1), 63-74.
- Walse, S.S., Morgan, S.L., Kong, L., Ferry, J.L., 2004. Role of dissolved organic matter, nitrate,

- and bicarbonate in the photolysis of aqueous fipronil. *Environmental Science & Technology* 38(14), 3908-3915.
- Watanabe, N., Harter, T.H., Bergamaschi, B.A., 2008. Environmental occurrence and shallow ground water detection of the antibiotic monensin from dairy farms. *Journal of Environmental Quality* 37(5), S78-S85.
- Watkinson, A.J., Murby, E.J., Kolpin, D.W., Costanzo, S.D., 2009. The occurrence of antibiotics in an urban watershed: From wastewater to drinking water. *Science of the Total Environment* 407(8), 2711-2723.
- Wells, J.L., Bordner, J., Bowles, P., Mcfarland, J.W., 1988. Novel degradation products from the treatment of salinomycin and narasin with formic-acid. *Journal of Medicinal Chemistry* 31(1), 274-276.
- Wenk, J., von Gunten, U., Canonica, S., 2011. Effect of dissolved organic matter on the transformation of contaminants induced by excited triplet states and the hydroxyl radical. *Environmental Science & Technology* 45(4), 1334-1340.
- Werner, J.J., Arnold, W.A., McNeill, K., 2006. Water hardness as a photochemical parameter: Tetracycline photolysis as a function of calcium concentration, magnesium concentration, and pH. *Environmental Science & Technology* 40(23), 7236-7241.
- Werner, J.J., Arnold, W.A., McNeill, K., 2006. Water hardness as a photochemical parameter: tetracycline photolysis as a function of calcium concentration, magnesium concentration, and pH. *Environmental Science & Technology* 40(23), 7236-7241.
- Westerhoff, P., Mezyk, S.P., Cooper, W.J., Minakata, D., 2007. Electron pulse radiolysis determination of hydroxyl radical rate constants with Suwannee river fulvic acid and other dissolved organic matter isolates. *Environmental Science & Technology* 41(13), 4640-4646.
- Westley, J.W., 1983. *Polyether Antibiotics: Naturally Occurring Acid Ionophores*, CRC Press.
- Wildenauer, F., Blotevogel, K., Winter, J., 1984. Effect of monensin and 2-bromoethanesulfonic acid on fatty acid metabolism and methane production from cattle manure. *Applied Microbiology and Biotechnology* 19(2), 125-130.
- Woodward, R.B., Sondheimer, F., Mazur, Y., 1959. The mechanism of the isomerization of steroidal sapogenins at C-25. *Journal of the American Chemical Society* 80(24), 6693-6694.
- Yang, N.C., Feit, E.D., 1968. Photochemistry of t-butyl alkyl ketones in solution. *Journal of the American Chemical Society* 90(2), 504-506.
- Yang, N.-C., Feit, E.D., Hui, M.H., Turro, N.J., Dalton, J.C., 1970. Photochemistry of di-tert-butyl ketone and structural effects on the rate and efficiency of intersystem crossing of aliphatic ketones. *Journal of the American Chemical Society* 92(23), 6974-6976.

- Yao, H., Sun, P., Minakata, D., Crittenden, J.C., Huang, C.-H., 2013. Kinetics and modeling of degradation of ionophore antibiotics by UV and UV/H<sub>2</sub>O<sub>2</sub>. *Environmental Science & Technology* 47(9), 4581-4589.
- Young, R.B., Latch, D.E., Mawhinney, D.B., Nguyen, T.H., Davis, J.C.C., Borch, T., 2013. Direct photodegradation of androstenedione and testosterone in natural sunlight: inhibition by dissolved organic matter and reduction of endocrine disrupting potential. *Environmental Science & Technology* 47(15), 8416-8424.
- Zafiriou, O.C., Jousset-Dubien, J., Zepp, R.G., Zika, R.G., 1984. Photochemistry of natural waters. *Environmental Science & Technology* 18(12), 358A-371A.
- Zepp, R.G., 1978. Quantum yields for reaction of pollutants in dilute aqueous-solution. *Environmental Science & Technology* 12(3), 327-329.
- Zepp, R.G., Hoigne, J., Bader, H., 1987. Nitrate-induced photooxidation of trace organic chemicals in water. *Environmental Science & Technology* 21(5), 443-450.